UNIVERSITY OF BIRMINGHAM

Understanding Molecular Interactions to Enhance Deposition of Perfume Microcapsules on Fabric Surfaces

by

Sen Liu

A thesis submitted to

The University of Birmingham

For the degree of

DOCTOR OF PHILOSOPHY

School of Chemical Engineering

The University of Birmingham

Sep 2018

Abstract

The fundamental purpose of this Thesis is to enhance the delivery of perfume microcapsules (PMC) containing fragrance active molecules to solid fabric surfaces in laundry process. This has been done through the study and screening of different polymers such as polyvinyl formamide, chitosan and polydopamine as surface coating and bridging molecules between PMC and fabric surfaces, and the fundamental understanding of their molecular interactions in different laundry conditions. The adhesive behaviours of polymer modified microcapsules on artificial and natural fabric surfaces were studied using AFM and a flow chamber technique. The surface compositions of both microcapsules and fabric surfaces before and after the modification were characterised using standard techniques including XPS, ESEM, light microscope, contact angle and zeta potential. The mechanical strength of the microcapsules was determined using a micromanipulation technique. The relationships between the surface properties of the microcapsules before and after the modification and their mechanical strength and adhesive performances at end-use applications have been established. Although the interactions of laundry liquid parameters such as surfactant type and concentration, hardness / salt concentration were proved to have significant influences, the adhesion of PMCs to model cellulose film has been demonstrated to be influenced largely by electrostatic interactions between the film and PMC surfaces, whilst the adhesion of PMCs to model PET film was dominated by hydrophobic interactions.

Acknowledgement

I would like to express my deepest gratitude towards my supervisor Prof. Zhibing Zhang for his excellent supervision, continuous encouragement and constant guidance. Without his valuable advice and support, it would be much more difficult for me to go this far.

Sincere thanks also go to Dr. James Bowen for the training of using AFM equipment and Dr. Yanping He for the training on flow chamber and micromanipulation rig, as well as the helpful discussions and suggestions on data analysis.

I would like to acknowledge the financial support provided by Procter & Gamble Belgium Innovation Centre (P&G BIC) and the School of Chemical Engineering, University of Birmingham to this research. Thanks to Pierre Verstraete in P&G BIC who continuous supported this project and gave me opportunities to visit P&G BIC to learn and collaborate with the industrial partners during the project.

I would like to express my sincere appreciations to the fellows, colleagues and staff in the School of Chemical Engineering, Lynn Draper, Dr. Mingming Du, Dr. Yan Zhang, Dr. Javier Marques De Marino, Bingyu Zhuo, Toni Bianca DiPaolo, Andrew Gray and Mariana Cardoso for their continuous assistance, support and encouragement. I cherish the friendship and the life experiences in the Micromanipulation Research Group.

Last but not least, I would like to express my thanks to my family, my parents and grandma back in China, and my dear wife Ella, who has companied and been patient with me through the journey. Thank you for all your love and support.

Table of Contents

List of Figures

List of Tables

List of Equations

List of Abbreviations

AFM	Atomic Force Microscopy
ATRP	atom transfer radical polymerization
BIC	P&G Belgium Innovation Centre
CMC	Critical Micelle Concentration
COS model	Carpick-Ogletree-Salmeron contact model
DDA	degree of deacetylation of chitosan
DI-water	de-ionised water
DLVO theory	Derjaguin-Landau-Verwey-Overbeek theory
DMT model	Derjaguin-Muller-Toporov contact model
EDX	energy dispersive X-ray spectroscopy
ESEM	environmental scanning electron microscope
HDL	heavy duty liquid
JKR model	Johnson-Kendall-Roberts contact model
L-DOPA	3,4-dihydroxy-L-phenylalanine
LAS	linear alkylbenzene sulfonate
MD model	Maugis- Dugdale contact model
MF	melamine formaldehyde
MSDS	material safety data sheet
P&G	Procter & Gamble
PA	polyamide
PAC-PVOH	polyacrylate-polyvinyl alcohol
PDAC	polydiallydimethyl ammonium chloride
PE	polyelectrolytes
PEI	polyethylenimine or polyaziridine

PET	polyethylene terephthalate
PMC	perfume microcapsules
PU	polyurea
PVAm	polyvinylamine
PVF	polyvinyl formamide
RMS	root mean square
SDBS	sodium dodecyl benzene sulfonate
SDS	sodium dodecyl sulphate
SEM	scanning electron microscope
SFA	surface force apparatus
SFE	surface free energy
SG	Specific Gravity
SPS	sulfonated polystyrene
TRIS	trisaminomethane
XPS	X-ray photoelectron spectroscopy

List of Symbols

λ_D	Debye length, m
ε_0	permittivity of free space, 8.854×10^{-12} F·m^{-1}
ε_r	dielectric constant of a material
γ_l	surface tension of liquid, N·m^{-1}
γ_l^d	dispersion interaction of liquid, N·m^{-1}
γ_l^p	polar interaction of liquid, N·m^{-1}
γ_s	surface free energy of a solid, N·m^{-1}
γ_s^{ab}	acid-base interaction of solid, N·m^{-1}
γ_s^d	dispersion interaction of solid, N·m^{-1}
γ_s^h	hydrogen interaction of solid, N·m^{-1}
γ_s^i	induction interaction of solid, N·m^{-1}
γ_s^p	polar interaction of solid, N·m^{-1}
γ_{sl}	interfacial tension of solid-liquid interface, N·m^{-1}
θ	contact angle, °
τ	wall shear stress, Pa
μ	dynamic viscosity of fluid, Pa·s
μ_T	Tabor parameter
ν_1, ν_2	Poisson's ratio
ρ	fluid density, kg·m^{-3}
ω	Adhesive energy per unit area, J·m^{-2}
A	total area occupied by microcapsules on one image, m^2
A_0	software calculated area of a blank film image, m^2

A_D	total area occupied by the microcapsules on a film image at the end of deposition step, m^2
A_i	surface area occupied by a single microcapsule on one image, m^2
A_t	total area occupied by the microcapsules on a film image at time t, m^2
A_{total}	total area taken by the image, m^2
a	area ratio of microcapsules occupied on one image, %
a_R	normalised area retention ratio, $\%\cdot m^{-2}$
C_i	molar concentration of ion *i*, $mol\cdot L^{-1}$
$D_{4,3}$	volume weighted mean diameters, m
D_h	hydraulic diameter, m
d_{10}, d_{50} and d_{90}	mean diameter values of related 10%, 50% and 90% cumulative volume / mass, m
e	elementary charge constant, 1.602×10^{-19}C
F	adhesive force, N
h	inner height of a flow chamber device, m
I	ionic strength of a solution, $mol\cdot L^{-1}$
K, K_1, K_2	effective Young's modulus, Pa
k_B	Boltzmann constant, 1.381×10^{-23} J/K
N_A	Avogadro number, $6.022 \times 10^{23} mol^{-1}$
N and n	number of microcapsules measured in AFM force analysis
n_i	concentration of a charged centre in the solution, $mol\cdot L^{-1}$
Q	flow rate, $m^3\cdot s^{-1}$
q_i	net charge of n_i, C
R	radius of a sphere in contact with a flat surface, m
r	contact radius of a microcapsule on film surface, m

Re	Reynolds number
S_q	RMS roughness of a surface, nm
T	absolute temperature in Kelvins, K
t	flow chamber time point, min
w	inner width of a flow chamber device, m
z0	interatomic equilibrium distance for solid–solid interactions, m
z_i	charge number of ion i

Chapter 1. Introduction

There is a growing need to deliver “active molecules” to solid surfaces, covering a wide range of industrial applications from personal cleansing care, household care to pharmaceutical drug delivery (Jain, 1999, Rodrigues *et al.*, 2009). Among all different applications, special interest is given to the controlled release of functional oils such as fragrance to fabric surfaces during laundry process in order to deliver the pleasant scent to clothes and improve the product usage experiences of the consumers.

Laundry product formula contains a large number of ingredients and has designed pH, ion strength once they are dissolved into detergent solutions (He, 2013, Liu, 2010). The detergents in laundry process help to remove dirt from fabric surfaces, which makes deposition of any other particles onto them difficult. In most cases, the perfume oils have to be delivered through microencapsulation (Thies, 2005). Microcapsule can not only protect the fragrance from evaporation or interaction between perfume and cleaning ingredients, but also provide a long lasting release of pleasant scent to consumers. Since the fragrance benefit is so important in consumer product, and it is rather expensive, even a very small amount of saving on the perfume usage will bring a big cost advantage to the industry. Thus, such features of the perfume-filled microcapsules (PMCs) have attracted great attention in personal and household care companies, especially big companies such as Procter & Gamble (P&G) where funding of this project has come from.

Most approaches chose polymers to be the wall material, considering the small size and the complexity of manufacturing microcapsules (Thies, 2005). Urea formaldehyde, melamine formaldehyde (MF) (He, 2013, Liu, 2010), polyurea (Rodrigues *et al.*, 2009) and polyamide(Poncelet *et al.*, 1993b) microcapsules are the examples which have been

researched by both academia and industries. Optimized wall thickness and mechanical strength are also crucial to a microcapsule. It needs to be thick (strong) enough to hold the particle shape and thin (weak) enough to be broken to release the fragrance under certain conditions (normally through mechanical friction or compression in this case, but also have other mechanism of release such as diffusion). Theoretically, a thin wall can be more effective when the mean particle size is small as well (Su *et al.*, 2012). Most commercial perfume oils were reported being encapsulated by MF which is facing more restrictions from both environmental and human health policies (Rodriguesa, 2010). Thus, polyvinyl-polyacrylate (Ganza-Gonzalez *et al.*, 2002) copolymer, has been chosen by P&G to be the wall material for this project because of its relatively environmental friendly properties.

The amount of current deposition rate of PMC on cleaned fabric surfaces is quite low (consumer research results from P&G BIC); based on the experimental results reported by Teixeira (2010), the estimated loss of PMC during one wash cycle could be up to 46%. Therefore, surface modifications using polyelectrolytes (PE) was introduced by the industry. He (2013) studied on MF microcapsules and fabric surfaces and the interactions of polyelectrolytes as bridging material between them.

Fundamental understanding is essential on the possible mechanisms of the adhesion between the microcapsules and different fabric surfaces through the wash cycles in order to improve the microcapsule deposition and retention efficiency. Readily developed theories of molecular interactions revealed van der Waals force and electrostatic forces are the origin of the adhesion between two surfaces. In ambient air, capillary force was found to be the main contributor, whilst in liquid, the combining relations of Van der Waals force, electrostatic double layer force and solvation forces are applicable generally (Israelachvili, 2011). These

theories can be applied to analyse certain phenomena of modified microcapsule-fabric interactions.

Fabrics can have complex chemical compositions and surface tomography. Modern fabrics have two large parts of fibre resources. Natural cotton fabric is the most common in industry. The other is synthetic, polyethylene terephthalate (PET) fabric as representative. Smooth model fibre film is needed to mimic the adhesion occurring in real washing conditions to eliminate the physical entrapment or steric effect. Thus, one initial purpose of the project includes finding the proper representative fabric films to replace real fabrics in the laundry process.

Flow chamber and microfluidic devices are not only powerful platforms for a number of cell biological assays (Sia and Whitesides, 2003), but also effective tools for physicochemical evaluation of behaviours of non-biological particles in liquid environment. With a light microscope, a flow chamber was introduced to adhesion measurement to understand interactions of microcapsules on fabrics. The device, initially developed by Decuzzi *et al.* (Decuzzi *et al.*, 2007), was modified by He (2013), producing reliable results in her studies.

Atomic Force Microscopy (AFM) has been used to study different polymers as bridging molecules between microcapsules and fabric surfaces to develop mechanistic understanding of the interactions. Through the combination of the above two analytical tools, the relationship between the surface properties of the microcapsules and their performance at application conditions were established (Liu, 2010, He, 2013). In this project, standard techniques were also used to characterise the surface composition of microcapsule and target fabric surfaces and their environmental conditions, and how they could affect the adhesion mechanisms.

Based on above, this Thesis is divided into following parts:

Chapter 2 is overall literature review which not only takes an overview of all the factors involved in surface interactions and laundry process in this project, but also gives focuses on the key parameters that possibly have significant influences on the microcapsule deposition and retention, such as shear stress range during the laundry process, current industrial approaches to deliver perfume microcapsules, as well as other potential adhesion promotion techniques that could be applied to laundry.

Chapter 3 introduces all the materials and equipment tools, experimental techniques used in this project. All the experiment processes and technical background are explained in detail. Related technical review of experimental techniques and the explanation of different choices are combined in this chapter as well.

Chapter 4 focuses on the validation and verification of different characterisation tools for the surface modified microcapsules and target fabric surface substitutions. Subsequently, screening a series of commercial polyelectrolytes, PVF polymers, in a simplified lab condition was carried out through the use of both the flow chamber technique and AFM. The results helped selecting the key candidates for further comprehensive studies and further proved the reliability and consistency of the lab tools and analytical techniques.

Chapter 5 compares the adhesion performances of two polymer categories in polyelectrolyte families: PVF and chitosan, both of which are positively charged and historically proved effective in enhancing the adhesion in different industrial applications. Intensive flow chamber and AFM experiments were designed and conducted, and the results are reported in

this chapter. The data analysis shows the possible mechanisms of the molecular interactions between the surface-modified microcapsules and target fabric surfaces.

Chapter 6 goes further by exploring the possibility to enhance the adhesion of microcapsules to fabric surfaces by introducing mussel-inspired "superglue", polydopamine, to coat the laundry PMCs. The conditions of the coating reaction, surface properties of the modified PMCs, their deposition and retention on the model fabric films and adhesion behaviours were studied and compared with the results of polyelectrolytes.

Chapter 7 summaries all the findings and experiences of this project, and proposes some important works for future, and possible new directions and explorations.

Chapter 2. Literature Review

2.1. Introduction

This chapter gives a brief overview on the background of this project. Domestic laundry process and the factors related to the cleaning of fabrics are introduced in this chapter. The development and use of fragrance encapsulation technologies in laundry detergents are reviewed, followed by a brief introduction of the methods which have been used to enhance the adhesion of perfume microcapsules (PMCs). The current problem of applying PMCs in the laundry detergent field and the industrial approaches are reviewed. Subsequently, particle adhesion and contact theories, as well as related model development work are reviewed. Finally, the tools applied to characterising the effect of adhesion and their advantages and disadvantages are summarised.

2.2. Modern laundry

Modern laundry has been introduced to human life since the synthetic detergent was introduced by German in 1916 (McNeil, 2002, Showell, 1997) and the electric washing machine being popular after 1950s (Cowan, 1976).

There are four main factors in a typical domestic laundry:

1. The fabrics involved such as cotton clothes, synthetic fabrics, linens, etc.

2. The dirt on the fabrics such as soil, food residues, etc.

3. The process that laundry is being conducted, e.g. agitation and tumbling process in a washing machine.

4. Laundry detergent which improves the cleaning during washing.

Though both washing machine and laundry detergent have been improved to meet different consumer needs and multiple benefits have been achieved since their first invention (McNeil, 2002, Bajpai, 2007), the basics of domestic laundry process have not been changed much, which include a series of physical steps and chemical reactions at interfaces (Bajpai, 2007, Showell, 1997). Because the purpose of this research is to study the mechanism of molecular interactions between the fabric and perfume microcapsules (PMC) in laundry washing cycles, the above factors are all involved. Thus an introduction and close review are done as follows.

2.2.1. Fabrics in laundry

According to a textile market report done by the market research institute Grand View Research (https://www.grandviewresearch.com/) in 2017, cotton fabric has accounted for 39.5% of global textile production in 2015, with 30 million tonnes produced worldwide throughout 50 countries; whilst synthetic fibres (generally referred to as polyester) held a market volume share of 54.5%. The market forecast for cotton fabrics is about 3 - 4% growing rate per annual, whilst for polyester being about 5 - 7%. The report also mentioned cotton being the most widely used raw material for textile production, due to the properties including excellent water absorbency, high strength and colour retention. The reason cotton is dominated by polyester fibre is that the latter is cheaper, easily available with superior properties including lightweight, good durability, easy to process and excellent resistance to wrinkle and shrinking. Furthermore, cotton is often used in combination with other fibres such as polyester as the blend offers properties superseding either of the materials.

2.2.1.1. Cotton fabric and cellulose

The most common fabric made from natural sourced ingredients is cotton fabric. Major composition of cotton is cellulose fibre which is composed of a linear polysaccharide of 1, 4 linked D-glucose units (Updegraff, 1969, Klemm *et al.*, 2005). Anhydro-beta-cellobiose or beta glucose is the repeating unit of the cellulose polymer chain. Figure 2.1 is the typical molecular structure of cellulose reported in various literatures (Aravindanath *et al.*, 1982, Ioelovich and Leykin, 2008, Leppanen *et al.*, 2009).

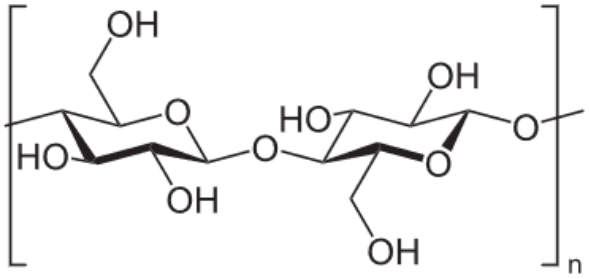

Figure 2.1 Typical molecular structure of cellulose

As one of the most abundant organic polymers on earth (Updegraff, 1969), a considerable number of studies on cotton fabric has been done since cellulose was first discovered in 1838 by French chemist Anselme Payen (Crawford, 1981, Young and Rowell, 1986). Although more than 90% of the composition in untreated mature cotton is cellulose fibre which is hydrophilic, the rest is a complex mixture of fatty acids, alcohols, alkanes, esters, glycerides and non-cellulosic polysaccharides which makes the cotton surface hydrophobic (Mitchell *et al.*, 2005). Therefore, the industrial scouring and bleaching process on the cotton fibres to make the commercial fabric has been designed to remove the impurities resulting in a product which is 99% cellulose (Wakelyn *et al.*, 2006).

Cotton cellulose has a degree of polymerisation (the number of repeating units in a single polymer chain) of 9000-15000 and about 73% of a cotton cellulose fibre is crystalline, whist wood pulp cellulose has a degree of polymerisation of 300-1500 and 35% crystallinity (Gibson, 2012). This higher cotton cellulose crystallinity indicates that most of the cotton fibre cellulose molecules are more closely packed and parallel to one another, relative to wood cellulose. Some literature reports have also stated higher crystallinity in both cotton (more than 90%) and wood (60-70%) sourced cellulose (Thygesen *et al.*, 2005). The high crystallinity makes the dissolution of cotton cellulose more difficult relative to wood cellulose under the same conditions. Figure 2.2 (a) and (b) are the illustrations of the crystallites in cellulose fibres (Ali and Gibson, 2013, Gibson *et al.*, 2010). Several different crystalline structures of cellulose are known, corresponding to the location of hydrogen bonds between and within the strands. Crystallite in natural cellulose is cellulose I; in regenerated cellulose fibre is cellulose II. The conversion of cellulose I to cellulose II is irreversible, suggesting that cellulose I is metastable and cellulose II is stable (Leppanen *et al.*, 2009, Fink *et al.*, 2001).

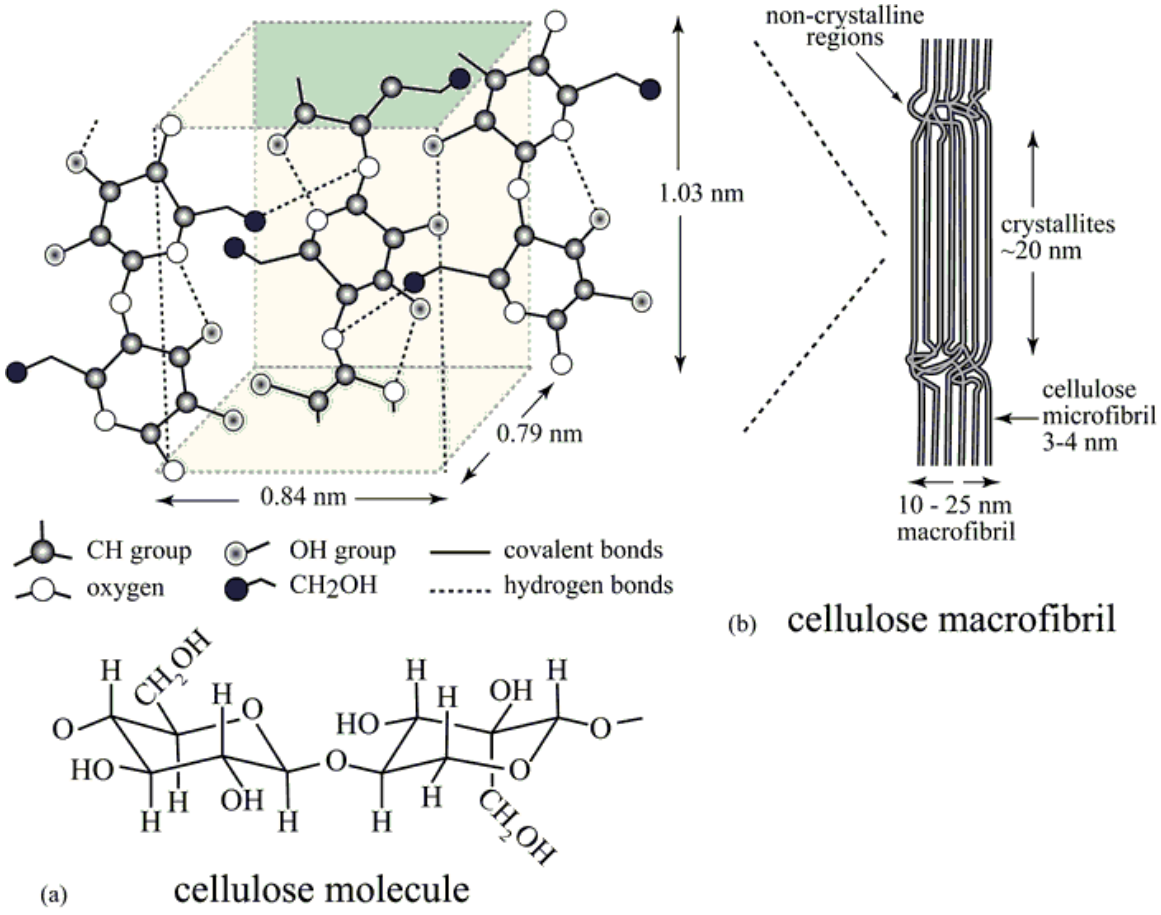

Figure 2.2 Structure of plant cellulose: (a) cellulose crystal structure; (b) cellulose macrofibril made up of several microfibrils (Ali and Gibson, 2013).

2.2.1.2. Surface properties of cellulose fabric

The surface properties of cellulose fabrics are extremely hydrophilic (Gassan *et al.*, 2000, Aravindanath *et al.*, 1982, Gibson *et al.*, 2010, Ioelovich and Leykin, 2008, Laity *et al.*, 2000, Mitchell *et al.*, 2005). Cotton fabric consists of cellulose fibres, therefore, the surface chemistry of such fabric is considered the same as the surface of the cotton cellulose fibre. Despite of the hydrophilicity, most cellulose fibres swell but do not dissolve either in water or most organic solvents because of their high degree of polymerisation and crystallisation due to long chain length, high molecular weight and inter- and intra-molecular hydrogen bonds

(Young and Rowell, 1986, Notley and Wågberg, 2005). Recently, Medronho *et al.* (Medronho *et al.*, 2012) reported that the cellulose is actually amphiphilic and the hydrophobicity in the molecular structure has also a marked contribution to its nature of insolubility in water and most organic solvents.

The illustrations in both Figure 2.1and Figure 2.2 reveal that there are hydroxyl (-OH) and hydroxymethyl (-CH_2OH) moieties at the surface of a cellulose fibre which makes it hydrophilic and able to form hydrogen bonds to external substrates (Aravindanath *et al.*, 1982, Young and Rowell, 1986, Gupta *et al.*, 2002, Scheirs and Long, 2005, Speight, 2005, Gardner *et al.*, 2008). Furthermore, as a result of the oxidation process (i.e. bleaching and dyeing in cotton fabric manufacture, and the kraft process in wood pulp manufacture), the surface hydroxy groups are converted to carboxylic acid moieties (-COOH) giving cellulose fibres a large surface electronegativity. Despite this, there are also hydrophobic alkyl (-CH- and -CH_2) groups taking about 25% surface area of a cellulose fibre (Paria *et al.*, 2005). Thus, the complex amphiphilic surface nature results in complex swelling behaviors, dissolution and adhesion of cellulose fabrics and films (Laity *et al.*, 2000, Falt *et al.*, 2003, Cuissinat *et al.*, 2008).

2.2.1.3. Synthetic fabrics

As technology develops fast, people want more diverse lifestyles and tend to have more choices of different clothing made of various fabrics. Such needs gave birth to a number of synthetic fabrics, among which polyethylene terephthalate (PET) fabric became the most common one (Scheirs and Long, 2005).

PET is thermoplastic polymer of the polyester family and is used in a wide range of industries such as beverage and foods packaging, thermoforming for manufacturing, engineering resins in combination with glass fibre and clothing. It is such an excellent barrier material to water and moisture that huge amount of PET plastic bottles are made around the globe exclusively for the use of drinking water and carbonated soft drink bottling (Gupta *et al.*, 2002). In addition, due to its thermo-plasticity, the PET bottles are recycled after their use for food package and processed into fibres, strapping tapes and non-food containers (Pickering, 2006). When used in clothing fabric industry, PET is referred to its common name, polyester. Globally, more than 60% of PET production is of fibres of which a large part fabricated into clothing (Gupta *et al.*, 2002, Speight, 2005).

2.2.1.4. Surface properties of polyester fabric

As the product of a series of synthetic process, PET consists of polymerized ethylene terephthalate repeating units (Figure 2.3). The 1, 4-substituted phenyl leads to a high degree of ordering through intra- and inter-molecular π-π stacking interactions enabling crystallite formation during the manufacturing processes, making the product (fibre, fabric or plastic film forms) stiff (Farrow and Preston, 1960). The synthetic polyester fibres and fabrics have a much greater tensile strength than those of natural cellulose. The ethylene and the phenyl units in the PET impart a much more hydrophobic material than cellulose, hence PET can be made into water bottles. However, the relatively polar ester groups in the backbone and hydroxyl end groups enable PET to interact with polar molecules as well, through hydrogen bonding and other polar interactions. As reported by Ellison and Zisman (1954) and Gotoh *et al.* (2011), the water contact angle of non-surface modified PET film is about 81-83°. Based on the general rule proposed by Förch *et al.* (2009) of judging if a solid surface is considered

hydrophobic or hydrophilic by seeing whether its water contact angle data exceeds 90° or not, it is concluded that PET surface does show certain degree of hydrophilic properties.

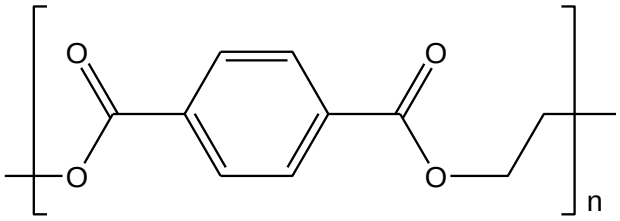

Figure 2.3 Typical molecular structure of PET polymer

2.2.1.5. Lab substitutions of fabrics

Due to batch differences and manufacturing variations, both industrial cotton and polyester fabrics are irregular in roughness, uneven in density and crystalline parts which make them difficult to be taken as standard samples to study their surface properties (Gassan *et al.*, 2000). Moreover, due to process variations (i.e. cleaning, bleaching, etc.), slight differences with regards to the chemical functional groups at the molecular level, such as ratio of oxycellulose, which is attributable to the oxidation of hydroxyl group into carboxyl, aldehyde or ketone moieties are inevitable. Therefore, model materials have been developed to replace the real fabrics in order to reduce the physical and chemical uncertainties of either material.

As illustrated in Figure 2.4, a fabric is non-continuous porous material formed from a network of yarns, which are formed from fibres. Model fabric structures neglect the irregularities and porous natures and are made as smooth, less-porous films, but of course made from the material to be studied, e.g. cellulose or PET, so that the surface chemical interactions can be studied, whilst eliminated the physical effects due to the hierarchical structure (Holmberg *et al.*, 1997, Fink *et al.*, 2001, Zauscher and Klingenberg, 2003). In this research, the same principle is followed to reduce the impact from physical properties of

fibres and focus on chemical interactions. Thus, both cellulose and PET film substitutions are needed.

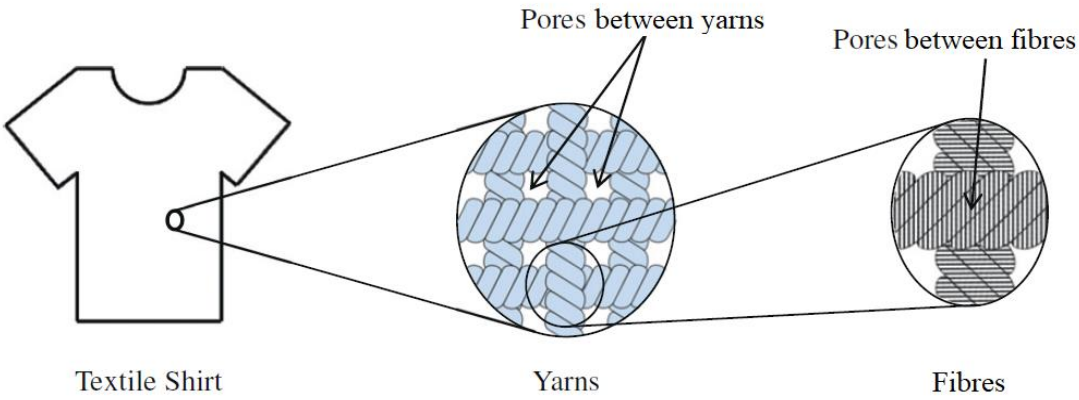

Figure 2.4 Schematic diagram of a typical textile and its dual porous structures due to spaces between yarns and spaces between fibres of the yarns, adapted from report of Mac Namara *et al.* (2012).

In order to study the surface chemical properties of cellulose, model cellulose films are fabricated by different methods to reduce or eliminate the interferences caused by the porous nature of cellulose fibres and fabrics (Aravindanath *et al.*, 1982, Holmberg *et al.*, 1997, Gunnars *et al.*, 2002). Among the methodologies, regenerated cellulose thin film deposited on a silicon wafer, or similar flat base, was the most commonly used (Gunnars *et al.*, 2002, Falt *et al.*, 2004, Liu, 2010, He, 2013). The fabrication is through a dissolve-redeposition process reported by Notley and Wågberg (2005), Liu *et al.* (2013) and He *et al. (2014)*.

Although this film formation process can be monitored for the amount of cellulose that is deposited therefore enabling control of the film thickness, it is a relatively complex multi-step and multi-parameters process, requiring 8 hours with precise material dosing, with a success rate being highly dependent on the experience of the operator, which affords surfaces that are not homogenous and of variable thickness or homogeneity. Thus, the method itself is not

efficient or reproducible for rigorous research needs. In addition, contact angle against deionized water of regenerated cellulose film on silicon wafer was reported around 25-30° (Gunnars *et al.*, 2002, Wågberg, 2000, Dankovich and Gray, 2011), whilst the contact angle of free standing cellulose film was reported below 20° (Falt *et al.*, 2004), indicating that the surface properties of both cellulose films still have some differences. Therefore, a more efficient, homogeneous, reproducible and sustainable model cellulose material is required, on which experiments can be performed to observe the chemistry in the absence of the hierarchical structure and porous nature of the cellulose.

For polyester, since the materials are coming from unnatural synthetic routes, a thin film should be much easier to fabricate, and indeed a number of commercially available PET films have been reported (Job *et al*., 2001, Inagaki *et al.*, 2002, Indest *et al.*, 2008, Indest *et al.*, 2010, He *et al.*, 2014). In this study, the same PET films were used as previously reported by He *et al.(2014)*.

2.2.2. Dirt

In laundry, dirt itself generally includes all the chemical categories people have ever known including, but not limited to: hydrophilic (clay, mud) and hydrophobic (oil, grease, lipid), natural (starch, protein) and artificial (pollution, soil) residues and their physical and chemical degradations, as well as microbes (Showell, 1997, McNeil, 2002). Clearly the target of the laundry industry is to remove dirt from fabric. Furthermore, as the objetives of this project do not include the understanding of the interactions of dirt, it is assumed that all dirt is cleaned off from the target fabric surfaces during a laundry process by either physical or chemical ways. Thus, dirt is not included in any of the test design, measurement consideration or data analysis in this research.

2.2.3. Washing machine

Washing machine is indispensable to modern life. They can be largely classified according to the washing method as drum type which is widely used in Europe and North America, agitator-type used mainly in America, and pulsator-type used in East Asia such as China, Korea and Japan; or in the view of rotational system as horizontal-axis type and vertical-axis type which includes both agitator-type and pulsator-type respectively (Lim *et al.*, 2010). For this study, the focus is put on the front loading drum type washing machine since it is the most commonly seen domestic washing machine in western Europe (Ward, 2000, Pakula and Stamminger, 2010, Kim *et al.*, 2015).

Of all the various built-in laundry process programs for different garments, the basic movement for all the substances inside a domestic washing machine is rotation driven by the tumbling of the inner drum. Warmoeskerken *et al.* (2002) introduced a concept of the stagnant core region in the textile yarn in which there is no flow at all. Therefore, transfer of dirt matter/water can only occur through molecular diffusion. Outside the stagnant core region and between the fibres within the yarn is a convective shell in which the washing liquid shear stress influences. The authors also confirmed the role of mechanical action in the washing machine is to deform, stretch and squeeze textiles, thus reducing the size of the stagnant core region and promoting transfer of materials, e.g. loosened dirt from within the fabric yarns, by convective flow (Figure 2.5).

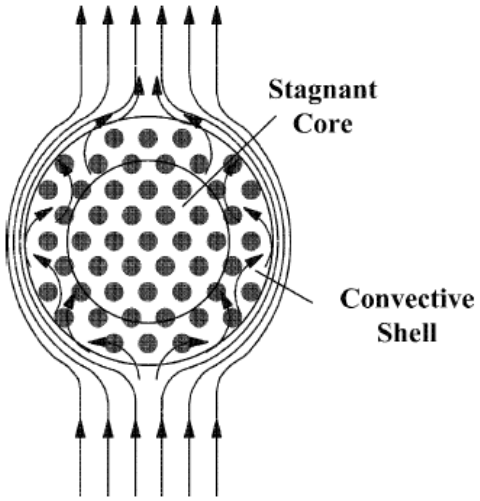

Figure 2.5 Liquid flow around and through a textile yarn. The dots represent the fibres in a yarn (Warmoeskerken *et al.*, 2002)

2.2.3.1. Mechanical action analysis in a washing machine drum

Motion and related force analysis on the materials inside a working drum washing machine has been done by multiple research teams. Not only different sensors capable of monitoring both liquid velocity and shear stress inside a washing machine drum were designed and applied, but modelling and simulations were introduced as well, and similar facts were discovered as follows, respectively:

- Shear stress magnitude is at 100 Pa near the inner wall of a washing machine drum (Van Den Brekel, 1987, Lazzaroni *et al.*, 2000, Ward, 2003, Mac Namara *et al.*, 2012).
- Fabrics bear a combined pulsating flow brought by the tumbling of the drum and undergo a set of repeated mechanical movements such as sliding, folding / unfolding, twisting, elongation, compression and rotation (Ganguli and Van Eendenburg, 1980, Lazzaroni *et al.*, 2000, Warmoeskerken *et al.*, 2002, Ward, 2003, Yun and Park, 2015).
- Three possible events which cause a shear stress across a piece of fabric: 1). pulling of the fabric through the liquid in the drum; 2). Lifting of the fabric out of the liquid; 3). impact

after free falling of the fabrics on the wall into the liquid (Van Den Brekel, 1987, Ward, 2003) are concluded to be the most significant physical movements in a washing process in terms of inducing a deformation and hence flow through the textile structure.

- The biggest shear stress is at the edge of a fabric surface inside the washing machine drum. The stagnant core region on the fabric, which enlarges when increasing the load of the textiles indicates the uneven distribution of shear stress (Warmoeskerken *et al.*, 2002, Mac Namara *et al.*, 2012).
- For fabric thickness being 6mm, convective flow through the fabric is at magnitude of 0.1 mm/s when the tumbling speed of the drum is between 35 and 50rpm (Van Den Brekel, 1987). For pore size on fabric of 3-150 μm with mean value at around 30-35 μm, the calculated shear stress through the pore is in magnitude of 0.5 Pa.

2.2.4. Water hardness

Water hardness is determined by the concentration of multivalent cations in water which are dicationic metal complexes. Common cations found in hard water include Ca^{2+} and Mg^{2+} (Crawford *et al.*, 1968). Since these ions enter a water supply by leaching from minerals of nature sources, water hardness is inevitable in most industrial applications. Only a few types of water such as rainwater, distilled water and deionised water (DI-water) are categorised as soft water because they contain few ions (Weingärtner *et al.*, 2000).

High water hardness is common in most industrial and consumer laundry processes since tap water is used, because of cost consideration. Therefore, water softening agents are commonly used to reduce hard water's adverse effects.

2.2.5. Laundry detergent, its compositions and their reactions in laundry solutions

Commercial laundry detergent began to be available in 1930s after the successful invention of synthetic surfactants, which was a response to the shortage of soap during World War I (McNeil, 2002). The forms of modern laundry detergent are mainly divided into two: powder and liquid, which have adapted usage conditions / requirements respectively (Liu, 2010). Regardless of its physical form, a laundry detergent is normally pre-formulated for certain purposes such as easy rinse, colour protection, white cleaning, and relatively concentrated for the ease to transport thus need to be dosed and dissolved /diluted before use (Showell, 1997).

Though the detailed ingredient lists could be different for each laundry detergent, they do share a relatively similar base formula which includes the following basic ingredients: dirt suspension agent, water softener, salt, filler, pH buffer, and some other beneficial functional ingredients such as bleach, optical brightener, enzyme, perfume. A brief summary of the percentages of these ingredient categories in a concentrated heavy duty liquid (HDL) laundry detergent formulation is presented in Table 2.1 based on the literature reports (Sachdev and Krishnan, 1996, Tan Tai, 2000), patents (Weinberger, 1983, Sajic *et al.*, 1999, Wood, 2004) and current market product information.

As main cleaning agent, surfactants are the most essential components in a laundry detergent. A surfactant molecule consists of two parts: a hydrophilic part which is soluble in water and a hydrophobic part that is insoluble in water. Industry usually refers the latter as “tail” of a surfactant and “head” for the former (Safran *et al.*, 1986, Nagarajan, 2002). The basic function of the surfactants is to remove dirt from the target fabric surface and more importantly, to keep them suspended in the washing liquid and prevent them from redeposition.

Table 2.1 A brief summary of typical compositions in concentrated HDL laundry detergents for European market

Components	Percentage, wt.%
Surfactants	
Anionic	15-35
Nonionic	3-7
Builders	20-40
Bleach	0-3
Optical brighteners	0-2
Enzymes	0-1
Perfumes	0-0.5
Preservatives	0-0.5
Dyes	0-0.2
Other agents	0-5
Water	Supplement to 100

The main surfactants used in current laundry industry are predominantly anionic surfactant which has a polar group head carrying negative charges when in aqueous conditions. The anionic nature is to prevent the redeposition of the dirt during the laundry process since most clay and oils are reported negatively charged in aqueous conditions (Lucassen-Reynders, 1981). Among the large group of anionic surfactants, linear alkylbenzene sulfonate (LAS) with a C10 - C14 tail (linear members of sodium dodecyl benzene sulfonate or SDBS families) is the lead option for laundry detergent because of its relatively strong hardness resistance by sulfonate head and large tail (due to benzene ring), as well as the good biodegradability due to linearity of the tail (branched molecules are the product of unnatural synthesis and cannot be digested by bacteria) and reasonably low cost (Hashim *et al.*, 1992, Showell, 1997, Bajpai, 2007, Yangxin *et al.*, 2008). Although sodium dodecyl sulphate (SDS) is a popular anionic surfactant (and almost the cheapest one among anionic surfactants) in the overall cleaning

industry, it is not used as main surfactant in laundry detergent industry because of its hardness sensitivity (Stellner and Scamehorn, 1989a), and it is less efficient in cleaning versus LAS, due to its small tail group and higher Critical Micelle Concentration (CMC) in aqueous solution (Savarino *et al.*, 2010). Nevertheless, SDS has been used as a complementary functional surfactant (i.e. foaming agent, co-surfactant) in laundry detergent (Scheibel, 2004). Figure 2.6 shows both molecular structures of LAS with a C12 tail and SDS.

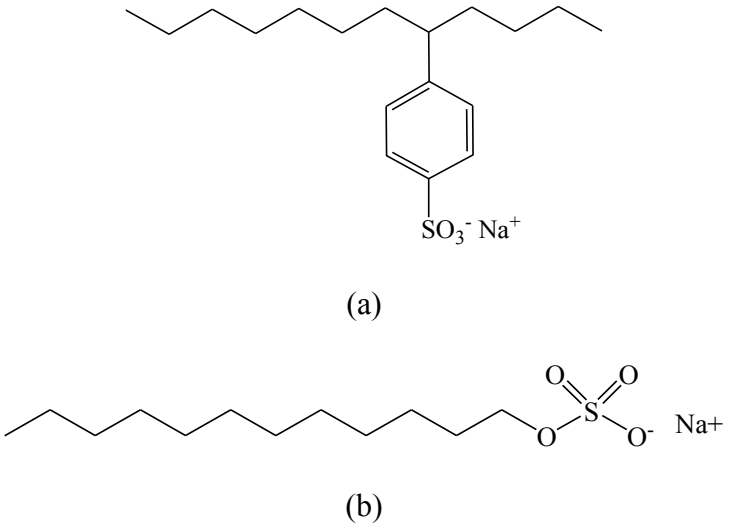

Figure 2.6 Typical molecular structure of C12-chain LAS (a) and SDS (b), respectively.

Nonionic surfactants have been introduced to laundry detergent formulation due to their insensitivity to the hardness of water, since the polar head group is not ionisable in aqueous conditions, and hence they do not react with the metal dications (Stellner and Scamehorn, 1989b, Bajpai, 2007, Yangxin *et al.*, 2008).

Water softener is often referred to as 'builder' in the laundry industry. It consists of chemical moieties that can chemically bind to the metal dications that cause water hardness, and hence

make the water softer, as they are no longer able to bind to the anionic surfactants (Talens *et al.*, 1998) or any other functional chemicals (Sachdev and Krishnan, 1996).

Functional polymers are normally added as another complementary cleaning agent with the main purpose of suspending the dirt and prevent it redeposition, although some of them have multiple additional benefits such as viscosity builder / stabiliser for the concentrated HDL formulation, water softener (Yangxin *et al.*, 2008).

Other ingredients including bleaching agents, optical brighteners, enzymes, preservatives, dyes and perfumes are also added to most laundry detergent products to differentiate products from competitors, and cater for multiple customer needs (Tan Tai, 2000).

2.2.6. Perfume in laundry

Perfume is usually a liquid form of a mixture of fragrant essential oils or aroma compounds used to give a pleasant scent. Reasonably selected perfumes added in modern laundry detergent not only deliver a certain sensory benefit during and/or after wash cycles to consumers, but also enhances the product brand and leads to a subjective reinforcement of product performances. This marketing of products is a critical determining factor to make a consumer purchase a particular product, and a number of P&G internal consumer studies have confirmed that perfume is one of the major motivations for repurchase of a laundry product. However, due to the complexity of its constituents and the overall hydrophobic nature, perfume oil brings problems if being directly incorporated into the detergent product. Most perfume ingredients are volatile, and are therefore easily lost through evaporation. Some perfume oil constituents, notably unsaturated hydrocarbons, aldehydes, that have been used in laundry product formulations, are oxidised by air and the peroxides used in cleaners

(Fisher and Dooms-Goossens, 1976, Blakeway *et al.*, 1987). Therefore, the loss of a perfume oil in a detergent can be significant depending on storage conditions, e.g. temperature and humidity, and the time of storage (Tan Tai, 2000). Moreover, since the detergent system is designed to clean any oils and suspend them during the wash cycles, the perfume oils may be extremely difficult to be directly deposited and retained on the target fabric surfaces during the laundry processes, due to their similarity in physical and chemical characteristics to those of oily soils (He, 2013, Liu, 2010). Therefore, industry puts special interest in the controlled release of functional fragrance oils to fabric surfaces during laundry process in order to solve the above problems and deliver a pleasant and long lasting scent benefits to clothes.

2.3. Perfume Microcapsules

Efforts have been made by previous researchers and industrial engineers to solve the problems of perfume application mentioned above, in order to protect the perfume oils during the production process and enable them to be stored in the final product without loss or degradation. One of the approaches is through microencapsulation in which perfume oils are encapsulated in a micron sized (1-100μm) polymeric capsule. This capsule acts as a barrier to evaporation of the perfume out of the capsule, as well as a barrier to peroxides (or air, or other ingredients in the formulation) coming into contact with the perfume oils.

A large number of capsule forming materials, as well as related manufacturing methods have been developed by the industries in order to encapsulate different types of active ingredients to suit specific applications. By modifying encapsulation process parameters and the capsule forming materials, the microcapsules properties (sizes, shell thicknesses and permeability) can be controlled. These capsules have been used extensively for several decades in

following areas: drug delivery (Jain, 1999, Rabanel *et al.*, 2009), pressure sensitive copying paper in printing industry (Seitz, 1988), controlled release of flavours in food (Desai and Jin Park, 2005, Nedovic *et al.*, 2011), pesticide protection and efficient delivery in agricultural applications (Tsuji, 1999, Tsuji, 2001), active ingredients delivery and / or extra functionalities in cosmetic products (Noda *et al.*, 1992, Martins *et al.*, 2014) and most recently, energy saving applications by embedding phase changing materials in construction industry (Giro-Paloma *et al.*, 2016).

2.3.1. Core-shell structure

A capsule is typically a sphere composed of a core material and a continuous shell material. The core material is usually referred to as core, inner phase or fill, whilst the shell surrounding the core is referred to as wall, coating or membrane. The core material is normally liquid, but could also be a solid. The liquid core can include dispersed and/or dissolved materials, as well as other functional components such as active ingredients, diluents. The ability to vary the core material composition not only provides the flexibility of the technique to a large number of applications, but also allows effective design and development of the desired microcapsule properties (Liebermann *et al.*, 1990). The shell material is capable of forming a film or membrane and does not react with the core material, at the same time providing the desired physical and chemical properties, such as mechanical strength, flexibility/elasticity, impermeability, optical, chemical and thermal stability. These different properties of the shell materials can be monitored by corresponding manufacturing process and microencapsulation methods (Bansode *et al.*, 2010). For perfume encapsulation where the core (fragrant oil) is hydrophobic, the shell material is chosen to be hydrophilic in nature, so that after forming the core-shell structure, the diffusion rate of hydrophobic core oil

through the shell is inhibited by the hydrophilic nature of the shell, leading to low leakage levels upon storage (Bône *et al.*, 2011).

The relative content weight ratio of core : shell materials (or sometimes expressed as core wt.%) in microcapsules is linked to wall thickness. Optimal core : shell ratio is of great importance for a commercial microcapsule product. The thicker the wall, the stronger the capsule and lower the leakage, but the lower the core payload (Thies, 2005 , Rodrigues *et al.*, 2009). Being properly made, a perfume microcapsule which contain up to 95 wt.% perfume oil, is physically strong to remain intact through detergent manufacturing process and washing cycles, but still weak enough to break and deliver the perfume oil on the target fabric after washing cycles (Tan Tai, 2000, Liu, 2010).

2.3.2. Microencapsulation methods and corresponding shell materials

Microencapsulation process methods can be categorised differently according to different classification standards. Moreover, each microencapsulation method has its advantages, as well as limitations, and choice of method will depend on the physicochemical properties that are required for the final product, which will be related to the core / shell properties of the microcapsules. A list of representative microencapsulation methods and the related particle size ranges of their products as well as common industrial application areas are summarised in Table 2.2 based on a number of literatures.

Table 2.2 Common particle size ranges and application areas of representative industrial microencapsulation methods adapted from the literature (Aymonier *et al.*, 2006, Madene *et al.*, 2006, Vemmer and Patel, 2013, Martins *et al.*, 2014).

Encapsulation Method	Suggested Particle Size	Major Application Areas	Technique
Co-extrusion	250 - 5000 μm	drugs, vitamins	Physical Process
Spray drying	6 - 1000 μm	pharmaceuticals, food flavourings	Physical Process
Fluid bed coating	20 - 1500 μm	pharmaceuticals, food flavourings	Physical Process
Spinning disc coating	5 - 1500 μm	pharmaceuticals, food flavourings	Physical Process
Coacervation / Complex coacervation	10 - 1200 μm	carbonless paper, fragrance, food flavourings	Physicochemical Process
Interfacial polymerisation	1 - 1000 μm	pesticides, carbonless paper	Chemical Process
In situ polymerisation	0.5 - 1100 μm	fragrances, adhesives, carbonless paper, cosmetics	Chemical Process
Supercritical fluids	from nano to < 2 μm	pharmaceuticals	Physical Process

Despite the three decades of research and development into the encapsulation of fragrant oils by industry most methods are focused on only complex coacervation and *in-situ* polymerisation, using a limited number of shell materials such as gelatin, melamine-formaldehyde (MF), polyurea (PU) and polyamide (PA) (Poncelet *et al.*, 1993a, Sun and Zhang, 2002, Rodrigues *et al.*, 2009, Liu, 2010, Bône *et al.*, 2011, Martins *et al.*, 2014). Among these methods and shell materials, MF microcapsule using *in-situ* polymerisation has been the market leader. Typical MF microcapsule is based on the co-polymerisation of an MF resin condensate and an acrylamide-acrylic acid copolymers (Figure 2.7) (Hong and Park, 1999) affording high shell density with low permeability, ease of control of the shell thickness, good mechanical properties and relatively low cost compared to other encapsulation methods.

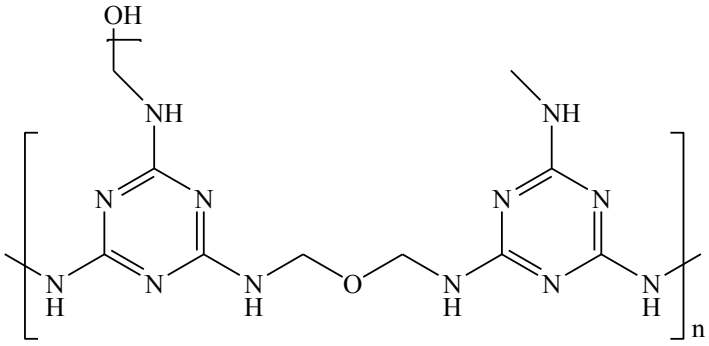

Figure 2.7 Typical molecular structure of MF polymer.

The major disadvantage for MF microcapsule is its potential risk of releasing toxic formaldehyde, through either an incomplete process reaction or decomposition through aging at low pH and/or high temperature conditions during storage and usage (Rodriguesa, 2010). Despite these concerns MF microcapsules are still intensively manufactured under strict controlled processes to limit the free formaldehyde formation in both laundry detergent products and industrial additive applications in construction materials where the requirement for toxicity is relatively low. However, due to the toxicity of formaldehyde, new shell materials and related process methods that are environmentally friendly are being developed.

2.3.3. PAC-PVOH PMC in laundry applications

As the world leading perfume manufacturing and application company, Procter & Gamble is developing environmental friendly and cost effective solution to replace the MF shell in PMC productions. The leading candidate is polyacrylate-poly vinyl alcohol (PAC-PVOH) copolymer shell PMC. Based on the patents which have been published between 2006-2014, Appvion Inc. (former Appleton Paper Inc.) invented a formulation and related oil-in-water free radical *in-situ* polymerisation process to make PAC-PVOH based PMC, Patent#

US7736695 (Stevenson and Sefton, 1992, Schwantes and Sands, 2010). The monomers used are amine modified acrylate and vinyl acrylate with an acid functionalised surfactant as emulsifier, an organic acid as pH buffer and a free radical initiator. Clearly, the resulted PAC-PVOH microcapsule does not contain any toxic ingredients such as aldehyde in MF microcapsule. Furthermore, there is no such concern when the shell material is decomposed because polyacrylate resins have been used for many applications in manufacturing industries, as well asin household goods such as the core materials in diapers since the 1970's. Appvion signed a supply agreement with P&G for this patented PAC-PVOH microcapsule technology in 2008, making P&G the only consumer goods company to use this unique product globally. Both companies did subsequent development on the technology, modifying the process to get the optimal PAC-PVOH microcapsules and filed several patents application in the following years, i.e. US-2012/0276210A1 (Dihora and Brown, 2012), US-2014/0079747A1 (Dihora *et al.*, 2014) and US-2014/0186630A1 (Schwantes, 2011) which focused on laundry and personal care areas. In P&G patent EP2418267B1 and US-2014/0079747A1, a number of favourable physical parameters were published as the company's preferable characteristics for PMCs in laundry detergent applications, which include the follows:

- Microcapsule shell thickness between 1 - 300nm.
- Particle size range of 3 - 30μm.
- Core: shell weight ratio between 0.25 - 4.
- Volume Weighted Fracture Strength (Smets *et al.*, 2011) in between of 0.1 - 16 MPa.
- Combined amine content of 0.1 – 1.0% of total polyacrylate mass.
- Combined carboxyl acid group content of 0.3 – 3.0% of total polyacrylate mass.

Obviously, the customised PAC-PVOH PMCs fit these strict requirements. Moreover, its successful applications into different laundry formulated products enables P&G to not only

reduce considerable raw material cost on perfume oils in delivering the target fragrant benefits, but also save a huge effort to screen/verify the compatibility of each fragrant system when developing a new formulation and process for future laundry products.

2.3.4. Problem in PMC applications in laundry: Retention of PMCs on Fabrics

Despite the successful manufacturing of PAC-PVOH PMCs and the application into laundry detergent products, one of the problems in the application is still unsolved in the industry: the relatively low efficiency of the PMC's deposition and retention on target fabric surfaces through the wash cycles. Similar to MF PMCs, PAC-PVOH PMCs have been found to have low particle deposition and poor retention on fabric surfaces during the wash cycle, based on both lab and consumer research results from P&G Belgium Innovation Centre (BIC). Thus, one of the objectives of this project is to investigate the mechanism of deposition and retention and find a possible solution to this problem.

2.3.5. Current approaches to enhance PMC deposition and retention in laundry

The enhancement of PMC deposition and retention in laundry applications can be divided into two categories: the modification of fabrics and the surface modification of PMCs.

2.3.5.1. Enhancement of PMC deposition and retention through the modification of the physical morphology of fabrics

By applying different weaving methods, the modification of the physical shape or surface morphology of target fabrics can be achieved. Physical traps between fibres formed in the

textile process may filter the microcapsules of the similar size range and lock them in during and after a motion process, such as tumbling in a washing machine during a laundry wash cycle, when the microcapsules frequently deposit on to or pass through the fabrics (Ono *et al.*, 1990, Rodrigues *et al.*, 2009).

Moreover, a number of patents and research reports have been published with a specific focus on the permanent bonding between PMCs and fibres which form in the textile process using different adhesives to give the end fabric product extra functions like long-lasting controlled-release fragrances which can withstand up to 20 – 30 cycles of washing. (Woo, 1985, Woo, 1988, Nelson, 2001, Holme, 2007, Rodrigues *et al.*, 2009, Miró Specos *et al.*, 2010).

However, since all of the above methods are related to the textile process and applications, which is not the focus of this project, the research on the approach to enhance the PMC's adhesion to the fabrics will need to be mainly on the surface modification of the PMC itself.

2.3.5.2. Enhancement of PMC deposition and retention through the surface modification of PMCs

Most surface modifications for the purpose of enhancing adhesion in both academic and industries are through plasma treatment, nanoparticle surface modification and surface coatings of certain functional molecules.

In the field of enhancing adhesion, plasma treatment has been used in surface modification of plastic films (Papakonstantinou *et al.*, 2007, Yoshida *et al.*, 2013) and various fibrous materials (Cheng *et al.*, 2010) to enhance the surface activity, strengthen the adhesive properties and improve the biocompatibilities of the target surfaces. However, the quality of the plasma modification is dependent on the nature of the target material and the plasma

atmosphere. Moreover, the plasma coating is normally within an ultra-thin layer (less than 1 μm) on the material surface. Therefore, the plasma coatings may have different degradation and aging issues which results in the plasma treatment being usually temporary, differing from just a few minutes to maximum months (Hegemann et al., 2003). Furthermore, the energy input for the process equipment is uneconomical; hence the cost of the process may be considerably high versus other industrial approaches (Ratner *et al.*, 1990, Morent *et al.*, 2008).

Although nanoparticle modifications for the purpose of enhancing adhesion have been reported (Balasundaram *et al.*, 2006, Hu *et al.*, 2007, Hou *et al.*, 2013), the majority have been pharmaceutical applications (more specifically, on promoting the adhesion of osteoblasts) because nanoparticulates are relatively difficult to handle at an industrial level due to their potential hazards to human health and the environment (De Jong and Borm, 2008, Warheit *et al.*, 2008).

Surface coating and modification in laundry process normally involves surface functionalisation of particles or the target fabrics, or both, using chemicals such as surfactants and polyelectrolytes. Since the types of the fabrics used in the real domestic laundry cycles can vary from cotton, to polyester to nylon, it is the laundry product which is designed with a strong formula of excessive surfactants and polymers to be able to treat and clean any fabrics in the washing cycle. Moreover, combining the review in §2.2.1 and §2.2.5, it is clear that most fabric surfaces are negatively charged through the laundry process. Therefore, with the addition of PMCs, it is the primary focus of manufacturers like P&G to monitor the surface of the PMCs used in the laundry product, other than to try to modify the target fabric surfaces, in order to improve the adhesion of the PMCs to such fabric. Theoretically, any positive charged molecules with certain surface activity such as cationic surfactant and positive charged polyelectrolyte may be suitable in this purpose. However, the relatively small molecular

radius of ionised surfactant usually leads to concentrated charge distribution in the solution, resulting in the incompatibility of anionic and cationic surfactants in the formulation. Consequently, positive charged polyelectrolytes with certain charge density became the optimum choice.

2.3.6. Polyelectrolyte to promote adhesion

Over the last 20 years, there have been a large number of literature reports on polyelectrolytes for surface modifications to promote adhesion in multiple fields. For example, in pharmaceutical applications, polyelectrolyte multilayer films of hyaluronic acid and chitosan were employed to modify the surface of substrate to promote and support attachment of cells (Salloum *et al.*, 2005, Chua *et al.*, 2008) and tissue engineering (Gribova *et al.*, 2011). polydiallydimethyl ammonium chloride (PDAC) and soluble sulfonated polystyrene (SPS) adhesive multilayer was reported by Kim *et al.* (2003b) to create a highly accurate soft mold in making dense and multilevel nanostructure pattern transfer in application areas including electronics and optics. Feng *et al.* (2007) found polyvinylamine (PVAm) had a stronger interaction with wet cellulose than carboxymethyl cellulose did, by measuring the force to delaminate pairs of regenerated cellulose membranes bound together with the polyelectrolyte complex. Furthermore, the interaction became much weaker when the PVAm was replaced with polymer bearing quaternary amine groups. The adhesion with complexes was highest at pH 4, where the amines were protonated, and rather insensitive between pH from 6 to 9, where the amines were neutral.

What these reports have in common is: the adhesion-promoting polyelectrolytes contain either multifunctional amino groups on their molecules or ammonium component when the application used a combination of at least two chemicals. As amine and ammonium

components are weak base, they can act as positive charge centres on the polyelectrolyte molecules in acid and neutral conditions, but still can be monitored to neutral by changing the surrounding environment into base condition. Moreover, patent applied by Wu *et al.* (1999) revealed such positive charge centre cannot be nitrogen heterocyclic group.

In recent years, polyvinyl formamide (PVF) (Khabbaz, 2007) and polyethylenimine (PEI, or polyaziridine) (Khan and Newaz, 2010) have been repeatedly reported to be the adhesives in multiple industries. With regards to enhancing the adhesion of microcapsules and microparticles to surfaces such as fabrics, He (2013) used PVF, PEI and chitosan to modify the model fabric surfaces in which PVF and chitosan showed better performance vs PEI.

2.3.6.1. Surface modification by polyvinyl formamide (PVF)

In previous studies by Yanping He (2013), PVF was reported to be effective in enhancing the adhesion of MF microcapsules onto cellulose covered silica wafer. P&G BIC also tested PVF surface modified MF PMCs in the same project and found the adhesion enhancement in experimental laundry processes through indirect fragrance longevity panel tests. However, if being considered as a raw material in laundry industry, PVF brings quite a lot of additional cost to the formulation than the other ingredients, which makes it uneconomical at present.

The main commercial PVF products in the globe are under the brand name of Lupamin® and Lupasol®, both from BASF. According to the product brochure “Water Soluble Polymers” of BASF chemicals 2012, Lupasol® series only have one amine derived PVF named Lupasol® VT (vinyl amine/vinyl formamide copolymer); Lupamin® series contain the main family of polyvinyl formamide polymers. The typical synthetic route and corresponding molecular structures of PVF are presented in Figure 2.7. The main functional groups of PVF are the

vinyl formamide (Figure 2.7, b) and its hydrolysed product, vinyl amine (Figure 2.7, c and d) side groups. Apart from molecular weight as an important feature of every polymer, hydrolysis ratio which defines the relative number of formamide to amino side groups is the other important parameter for a PVF polymer, as it determines the various coating properties of PVF, resulting in differences in adhesion performances. The formamide group in PVF polymer is polar but cannot be protonated with pH change; actually, it is easier for the formamide to be hydrolysed than protonated (Antonczak *et al.*, 1994). After hydrolysis, the resulting alkyl-amine group has a p*K*a value around 10.5 (Perrin *et al.*, 1981, Toney and Kirsch, 1989) meaning it can be protonated under pH 10 and becomes positively charged. Therefore, the charge and charge density on PVF polymer is dictated by the molecular weight and hydrolysis ratio of the polymer (thus the proportion of the amine groups) and pH of the solution. In addition, the $-NH_x$ ($x \geq 1$) group on both formamide and amine side groups can form hydrogen bond with other hydrolysis molecules as well as water molecules in the solution. Furthermore, the steric hindrance of both groups is relatively small thanks to the relatively simple and compact side molecular structures. All these factors make PVF an ideal positively charged polyelectrolyte to surface modifications. Based on above, PVF polymer is continued to be chosen as the positive benchmark in this project.

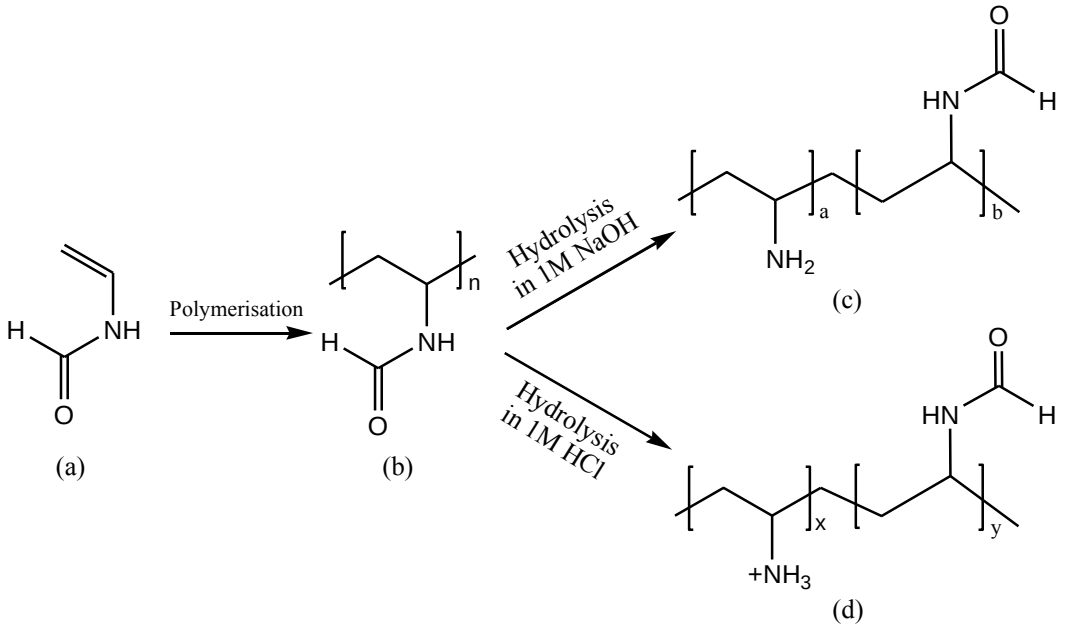

Figure 2.8 Typical molecular structures of PVF polymer: (a). Vinyl formamide monomer; (b). PVF polymer; (c). PVF polymer after partial hydrolysis in basic condition (e.g. 1M NaOH); (d). PVF polymer after partial hydrolysis in acidic condition (e.g. 1M HCl).

2.3.6.2. Surface modification by chitosan

Chitosan is commercially produced by the partial basic deacetylation of chitin (natural sourced from crustaceans and fungi) to produce a polymer with both amide and amine moieties in it (Figure 2.8), whereby the amine moieties can be protonated and form cationic centres in the polymer, which is similar to that of PVF described above. The ratio of both the amide to amine groups on chitosan polymer can be customized through the process of deacetylation during its production. Thus, the two most important features of chitosan are its degree of deacetylation (DDA) and its molecular weight (Büşra and Nevin, 2015). Normally, a chitosan has a DDA of 60 – 100%. The amino groups in chitosan has a p*K*a value of ~6.5, which leads to a protonation in acidic to neutral solution with a charge density dependent on pH and the DDA-value (Lee *et al.*, 2013). Moreover, chitosan itself is reported as good antimicrobial material and dietary fibre (Kumirska *et al.*, 2011, Büşra and Nevin, 2015). All

these properties mean chitosan is suitable for surface applications such as anti-spoilage in wine-making (Gallifuoco *et al.*, 1998, Krajewska, 2004), surface coatings for biomedical active delivery (Bhattarai *et al.*, 2010, Dash *et al.*, 2011, Wang *et al.*, 2013) and surface modification (Liu *et al.*, 2002, Enescu, 2008) including surface modification of model fabric films to enhance the adhesion of PMCs to film surfaces (He *et al.*, 2014). Therefore, chitosan is chosen as a candidate in the research presented in this Thesis to get more in-depth understanding on the properties of PMC modification and surface interactions.

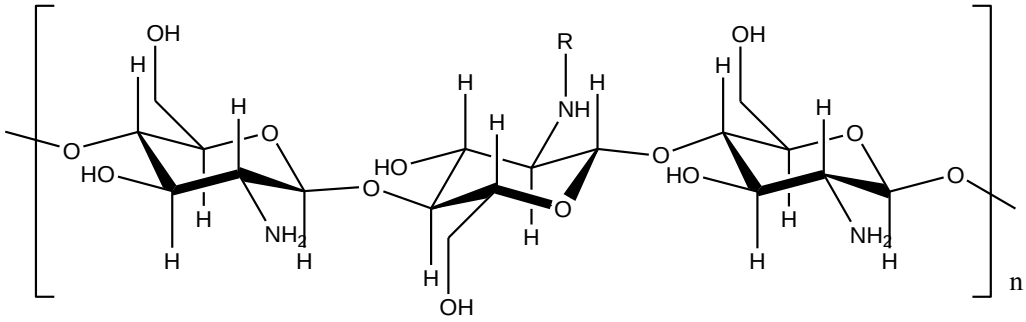

R = H or $COCH_3$

Figure 2.9 Typical molecular structure of chitosan polymer.

2.3.6.3. Surface modification by polydopamine

Since catechol functional groups in DOPA-containing proteins was found to be responsible for the enormous power of mussel shells for adhesion to all kinds of surfaces (Lee et al., 2007, Waite, 2008), catechol-containing molecules and polymerised catecholamines have been applied to coat various materials such as metals, metal oxides, nonmetal oxides, silica, ceramics, polymers, and nanomaterials (Ye *et al.*, 2011, Liu *et al.*, 2014, Kang *et al.*, 2015b, Liang *et al.*, 2016, Li *et al.*, 2017). The most frequently reported chemicals of such type are dopamine (3, 4-dihydroxyphenylamine), which is also with the simplest molecular structure

from the catecholamine group, and more importantly its polymeric form, polydopamine (PDA) with a molecular structure similar to that of DOPA (Liu *et al.*, 2014).

Normally, dopamine is commercially available as a stable clear powder form, dopamine hydrochloride; it can be also produced by hydrolysis of L-tyrosine amino acid (resulting in 3,4-dihydroxy-L-phenylalanine, or L-DOPA) followed by a decarboxylation. Having a p*K*a (with the amino group) of about 8.8 - 8.9 (Wang *et al.*, 2009), dopamine was reported being able to go through a series of subsequent oxidation processes and polymerised into PDA (Lee et al., 2007, Liebscher et al., 2013, Liu et al., 2014, Ponzio et al., 2016a). It is also worth noting that the polymerisation process can be self-initiated under basic condition in ambient air (Lee *et al.*, 2007), but needs an oxidant such as ammonium persulfate, sodium periodate or potassium chlorate in neutral or acidic environment (Wei *et al.*, 2010, Bernsmann *et al.*, 2011), because dopamine has been found to be much more reactive when in its free base form in basic condition (Carter *et al.*, 1982). A proposed primary pathway of the reactions is illustrated in Figure 2.9.

However, although the fabrication and broad applications of PDA based materials have rapidly advanced since 2007 as indicated by the large number of publications, the research of the polymerisation mechanism, characterisation of the properties of the PDA coatings and further broad applications of polydopamine in different research and industrial fields are still being pursued globally (Lynge *et al.*, 2015, Schanze *et al.*, 2018). Based on above analysis, polydopamine coating will also be explored in this Thesis.

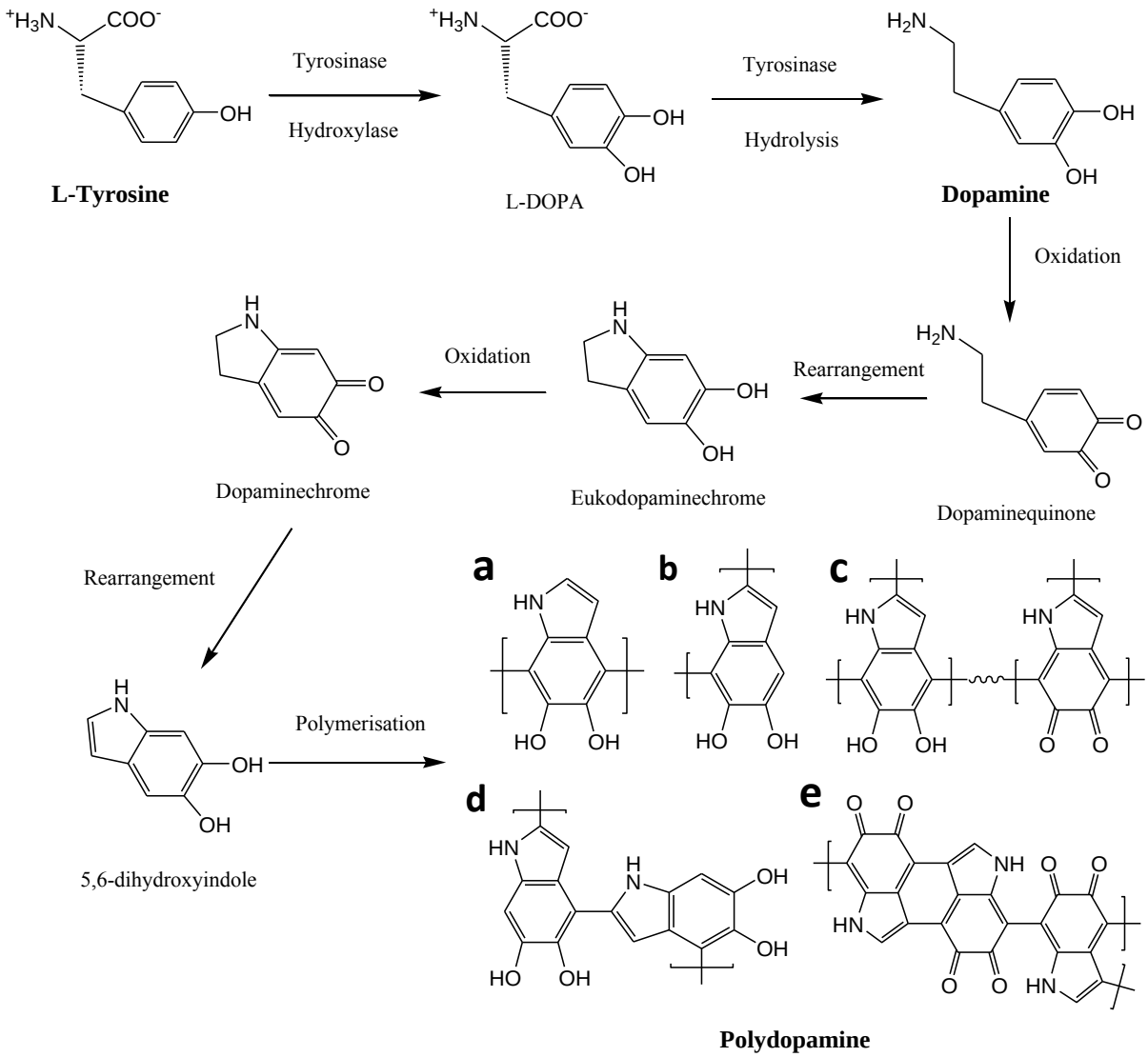

Figure 2.10 Primary pathway of reactions from L-tyrosine through dopamine to PDA (summarised and adapted from Lee *et al.* (2007) and Liebscher *et al.* (2013)).

2.4. Adhesion

Fundamental understanding is essential on the possible mechanisms of the deposition and retention for the adhesion between microcapsules and different fabric surfaces through the wash cycles in order to improve the delivery efficiency of the PMCs. The related literature, existing knowledge and concepts are reviewed in this section.

Adhesion between two objects arises from the molecular interactions between them (Johnson, 1987, Sohail *et al.*, 2013). Adhesion plays a vital role in biology, such as cell-tissue interactions (Gumbiner, 1996, Lei *et al.*, 1999, Bafna, 2016), and contributes substantially in many industrial applications including electrophotography (Hays, 1995), biotechnology (Fletcher, 1996), semiconductor (Lee, 2013, Mittal and Jaiswal, 2015) and pharmaceutical (Podczeck, 1998, Felton and McGinity, 1999, R Williams, 2015) industries. Since the laundry process taken into account in this research is in aqueous detergent solutions, the adhesive interactions and corresponding theories in liquid condition, including colloidal interactions, particle-particle and particle-surface interactions in liquid conditions may be most applicable to this project.

2.4.1. Interparticle forces in aqueous solution

A detailed classification with regards to the interparticle forces in an aqueous solution has been developed and refined through the past decades. Whilst capillary forces were found to be the main contributor in ambient air, other forces including Van der Waals force, electrostatic double layer force and solvation force are applicable in liquids (Israelachvili, 2011). Liang *et al.* (2007) discussed the different interactive forces between colloidal particles and their measurement in aqueous conditions, and concluded that the stability of colloidal dispersions in aqueous solutions can be described by the combination of London-Van der Waals and electrostatic double layer forces through the Derjaguin-Landau-Verwey-Overbeek (DLVO) theory (Verwey *et al.*, 1999); in some cases when other non-DLVO forces such as solvation force, hydrophobic force and steric force arises, direct measurement tools need to be introduced, because there is still no clear readily available theory. All these

approaches and conclusions can be possibly used to analyse certain phenomena of microcapsule-fabric interactions.

As an important parameter in colloids DLVO theory, Debye length (also called Debye radius) is a characteristic length or "thickness" of the diffuse electric double-layer which describes the ionic atmosphere near a charged surface (Israelachvili, 2011). It is a measure of a charge centre's net electrostatic effect in solution and how far its electrostatic effect persists. All charged species contribute to the Debye length in the same way, regardless of the sign of their charges in the solution. With each Debye length, charges are increasingly electrically screened. For an electrically neutral system, Debye length λ_D can be calculated as:

$$\lambda_D = \left(\frac{\varepsilon_0 \varepsilon_r k_B T}{\sum_{i=1}^{N} n_i q_i^2}\right)^{1/2} \qquad \text{Equation 2.1}$$

Where ε_0 is the permittivity of free space (physical constant of the value of the absolute dielectric permittivity of classical vacuum, which equals to 8.854×10^{-12} F·m^{-1}); ε_r is the dielectric constant (for water, it is 78.4 at 25°C); k_B is the Boltzmann constant (1.381×10^{-23} J/K); T is the absolute temperature in Kelvins; n_i is the concentration of a charged centre in the solution; q_i is the net charge of n_i.

For an aqueous solution with electrolytes, the Debye length can be also written as:

$$\lambda_D = \left(\frac{\varepsilon_0 \varepsilon_r k_B T}{2 \times 10^3 N_A e^2 I}\right)^{1/2} \qquad \text{Equation 2.2}$$

Where N_A is the Avogadro number (6.022×10^{23}mol^{-1}); e is the elementary charge (1.602×10^{-19}C); I is the ionic strength of the solution, calculated as:

$$I = \frac{1}{2}\sum_{i=1}^{N} C_i z_i^2 \qquad \text{Equation 2.3}$$

Where C_i is the molar concentration of ion i (M, mol/L), z_i is the charge number of that ion.

Since the hardness ions are normally simplified as Ca^{2+} or the combination of Ca^{2+} and Mg^{2+} and the corresponding counter ions (such as Cl^- or SO_4^{2-}) in the laundry industry, once the hardness model system is decided, the Debye length of the solution can be calculated using above equations. For example, for hardness water made with $CaCl_2$ and $MgCl_2$ in 3:1 weight ratio, the Debye length is simplified as:

$$\lambda_D = \frac{1.76 \times 10^{-10}}{\sqrt{I}} \qquad \text{Equation 2.4}$$

Wagberg (2000) summarised the main factors influencing the adsorption of polyelectrolytes onto cellulose fibres as: a) charge density of both polyelectrolyte and cellulose fibre, b) molecular mass of the polyelectrolyte, c) ionic strength. The Wagberg study was based on paper industry; however, the theoretical considerations and conclusions may be reapplied to this project as well.

Surface modifications using polyelectrolytes was also studied by He (2013) on MF microcapsules and fabric surfaces. By comparing the surface modifications made by linear PVF, chitosan and branched PEI, long linear PVF was found to be a better adhesion promoter than similar amino-containing branched materials, due to the ability for the polymer to have more hydrophobic interactions and less steric repulsions, resulting in more efficient in establishing polymer bridging.

2.4.2. Contact and contact models

PMCs in this project are all liquid (perfume oil) core, with strong, but relatively elastic, spherical solid shell. The elasticity of the shell means the microcapsule is soft and could deform when under external force, such as shear stress during agitation in a washing cycle, or compressive force when in contact with other particles in the solution, or the wall of the

washing machine. The theories and models below were developed to be applied to the contact and adhesion problem of a spherical particle with limited particle size in contact with a flat surface:

a. Bradley model (Bradley, 1932) which only considers purely Van der Waals force with rigid spheres.
b. Classical Hertzian contact theory and the fully elastic deformation model (Hertz model) (Johnson, 1987), which neglects any adhesion force, e.g. Van der Waals force.
c. Johnson-Kendall-Roberts (JKR model) (1971) that includes the effect of adhesive forces on the fully elastic (Hertz) deformation of the sphere in contact to an elastic flat surface. The adhesive forces are assumed to be short-range surface forces acting only within the contact area. The JKR model adhesive force is calculated as:

$$F = \frac{3}{2}\omega\pi R \qquad \text{Equation 2.5}$$

Where R is the radius of a sphere in contact with a flat surface, ω is the adhesive energy per unit area.

The contact radius is as below:

$$r = \left[\frac{R}{K}\left(F + 3\omega\pi R + \sqrt{6\omega\pi R + (3\omega\pi R)^2}\right)\right]^{1/3} \qquad \text{Equation 2.6}$$

Where K is the effective Young's modulus,

$$K = \frac{4}{3}\left[\left(\frac{1 - \nu_1^2}{E_1} + \frac{1 - \nu_2^2}{E_2}\right)\right]^{-1} \qquad \text{Equation 2.7}$$

E_1 and E2 are the corresponding Young's modulus for particle and glass substrate, ν_1 and ν_2 are the Poisson's ratio for particle and glass substrate (Xu *et al.*, 2007).

d. Derjaguin-Muller-Toporov (DMT model) (1975) that includes the effect of adhesive forces and assumes the fully elastic (Hertz) deformation. Moreover, the adhesive

forces are assumed to be long-range surface forces (Van der Waals force), but act only outside the contact area. The adhesive force under DMT model is:

$$F = 2\omega\pi R \qquad \text{Equation 2.8}$$

The contact radius is:

$$r = \left[\frac{R}{K}(F + 2\omega\pi R)\right]^{1/3} \qquad \text{Equation 2.9}$$

e. Tabor (1977) reported that both JKR and DMT theories were the extreme limits of a single theory parameterised by the Tabor parameter μ_T (Xu et al., 2007).

$$\mu_T = \left(\frac{16R\omega^2}{9K^2 z_0^3}\right)^{1/3} \qquad \text{Equation 2.10}$$

Where z_0 is the interatomic equilibrium distance in the Lennard-Jones potential for solid–solid interactions. In solid–solid adhesion, z_0 is a measure of the range of adhesive interactions. If the Tabor parameter is large (>5), implying that the gap outside the contact zone is much larger than z_0, it is not necessary to consider the adhesion force outside the contact zone and the JKR model then applies. If the Tabor parameter is small (<0.1), the adhesion force outside the contact zone can be considered to be an external load and the DMT model holds. Therefore, the JKR theory applies to large, compliant spheres for which the Tabor parameter is large; the DMT theory applies for small, stiff spheres with small values of the Tabor parameter.

f. JKR and the DMT models assume elastic deformation. However, there is quite a lot of experimental data that suggested plastic deformations in many cases. Therefore, Maugis (1992) developed a method based on the model proposed by Dugdale (1960) (MD model) which included plastic deformation to be taken into consideration. MD model provides an analytical solution, but the resulting equations are a bit too

cumbersome for it to be compared with experimental data and get solved. Consequently, Carpick-Ogletree-Salmeron (COS model) (Carpick et al., 1999) came up with a simplified model based on MD one.

2.4.3. Measuring techniques of adhesion

Although the direct measurement on real fabric movement in a working washing machine has become possible (Lazzaroni *et al.*, 2000, Palanisamy, 2015), most of the reported results were still in the macroscale, involving quite large dynamic variations, even with the help of modern computer modelling techniques (Ward, 2000, Akcabay, 2007, Lim *et al.*, 2010), which is still not sufficient for the study of microscale PMCs' adhesion to local fabric surfaces. Therefore, the alternatives have become popular such as direct measurement of adhesion analysis in a flow chamber device (Decuzzi *et al.*, 2007, Lane *et al.*, 2012), adhesive force analysis using atomic force microscopy (AFM) (Weisenhorn *et al.*, 1992, Butt *et al.*, 2005, Liang *et al.*, 2007) or surface force apparatus (SFA) (Israelachvili and McGuiggan, 1990, Sridhar *et al.*, 1997, Israelachvili *et al.*, 2010) in the liquid phase.

The flow chamber is a common technique used to study adhesion of particles on a surface in a liquid environment. Using a parallel-plate and a continuous pump or flow circuit to generate laminar shear flow, the flow chamber device has been successfully applied to investigate the adhesion of microparticles and cells on substrates (Pierres *et al.*, 2008, Guillemot *et al.*, 2007, He, 2013). The removal of particles from a surface inside the chamber can be adjusted by monitoring flow velocity, and thus, the shear stress imposed upon the particles. Particles exposed to shear flow are expected to be removed by lifting, sliding, rolling or a combination of them (Sharma *et al.*, 1992, Zoeteweij *et al.*, 2009). The adhesion

of the particles is directly correlated with their removal profiles from the surface caused by the shear stress and torques induced. More importantly, the technique provides adhesion information for a population of particles, providing statistically significant information in a short period of time (He *et al.*, 2014).

In contrast, the force spectroscopy done by AFM is to measure micro- or nano-scale forces between a single microparticle or cell and interested surface (Ducker *et al.*, 1992, Cooper *et al.*, 2000). Adhesion is investigated either by comparison of the detected peak forces on the samples with different chemical compositions and surface roughness (Schaefer *et al.*, 1995) or through interpretation of the force–displacement curve by monitoring relative humidity, ionic strength, pH (Jones *et al.*, 2002). The adhesion mechanisms are explored such as capillary force, electrostatic interaction, hydrophobic interaction and molecular bridging (Hult *et al.*, 2003, van Honschoten *et al.*, 2010).

2.4.4. Other surface characterisation methods

As mentioned in a large number of literature, surface parameters such as Zeta-potential (Kusuma *et al.*, 2014) in aqueous solutions, surface roughness and contact angle (Matijevic and Good, 2012) of the target fabric substrates, as well as X-ray Photoelectron Spectroscopy (XPS) elemental analysis (Hofmann, 1986), Scanning Electron Microscope (SEM) and light microscope image analysis (Ren *et al.*, 2007b) of surface modified PMCs, will be greatly useful in helping to confirm, or further interpret, any deposition and adhesion results.

2.5. Conclusions and objectives of this project

The current perfume delivery business in the laundry industry has been reviewed. The emergent needs for the consumer, and therefore for the company, is to provide a cost effective solution to the problem of delivering the fragrance benefit more efficiently. Perfume microcapsule technology has become one of the choices with good potential for business and application interests.

This project has been established based on previous research projects (Liu, 2010, He, 2013), as a co-research project with P&G R&D BIC. As it is mainly a research project targeting end-use applications, which lies both on the business needs from the company and the academic expectations from the technology development, there are a number of parameters involved which need to be determined, including material (ingredients and test substrates) choices, formula options (detergent type, concentrations and process parameters) and experimental conditions (solution hardness, etc.).

As previous surface modifications of PMCs have been explored, PVF was shown to be the lead candidate for enhancing the deposition and retention of current PAC-PVOH PMCs. Chitosan and other modification options, such as novel polydopamine coatings, will be explored in this Thesis.

The flow chamber technique and AFM force analysis have both been utilised in several research fields, and proved to be effective tools to investigate the adhesion of microparticles, cells, respectively. As such they will be used in this research project as the major analytical tools to reveal the possible mechanisms.

In summary, the objectives are divided into two parts:

1) Screen and find the best candidate/application conditions of shell surface modified PMCs. Samples including non-modified PMC and surface modified PMC will mainly be provided by P&G BIC.

2) Make fundamental understandings towards the interactions between shell surface modified PMCs and different model fabric surfaces, including real laundry washing conditions.

Since one of the purposes of this project is to understand the mechanisms of the adhesion between surface-modified PMCs and fabrics, both flow chamber and AFM equipment are critical to the research. Other research techniques such as microencapsulation, micromanipulation and surface characterisation techniques will be necessary as well.

Chapter 3. Materials and Methodology

3.1 Introduction

This chapter introduces the materials, techniques and experimental methods applied in this work. It is divided into two parts. The first part describes all the materials, samples and the related producing procedures used in this work including commercialized cellulose and PET films which performed as model fabric surface substitutions, polymer surface modified PAC-PVOH microcapsules with an industrial perfume oil precursor as core material, chemicals used to synthesize melamine-formaldehyde microcapsules and chemicals used to conduct polydopamine surface treatments. The second part concerns on all the techniques and experimental methods to measure and characterise model fabric substitutions, surface modified perfume microcapsules in different environmental conditions, deposition and retention of perfume microcapsules on model fabric substitutions in a flow chamber, as well as the AFM techniques on the adhesion and detaching behaviour of single microcapsule on model fabric films.

3.2 Materials and related synthesis and surface modification methods

The main materials used in this research include commercial model fabric films, perfume microcapsule samples and the chemicals to either synthesize the microcapsules or conduct the surface modifications. They were introduced as follows.

3.2.1 Model fabric films

3.2.1.1 Non-surface-modified cellulose film

Commercially available cellulose film samples was provided by the company Innovia Films Ltd. (www.innoviafilms.com), which has world's leading technologies of making different cellulose films from wood pulp. The chosen type of cellulose film for this project was uncoated regenerated cellulose, brand name Cellophane™, product code 350P00. According to the company Innovia Films, though the film has gone through industrial treatments to eliminate any of the impurities or artificial additions, it still remains chemical properties of cellulose and its hydrophilic surface functionalities. The cellulose film is dry and amorphous with a thickness of about 40μm. The detailed surface properties were characterised and results are shown in Chapter 4. Since the cellulose film will swell and becomes wrinkle by absorbing moisture at the beginning of touching aqueous solutions or being exposed to high humidity conditions, it is always cut into needed sizes and soaked in DI-water for more than 20 minutes before used in experiments (Chapter 4, 5, 6 and 7).

3.2.1.2 Non-surface-modified polyester (PET) film

The PET film used in this work was purchased from Goodfellow (www.goodfellow.com), product code ES701335. The supplier confirms there is no surface modification after the production of the film. The PET film is amorphous with a thickness of about 250μm. The detailed surface properties were characterised and results are shown in Chapter 4. The PET film was cut into needed sizes and directly used in experiments (Chapter 4, 5 and 6) without further modification.

3.2.2 Samples and related synthesis and surface modification methods

A number of microcapsule samples were used in this project including non-surface-modified and surface-modified PMC samples. They were either provided by the company Procter & Gamble Belgium Innovation Centre (P&G BIC) at Brussels, Belgium or synthesized and modified in lab in School of Chemical Engineering, University of Birmingham. All the samples were separately diluted to target concentrations before each experiment using DI-water or designed aqua solutions such as 850ppm SDS surfactant solution.

3.2.2.1 Perfume oil filled polyacrylate (PAC) - polyvinyl alcohol (PVOH) microcapsules

Four commercial batches of non-surface modified microcapsule samples with PAC-PVOH shell and perfume oil core were used in this work. The batch numbers of them are PDS060412, PDS082813A, PDS101713 and PDS091714B. Since such commercial manufactured PMC has an expiration period of six months in this concentrated form, they were specially made by P&G together with its supplier Appvion, Inc. and sent to the university lab every six months. These non-surface modified PMC batches were then used not only as negative control to conduct comparisons such as adhesion performances with surface modified PMC samples, but also as base materials for such different surface modifications.

Typically, the manufacture of the PAC-PVOH microcapsule was based on *in-situ* polymerisation and could be referred to US Patent 7736695 (Schwantes and Sands, 2010). The general process includes the major steps in Figure 3.1. Microcapsules with different properties can be made by altering the process parameters including shell material formula, core/shell ratio (the relative content of core and wall materials), reaction temperature and

polymerisation time. Less core materials, higher temperature and longer reaction time would lead to thicker and stronger shell of the microcapsules.

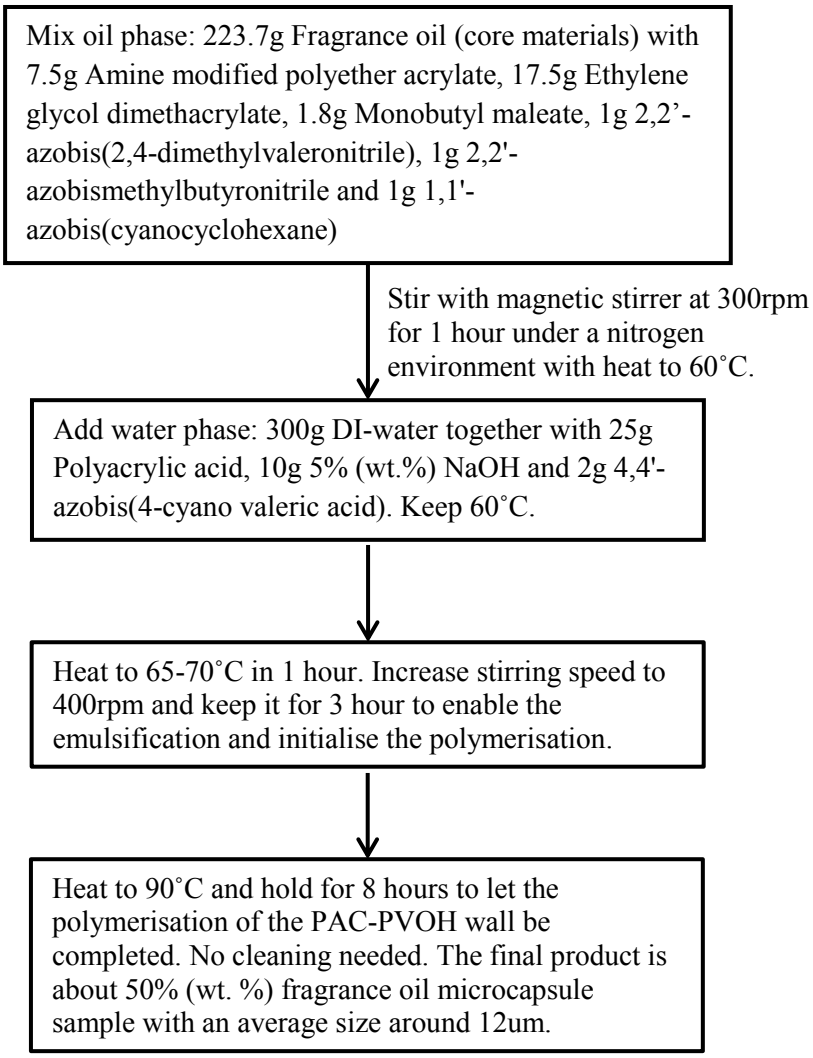

Figure 3.1 General manufacturing process example of PAC-PVOH microcapsules, derived from US Patent 7736695 (Schwantes and Sands, 2010)

All the microcapsule samples were about 50% (wt. %) concentrated water slurries when received. The Specific Gravity (SG) of the encapsulated perfume oil is 0.8958 as told by P&G BIC. Although the SG of PAC-PVOH resin (the shell material of the PMC) is about 1.19 – 1.3, the PAC-PVOH PMC particles are still lighter than water and float in the slurry

since the payload of the perfume oil is about 90 - 95% according to the P&G company information. Some of the microcapsule properties such as particle size distributions and shell strength including shell thickness will be shown in Chapter 4. However, the other details of their preparation methods and chemical compositions are not known because of commercial secrets. Before each experiment, a gentle stirring by metal sampling spoon was applied to make sure the microcapsule slurry was homogeneous. All the microcapsule samples were directly used without further modification.

3.2.2.2 Polyvinyl formamide (PVF) surface modified PAC-PVOH microcapsules

PVF polymer coating was chosen as positive control for this project. The polymer raw materials were supplied by BASF chemicals. The information of the batches of coated PAC-PVOH PMC samples and the chosen PVF polymers are in Table 3.1 and Table 3.2 respectively.

Table 3.1 Sample information of PVF coated PAC-PVOH PMCs

Coated Sample Lot#	Polymer Information Used for the Surface Modification
PDS060412-A:	0.25% PVF, 0.34MDa 30% Hydrolysis (BASF Lupamin® 9030)
PDS060412-B:	0.50% PVF, 0.34MDa 30% Hydrolysis (BASF Lupamin® 9030)
PDS060412-C:	0.25% PVF, 2MDa 20% Hydrolysis (BASF Lupasol® VT)
PDS060412-D:	0.50% PVF, 2MDa 20% Hydrolysis (BASF Lupasol® VT)
PDS101713-PVF	0.25% PVF, 0.34MDa 95% Hydrolysis (BASF Lupamin® 9095)
PDS091714B-PVF	0.25% PVF, 2MDa 20% Hydrolysis (BASF Lupasol® VT)

Table 3.2 Sample information of PVF polymers used in PMC surface modifications

PVF Polymer Name	Lupamin® 9030*	Lupamin® 9095*	Lupasol® VT**
Chemical Type	Ethenylformamide, homopolymer, hydrolysed	Ethenylformamide, homopolymer, hydrolysed	Vinylamine / Vinylformamide copolymer
CAS#	183815-54-5	183815-54-5	NA
Physical Form	Liquid	Liquid	Liquid
pH (1% in DI-water)	7 - 9	7 – 9	~3.5
Relative Density (15°C)	1.08	1.08	1.14
Solid, wt%	10 - 15	10 - 15	46
Polymer, wt%	10 - 12	6 – 8	NA
Hydrolysis, mol%	30	95	20***
Average molecular weight, kDa	340	340	2000***
Dynamic Viscosity, mPa·s at 20°C	500 - 3500	500 - 2500	~3000

* Source from EU patent EP2331059A2 (Verboom, 2013) and related Material Safety Data Sheet (MSDS) of BASF chemicals.

** Source from "Water Soluble Polymers" product brochure of BASF chemicals 2012.

*** Data provided by P&G BIC.

The surface modification on perfume microcapsule samples were done by P&G BIC. The process is as following: the PVF polymer raw material was weighted to the target ratio and directly mixed into the 50% (wt. %) PAC-PVOH microcapsule slurry in a 20mL or 50mL

glass vial. Then the vial was put on a roller mixer for 24 hours mixing before being sent to us. The PVF modified PAC-PVOH microcapsule slurry was used without further modification.

3.2.2.3 Chitosan surface modified PAC-PVOH microcapsules

Chitosan polymer coating was another option on surface modification of PAC-PVOH microcapsules. According to P&G BIC, the polymer material was supplied by Sigma Aldrich. The chosen chitosan had an average molecular weight of 50k Da with 75~85% (mol. %) deacetylation ratio and it was the only batch of chitosan used to do the surface modification on microcapsules in this project. The modification process was done by P&G BIC which includes the following steps (He, 2013): chitosan powders were dissolved into 10% (wt. %) acetic acid (Sigma-Aldrich, UK) solution and then directly mixed with 50% (wt. %) PAC-PVOH microcapsule slurry in a 50mL glass vial at target weight ratio. The ratio of chitosan polymer to microcapsule was used at 0.25% w/w. After that, the pH was adjusted to 6 using 10% (wt. %) NaOH solution and the vial was capped and put on a roller mixer for 24 hours mixing. Finally, the modified sample slurry was sent to us and used without further modification.

3.2.2.4 Vegetable oil filled melamine formaldehyde (MF) microcapsules

In Chapter 7, vegetable oil filled melamine formaldehyde microcapsule was synthesized by the method described in US patent 4552811 (Brown and Bowman, 1985). The purpose of making MF microcapsule was to study the coating properties of polydopamine (PDA), since the amount of PAC-PVOH control samples provided by P&G was not sufficient. It also provided an opportunity to compare the novel PDA coating with current microcapsule surface

modifications such as PVF and chitosan polymer coatings. The detailed process of MF microcapsule synthesis was based on an *in-situ* polymerisation technique and it can be found in Sun and Zhang's paper (Sun and Zhang, 2001). A variation of parameters such as reaction temperature, polymerisation time and production scale was introduced to adapt the real lab conditions.

The core oil for the MF microcapsule was Solesta branded vegetable oil 1L pack purchased in Aldi supermarket, UK and was used without further modification. The SG of the oil and MF resin are about 0.85 and 1.5, respectively. The same as PAC-PVOH PMC, the MF microcapsule has a smaller SG value versus water since the payload is >90% (He, 2013).

Procedure of synthesizing vegetable oil filled MF microcapsules (He, 2013): 0.78g poly(acrylamide-acrylic acid copolymer (Sigma-Aldrich) together with 2.5g melamine formaldehyde precondensate (P&G provided) and 1.0g 37% (wt. %) formaldehyde (Sigma-Aldrich) were mixed with 70 mL DI-water while being agitating on an IKA magnetic stirrer plate at 400 rpm in room temperature 25˚C. Adjusted pH to 4.0 with acetic acid and kept agitation at 400rpm, 25˚C to let the mixture react. The solution should become homogeneously white after 105min. 9.33g vegetable oil, as core material, was added into the solution and the whole solution was emulsified at 2500 rpm using a Silverson shear mixer for 30 min at 15˚C (water cooling system was used to control the temperature). After that, the dispersion was stirred at 400 rpm again for an extra 30min under 15˚C water cooling. The temperature of the water cooling system was then increased to 75˚C to speed up the polymerising reaction in the dispersion. Both the agitation of 400 rpm and the 75˚C temperature were hold for 6 hours to let the dispersion form the solid microcapsule walls. After that, the heating was removed and the dispersion was cooled to room temperature. The pH was raised to 10.0 by addition of 1 M sodium hydroxide to stop the reaction. Finally, the

dispersion was centrifuged and MF microcapsules, as upper part was taken out and washed by both ethanol and DI-water for three times.

3.2.2.5 Polydopamine (PDA) surface modified MF microcapsule

A PDA coating was formed on the surface of synthesized MF microcapsules. Three approaches were used to fabricate the PDA coatings. All were conducted in room temperature (20~25 ˚C), and two of them following the methods reported by Kang *et al.* (2015a).

The first method was the most common one in literatures (Lee et al., 2007, Waite, 2008, Kang et al., 2009, Postma et al., 2009, Yang et al., 2011). 0.2g MF microcapsules were dispersed in a 10 mL pH 8.4 buffer solution. The solution was agitated on an IKA magnetic stirrer plate at 350 rpm. 0.04g Dopamine Hydrochloride (99%, supplied by Alfa Aesar, Fisher Scientific) was then added. The solution turned brown within 20 min, indicating the polymerisation of dopamine. After 24 hours, the coated microcapsules were formed. The samples were then centrifuged. The upper part was taken, rinsed and centrifuged with DI-water for three times. The pH 8.4 buffer contained 0.1 M trisaminomethane (TRIS) in DI-water. 1M HCl was used to adjust the pH to 8.4.

The second method contained following steps: 0.2g MF microcapsules were dispersed in a 10mL pH 7.0 buffer solution. 0.04g dopamine hydrochloride and 0.04g ammonium persulfate were then added to the solution while stirring at 350 rpm on an IKA magnetic stirrer plate. After 24 hours, the PDA coated microcapsules were collected using the same procedure described in the first method. The pH 7.0 buffer solution contained 0.1 M sodium phosphate monobasic monohydrate and 0.1 M sodium citrate dihydrate. 1M Sodium Hydroxide was used to adjust the pH to 7.0.

In the third method, a pH 5.0 buffer solution was used to replace the pH 7.0 buffer in the second method. Otherwise, all the other conditions and procedures were the same as the second one.

3.2.3 Other chemicals to mimic environment of laundry process

The sample detergent was chosen and supplied by P&G BIC. The name of the detergent was Senso (Lot#ETF1873-063). It was a type of Heavy Duty Liquid (HDL) detergents and specially made with the full formula of the company's lead liquid detergent without any perfume ingredients. The detailed full formula of the detergent was trade secret thus not disclosed by the company. It was only told that the level of LAS was 15% in the detergent formula and the target application was for US laundry condition which is 5675ppm of total detergent concentration in 15gpg hardness water. Therefore, the LAS level is then calculated as 850ppm in such real wash condition in this project.

The water hardness for US condition was chosen as 15gpg by P&G BIC as well. The composition of the hardness was set as Ca^{2+}:Mg^{2+} = 3:1 (weight ratio), corresponding to 77.2ppm (1.9mM) of Ca^{2+} and 15.4ppm (0.64mM) Mg^{2+}, respectively. The chemicals chosen to make lab hardness water were calcium chloride dehydrate and magnesium chloride hexahydrate. Both were supplied by Sigma Aldrich. In Zeta potential and AFM adhesion measurements, 1gpg hardness (Ca^{2+}: Mg^{2+} = 3:1 by weight) water was used as well, which corresponded to 5.2ppm (0.13mM) Ca^{2+} and 1.0ppm (0.04mM) Mg^{2+} in DI-water.

To conduct the mechanism understandings on the adhesion behaviors of coated PMC and non-coated ones, Sodium Lauryl Sulfate (SDS, 98% activity, powder form, supplied by Sigma Aldrich, Cat#436143, UK) and LAS (92% activity, spray-dried granule, supplied by

Stepan, Cat#Nacconol 90G, Lot#7587931, UK) were used as references to compare the data generated in DI-water and real washing conditions with P&G Senso detergent.

3.3 Characterisation techniques

3.3.1 Optical Microscopy

As optical microscope can magnify small samples or objects using the visible light, a Leica DM RBE microscope (Leica Microsystems GmbH, Germany) equipped with a series of lenses, a real time Moticam Pro 205B digital camera and both Leica QWin Pro V2.8 (Leica Microsystems Imaging Solutions Ltd., UK) and Motic Images Advanced 3.2 (Motic Inc., China) software was employed to do the different observation tasks in this project.

The morphology of microcapsule samples from different manufacturing process and with certain surface modifications were observed under the microscope in order to make sure the correct samples were used in later experiments and analysis. Some microcapsule slurries formed aggregates which were impossible to be dispersed using only the stirrer method in water solution. A few microcapsule samples had surface defects (hollow or indentation) after being manufactured, shipped and stored some time before being further tested. All these characteristics were taken pictures and considered in the later analysis and data interpretations.

The same optical microscopy system was also used to capture and process the images of deposited and retained microcapsules on the model fabric films in flow chamber experiments (details in §3.3.10).

The third task the optical microscopy system involved was to capture the images of the microcapsule colloidal probe to ensure a proper attachment of single microcapsules to the end of tipless cantilevers for adhesion measurements by AFM (details in §3.3.11).

3.3.2 Interferometry

A vertical scanning white light interferometer (MicroXAM2, Omniscan, UK) was used to study the surface topography of both model fabric films. The image data were analysed using Scanning Probe Image Processor software (Image Metrology, Denmark). When light waves combine, the superposition properties of the combined waves can give diagnostic information of the original state of the waves. If a single beam has been split into two paths, then the phase difference is diagnostic of anything that changes the phase along the paths (de Groot and Deck, 1995). The white light interferometer and software utilise this light wave property by scanning vertically over the given height range of the sample using one of the split beam and measuring the phase differences between the two afterwards to give both numerical and image details of the sample surface.

Both PET and cellulose films were directly cut into sample sizes and measured without further modification. The measurement area was 669μm × 319μm and three separate images were acquired for each sample to calculate the root mean square (RMS) roughness.

3.3.3 Atomic Force Microscope (AFM) imaging

Both PET and cellulose films were scanned by a NanoWizard®II AFM with an attached CellHesion module (JPK Instruments, UK) in order to confirm the surface roughness results

measured by interferometry as well as getting the images of the surfaces this research was conducting on. AFM is a type of scanning probe microscopy with demonstrated resolution on the order of fractions of a nanometer, which is more than 1000 times better than the optical diffraction limit (JPK Instruments, 2009a, Binnig *et al.*, 1986). The measurement principle of AFM imaging is based on a mechanical probe which is called cantilever with a sharp and rigid tip scanning with the sample surface and the transfer of the tip and surface interactions into electronic signals and later processed into images. The signals are detected by monitoring the reflection of a laser which is focused on the back of the cantilever during the time of the measurement (Binnig *et al.*, 1986, Giessibl, 2003). There are three commonly used modes on AFM: contact mode, intermittent (tapping) mode, non-contact mode in which the former two are mostly used for imaging. Some literature listed a newly developed fourth mode, force modulation mode, which could be categorised as an alternation of contact mode (Giessibl, 2003, He, 2013). Cantilever tip never leaves the target surface in contact mode which results in precise details and good resolution of images but it always bring higher lateral force (dragging force) and leads to the disruption of the sample (Hutter and Bechhoefer, 1993). In intermittent and non-contact mode, the tip has less or no touches of the target surface respectively and this significantly decreases the lateral force applied on both the sample and the cantilever (Butt *et al.*, 2005, JPK Instruments, 2009a). Base on above, intermittent mode was selected to do AFM imaging of both films. By using a pyramidal-tipped Si cantilever (RTESP, Veeco, France) with a nominal spring constant of 40 N/m, the scanning was conducted in ambient conditions. The scan rate of 1 Hz and a resolution of 512 × 512 pixels were set for all the scans. Considering the AFM images are combining a number of line scans results, line fitting could have neglected the connections between scanning lines and introduced more variations to the results. Thus, polynomial surface fitting is chosen to process the AFM image data.

3.3.4 Contact Angle

Contact angle is used to indicate the affinity of a liquid droplet to the target surface (Good, 1992). Surface hydrophobicity of both PET and cellulose films were characterised using a Drop Shape Analyser (DSA30E, Krüss, Germany). The measurement method is based on imaging analysis of a static sessile drop at the points of intersection (three-phase contact points) between the drop contour and the solid sample surface, also mentioned in the literatures as pendant drop method (Shimizu and Demarquette, 2000).

Based on the reports by Shimizu and Demarquette (2000), Żenkiewicz (2007), Kwok and Neumann (Kwok and Neumann, 1999) and Good (2012), surface free energy (SFE) of a solid polymer can be calculated using its contact angle data by solving the corresponding theoretical equations combined with Young's equation (Young, 1805):

$$\gamma_{sl} = \gamma_s - \gamma_l \cos\theta \qquad \text{Equation 3.1}$$

Where γ_s is the SFE of a solid, γ_{sl} is the interfacial tension corresponding to the solid-liquid interface, γ_l represents the surface tension of a measuring liquid, and θ is the contact angle between the solid and the measuring liquid.

Fowkes (1964) assumed the SFE of a solid is a sum of independent components including dispersion (γ_s^d), polar (γ_s^p), hydrogen (γ_s^h, related to hydrogen bonds), induction (γ_s^i) and acid-base (γ_s^{ab}) interaction, respectively. Moreover, γ_s^d is connected with London dispersion force (London, 1937) and independent from other types of interactions. Considering in most contact angle measurement, both solid and liquid phase can be pure which the dispersion interaction appears only, Fowkes determined the SFE of solid-liquid interface as:

$$\gamma_{sl} = \gamma_s + \gamma_l - 2\sqrt{\gamma_s^d \gamma_l^d} \quad \text{Equation 3.2}$$

Where γ_l^d represents the dispersion interaction of the liquid.

Owens and Wendt (1969) kept Fowkes' assumption that SFE is the sum of all the components but significantly changed the expression of γ_s^d and considered it associated with γ_s^p. Consequently resulting in:

$$\gamma_{sl} = \gamma_s + \gamma_l - 2\left(\sqrt{\gamma_s^d \gamma_l^d} + \sqrt{\gamma_s^p \gamma_l^p}\right) \quad \text{Equation 3.3}$$

Where γ_l^p is the polar interaction of the liquid.

Wu (1971, 1973) further developed the idea of Owens and Wendt by replacing the geometric means with harmonic means and derived the equation below:

$$\gamma_{sl} = \gamma_s + \gamma_l - 4\left(\frac{\gamma_s^d \gamma_l^d}{\gamma_s^d + \gamma_l^d} + \frac{\gamma_s^p \gamma_l^p}{\gamma_s^p + \gamma_l^p}\right) \quad \text{Equation 3.4}$$

Combined with Young's Equation 3.1, Equation 3.3 and Equation 3.4 can be expressed as following, respectively:

$$\gamma_l(1 + \cos\theta) = 2\left(\sqrt{\gamma_s^d \gamma_l^d} + \sqrt{\gamma_s^p \gamma_l^p}\right) \quad \text{Equation 3.5}$$

$$\gamma_l(1 + \cos\theta) = 4\left(\frac{\gamma_s^d \gamma_l^d}{\gamma_s^d + \gamma_l^d} + \frac{\gamma_s^p \gamma_l^p}{\gamma_s^p + \gamma_l^p}\right) \quad \text{Equation 3.6}$$

As there are notably two unknowns (γ_s^p and γ_s^d), two different liquids with known γ_l^p and γ_l^d are needed in the contact angle measurement to solve Equation 3.5 (geometric mean) or Equation 3.6 (harmonic mean) and obtain the γ_s^p and γ_s^d for the target solid surface. The most recommended pair of liquids by above literatures is DI-water and diiodomethane, also as representatives of polar and non-polar liquids, respectively. Though some of the literature

suggested to use Equation 3.5 for calculations involving larger SFE values and Equation 3.6 for smaller ones based on the different mathematical meanings of both to get more theoretically accurate results, the approach by Owens and Wendt has been the most widely applied one in the studies of the wettability and SFE of polymeric materials (Kwok and Neumann, 1999, Żenkiewicz, 2007). Therefore, Equation 3.6 was chosen to calculate the SFE of the model fabric films in this project. The literature data of γ_l^p and γ_l^d for both DI-water and diiodomethane used in the calculations are listed in Table 3.3. Subsequently, the calculated SFE results were compared to the ones of a series of real fabrics measured and provided by P&G.

A liquid droplet volume of 3 μL was placed on a piece of flat film sample and the profile of the droplet was observed by a side view digital camera. The sample image taken during the contact angle measurement with DI-water on cellulose film was set to be done within a strictly 3 seconds time. The other image taken time for DI-water on PET film and diiodomethane conditions was controlled within 20 seconds in order to obtain the equilibrium contact angle data. At least four separate measurements were acquired for each condition to calculate the mean contact angle. The images were processed subsequently using the equipment software (DSA30E, Krüss, Germany). Diiodomethane used in this project was purchased from Sigma Aldrich, Cat#158429, UK. All the contact angle measurements were performed at room temperature of 20˚C. Both PET and cellulose films were directly cut into sample sizes and used without further modification.

Table 3.3 Polar (γ_l^p) and dispersion (γ_l^d) components of liquid surface tension (γ_l) at 20°C of both DI-water and diiodomethane used in this project.

Liquid	γ_l^p (mN/m)	γ_l^d (mN/m)	γ_l (mN/m)
DI-water*	50.7	22.1	72.8
Diiodomethane*	0.4	50.4	50.8

* Data adapted from Shimizu and Demarquette (2000)

3.3.5 X-ray Photoelectron Spectroscopy (XPS)

In order to confirm the surface chemistry of both model fabric films, a highly sensitive surface analysis equipment X-ray Photoelectron Spectroscopy (Kratos AXIS ULTRA DLD, UK) located at Nanoscale and Microscale Research Centre, University of Nottingham was used. The XPS analysis is based on the measurement of surface composition. The incident X-rays cause the ejection of both valence and core-level electrons from atoms close to the surface of the sample. Since the energy of a photo emitted core electron is a function of its binding energy and is characteristic of the element from which it is emitted, analysis of the energy spectra of the emitted photoelectrons can determine the surface elemental composition and their binding states. The sensitivity of the equipment derives from the escape depth of the excited electrons which typically come from the uppermost 2-10 nm layer and is normally around 1 ppt. By counting the number of photoelectrons as a function of their energy, a spectrum representing the surface composition can be obtained. The energy corresponding to each peak is characteristic of an element and its bonding environment (Hofmann, 1986).

The XPS equipment was operated under a pressure below 1.0×10^{-9} mbar. It equipped with a monochromated Al Kα X-ray source at 1486.6 eV. Both model fabric films were cut into small pieces of approximately 10 x 10mm size using a clean scissor and a sample spot size of ~0.2 mm2 was analysed. No further surface modification was conducted to the samples. A

pass energy of 20 eV over a binding energy of 0 to 1200 eV was applied to obtain the survey spectra with 0.69 eV increments as the energy resolution. Since both PET and cellulose films are insulating, the surfaces can become positively charged as electrons leave the film surface. Therefore a flux of 1 eV electrons was used to compensate (Barth *et al.*, 1988, Stamm, 2008). All data were analysed using the CasaXPS software package using Voigt line shapes, a mixture of Gaussian and Lorentzian lines. After that, software fittings were done based on the standard library comparisons to give the estimated atom status or bonding environment of target elements. Two different pieces of each film sample and three different locations on each piece were tested separately. Average data were taken into further calculation and fittings to get representative results.

3.3.6 Zeta Potential

In aqueous condition, the dispersed particle is strongly bound with an inner layer (stern layer) counter ions and an outer diffuse region. Within the diffuse region there is a boundary (slipping layer) inside which the ions, counter ions and the particle form a stable entity – stationary interfacial double layer. The ions beyond the boundary stay with the bulk dispersant. Surface charge of such double layered particle in the fluid is called zeta potential which indicates the potential difference between the dispersion medium and the double layer (McNaught, 1997, Kirby, 2010). It is a joint interactive result of both the particle and the liquid medium system which means different liquid parameters such as pH, icon strength, etc. alter zeta potential of the same dispersed particle (Malvern Instruments Ltd, 2013). A schematic diagram of zeta potential was illustrated by Yanping He (Figure 3.2) (2013).

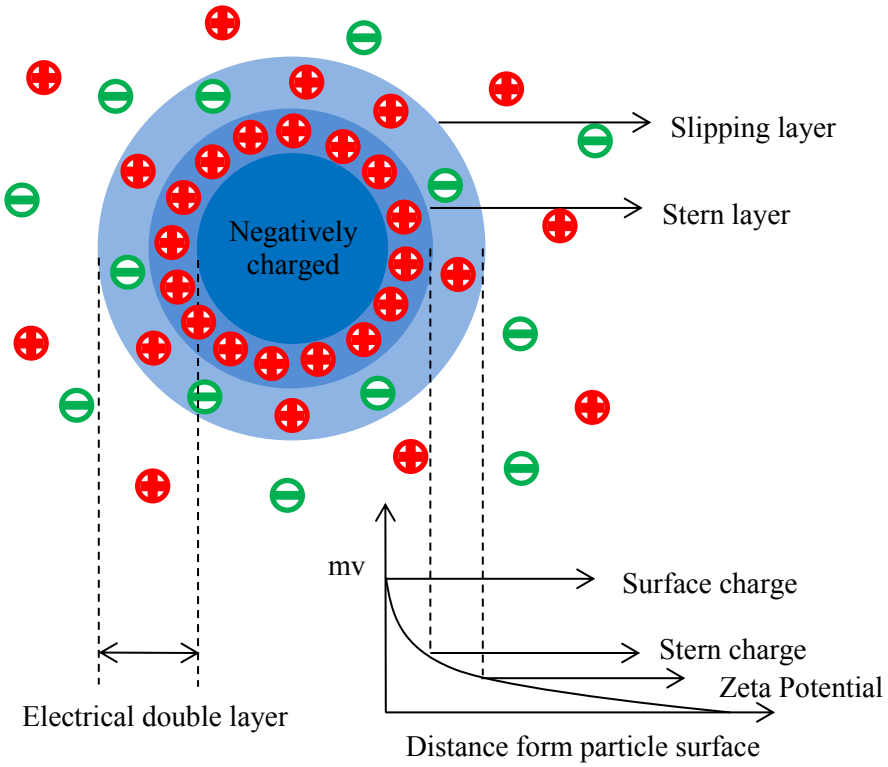

Figure 3.2 A schematic diagram to illustrate Zeta Potential (Adapted from He (2013))

Zeta potential is often termed of "a remote surface charge", but particle surface charge itself requires other technique to determine. The zeta potential of different microcapsule samples before and after the surface modifications were measured at varying pH, ion and surfactant concentrations in order to determine their interactions in those solutions, providing evidences to help explain and validate the adhesion measurement results from other techniques, such as flow chamber and atomic force microscopy.

A Zetasizer Nano ZS (ZEN3500, Malvern Instruments Ltd, UK) with disposable folded capillary cells (DTS1070, Malvern Instruments Ltd, UK) was employed to measure the zeta potential of the microcapsules in aqueous solutions. The equipment is capable of measuring zeta potential of particles with a diameter ranging from 3.8nm to 100μm (Malvern Instruments Ltd, 2013). The pH of 0.01M NaCl solution was adjusted from 3 to 11, at 2

interval. The pH of hardness (US hardness condition, at 1gpg and 15gpg respectively), SDS and LAS surfactant solutions (both at different concentrations respectively) was adjusted to 5, 7 and 9 only. All solutions contained 0.25% target microcapsules and after adjusting the pH, immediate measurement was conducted by Zetasizer. All measurements were repeated 3 times separately in order to calculate mean value.

3.3.7 Particle Size and Size Distribution

A Mastersizer 2000 (APA 2000, Malvern Instruments Ltd, UK) with liquid sample dispersion unit Hydro 2000SM was employed to measure the volume weighted mean diameter size and size distribution of microcapsules in aqueous suspension. The principle of the measurement is based on Dynamic Light Scattering (laser diffraction) techniques and Mie Theory (Merkus, 2009) which predicts the way light is scattered by spherical particles and deals with the way light passes through or is adsorbed by the particles (Malvern Instruments Ltd, 2007). To apply Mie Theory in the measurement, some specific parameters about the particle and the medium needs to be known, such as their reflective index and absorptions. By identifying the shell materials of the microcapsules, reflective index was determined as 1.65 for MF microcapsule (Brydson, 1999), 1.49 for PAC-PVOH microcapsules (Sultanova *et al.*, 2012) and 1.332 for water medium (Bashkatov and Genina, 2003) respectively. The equipment uses red light laser source at wavelength of 633nm and is capable of measuring particles sizing from 0.02 to 2000μm in diameter (Malvern Instruments Ltd, 2007).

The mixed microcapsule slurry was first gradually added into the sample dispersion unit under constant stirring at 2500rpm until the Mastersizer 2000 software indicated that the ideal concentration of the sample had been achieved. Then, the measurement was started whilst the dispersion unit continuing circling the sample suspension. Each measurement was set to

complete in 10 seconds in order to get enough data to enable the software to do the calculation. Each sample was repeated 3 separate times on measurement and the mean value was calculated and used in data reports.

3.3.8 Micromanipulation

A well-established micromanipulation technique has been used to measure the mechanical properties of microcapsule samples. The technique is based on the compression of a single microcapsule between two parallel surfaces (Zhang, 1999, Sun and Zhang, 2002, Liu, 2010, He, 2013). The detailed scheme of the micromanipulation rig is shown in Figure 3.3. During the measurement, one of the surfaces moves towards the other in a constant speed and the force signal compressed on to the surface is recorded simultaneously with time spent. With selection of an appropriate probe, probe size (all lab made) and transducer force (various models from Aurora Scientific Inc., Canada) scale, the micromanipulation rig is capable of measuring a number of force related static and dynamic parameters on particles ranging from 1μm to 1000μm. In this research, a compression-rupture test was conducted using the micromanipulation technique to determine the strength of the related perfume microcapsule samples.

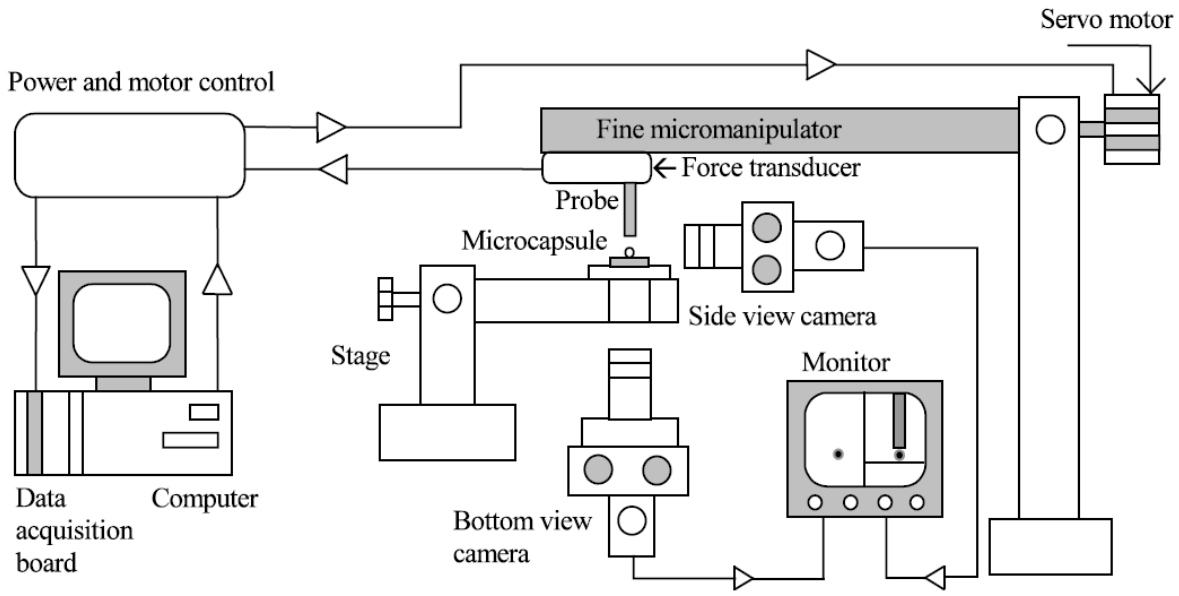

Figure 3.3 Schematic diagram of the micromanipulation rig (Sun and Zhang, 2002)

For each sample, at least 3 size bands with 10 microcapsules from each band were compressed in order to obtain statistically representative mechanical strength data of the bulk (Liu, 2010, Gonzalez, 2012).

A polished flat surface glass probe with a tip diameter of 30-40μm was glued (Loctite Glass Bond, Henkel, Germany) to a force transducer which was firmly screwed on to the micromanipulation rig and connected to the computer controlling system. The microcapsule sample was well mixed by gentle stirring using a tiny metal or glass stick and diluted by 1 : 300-500 (v/v, exact dilutions depend on the concentration of each slurry) with DI-water. Then one drop of the diluted suspension was placed on a pre-cut microscope glass slide (about 25 × 9 mm size, 1mm thick) and dried in room temperature. After that, the sample slide was firmly secured on to the micromanipulator sample stage under the probe. The position of the side view camera was adjusted to focus on the probe first. Then, by carefully moving the sample stage, an isolated microcapsule on the slide was focused into the side

view camera (on the screen view). Bottom view camera was then adjusted to focus on the microcapsule. Once a microcapsule was chosen, its diameter was measured on the monitor with a normal ruler and the compression took place measuring simultaneously the force imposed on the single microcapsule and the compression time. Each microcapsule was compressed to burst under a constant compression speed of 2μm/s. The recorded compression force vs distance data were collected by the computer controlling system and exported to a Microsoft Excel file where they were analysed using already built-up calculation sheet by (Zhang, 1999, Liu, 2010, He, 2013).

The dimensions of the monitor connected to the microscope camera were previously calibrated using a 1000μm size microscope standard scale on the sample stage. The compression speed of the probe was calibrated subsequently by conducting a compression movement for a certain time and measuring the distance of the probe image moved on the monitor using the ruler whilst counting the compression time using a stopwatch. Sensitivity of force transducer was calibrated following the method reported by Liu (2010) using carefully cut and weighted papers. Compliance of the system (Liu, 2010) was calibrated before each experiment by compression the blank sample slide fixed on the sample stage using the transducer which was pre-glued a flat probe. The compliance measurement was repeated at least 3 times at different point of the sample slide and average result was used in later sample data calculations.

3.3.9 Scanning Electron Microscope (SEM)

An Environmental Scanning Electron Microscope (ESEM, Philips XL30 ESEM-FEG, The Netherlands) fitted with a detection mode of Energy Dispersive X-ray (EDX) spectroscopy (Oxford Inca 300 EDX system) was employed to investigate the surface topography of

different microcapsules and to study the elemental proof of any surface modification (Goldstein *et al.*, 2012).

ESEM was used for high magnification electron micrographs for samples to study the surface topography of them. Comparing to normal SEM, ESEM not only allows for a more gaseous environment which can be in high pressure and high temperature but also allows samples to be more in their natural status which are dry, wet, oily, non-conductive or uncoated conditions. Since all the experiments in this study were conducted under dry condition, the ESEM acted as a normal SEM (Reimer, 2000, Joy, 2006).

The microcapsule particles were first dried on a glass slide, then coated with a thin layer of Platinum with a thickness of 5 to 6 nm in a sputter coater (Polaron S07640, Quorum Technologies Ltd, UK) to make their surface conductive. After that, the whole glass slide was moved into ESEM chamber to be investigated. According to the report of Ren *et al.* (2007a), MF microcapsule could resist an accelerating voltage up to 20kV within a radiation time up to 1 minute before a significant damage could be observed under ESEM dry condition. In the single microcapsule compression experiment which conducted on a micromanipulation rig in dry condition (details reported in chapter 4), PAC-PVOH microcapsules had similar mechanical strength vs. literature data of MF microcapsules (Liu, 2010), plus the fact that there is little literature reported on how the radiation may affect the mechanical properties of the PAC-PVOH microcapsule, it is assumed that PAC-PVOH microcapsule shares similar mechanical properties with MF ones under dry ESEM conditions. Hence, it was always ensured that the accelerating voltage was below 20kV and the exposure time of all microcapsule samples were controlled below 1 minute during the ESEM investigation in this study. On average, 5 to 10 ESEM images at different magnification were acquired for each

microcapsule sample. EDX was applied to the some of the coated microcapsule samples to confirm the elemental proof of such surface modifications.

3.3.10 Flow Chamber Adhesion Characterisation

3.3.10.1 Flow chamber technique

A flow chamber consists of a pair of parallel plates in which there are fluid passageways, inlet and outlet. It is normally custom built for the study of deposition and removal behaviours of certain particles. It utilises hydrodynamic force and liquid-solid molecular interactions to distribute the particles (Decuzzi *et al.*, 2007, He, 2013).

Wall shear stress (τ) is dependent on the design of the flow chamber. Reported in literature (Guillemot *et al.*, 2007, Wang *et al.*, 2011, Lane *et al.*, 2012), in a rectangular flow chamber, τ can be calculated using Equation 3.7:

$$\tau = \frac{6\mu Q}{wh^2} \qquad \text{Equation 3.7}$$

Where μ is the dynamic viscosity of the fluid, Q is the flow rate set on the syringe pump, w and h are the inner width and height of the flow chamber, respectively.

The flow pattern inside a flow chamber must be laminar and it is verified by calculating its Reynolds number Re, which is the ratio of fluid inertial forces to viscous forces. When Re is small (usually Re < 2100), the fluid dynamics are dominated by viscous drag; and the flow is laminar or fully developed. If inertial forces predominate, the flow becomes more and more random until it is turbulent, in which case Re > 4000. According to the reports of Cao *et al.* (1997) and Lane *et al.* (2012), Re in a rectangular flow chamber can be calculated as:

$$\mathrm{Re} = \frac{\rho Q D_h}{\mu w h} \qquad \text{Equation 3.8}$$

Where ρ is the fluid density; D_h is the hydraulic diameter, defined as (Lane *et al.*, 2012):

$$D_h = \frac{4 \times Cross - Sectional\ Area}{Wetted\ Perimetre} = \frac{4\,wh}{2(w+h)} \qquad \text{Equation 3.9}$$

Therefore, Equation 3.8 can be written as:

$$\mathrm{Re} = \frac{2\rho Q}{\mu(w+h)} \qquad \text{Equation 3.10}$$

The flow velocity and shear stress need to be fully developed along the inside of flow chamber. Thus, the flow chamber must be longer than the entrance length L_e from the fluid inlet. More importantly, any observing point needs to be setup later than L_e in order to get consistent data. For a rectangular chamber and $w > h$, L_e is calculated as (Cao *et al.*, 1997):

$$L_e = 0.044h\mathrm{Re} \qquad \text{Equation 3.11}$$

Moreover, in order to ensure that the fluid velocity and shear stress in the lateral direction do not vary significantly from the value of the flow direction, the ratio h/w must be much less than 1.0 (Lane *et al.*, 2012), which will result in the increase of data consistency from the flow chamber.

3.3.10.2 Construction of flow chamber system

The flow chamber used in this study was applied from the report of Lane *et al.* (2012). The detailed design is shown in Figure 3.4. The chamber was built with two 6061 Aluminium alloy plates by Physics Workshop, University of Birmingham. Two pre-fitted cut microscope glasses were glued (Loctite Glass Bond, Henkel, Germany) separately to each plate as chamber window. 10 stainless steel screws and 2 standard silicone O rings (AS568A-044 and

046) were used to fasten and seal the chamber. The other materials like 3 way stopcocks, soft tubing, male and female luer adaptors and 10 mL luer lock tip syringes (for sample injections) were all the same as the report of Lane *et al.* (2012) and supplied by Cole-Parmer Instrument Co., Ltd. This design typically results in a flow chamber with length 105mm, width 17mm and height range of about 200 - 350μm. Accordingly, the h/w value is in the range of 0.011 – 0.02 which means at lateral direction, the wall shear stress would be only reduced about 1.1 – 2% versus that in the flow direction.

Before each experiment, one piece of model fabric film (either PET or cellulose film) was cut into the size of 160 (±5) mm × 29 (±3) mm which fit in between the space of the large O ring (AS568A-046) and the screws on the bottom plate in Figure 3.4.B in order to fully cover the internal flow area. Then the top plate (Figure 3.4.A) was put on to the film and screws were fastened using an electronic screw driver (Model#AS6NG cordless, Black & Decker). A 3D schematic assembly was shown in Figure 3.4.C.

After the assembly, the inlet of flow chamber was connected to a syringe pump (PhD Ultra 70-3007, Harvard Apparatus Inc., USA) together with the luer adaptors and soft tubing. The outlet was connected to a waste tank. A dual 60mL syringe settings (both BD disposable syringe, supplied by Cole-Parmer Instrument Co., Ltd.) was used on the syringe pump to provide enough stock of the test solution in order to complete the designed flow chamber measurement.

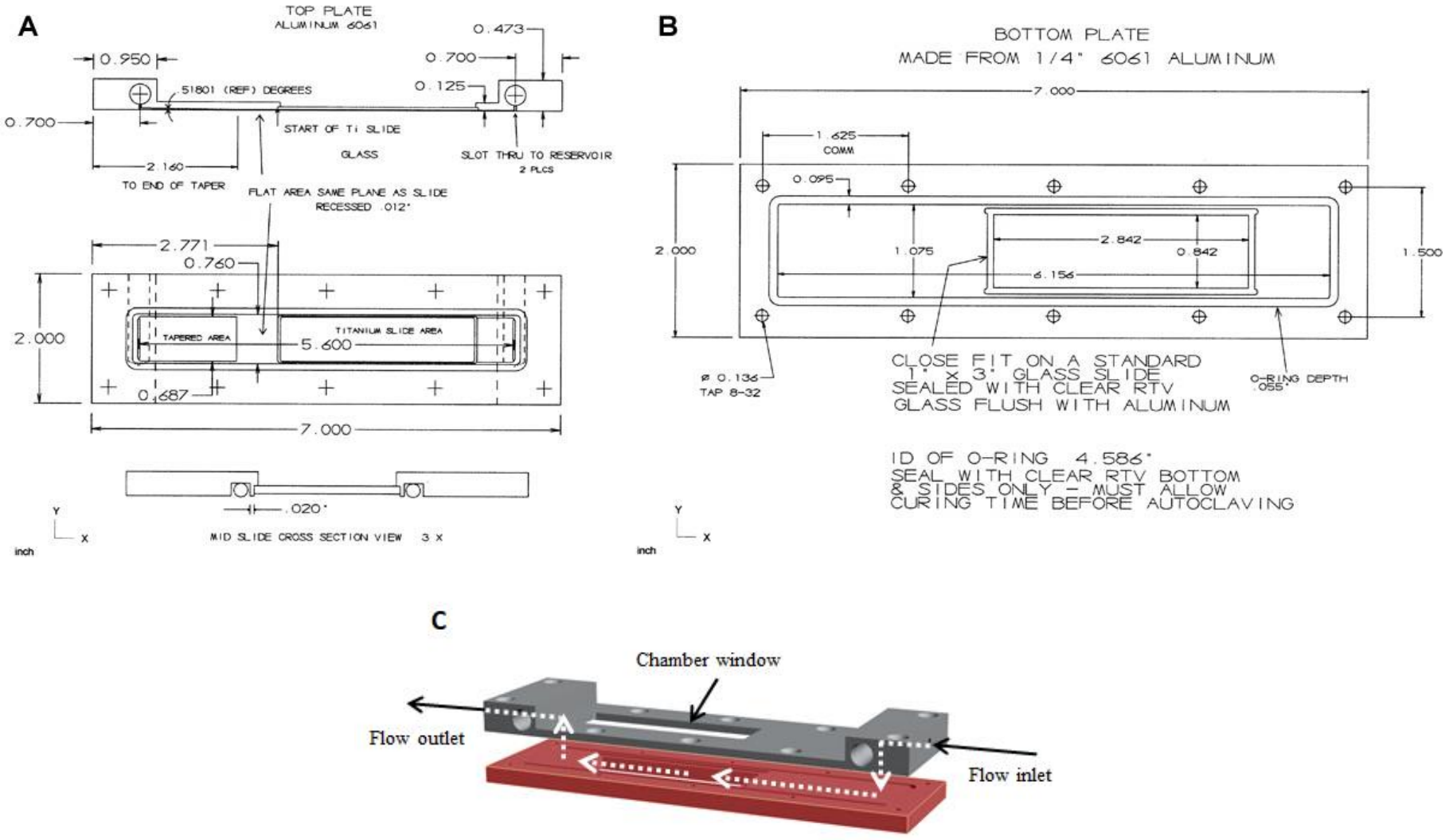

Figure 3.4 Design of the flow chamber from Lane *et al.* (2012): A. Top plate, B. Bottom plate and C. 3D schematic assembly and the designed flow of the flow chamber. Also see in Appendix A.

3.3.10.3 Sample preparation

Since the functional groups including the negative charged carboxylic acid and hydroxyl groups on PAC-PVOH microcapsule surface and the positive charged amide and amine groups on PVF and chitosan molecules are interactive with a number of environmental factors in aqueous conditions such as solution components, mixing rate and mixing time, etc., sample preparation method is believed to be one of the factors which will influence the surface properties of the microcapsule samples. However, in real washing conditions, the preparation processes of detergent solutions could vary a lot among different types of washing machines and consumer habits. In order to reduce variation, P&G has developed one standard method to prepare the detergent solutions for the lab tests. Likewise, in this project, following sample preparation steps were applied prior to the flow chamber experiment for the microcapsule flow chamber tests: First, each microcapsule slurry was gently stirred evenly with a small weighing spoon / spatula. Then, the sample was weighted and added with a certain volume of the target aqueous solution such as DI-water, hardness water or any surfactant / detergent solutions in this project to make 0.25% (wt.%) microcapsule sample suspension. Gentle shakings were applied subsequently to mix the suspension. Afterwards, a resting time of 20 min was given to allow the components in the suspension to achieve equilibrium which was also to mimic the detergent dissolving and mixing processes in real washing conditions. Finally, another round of gentle shakings was applied to homogenise the suspension before the syringe sampling and injection into the flow chamber.

3.3.10.4 Adhesion measurement by flow chamber

A previous flow chamber method reported by He (2013) was modified to fit the test conditions and microcapsule samples in this study. Since the overall SG of both microcapsule sample types (PAC-PVOH shell samples received from P&G and the other in-lab synthesized MF shell samples) was smaller than that of water, all the particle samples float in the flow chamber experiments. Thus, the flow chamber was put reversed under the microscope lens with top plate in Figure 3.4A towards downside so that the target fabric film surface was at the top inside the chamber. A schematic diagram in Figure 3.5 shows the flow chamber system in this project.

DI-water or target aqueous solution was firstly pumped through the entire system at 0.6 mL/min until there was no visible air bubble through the tubing, luer connections and the inside of syringes. Careful attention was paid to ensure there was no air bubble in the chamber by slightly lifting up the outlet end of the flow chamber until it was filled by the fluid. The device was then fixed flat onto the sample stage of the optical microscope described in §3.3.1. The microscope image taking window was adjusted onto a position which included the crossing area of the chamber's half width line and 10-15 mm towards the fluid entry of the chamber window. Since the model fabric film inside the flow chamber was fixed on the upper layer of the chamber wall, the microscope was adjusted to focus on the lower surface of the film where the PMC would deposit on. After that, the flow was stopped, 2 mL sample suspension was injected into the chamber and the microcapsules were allowed to set for 20 min (deposition step). Subsequently, the system was subjected to a flow of 13μL/min for 3min in order to remove any suspended free oil droplets introduced by occasional breakage of microcapsules when imported by injection or any non-deposited microcapsule (cleaning step). After that, the flow rate was increased using a 30 seconds

smooth flow rate increase settings / program in the pump (flushing step) and held at 0.03, 0.065, 0.125, 0.3, 0.6, 1.2, 2.4, 4.8 and 9.6 mL/min for 2.5 min respectively.

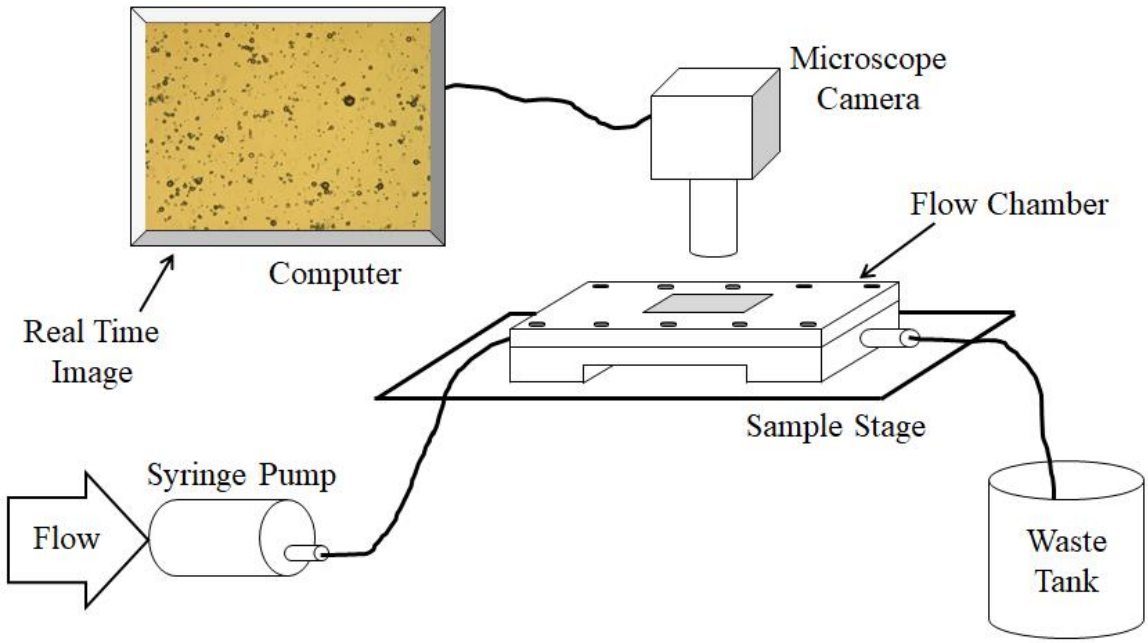

Figure 3.5 Schematic diagram of a flow chamber system

According to the shear stress data that fabrics experience inside the washing machine from §2.2.3.1, if maximum τ in the flow chamber tests was set to 1.0Pa, calculated using Equation 3.7, the maximum Q should then be just less than 18.5mL/min. Consequently, the maximum Re of the aqueous fluid in the flow chamber device would be 35.5 (calculated by Equation 3.10), which is obviously much smaller than 2100. Therefore, the flow inside the flow chamber must be laminar within the scope of the test design. Moreover, L_e would be 0.51mm in this condition (by Equation 3.11) which is well below 10-15mm where the observing window was set on the flow direction.

Images of microcapsules through the chamber window were taken every 3 min from the fixed position to get consistent data vs. the increasing flow rate. Each sample suspension was separately prepared and diluted using the same flow fluid and mixed well 30min before being used in experiment.

3.3.10.5 Results calculation for flow chamber experiment

Open source image analysis software ImageJ and commercial software package Matlab (R2015b, Mathworks Inc., USA) were used and compared to verify each other for analysing images taken from flow chamber experiments. The Matlab code (see Appendix B) for area calculation was generated by Dr James W. Andrews and Dr Yanping He in the School of Chemical Engineering, University of Birmingham (He, 2013). An example procedure of image analysis is shown in Figure 3.6.

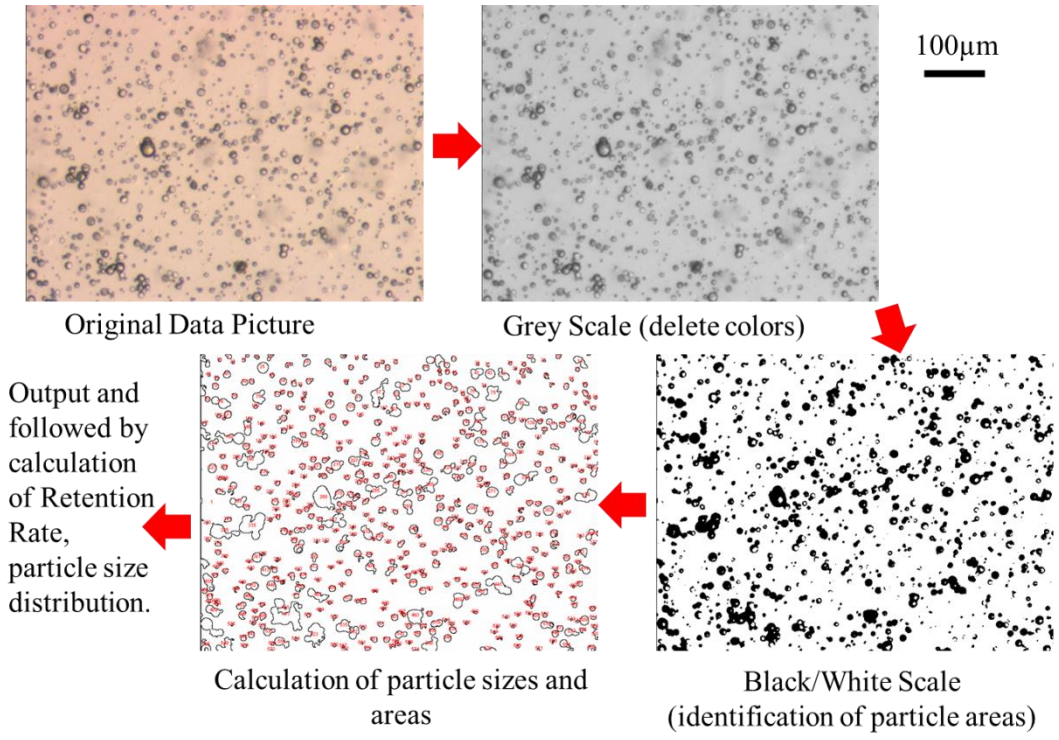

Figure 3.6 Example image analysis procedures of microcapsules on a model fabric surface

The principle is to calculate the area ratio covered by microcapsules (the black spots in the original image) of microcapsules for each image. The original image was firstly converted into grey-scale image (remove colour). Then black and white image was generated to remove the shadow and fill the hollow holes. Finally, the particle size distribution and surface area covered by the microcapsules on the capture area were calculated by software measuring of the spot size (diameter) and area, counting of the total spot numbers and statistical analysis of the data.

The surface area occupied by a single microcapsule was recorded as A_i. The total area (A) occupied by microcapsules on one image is:

$$A = \sum_{i=1}^{n} Ai \qquad \text{Equation 3.12}$$

The area ratio (a) of microcapsules occupied on one image is:

$$a = \frac{A}{A_{total}} \qquad \text{Equation 3.13}$$

Where A_{total} is the total area taken by the image.

Since defects are inevitable on the surfaces of commercialised model films, the normalised area retention ratio (a_R) of remained microcapsules after a certain removal process on the image position was calculated as:

$$a_R = \frac{A_t - A_0}{A_D - A_0} \qquad \text{Equation 3.14}$$

Where A_t is the total area occupied by all the microcapsules on the film surface at the time t; A_D is the total area occupied by all the microcapsules on the film surface at the end of

deposition step; A_0 is the software calculated result of the blank film image before deposition step starts or base line image area ratio.

3.3.11 AFM Adhesion Force Measurement

3.3.11.1 AFM force spectroscopy

The NanoWizard® II AFM with an attached CellHesion module and a 15 μm z-piezo (JPK Instruments, UK) mentioned in §3.3.3 was used for measuring adhesion properties between a single microcapsule particle and model film surfaces in both ambient air and aqueous solutions. The force spectroscopy mode of the AFM system was applied to all the force measurements in this research. Figure 3.7 schematically showed the principle of the AFM force measurement.

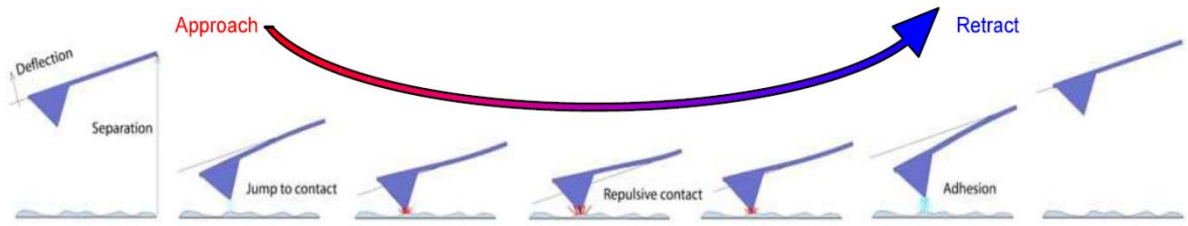

Figure 3.7 Schematic flow of the AFM force measurement (JPK Instruments, 2009a)

When the cantilever tip is brought close to or contact the target sample surface, interatomic forces such as electrostatic and Van der Waals forces between the tip and the sample lead to a deflection of the cantilever according to Hooke's law. The deflection is measured using a laser spot reflected from the top surface of the cantilever tip on to an array of photodiodes.

Then the electronic signal is further converted into force by the software control system (JPK Instruments, 2009b).

3.3.11.2 Preparation of AFM colloidal probe

In order to measure the interaction between single microcapsule and model fabric substrate, the traditional cantilever tip needs to be replaced by microcapsule. Thus, AFM colloidal probe technique (Zauscher and Klingenberg, 2001, Cho and Sigmund, 2002, Liu, 2010, He, 2013) was applied in this research.

Tipless rectangular Si cantilevers (uncoated NSC35 and CSC37, MikroMasch, Estonia) were used to make the microcapsule colloidal probe. A two-component epoxy glue (Araldite Rapid, Bostik Findley Ltd., UK) was used as adhesive. The micromanipulation rig introduced in §3.3.8 was used for precise operations on gluing a single microcapsule onto the end of a tipless cantilever. The detailed procedure was described as follows: one drop of microcapsule slurry was diluted by 13mL DI-water. One drop of such diluted suspension was then taken onto a clean microscope slide and dried in room temperature. A rectangular tipless cantilever was hold reversed in the sensor position of the micromanipulation rig with a fine glass tube and Blu Tack whilst waiting the sample on the slide to be fully dried. Focus was adjusted onto the target tipless cantilever. The sample slide was then put onto the sample stage of the micromanipulation rig and moved into focus. A tiny drop of well mixed epoxy glue was placed on a clean location on the slide. After that, careful operation was made on the micromanipulation rig to move the cantilever towards the epoxy drop until the tipless end slightly touched the top surface of glue. Then the cantilever was lifted away from the bulk glue, moved on top of a selected microcapsule and lowered down until the glue on the tipless

end touched the surface of the particle. A gentle press was retained on the cantilever by controlling the micromanipulation rig to hold its position for a few minutes until the glue fully dried. Finally, the cantilever was gently lifted to remove the attached microcapsule from the sample slide and the colloidal probe was then taken off from the micromanipulation rig. After being taken an image under a light microscope, the colloidal probe was stored in AFM cantilever box for further experiment. The captured image was further analysed by optical microscopy system (§3.3.1) to measure the diameter of the microcapsule, the distance between the end of the cantilever tip and the centre of attached microcapsule, together with the width and length of the tipless cantilever. All the information were further used to calculate the spring constant of the colloidal probe (Bowen *et al.*, 2010). Since it was revealed in the literature that there is little variation in adhesive force with particle size differences (Hodges *et al.*, 2002, Hodges *et al.*, 2004, Liu, 2010), microcapsule with a diameter of around 10-20 μm was chosen to make colloidal probe for the ease of handling during the above process. Figure 3.8 shows a benchtop SEM (TM3030, Hitachi, Japan) image of a chitosan modified PAC-PVOH microcapsule with diameter of 19.0 μm attached to a tipless cantilever. The image confirms there was no glue or any other external materials over the upper surface of the microcapsule where adhesion measurement takes place.

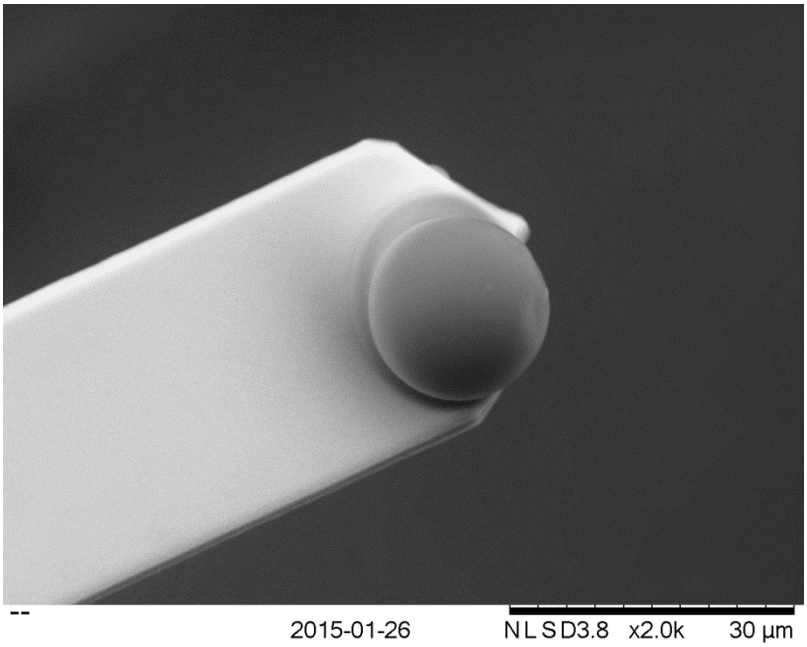

Figure 3.8 A benchtop SEM image of a chitosan modified PAC-PVOH microcapsule with diameter of 19.0 µm attached to a tipless cantilever

3.3.11.3 AFM measurement operations and test conditions

Model fabric substrate was firstly cut into 30mm × 15mm piece and attached (using transparent double sided tape) to polystyrene petri dish with a diameter of 60mm and 6mm height which was then fixed to the AFM sample stage. Contact mode was chosen for all the force measurements in this research. For the experiment performed in ambient condition, the room temperature and relative humidity were set to 17±1 ℃ and 40±2% respectively. For aqueous condition, sufficient target liquid (various aqueous solutions according to different experiment requirement) was added into the petri dish to ensure there was a minimum of 2-3 mm liquid depth above the upper surface of the film. Upon immersing the cantilever into the liquid, the whole AFM system was left thermally equilibrate for at least 20 minutes before each experiment. A 4 × 4 matrix measurement points were chosen over an area of 45µm ×

45μm around the central surface of the film substrate for each microcapsule and test condition. The approach velocity of the cantilever colloidal probe was set at 20μm/s which was adopted and modified from Jones *et al.* (2002), Liu (2010) and He's (2013) work. JPK data processing software (JPK Instruments AG, Germany) were used to process all the AFM measurement data. After that, all the data was further calculated and compared using Excel (Microsoft, US) and Origin 9.0.0 (OriginLab Coporation, US).

Chapter 4. Investigation of adhesion behaviour of PVF modified PAC-PVOH microcapsules on both cellulose and PET films

4.1 Introduction

The work presented in this chapter mainly focuses on establishment and verification of analytical methods, as well as characterisations of control microcapsule samples for this study. Because PVF polymer was found to be effective in modifying PAC-PVOH microcapsules and enhancing their adhesion to fabric surfaces by P&G BIC in their previous researches, it was selected as the initial benchmark in this project. In addition, commercially available fabric substitution of cellulose and PET films were purchased and used to replace self-made films. Multiple analytical equipment were employed to characterise the model films, the control and PVF modified microcapsule samples. Furthermore, AFM was used to characterise adhesion of the microcapsule samples to different fabric surfaces exposed to DI-water. Initial understanding of how different parameters impact on the adhesive interactions has been established accordingly.

4.2 Characterisation of cellulose and PET films

A number of technical measurements were conducted at the University of Birmingham to characterise the surface properties of both commercially available model cellulose and PET films. By comparing to the characterisation results reported by Yanping He (2013) on self-made cellulose films and the results on real cotton and polyester fabrics characterised by

P&G BIC research lab, conclusions may be made to confirm whether there is similarity among the sample groups in two categories of 1). commercial cellulose film, self-made cellulose film and real cotton fabric and 2). commercial PET film and real polyester fabric.

4.2.1 Film surface roughness measured by AFM and interferometry imaging

Surface topography images obtained using AFM and interferometer imaging for both surfaces of cellulose and PET films are shown in Figure 4.1 and Figure 4.2, respectively. Polynomial surface fitting of the smaller AFM scan area 45μm × 45μm shows that the difference between the highest and lowest peak is 90nm on cellulose film and 118nm on PET film. The RMS roughness parameter S_q of this area from the interferometer scan on cellulose film and PET film are 184nm and 98nm respectively on a large scan area of 669μm × 319μm. Combining both image analysis results, the surface roughness of the cellulose film is about the same as that of PET film and both are at 100 ~ 200nm level. As mentioned in §2.2.1.5, both industrial cotton and polyester fabrics are irregular due to manufacturing variations. Akgun (2014) reported the surface roughness of different cotton fabrics are at 30 – 50μm level and depending on the yarn properties (i.e. type, count, twist level and unevenness) and fabric constructional properties (i.e. thickness and balance). In another report, Akgun *et al.* (2012) measured the surface roughness of different polyester fabrics and the results to be in the range of 25 – 50μm. Clearly, both cellulose and PET films are much smoother than their fabric forms. Furthermore, both film surfaces are considered smooth if comparing to the PMC sizes used in this research (shown in §4.3.1, the majority PMCs are in about 7 – 37μm size range). All above indicate that the geometric effect on the PMC adhesion / detaching process on the cellulose and PET films may be neglected and both films could be suitable for

following measurement in this research. However, comparing to the RMS roughness data of less than 1nm for regenerated cotton cellulose or PET films deposited on silicon wafer which were made in the lab (Osterberg and Claesson, 2000, Liu, 2010, He, 2013), the current commercial model cellulose and PET films have relatively larger asperities. Therefore, the real impacts brought by the surface roughness of the films on the microcapsule-substrate interaction behaviours (e.g. adhesion, detachment, sliding and rolling) could be difficult to predict and will be studied and discussed in later sections and chapters.

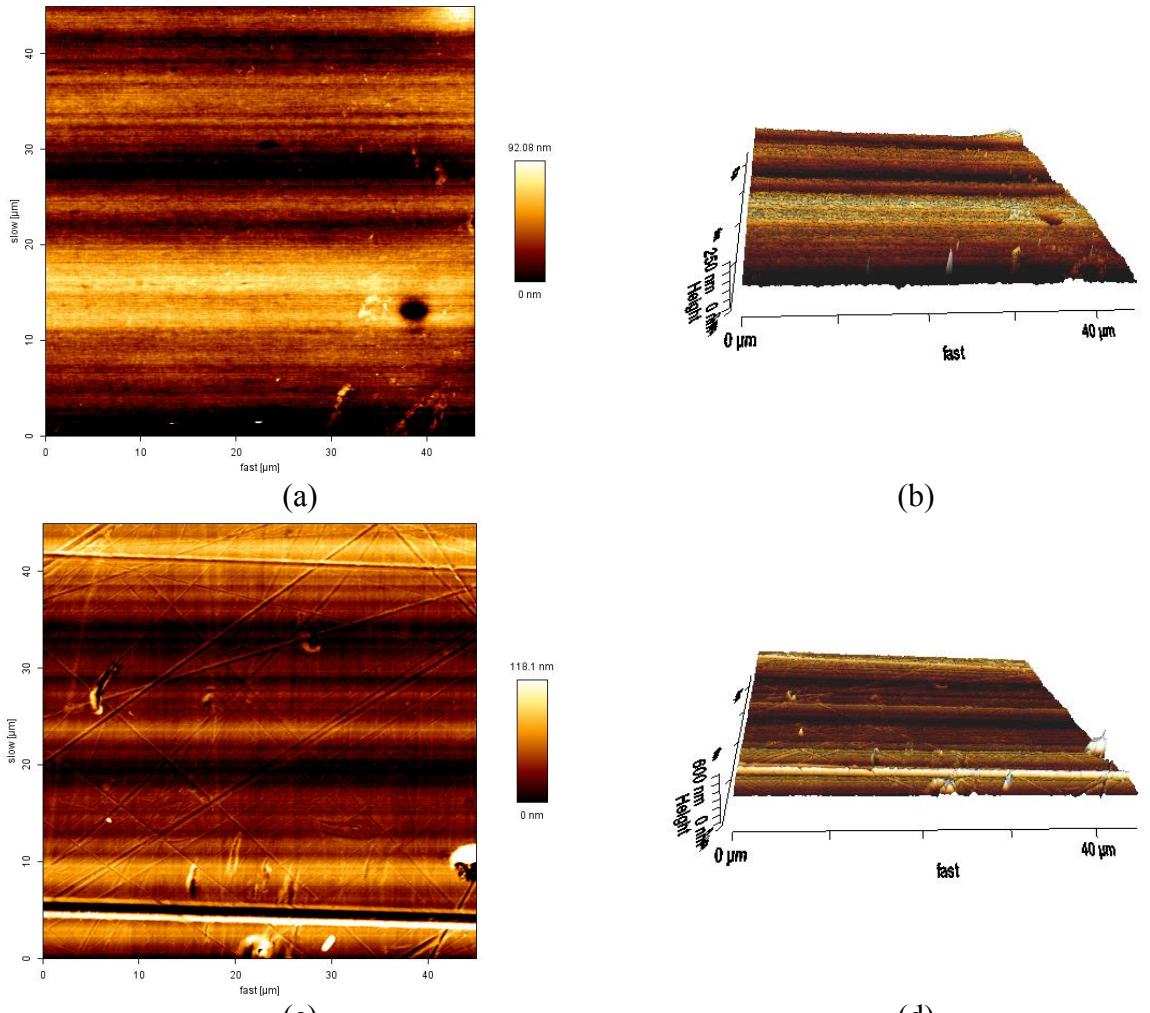

Figure 4.1 AFM images of cellulose film surface (a) 2D view; (b) 3D view and PET film surface (c) 2D view; (d) 3D view. Both scan areas are 45µm × 45µm

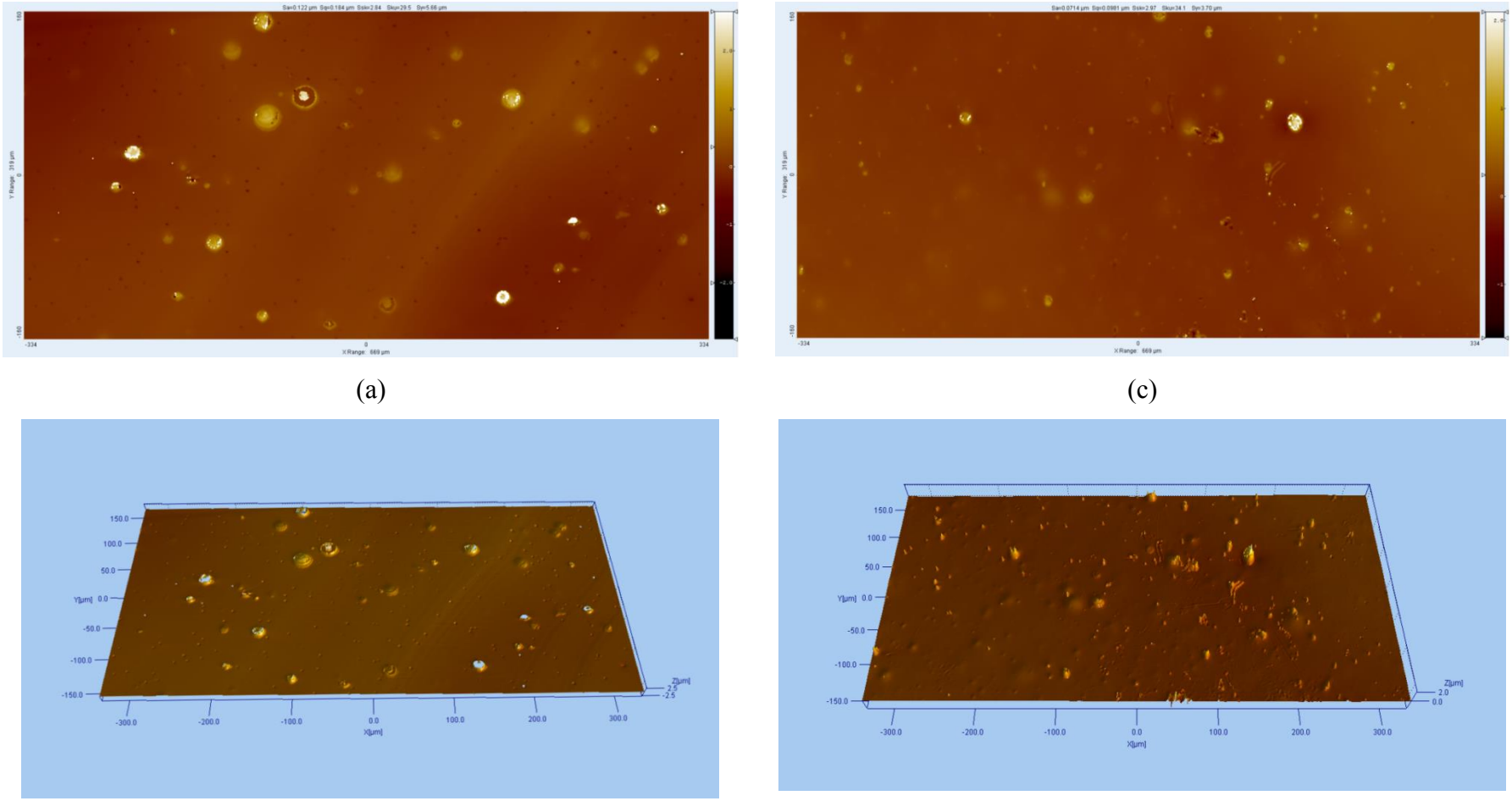

Figure 4.2 Interferometer images of cellulose film surface (a) 2D view; (b) 3D view and PET film surface (c) 2D view, (d) 3D view. Both scan areas are 669µm × 319µm. RMS area roughness for cellulose and PET films are 184nm and 98nm respectively.

4.2.2 Film surface elemental analysis using XPS

Surface composition scan was done on both cellulose and PET films using XPS. No H signal is shown since XPS technique is not able to detect H element (Hofmann, 1986).

Elemental results and spectra of cellulose film are shown in Table 4.1 and Figure 4.3 (a) respectively. According to both data, only C and O elements are detected from cellulose film surface and the element ratio are 56.21% and 43.79% respectively. The spectra of distinctive C 1s and O 1s elements were matched to the existing XPS spectra library built within the data processing software and the matching results are in Figure 4.3 (b) and (c). Comparing to the XPS data reported by Briggs and Beamson (1992), Chastain *et al.* (1992) and Gerin *et al.* (1995), the software matching result of C 1s shows there are a large amount (90% of C element) of C-O-H and C-O-C (286.8 eV) and small amount of C-C and/or C-H (285.0 eV) components on the surface of the cellulose film, while the matching of O 1s confirms there is only one kind of O element which is presented as hydroxyl C-OH or C-O-C (533.1 eV). All these results indicate that the surface of the film is similar to the structure of cellulose molecule which is highly hydrophilic. It also confirms the commercial model cellulose film samples were as pure as Innovia Films Ltd. (www.innoviafilms.com) claimed that there was no extra added chemical during manufacturing other than the raw materials from wood pulp and no post surface modification was done to the film products.

Table 4.1 Surface elements and atomic concentration (%) on cellulose film analysed by XPS

Element	Peak Position(eV)	Matched Component by XPS Library	%Atomic Conc.	%Total Conc.
C 1s	285.0	C-H / C-C	5.7	56.2
C 1s	286.8	C-O-H / C-O-C	50.5	
O 1s	533.1	C-O-H / C-O-C	43.8	43.8

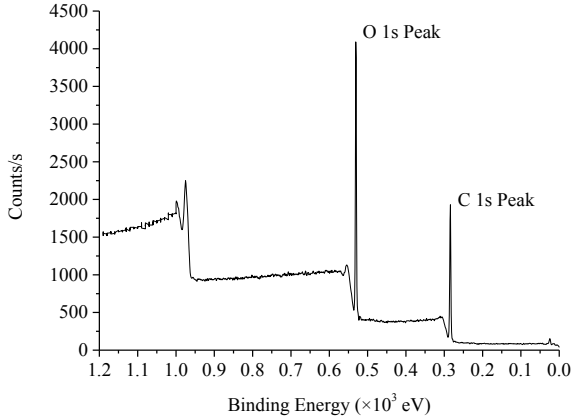

(a)

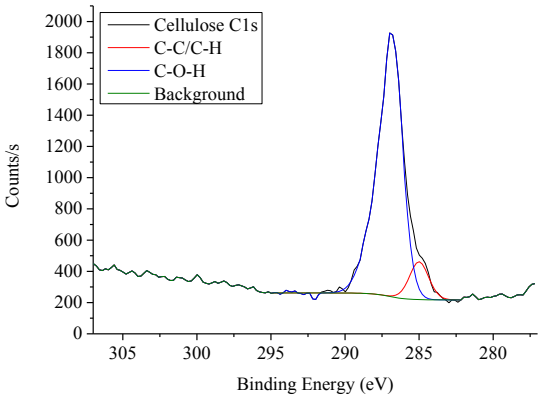

(b)

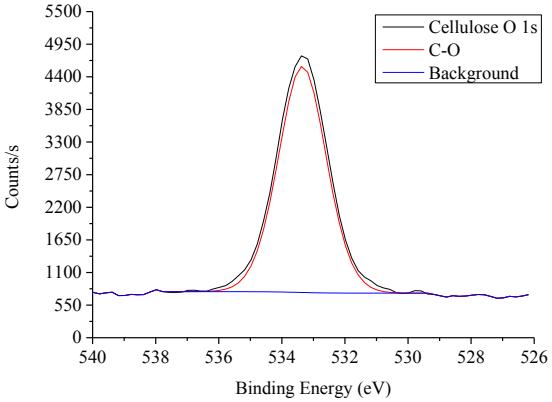

(c)

Figure 4.3 Surface composition spectra (a) and software library matching results for element C 1s (b) and O 1s (c) on model cellulose film obtained using XPS.

Table 4.2 and Figure 4.4(a) are the analytical results of PET film surface elements. Figure 4.4 (b) (c) (d) are the software library matching results on distinctive C 1s, O 1s and Si 2p elements. The matching results combined with literature data (Gerin *et al.*, 1995, López *et al.*, 1991, Chastain *et al.*, 1992, Beamson and Briggs, 1992) show more than 75% C 1s element on the PET surface are C-H or C-C (284.7eV) and more than 40% of O element are in C-C=O and C-O-C=O components. Further, because of the majority C-H / C-C result, C-O-C could dominate O element at 533.2eV. By considering the molecular structure of PET (Prevorsek *et al.*, 1977), a small amount of C-O-H could be present on the film surface as end group of the polymer. However, this doesn't change the conclusion that the majority of functional groups on the surface of the PET film are hydrophobic.

Table 4.2 Surface elements and atomic concentration (%) on PET film analysed by XPS

Element	Peak Position (eV)	Matched Component by XPS Library	%At Conc.	%Total Conc.
C 1s	284.7	C-H / C-C	16.47	
C 1s	286.4	C-O-H / C-O-C	2.96	21.41
C 1s	288.8	C-C=O / O-C=O	1.98	
O 1s	531.7	C-C=O / C-O-C=O	31.81	75.42
O 1s	533.2	C-O-H / C-O-C	43.61	
Si 2p	101.9	SiO_2	3.18	3.18

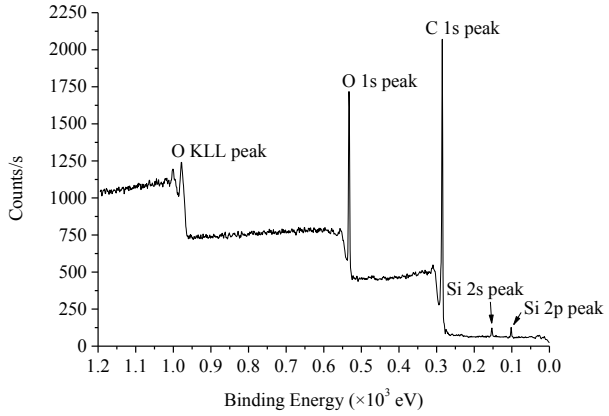

(a)

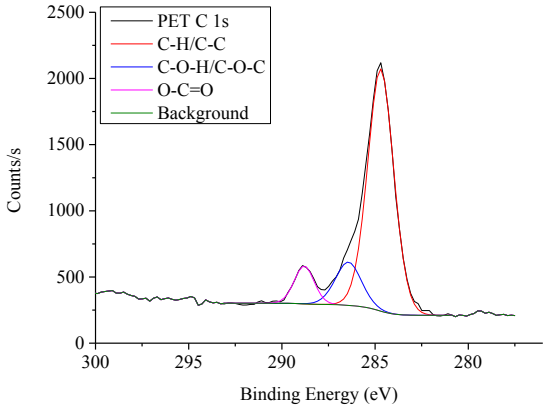

(b)

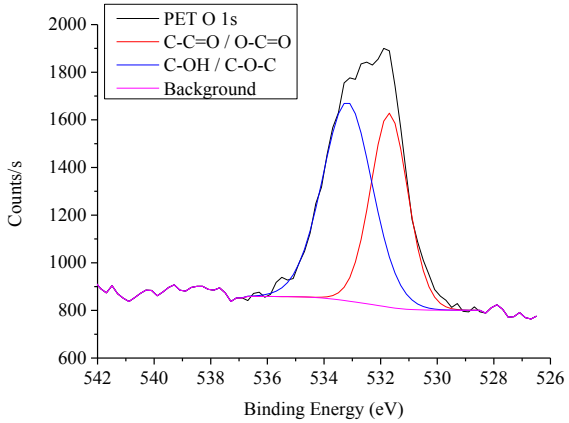

(c)

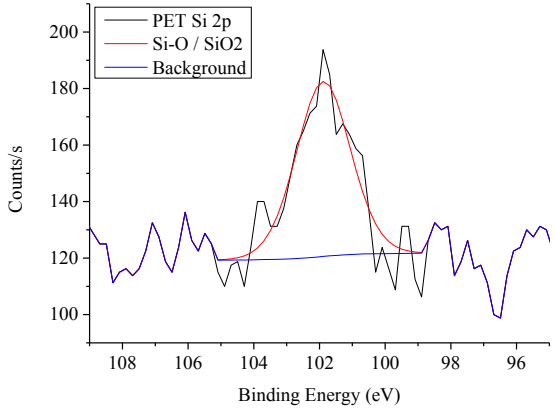

(d)

Figure 4.4 Surface composition spectra (a) and software library matching results for element C 1s (b), O 1s (c) and Si 2p (d) on PET film obtained using XPS.

In addition to the atomic concentrations of elements C (21.41%) and O (75.42%), the PET film has a level of 3.18% Si detected on the surface. The software library matching result of the Si 2p is for SiO_2. In spite of the literature data reported by Chastain *et al.* (1992) and Beamson and Briggs (1992) that Si 2p peak in SiO_2 was around 103±0.5eV, Lucovsky *et al.* (1985) and Ulgut and Suzer (2003) showed that the binding energy of Si 2p in SiO_2 could be lower due to environmental differences. Though the PET film supplier Goodfellow (www.goodfellow.com) didn't disclose any of the process information, it is quite common in industry that materials (e.g. silica particles or powders) containing a very small amount of inorganic silicon can be added as an anti-blocking aid during plastic film production (Sobottka, 1994, Xanthos, 2010). It is also possible that after rinsing by DI-water, during the drying stage or the stage of transferring it into the XPS chamber, the PET film sample attracted some dusts from the air containing the inorganic silicon to its surface due to electrostatic effect. Since the XPS data presented are the mean results based on scans on three different areas, this small amount of inorganic Si is considered evenly distributed on the PET film surface.

4.2.3 Contact angle measurement results

Cellulose molecule contains a large amount of hydroxyl groups which makes the cellulose film highly hydrophilic. Actually, this property allows water molecules to penetrate into the film when they are in contact and makes the film swell (Falt *et al.*, 2003). It was observed in this work that the water penetration process on a 40 μm thick cellulose film was so fast that the size of a water droplet significantly decreased after 3 seconds and was completely absorbed by the film within 6 seconds. Simultaneously, the film began to twist and this transformation lasted for an extra 2 to 3 seconds after the

complete absorption of the water droplet. Then, the film became stiffly distorted and no longer suitable for a contact angle measurement since the software associated with the instrument could not recognise the base line from the image with such an uneven intersection. Only after soaking the entire substrate into excessive water, the cellulose film could be softened and stretched again into a flat piece. This swollen phenomenon of cellulose which was previously studied by Laity *et al.* (2000), Falt *et al.* (2003) and Cuissinat and Navard (2006a, 2006b, 2008) indicates that not only the molecular functional groups on the surface but also the interior polymeric molecules inside the cellulose film attract and bond with water molecules in a very short time. However, water molecules and possible aqueous ions existing are not capable enough to break the internal hydrogen bonds between cellulose molecules and dissolve the cellulose film. Therefore, as a result, swollen and distortions are caused to the entire film structure. Hence, in order to get valid contact angle data, the time to take the image of aqueous droplet on cellulose film was strictly controlled within three seconds before severe swollen and distortions take place. In real measurement, most contact angle images were taken within one second after the dropping of an aqueous droplet.

The representative images from contact angle measurement on cellulose film using DI-water and diiodomethane are shown in Figure 4.5 (a) and Figure 4.5 (b) respectively. The mean values of the contact angle were 19.1˚±0.5˚ and 38.1˚±1.7˚ respectively. The contact angle value for DI-water droplet on cellulose film is consistent with those reported by Liu (2010) and He (2013) on self-made thin cellulose films and is within the range suggested by Gunnars *et al.* (2002) for pure cellulose. As the DI-water contact angle on the film is much less than 90˚, it confirms that the cellulose film surface is hydrophilic.

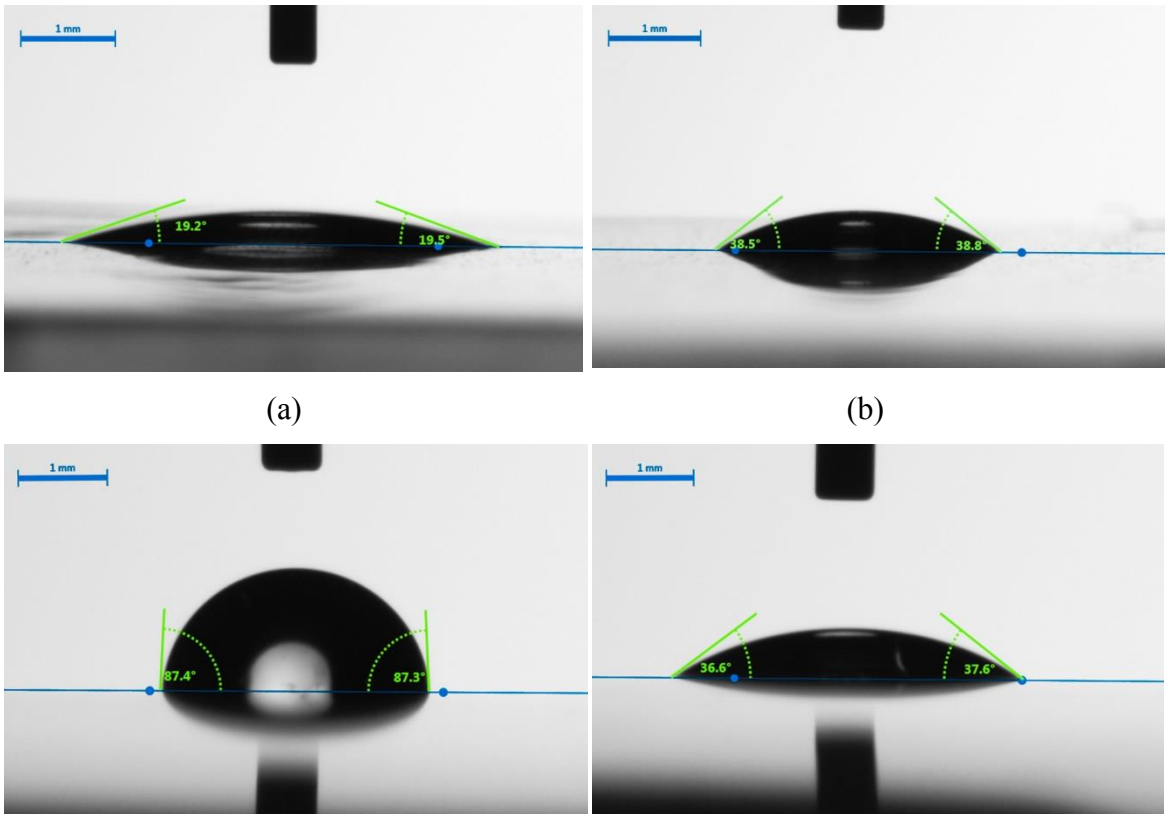

(a) (b)

(c) (d)

Figure 4.5 Representative contact angle measurement images on cellulose (a. DI-water droplet; b. diiodomethane droplet) and PET (c. DI-water droplet; d. diiodomethane droplet) film surfaces

For the PET film, there was no such time limitation on the measurement since its surface is relatively hydrophobic and no water penetration observed. Thus, the time to take images was set to be within 20 seconds in order to obtain the equilibrium contact angle data. Same measurements were conducted on the PET film and the contact angle results using DI-water and diiodomethane were 84.9˚±5.4˚ (Figure 4.5 (c)) and 37.4˚±3.4˚ (Figure 4.5 (d)) respectively. The contact angle data of the PET film for DI-water is consistent with those reported in the literature (Inagaki *et al.*, 2002, Liu *et al.*, 2005).

Table 4.3 presents the SFE results calculated from contact angel data using Equation 3.5 which was originally proposed by Owens and Wendt (Owens and Wendt, 1969), then evaluated and verified by multiple researchers like Shimizu and Demarquette (2000) and Good (2012), et.al. The data in Table 4.3also includes the SFE data for four real fabrics measured by P&G BIC and calculated using the same equation. The results for glass are used as control as well.

Table 4.3 Calculated surface free energy for different substrates

Substrate		SFE (mN/m)	
		Nonpolar (γ_s^d)	Polar (γ_s^p)
Commercial Model Fabric Film	Cellulose Film	40.6 ±0.8	31.3 ±0.5
	PET Film	40.9 ±1.6	1.0 ±1.1
Real Fabric	100% Cotton W120*	38.9 ±0.5	16.7 ±1.5
	100% Cotton*	41.3 ±0.8	17.9 ±1.0
	100% Cotton Twill*	35.7 ±0.9	27.0 ±1.5
	100% Polyester*	43.0 ±0.5	0.8 ±0.5
Control	Glass*	31.3 ±0.9	36.1 ±1.2

* Data provided by P&G BIC.

From these surface energy data, it is clear that all the materials made of cellulose and polyester have similar nonpolar SFE values in a range of 31 - 44 mJ/m^2; however, there are significant differences in polar ones. According to the results, the polar SFE of cellulose film used in this research is most similar to that of 100% cotton twill fabric. Thus it was used as a substitution of such real cotton fabric in later experiments. Since there are a number of weaving methods to produce cotton fabrics in the industry and

each produces cotton fabrics with different surface patterns, subsequently resulting in different surface properties, the commercial model cellulose film is not expected to fully represent the real cotton fabrics.

In terms of polar and nonpolar SFE values, the PET film was very similar to 100% polyester fabric, which indicates that the PET film may be suitable to mimic real polyester fabric, and was therefore used in later experiments. It is also important to note that both polyester fabric and model PET films showed almost no polar SFE, which means their surfaces were highly hydrophobic.

4.3 Characterisation of PVF modified PAC-PVOH PMCs

A number of characterisations were done on both control and PVF modified PMC samples. By comparing the physicochemical, chemical and mechanical properties of both samples, questions regarding the choice of following experimental parameters as well as the concern on whether any physical / chemical properties were changed by the PVF polymer modifications were addressed.

4.3.1 Particle size and size distribution

Three control samples were characterised by a Mastersizer (APA 2000, Malvern Instruments Ltd, UK) equipped with a liquid sample dispersion unit Hydro 2000SM to get their size and size distribution data. Although all three samples have a size distribution range from about 1μm to 70μm (shown in Figure 4.6), the calculated mean diameter values (the intercepts of related 10%, 50% and 90% cumulative volume/mass

as d_{10}, d_{50} and d_{90}) (Bittelli *et al.*, 1999) as well as volume weighted mean diameters ($D_{4,3}$) of each control sample listed in Table 4.4 (with 2× std error) indicate that the majority of the microcapsules in the control samples are in about 7 - 37μm size range.

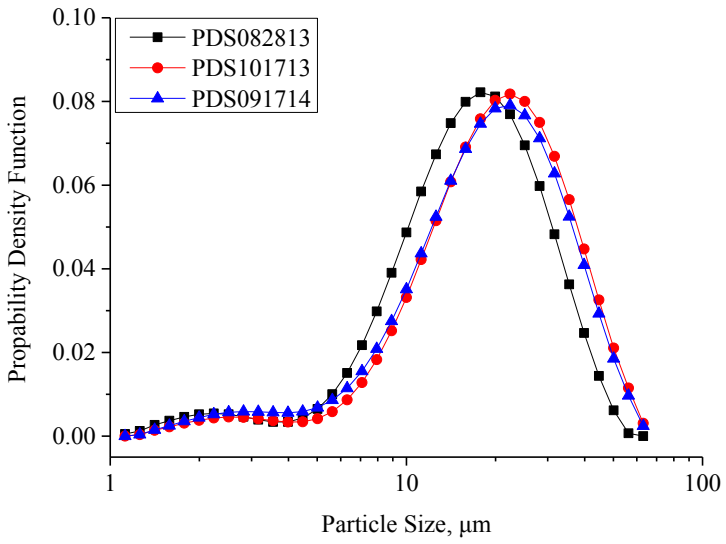

Figure 4.6 Differential particle size distribution of different control samples.

In this research, surface modification of PMCs is expected to play a part in the interactions between them and the targeted deposition surfaces such as model fabric films. Since the modification process was through gentle mixing of a polymer solution with PMC slurry, the mixing force was not expected to break any of the particles and change the size distribution of the original samples. Moreover, the amount of polymer used was limited (0.25 - 0.5wt.%), and no significant agglomeration by the polymer modifications during and after the process was expected. Therefore, the particle size and size distribution data of the control samples may be applied to the related PVF, chitosan and any other modified samples.

Table 4.4 Mean diameters of different control samples measured by Malvern particle sizing

Sample Batch#	d_{10}, μm	d_{50}, μm	d_{90}, μm	$D_{4,3}$, μm
PDS082813	7.02 ±0.03	15.85 ±0.04	30.21 ±0.05	17.36 ±0.04
PDS101713	8.40 ±0.02	19.21 ±0.06	36.58 ±0.08	21.01 ±0.05
PDS091714	7.32 ±0.03	18.36 ±0.02	35.56 ±0.02	20.10 ±0.02

4.3.2 Surface morphology of PMCs characterised using ESEM

The ESEM images of PMCs are shown in Figure 4.7. Figure 4.7 (a) and (e) present the overview of both samples. Figure 4.7 (b) (c) (d) show the detailed morphology of non-coated (control sample) PAC-PVOH microcapsules in different magnifications whilst Figure 4.7 (f) (g) (h) show those of 0.25% (w/v) PVF modified PAC-PVOH microcapsules respectively. Overall, all the ESEM images show spherical geometry with relatively smooth surface. The dimples found on some microcapsules under high magnifications were probably formed due to the strong electron beam radiation which was used to focus on the samples during the scanning and imaging according to the investigation results of Ren *et al.* (2007b).

Observed from Figure 4.7 (b) (c) (d), it is clear that the surface of control sample is smooth and no coating material can be seen as there is clear edge between contacting particles. Comparing to control sample, a thin layer of substances can be observed at the contacting areas between particles in Figure 4.7 (h) which blurs the edge. This phenomenon indicates a thin layer of coating material formed on the shell of the 0.25% PVF modified PAC-PVOH microcapsules. Although it is difficult to identify from the images whether the coating makes a full coverage on the PAC-PVOH microcapsules or not, the fact that the number of smaller sized (from nano to 2μm size range, shown on

Figure 4.7 (f) and (g)) particles staying on the surface of the bigger microcapsules is significantly larger than that on control sample clearly shows the existence of adhesive coatings on most of the surfaces. Since there was only PVF polymer added into the bulk PAC-PVOH microcapsule slurry to make the PVF modified sample, the coating material on the microcapsule shell should be PVF polymer theoretically, however, it is necessary to use other techniques to confirm.

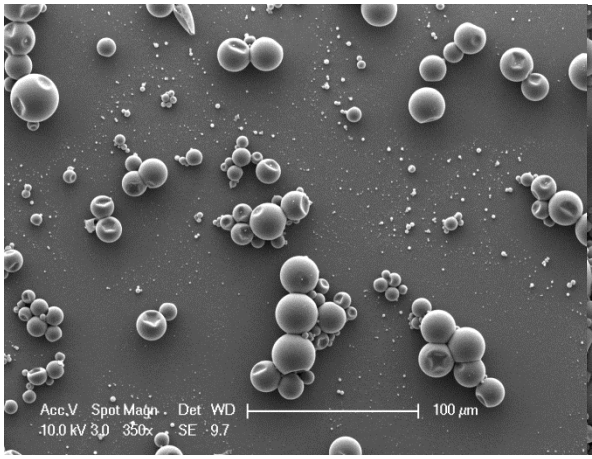

(a)

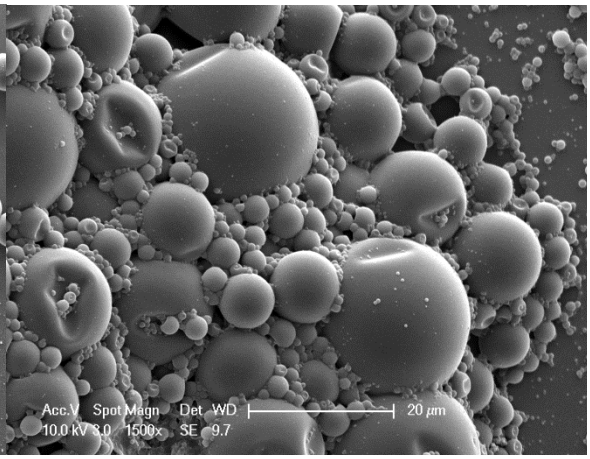

(e)

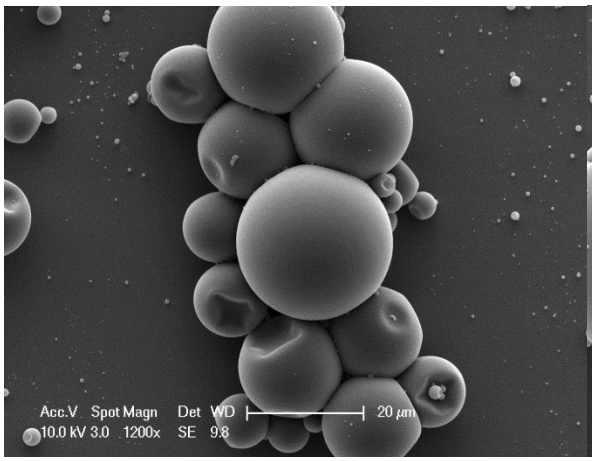

(b)

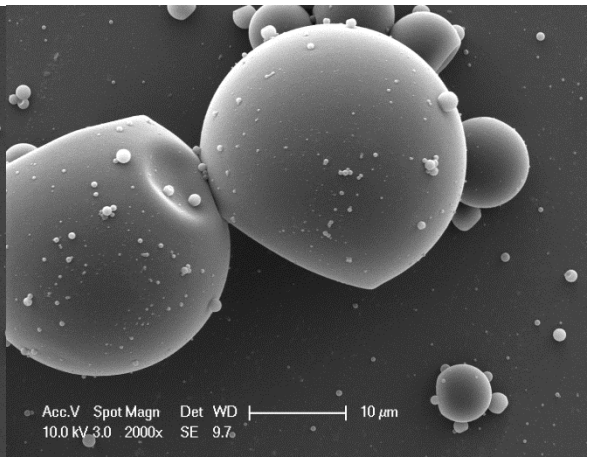

(f)

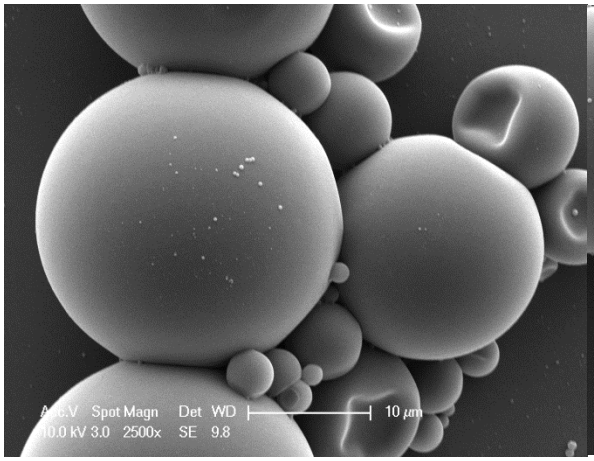

(c)

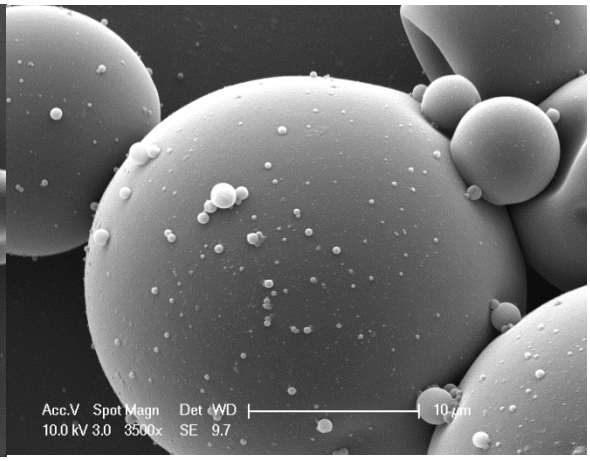

(g)

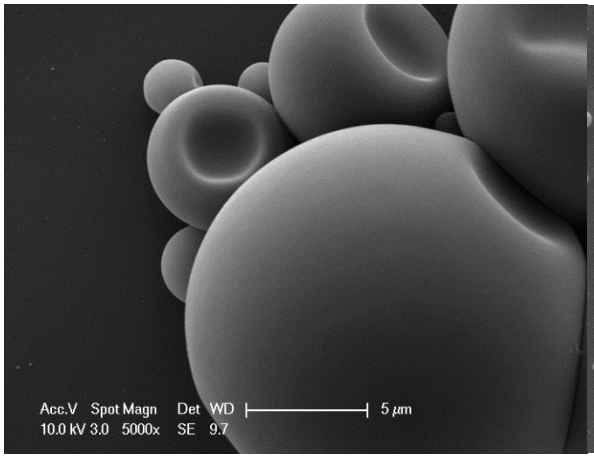

(d)

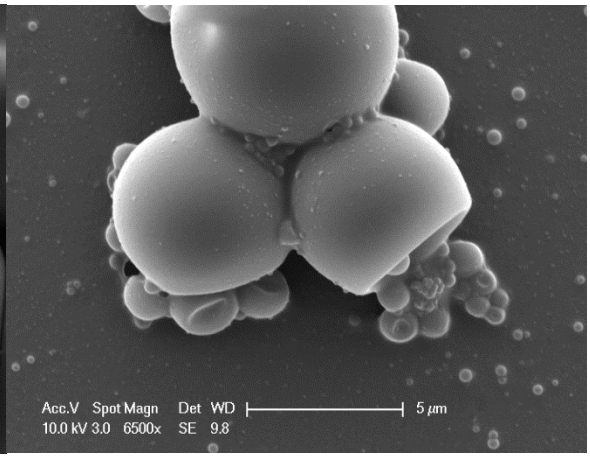

(h)

Figure 4.7 ESEM images of non-coated control sample (Lot#PDS091714B, image a, b, c, d) and 0.25% PVF modified PAC-PVOH microcapsules (Lot#PDS091714B-PVF, image e, f, g, h) at different magnifications

4.3.3 Surface elemental analysis by SEM-EDX

SEM-EDX was then employed to analyse the surface elements on the PVF modified microcapsule samples. PAC microcapsule shell consists of polyacrylate and polyvinyl alcohol copolymer which doesn't contain nitrogen in their molecular formula (Finch, 1973, Stevenson and Sefton, 1992, Schwantes and Sands, 2010); whilst PVF polymer has formula combination of $(C3H5NO)_n$ and $(C2H5N)_m$ depending on the hydrolysis

ratio, in which N element takes about 14 - 19%, respectively (Verboom, 2011). Therefore, N element was chosen to be the target in EDX elemental scan to determine if there is PVF polymer coated on the shell of PAC microcapsules. Figure 4.8 shows the representative scan results of EDX analysis of both non-coated and 0.25% PVF modified PAC microcapsule samples. The data indicates no N elemental signal was detected in any of the control samples (Figure 4.8 a and b) whilst small N peak was identified in PVF modified ones (Figure 4.8 c, d, e and f). However, not all of the elemental scans on the PVF modified sample showed N elemental peak (Figure 4.8 g and h). Considering the PVF polymer concentration used in the modification was relatively low due to the cost consideration, it is possible that the PVF polymer coating was uneven or only partial coating coverage was achieved for most of the microcapsule surfaces. Nevertheless, it is clear that the EDX results proved the coating of the PVF polymer on the PAC microcapsule surface.

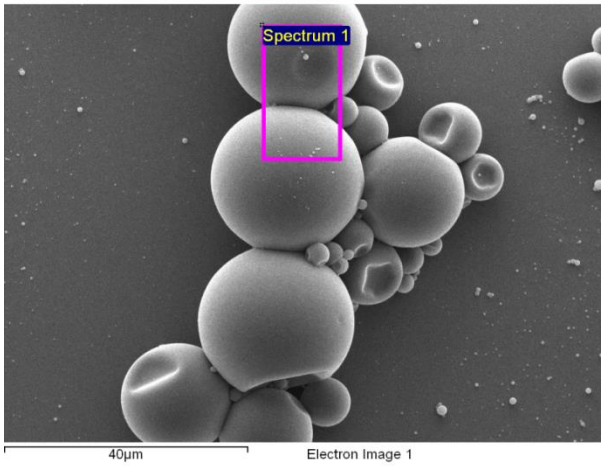

Element	Weight%	Atomic%
C	80.37	84.50
O	19.63	15.50
Totals	100.00	

(a)

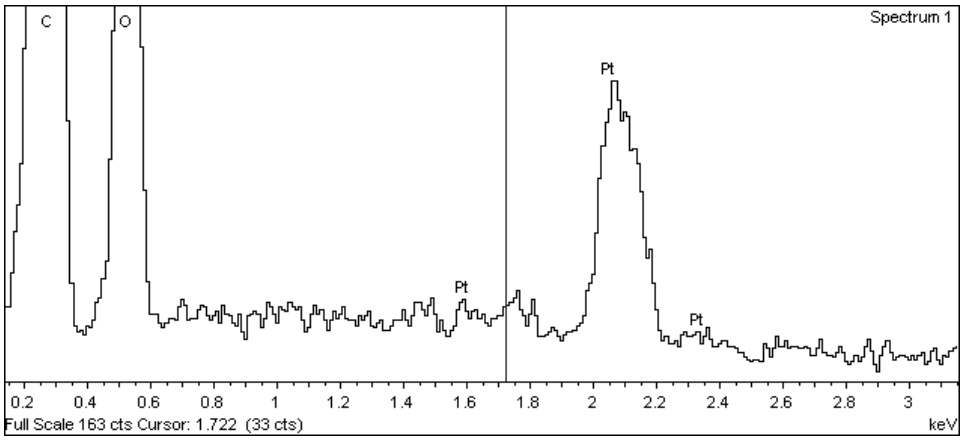

(b)

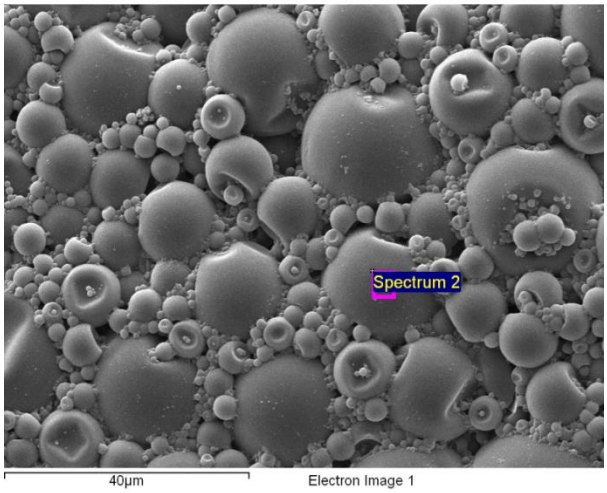

Element	Weight%	Atomic%
C	77.20	81.83
N	0.38	0.35
O	22.42	17.82
Totals	100.00	

(c)

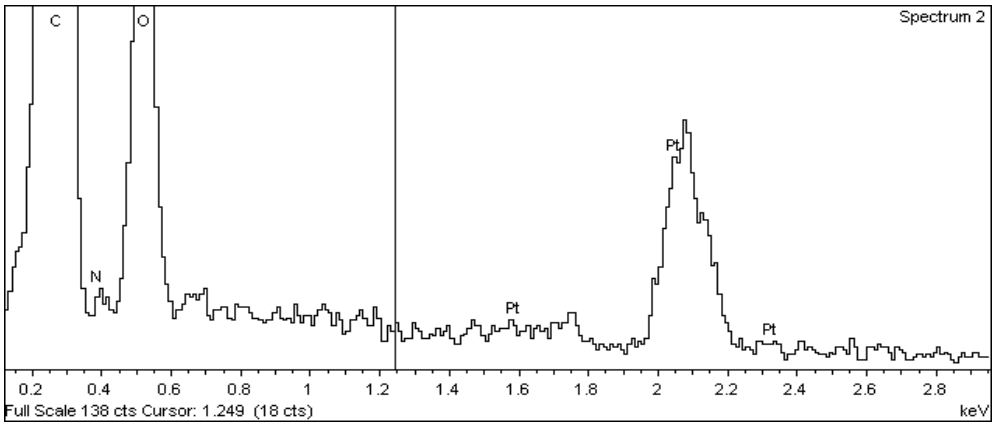

(d)

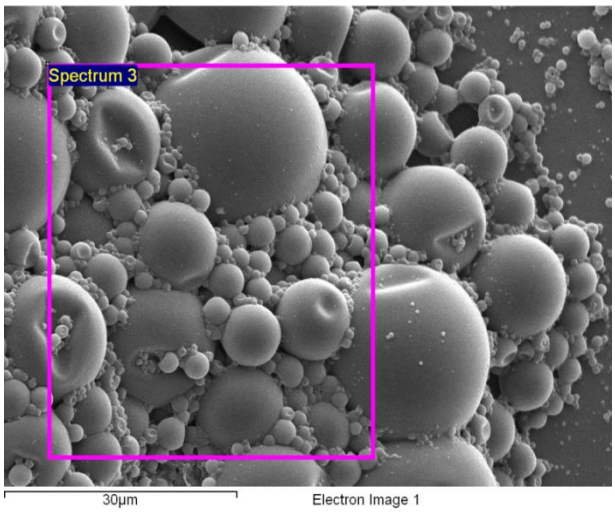

Element	Weight%	Atomic%
C	72.42	77.76
N	0.26	0.24
O	27.32	22.00
Totals	100.00	

(e)

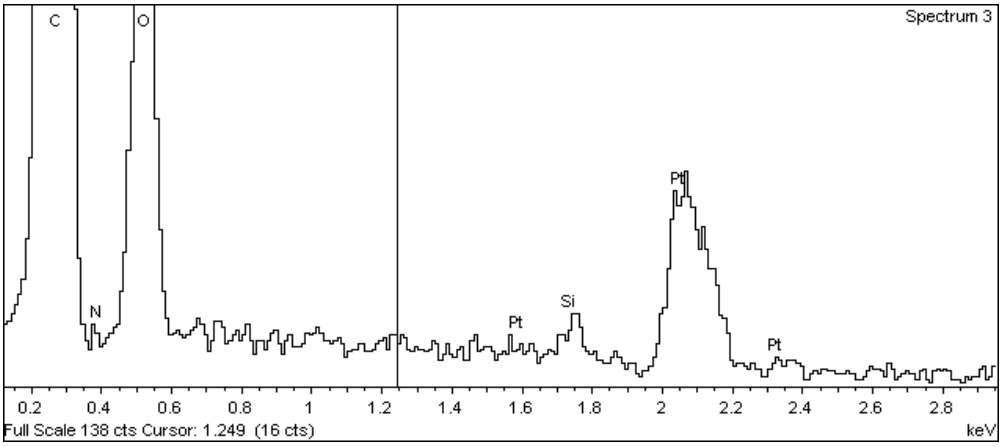

(f)

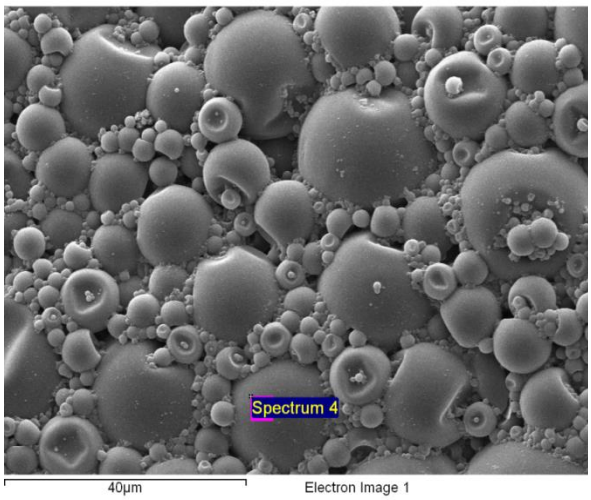

Element	Weight%	Atomic%
C	82.36	86.15
O	17.64	13.85
Totals	100.00	

(g)

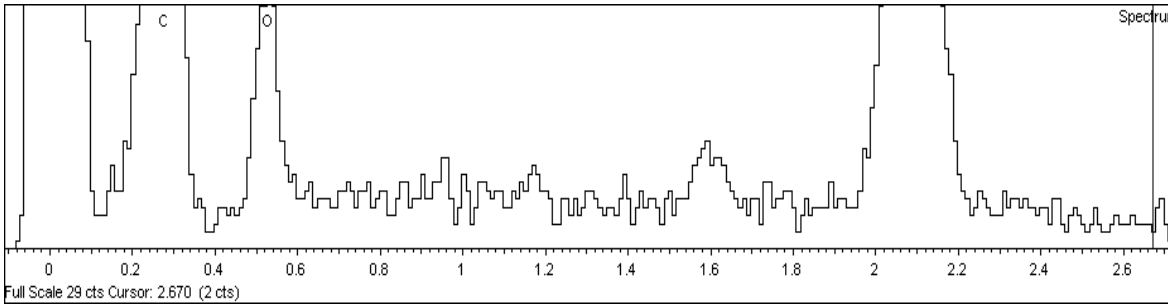

(h)

Figure 4.8 SEM-EDX analysis of non-coated control sample (a: SEM image and elemental data; b: EDX spectrum) and 0.25% PVF modified PAC microcapsule samples in different scanning areas (c, e and g: SEM image and elemental data; d, f and h: EDX spectrum)

4.3.4 Mechanical properties

The mechanical properties of PMCs are important in ensuring their integrity when they are exposed to mechanical forces, which can help to determine the test conditions for both flow chamber and AFM measurements. Both control and 0.25% PVF modified PMCs were characterised by diametric compression using a micromanipulation rig.

From the data in §4.3.1, most of the particle sizes were in the range of 7 - 37μm. Therefore, 10 - 20 - 30μm size bands (±2μm for each band) were chosen for measuring their mechanical properties. At least 10 particles in each size band were randomly picked, their sizes measured and compressed to rupture using a force transducer (Model#403A, 0 - 5mN force range, Aurora Scientific Inc., Canada). The force and probe displacement data from the micromanipulation rig when compressing individual PMCs from both control and PVF modified samples were collected, respectively.

4.3.4.1 Analysis of the force vs displacement data up to rupture of PMCs

A typical force vs displacement curve for compressing single PAC-PVOH perfume microcapsules to rupture is shown in Figure 4.9. Point A represents the starting point of the measurement when the force transducer (probe) begins to travel down towards the chosen particle. Point B is the starting point of the compression which corresponds to the initial contact of the probe with the microcapsule. Curve B-D corresponds to the microcapsule deformation until it was ruptured at point D, where the compression force reaches the highest, which is defined as rupture force. As a result of a quick energy release caused by the rupture of the microcapsule, the force quickly reduced to point E. Curve E-F is generated when the probe continues to compress the debris of the microcapsule until it touches the bottom glass surface, which induces a large force that triggers the system to terminate the measurement automatically at point F.

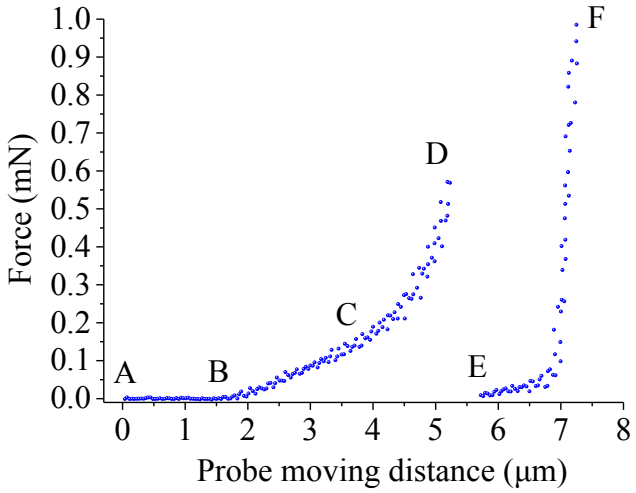

Figure 4.9 Representative compression force-displacement curve for compressing single PAC-PVOH perfume microcapsules in control sample (d = 9.7μm).

From the compression force-displacement curve, it is possible to identify the elastic and plastic regions to determine several intrinsic material property parameters (Liu, 2010, Mercade-Prieto and Zhang, 2012), e.g. the elastic region (curve B-C) and a plastic region (curve C-D) (Mercadé-Prieto *et al.*, 2011). In the case in Figure 4.9, the microcapsule (with a diameter of 9.7μm) was from PAC-PVOH control sample, lot# PDS091714B. To calculate the mechanical properties, the actual compression force-displacement of the capsule was obtained by removing the none-compression stage A-B on the curve. Therefore, the actual compression went through an elastic region up to about 1.7μm displacement and the microcapsule was ruptured at around 3.4μm. The calculated elastic limit is approximately 18% nominal deformation defined by the ratio of the displacement to initial diameter and the nominal deformation at rupture was 35%.

In the elastic region, a microcapsule can fully recover to its original shape after the external force is removed. In this project, for the flow chamber used, the maximum wall shear stress was set to be less than 1.0 Pa (corresponding to a flow rate of 20.7mL/min).

Under such condition, for a microcapsule with a typical diameter of 20μm which is deposited on the film attached to the chamber wall, the shear force applied by the fluid would be approximately 0.3nN. The Young's modulus at elastic range for the capsule is about 1.5GPa. When using AFM to measure adhesion of single PMCs to a substrate, the maximum compression force was set to be 20nN. From Figure 4.9, the force at the elastic limit is nearly 0.1mN, which is significantly greater than all the forces experienced by PMCs in the flow chamber and AFM measurements. Therefore, the PMCs are considered to experience only elastic deformations in such experiments.

4.3.4.2 Mechanical strength of PAC-PVOH microcapsules

The rupture stress nominalized by the contact area when microcapsule ruptures reflects the nature of the microcapsule's intrinsic physical properties (Sun and Zhang, 2002, Liu, 2010). However, the contact area at the rupture is not known unless a sophisticated finite element analysis is applied (Mercade-Prieto *et al.*, 2011, Mercadé-Prieto *et al.*, 2012), which is beyond the scope of this project. Therefore, the nominal rupture stress defined by the rupture force normalised by the initial cross-sectional area was calculated instead, which may be used to compare the relative mechancal strenghths of different microcapsule samples. Figure 4.10 shows the nominal rupture stress data for two control samples from different production batches made using the same formulation and processing conditions, which look consistent and there is no significant difference between them.

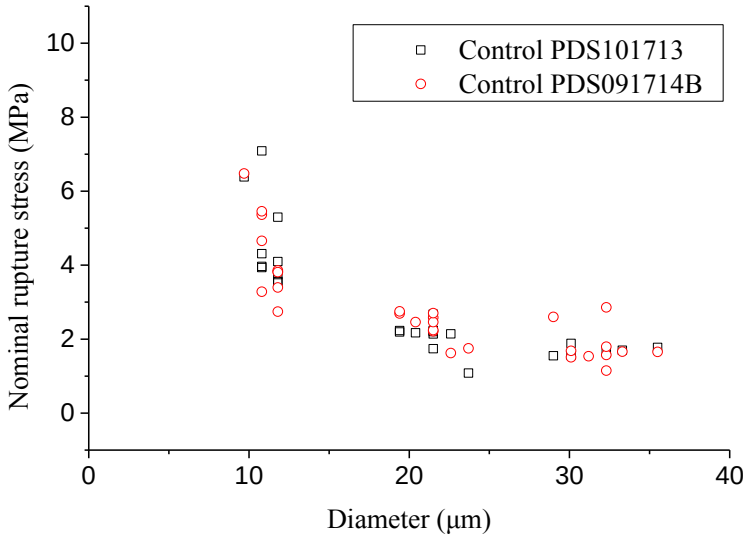

Figure 4.10 Nominal rupture stress vs diameter data for 2 control PAC-PVOH microcapsule samples from different batches made using the same formulation and processing conditions.

The nominal rupture stress versus diameter for a control sample modified by 0.25% PVF shows similar trend to the control sample (Figure 4.11). The mean nominal rupture stress values for the two control samples and one PVF modified PAC-PVOH microcapsules are compared in Figure 4.12. Using one-way analysis of variance (one-way ANOVA) with confidence level of 95%, the p-values of all three size bands are greater than 0.1 respectively. Therefore, it is concluded that no significant difference among the 3 samples, which means the PVF modification had no significant impact on the mechanical properties of the PAC-PVOH microcapsules.

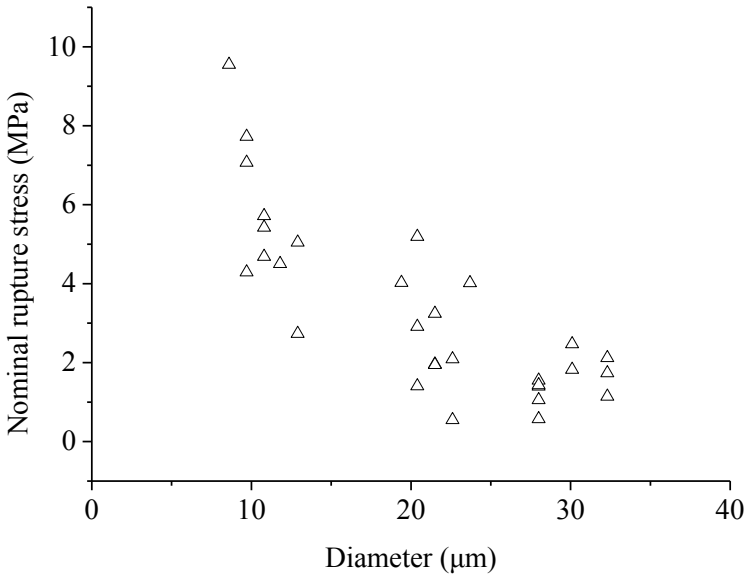

Figure 4.11 Nominal rupture stress vs diameter data for 0.25% PVF modified PAC-PVOH microcapsule sample (Batch# PDS091714B-PVF).

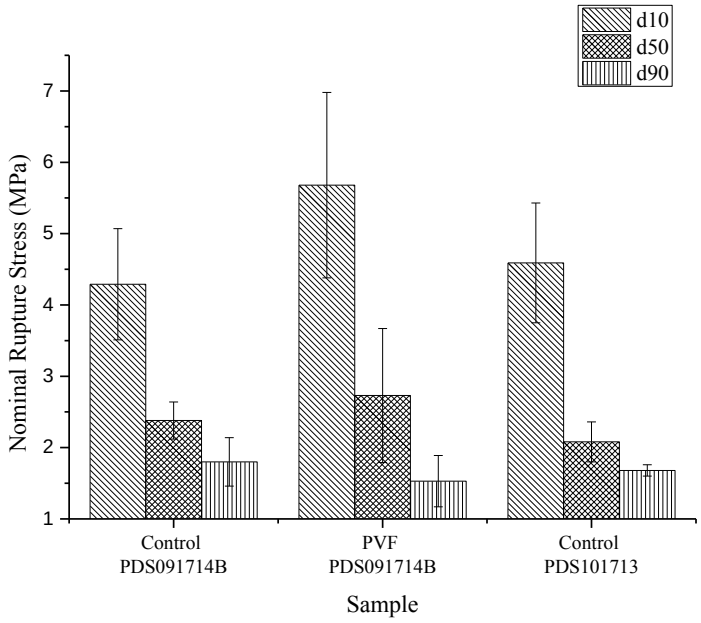

Figure 4.12 Mean nominal rupture stress of two control samples and one PVF modified PAC-PVOH PMC sample in all three size bands. The error bar represents the standard error.

4.3.5 Surface charge of PMCs in aqueous suspension

Zeta Potential analysis results (mean value of 3 measurements, each measurement lasted for 30s) of control PAC-PVOH PMCs (batch# PDS091714) and the corresponding 0.25% PVF modified microcapsules (batch# PDS091714B-PVF) at varying pH are shown in Figure 4.13. Overall, the zeta potential of both control PAC-PVOH microcapsules and PVF modified ones dropped as pH increased. It is also clear that the control PAC-PVOH microcapsules remained negatively charged through the tested pH range, whilst the PVF modified PAC-PVOH microcapsules kept positively charged. The changes of the absolute zeta potential values for the control and PVF modified samples from pH 3 to pH 11 were 3.78mV and 11.89mV, respectively. These data suggest following results:

(1). The surface charge of the control PAC-PVOH microcapsule shell did not change much with pH in the aqueous solution with low concentration of a strong electrolyte salt (in this case 580ppm NaCl).

(2). The PVF polymer interacted with PAC-PVOH microcapsule surface even at a low concentration of PVF (in this case 0.25wt.%) and modified the surface property from negative charge to positive charge in a range of pH 3 - 11.

(3). Although the microcapsule sample maintained the overall positive charge, there was a significant drop of absolute zeta potential from pH 3 to 11, which could be due to some of the amino groups in the PVF molecular backbone being neutralised by increasing pH. This indicated that the PVF modification of the PAC-PVOH microcapsule surfaces made the particle surfaces more sensitive to pH change.

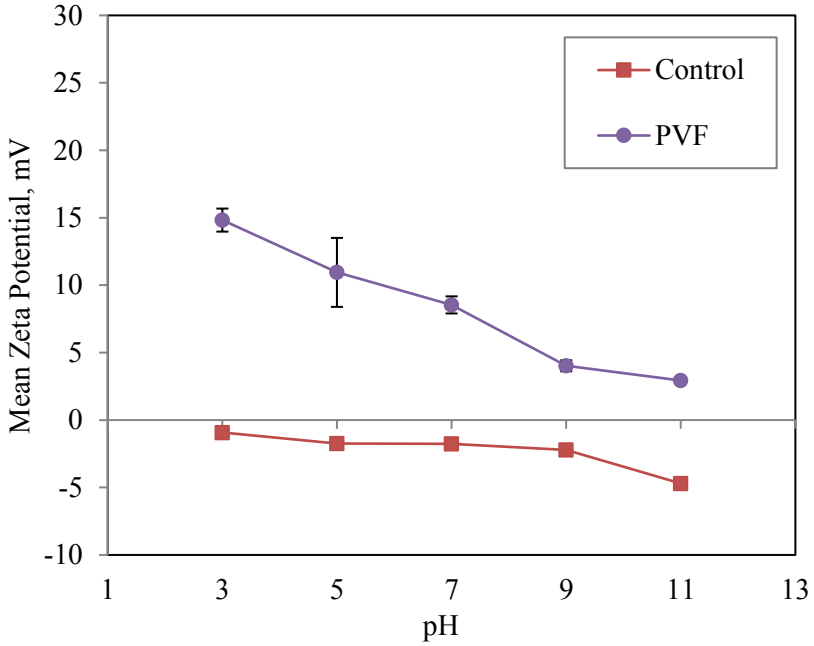

Figure 4.13 Mean (N = 3) Zeta potential of control PAC-PVOH microcapsules (Batch# PDS091714) and the corresponding 0.25% PVF modified microcapsules (Batch# PDS091714B-PVF) in 0.01M (580ppm) NaCl solution at varying pH. The error bar represents the std. error of the mean.

4.4 Adhesion between single PVF modified PAC-PVOH PMC and model fabric films in DI-water measured using AFM

4.4.1 AFM force measurement

AFM force measurements were conducted to study both attractive and adhesive properties between single PAC PVOH PMCs (either control or PVF surface modified) and a model fabric film. The surface roughness results from §4.2.1 for model fabric films, and SEM images from Figure 3.8 and §4.3.2 for microcapsules proved that both sample surfaces were relatively smooth and suitable for such measurements. Because the cantilever deforms once it bears a bending force, the real distance between microcapsule and target film surface cannot be always the same as the moving distance

of the cantilever. Based on this, the displacement data was adjusted by subtracting the deflection of the cantilever calculated from force data and cantilever spring constant. Therefore, a force-distance curve with force data vs the adjusted displacement which represents the real distance between the microcapsule and the PET film surface is obtained.

Figure 4.14 (a) (partially enlarged in b) shows a typical force measurement cycle between a non-surface modified (control) PAC-PVOH microcapsule and PET film in DI-water. The microcapsule in the control sample used in this measurement had a diameter of 18.5μm. The "Force" data are the calculated results from the electrical readings of AFM whilst the "Displacement" represents the distance between the microcapsule and the PET film surface. Combined with the schematic AFM force measurement principle (Figure 3.7) and literature results (Liu *et al.* (2013) He (He, 2013), Figure 4.14 is also used to explain the detailed procedures of the measurement between a single microcapsule and model fabric film surface.

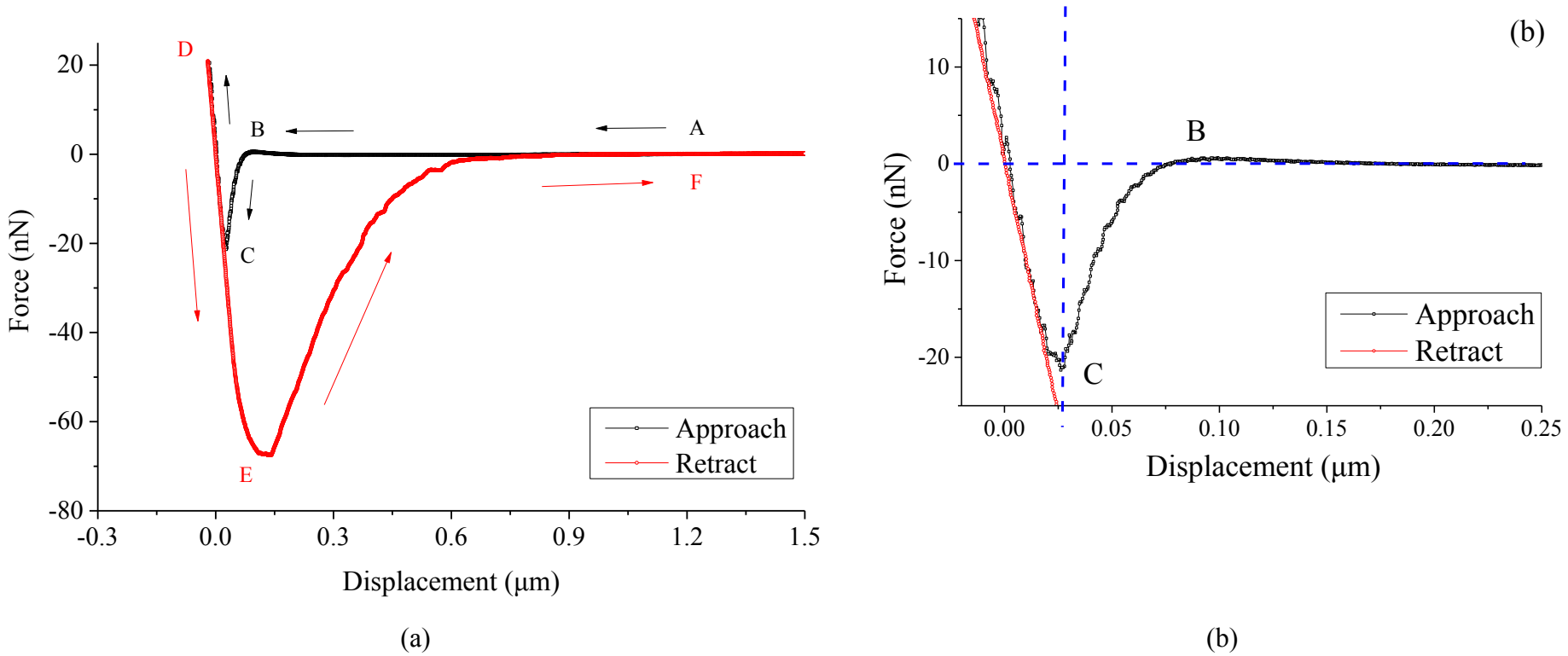

(a) (b)

Figure 4.14 A typical AFM force measurement cycle (a) between a control microcapsule with diameter of 15.8 μm and a model PET film in DI-water. (b) is the enlarged area of curve B-C to show more details. Point A and F represents the beginning of approach and end of retract curves respectively. Point D is the maximum compression force applied by the AFM cantilever to the microcapsule. Point B, C and E represent force peaks of repulsion, attraction and adhesion between the microcapsule and PET film respectively during the measurement.

First, the cantilever with one single microcapsule glued as colloidal probe was taken by the z-piezo to approach from a relatively far displacement (point A, which was more than 3μm away from the substrate in this measurement) towards the target PET fabric film surface. When the microcapsule approached to less than 200 nm displacement from the PET film, the repulsive force dominated the interaction for a short moment until point B (about 90 nm away from PET film surface). After that, a strong attractive interaction began to occur, pulled the microcapsule and bent the cantilever towards the film surface which resulted in the microcapsule quickly "jumping" to touch the film (point C). As the z-piezo continued to drive the cantilever towards the PET film, the elastic deformation of the cantilever was released gradually to zero and it then started to compress the microcapsule against the PET film (curve from C to D). The compression continued until the force reached a pre-set value at point D (20nN in this case) where the z-piezo stopped approaching process and started to retract the cantilever. Subsequently the compression force on the microcapsule started to decrease as the cantilever released its elastic deformation again. The applied force to the microcapsule became increasingly pulling as the cantilever continued to be retracted and started to pull the microcapsule away from the PET film surface. The retract force reached its highest peak at point E where the microcapsule bore the highest pulling force from the cantilever as well. At the same time, the elastic stretching of the microcapsule reached its peak and was equal to the adhesion force between the microcapsule and the film surface. Consequently, the microcapsule bounced and left the PET film surface at the next moment since the adhesive interaction could not compete with the retraction after point E. After that, the retract force gradually reduced to zero (point F) as any long-range interaction between the microcapsule and film surface decreased to zero and the cantilever recovered from its elastic deformation. The microcapsule returned to its

spherical shape and became further away from the film surface again. The force measurement was auto-stopped when the cantilever returned to its starting position and the AFM system moved on to the next measurement circle.

It is noted that the cantilever used in this experiment had a spring constant of about 2.5 N/m. This results in the cantilever being deformed to approximately 8nm and 24nm when the interaction force exceeds 20nN and 60nN, respectively. The scope of the cantilever deformation is considered insignificant comparing to the scales of the microcapsule size, the cantilever moving distance (both at magnitude of 10μm) and adhesive interaction distance (magnitude of 0.5 - 1μm). It should also be noted that the microcapsule is highly likely to undergo a compressive deformation through C to D and a tensile deformation during later pull-off stage (in later part of D to E) and be stretched upwards. Moreover, in above experiment, attractive forces dominated the interactions between the microcapsule and PET film during approaching process. Therefore, there is an attractive force peak (as point C) on the approach curve. However, in some cases, the repulsive force becomes dominant during the whole approaching process and it results in no force peak or inflection point on the approaching curve. Furthermore, the pattern of the force curves from point B through C, D and E to F is a complicated interactive result of a number of factors (Bowen and Doneva, 2000, Butt *et al.*, 2005, Götzinger *et al.*, 2007, He, 2013) which include:

1). Maximum compression force applied by the AFM cantilever.

2). Overall contact time between the microcapsule and film surface during the measurement process from C to E.

3). Surface properties of both microcapsule and model fabric film, such as roughness, charge and charge density (therefore static and dynamic electrical forces), surface coatings, hydrophobicity or hydrophilicity.

4). Molecular interactions when and after the microcapsule and model fabric film are in contact with each other, such as van der Waals force.

5). Environmental impacts such as capillary force in air, solvation forces and hydrodynamic forces in liquid conditions.

In order to obtain meaningful results from the force measurement and to study the key adhesive behaviours, a series of single-variable AFM measurements were designed. More details will be discussed in following sections and chapters.

4.4.2 Comparison of adhesion in ambient air and DI-water

It has been reported in literature that capillary force can dominate adhesion between micro-particles under ambient air condition when its relative humidity reaches a level above 40% (Jones *et al.*, 2002, Rabinovich *et al.*, 2002, Weeks *et al.*, 2005, van Honschoten *et al.*, 2010, Liu, 2010, Liu *et al.*, 2013, He, 2013). Therefore, AFM measurements were firstly conducted to compare adhesion of single microcapsules to a model fabric film in ambient air and in DI-water conditions.

In order to reduce variables, the AFM compression force was set to be 20nN with a contact time of 0.01s. Control PAC-PVOH microcapsules (batch# PDS060412), different PVF modified microcapsules in batch# PDS101713-PVF (modified with 0.25% Lupasol 9095) and Sample D (batch# PDS060412-D, modified with 0.5% Lupasol VT) were chosen for the experiments. The other parameters were the same as described in

§3.3.11.3. Multiple microcapsules in a sample were made into colloidal probe and each of them was measured under both air and DI-water conditions following the method described in §3.3.11.3. As the adhesion between microcapsules and model fabric films is of most interest in this project, the forces during retraction were analysed and the results are presented in Figure 4.15. Because the sizes of the microcapsules were different, the force data are nominalised by the diameter of the related microcapsule.

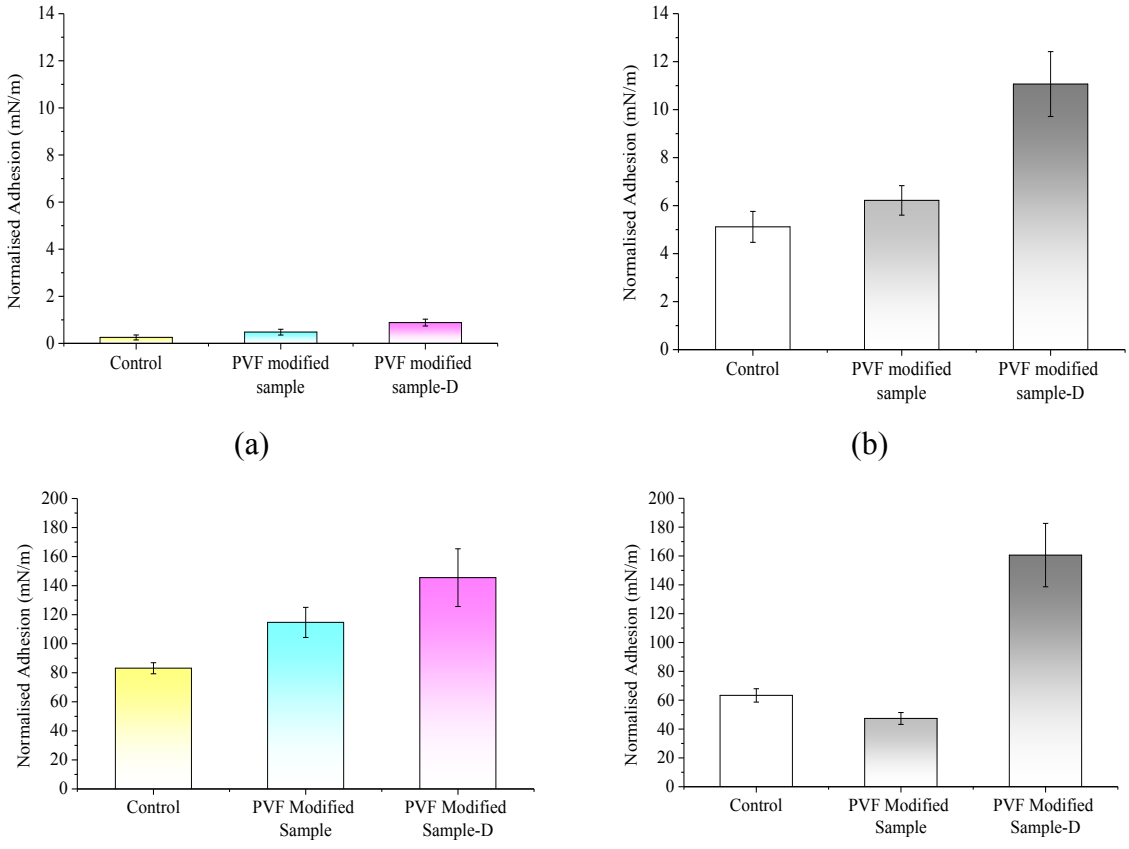

Figure 4.15 Comparison of mean normalised adhesion of single microcapsules on model cellulose film (a, c) and PET film (b, d). (a) and (b): in DI-water condition. (c) and (d): in ambient air condition. For control sample (batch# PDS060412), n (number of microcapsules measured) = 4; for PVF modified sample (batch# PDS101713-PVF), n = 6; For PVF modified sample D (batch# PDS060412-D), n = 2. The compression force was set to be 20nN with 0.01s contact time. The error bar represents the standard error of the mean.

It can be calculated from the data in Figure 4.15 that, in ambient air condition, the ratios of the values of normalised adhesion of microcapsules to cellulose film (Figure 4.15 (c)) to those to PET film (Figure 4.15 (d)) are 1.3, 2.4 and 0.9 for control sample, PVF modified sample (batch# PDS101713-PVF) and PVF modified sample D (batch# PDS060412-D), respectively. This indicates the measured values of normalised adhesion of the same microcapsules to both films are similar in ambient air condition. However, such ratios decreased to 0.05, 0.08 and 0.08 corresponding to DI-water condition (Figure 4.15 (a) and (b)) for the same samples, respectively. It is also noted that the mean normalised adhesion values are more than 100 times greater in ambient air condition, than those in DI-water condition for all the microcapsule samples interacting with the cellulose film; such forces are about 8-10 times greater for the PET film in ambient air condition than the ones in DI-water condition.

In DI-water, since all the samples and film substrates are immersed in water, no capillary force exists (Butt and Kappl, 2009). Therefore, above data confirm the reported results that the capillary force resulting from water vapour between single microcapsules and a model fabric film was so strong that it dominated the measured adhesion in ambient air condition. In consequence, the difference in measured adhesions between single microcapsules to the cellulose or PET film is more obvious in DI-water condition to reflect the real difference of the adhesive interactions caused by the two substrates. Moreover, understanding the adhesion and its impact on microcapsule deposition / retention on fabric surface immersed in water is the main objective of this project. Hence, all the following AFM force measurements in this study were conducted in aqueous condition.

Combining the AFM data in Figure 4.15 and the sample information in Table 3.1, one can conclude that PVF modification with Lupasol® VT (sample D) could be better than Lupamin® 9095 modification in enhancing the adhesion of PAC-PVOH microcapsules to either cellulose or PET model fabric film, which was probably due to a greater amount (by 100%) of polymer used in the former modification than the later. In order to investigate the real difference made by both PVF polymer modifications, a comparison of both 0.25% of Lupamin® 9095 and 0.25% Lupasol® VT modified PAC-PVOH microcapsule samples were conducted and will be discussed in later sessions.

4.4.3 Effect of compression force on adhesion measured by AFM

Hooke's law (Murnaghan, 1944) suggests that the stress on a material is proportional to its strain within its elastic range. In addition, the DMT-JKR contact model and a number of other models (Johnson and Greenwood, 1997, Schwarz, 2003, Grierson *et al.*, 2005, Barthel, 2008, Popov, 2010) suggest that adhesion between an elastic microcapsule and a flat surface is proportional to their contact radius. Therefore, during AFM measurement of single microcapsules on a model fabric film, a series of compression forces were applied to the model fabric films to choose appropriate compression force which can be used for later AFM studies. Since the surface of microcapsules in the control sample was smooth, they were used to investigate the effect of compression force on the adhesion. Figure 4.16 shows the normalised adhesion versus compression force of a microcapsule (22μm) from a control sample to both cellulose (a) and PET (b) films in DI-water.

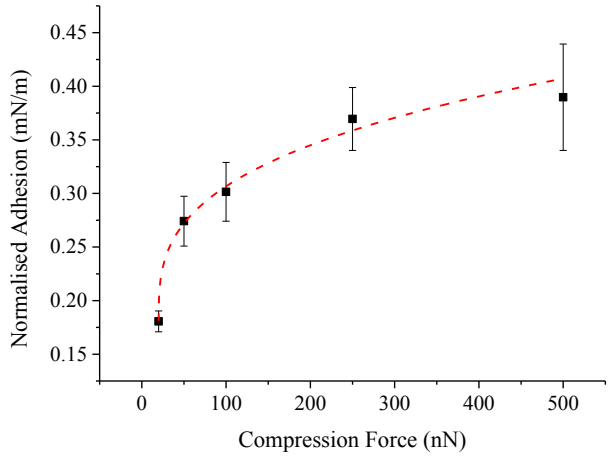

(a)

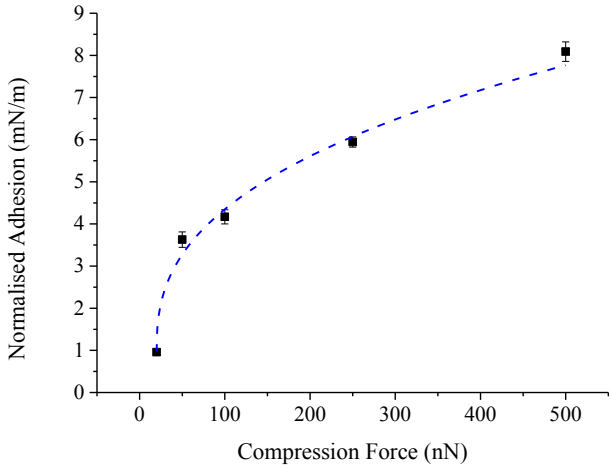

(b)

Figure 4.16 Mean normalised adhesion of a single microcapsule (22μm) in control sample (Lot# PDS091714B)) to both model cellulose (a) and PET (b) films in DI-water. The contact time was set to be 0.01s. The short dash curves represent the trend. Error bar represents the standard error of the mean.

It is clear from the data that the normalised adhesion to each film continuously increases with compression force, which might result from that higher compression force causes bigger contact area between the microcapsule and the substrate, leading to greater adhesion. Nevertheless, if a large compression force were applied, the AFM cantilever

used should be very stiff. In this case, the force measurement system may not be sensitive enough to detect very small force from molecular interactions. Thus, though the elastic range of the microcapsule could be up to around 0.1mN (results from §4.3.4.1), the AFM compression load was fixed to be 20nN for all the later AFM measurements in this project.

4.4.4 Effect of contact time on adhesion measured using AFM

The normalised adhesion between a microcapsule (22μm) in a control sample to both cellulose (a) and PET (b) films for contact times from 0.01s to 30s and a constant compression force of 20nN are shown in Figure 4.17.

According to Figure 4.17, the normalised adhesion increases with contact time up to 10s and then becomes almost flat. This means that the interaction between a microcapsule and the model fabric films may have reached equilibrium after their contact for 10s. Therefore, for practical reasons, the contact time in later AFM measurements were chosen at both 0.01s and 10s to analyse the influence of short and long time interactions, respectively.

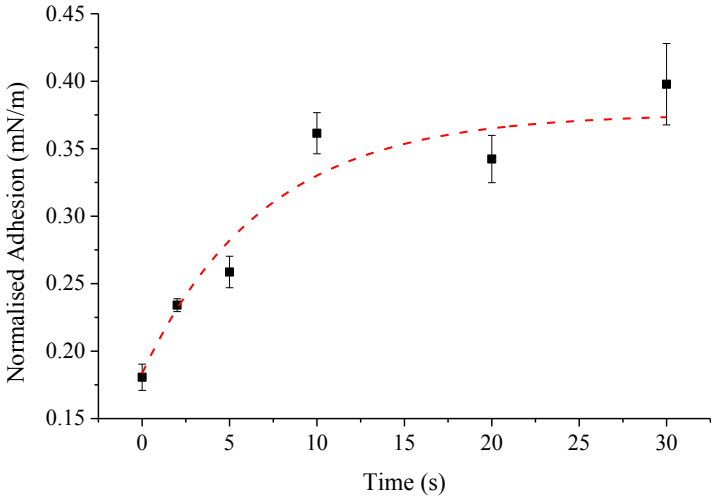

(a)

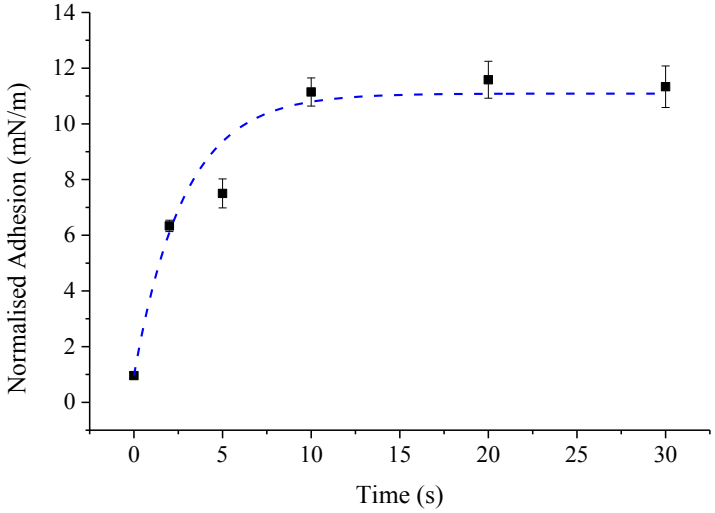

(b)

Figure 4.17 Mean normalised adhesion of a single microcapsule (22µm) from a control sample (Lot# PDS091714B) to both model cellulose (a) and PET (b) films in DI-water measured by AFM. Compression force was set to be 20nN. The short dash curves represent the trend. The error bar represents the standard error of the mean.

4.4.5 Adhesion measurement results of single PVF modified PAC-PVOH microcapsules to model fabric films in DI-water

Figure 4.18 shows the normalised adhesion data for PAC-PVOH PMCs from a control sample and three PVF modified samples to both cellulose (a) and PET (b) films in DI-

water with a contact time of 0.01s. Clearly, the three PVF modifications enhanced the adhesion of the PAC-PVOH microcapsules to the two films at this short contact time; the two samples modified by Lupasol® VT showed the most significant improvement in adhesion among all.

Figure 4.19 presents mean normalised adhesion data of control and PVF modified (0.25% Lupasol® VT) microcapsules to both cellulose (a) and PET (b) films with a contact time of 10s. The overall increase of the normalised adhesion after extending the contact time from 0.01s to 10s for both control and PVF modified microcapsules is consistent with what was found by He (2013). It is noted that PVF modified microcapsules resulted in a similar normalised adhesion as non-surface-modified control sample did in this test condition on both model fabric films, respectively. This phenomenon indicates that there may be similarity in the adhesive interactions of non-surface modified and surface modified microcapsules on both model fabric films in DI-water.

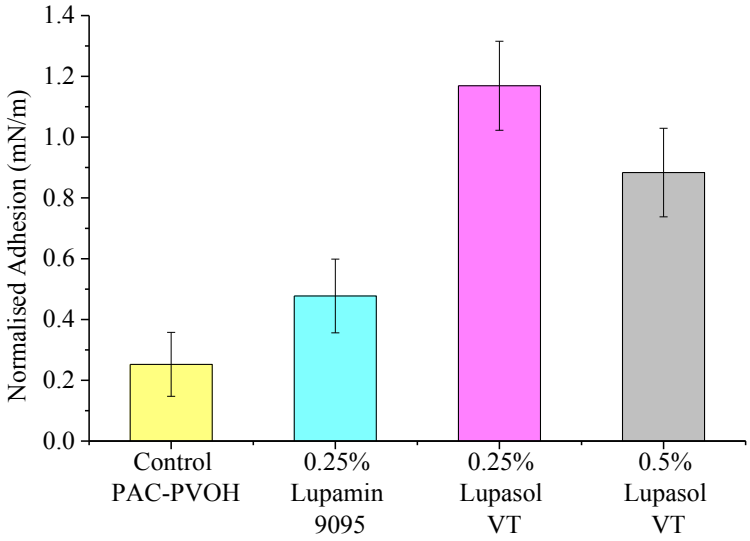

(a)

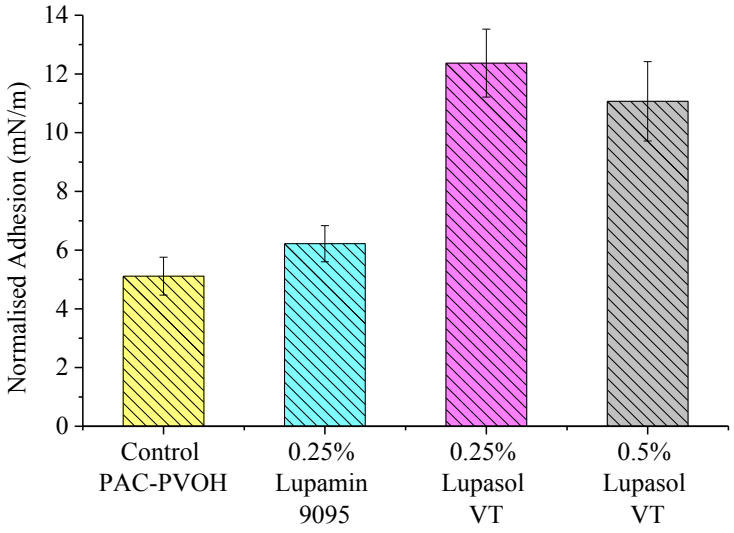

(b)

Figure 4.18 Mean normalised adhesion comparisons of control PAC-PVOH (N=6) and three PVF modified microcapsules (n=6 for PDS101713-PVF, modified with 0.25% Lupamin® 9095; n=4 for PDS091714B-PVF, modified with 0.25% Lupasol® VT; and n=2 for PDS060412-D, modified with 0.5% Lupasol® VT) to both model cellulose (a) and PET (b) films in DI-water with a contact time of 0.01s using AFM. The error bar represents the standard error of the mean.

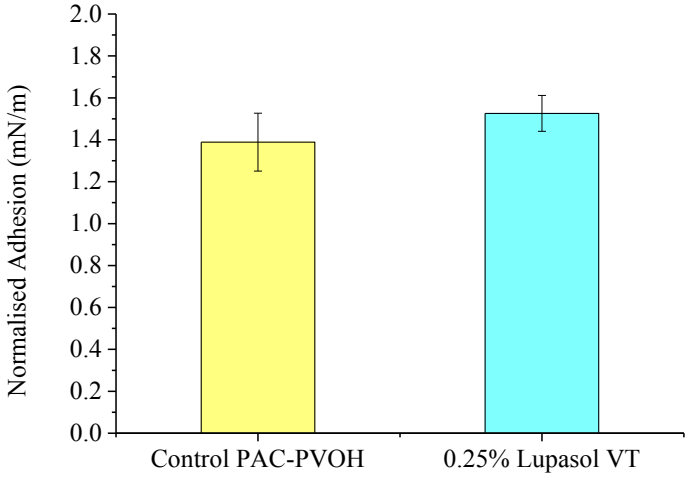

(a)

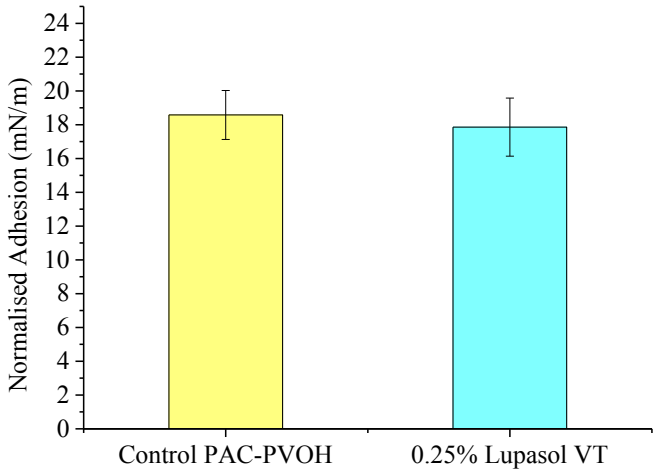

(b)

Figure 4.19 Mean normalised adhesion of control (n = 6) and PVF modified microcapsules (batch# PDS091714B-PVF, 0.25% Lupasol® VT coating, n = 4) to both model cellulose (a) and PET (b) films in DI-water with a contact time of 10s. The error bar represents the standard error of the mean.

4.5 Discussion: factors to impact on adhesion in DI-water condition

Because only DI-water condition was used in the AFM analysis of adhesive interaction in this chapter, surface properties of model fabric films become important when considering the factors to impact on adhesion.

The Young's modulus and Poisson's ratio of glass substrate are reported 70GPa and 0.23 (Akhtar *et al.*, 2009), respectively. Assume a microcapsule with diameter of 20μm, the Young's Modulus is about 1.5GPa according to §4.3.4.1. The Poisson's ratio is assumed to be 0.5 (Liu, 2010), the adhesive energy to be around 100μJ/m^2 (Liu, 2010, He, 2013) and the equilibrium separation to be 3Å (Tabor, 1977). Following Equation 2.7 and Equation 2.10, the calculated Tabor parameter is 0.1. Therefore, DMT model has been used to calculate the contract radius of the microcapsule on model fabric surface. Using maximum compression force 20nN and Equation 2.9, the calculated contact radius is 46.6nm.

4.5.1 Surface roughness

Comparing to the 7 ~ 37μm size (from the particle size distribution data in §4.3.1) of the PMCs used in this research, both RMS surface roughness data of 100 – 200nm from §4.2.1 suggest that commercial model cellulose and PET films may be relatively smooth. Moreover, cellulose film does have almost twice the RMS surface roughness of PET film in ambient air according to the experimental results in §4.2.1. As suggested by a number of researches that an increase of surface roughness results in a decrease of solid-solid adhesion (Fuller, 1975, Rabinovich *et al.*, 2000, Peressadko *et al.*, 2005, Rumpf, 2012), it is highly likely that the adhesion of a microcapsule on cellulose film

surface may be smaller than PET film surface. Furthermore, since cellulose film is hydrophilic and PET film is hydrophobic, when in contact with liquid water, molecules on cellulose film surface swell and stretch into water phase (Cuissinat and Navard, 2006b, Osterberg and Claesson, 2000) whilst PET molecules keep packing closely on the surface (Ellison and Zisman, 1954). Consequently, molecules on the surface of cellulose film may have more mobility than those on PET film surface in aqueous conditions. This may result in a further increase of the surface roughness of cellulose film than that of PET film thus less adhesion achieved of PMCs on to cellulose film. As RMS surface roughness is calculated by mean values, the actual maximum peak-valley difference on the surface could reach 1-2μm. From the size distribution chart in Figure 4.6, there are a small portion (about 2%) of microcapsules in the size range of 1-6μm which are likely to be impacted by the RMS roughness of both film surfaces during analysis. However, due to the limitation of this project, there is no introduction of further methods either in cleaning of the samples or in post-analysis of the image data from flow chamber tests to reduce the roughness impact on the particle size.

According to the surface morphology in the ESEM images from §4.3.2, the surface of control PAC-PVOH microcapsules should be very smooth (at nanometre scale). Although the surface of PVF-modified microcapsule could be more uneven possibly because of the tiny particles (at about sub-micrometre scale from the images) attached to its surface, the increase of the surface roughness versus the control sample should be limited since the particle still keeps clear in most of the surface areas. However, this difference could contribute to the instability of adhesive interactions of PVF-modified samples and cause larger variations in the AFM single particle adhesion measurement.

4.5.2 Surface charge and charge density

4.5.2.1 Surface charge and charge density of model fabric films in DI-water

As mentioned in §2.2.1.2, because of the oxidising manufacturing process in wood pulp or cotton cellulose, the surface of model cellulose film has great possibility to contain a considerable amount of carboxyl () end groups together with the vast majority of hydroxyl (-OH) groups. In contrast, PET film surface is dominated by ester (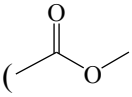) and phenyl (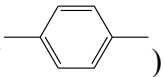) groups with a small amount of hydroxyl end groups mentioned in §2.2.1.4. Consequently, in DI-water, a number of deprotonation process take place on carboxyl groups and a large amount of hydrogen bonding form which makes the molecules on cellulose surface interact with water molecules. As a result, both electrostatic and steric repulsions push the cellulose surface molecules stretched into water phase (Liu, 2010, Israelachvili, 2011). However, only limited number of hydrogen bonding forms on PET film through the interaction between hydroxyl groups and water molecules; majority PET molecules and the hydrophobic functional groups remain inactive and densely packed on the surface. Therefore, cellulose film surface behaves much more hydrophilic whilst PET film hydrophobic. The charge of both films is overall negative with a relatively high charge density on cellulose film surface versus PET film.

As the model film surfaces are the substrates of the adhesion interactions being interested in this project, their charge and charge density variations may have significant influence on the approach and deposition steps of a microcapsule through electrostatic interactions. However, once a microcapsule gets close enough and contacts with the film, the charge and charge density of both parts may change due to electrical

neutralisation including any chemical bonding formation (ion pairing, etc.), molecule rearrangement caused by steric interactions and surface material / molecule exchanging. Therefore, adhesion and adhesion energy are dependent on the combined interactive results of a number of factors such as van der Waals force, contact mechanics, surface properties of both microcapsule and model film (Burnham *et al.*, 1992, Meyer *et al.*, 2005). Thus, the original surface charge and charge density on both model film surfaces may be less important during adhesion and separation stages between a microcapsule and the film surface involved. As it is practically difficult to accurately measure such change in charge and charge density before and after the contact of a microcapsule and a related model film surface, no further analysis was done to quantify this parameter on either film.

4.5.2.2 Surface charge and charge density of PVF modified PMCs in DI-water

Microcapsules are the counter part of the concerned adhesive interactions in this project. Despite PAC-PVOH PMC shell contains an amount (detailed number not disclosed) of amino groups from the patent description by Schwantes and Sands (2010), the overall charge of the PMC shell is slightly negative according to the Zeta potential results of aqueous condition through the pH range of 3 – 11 from §4.3.5, which indicates that the total number of amino groups on the surface of the PAC-PVOH PMCs is relatively small comparing to the amount of negatively charged groups. This is further confirmed by the AFM approach curves from the adhesion measurement (Figure 4.20) that when a control PAC-PVOH PMC approached to cellulose film surface, repulsive behaviour was observed as a result of identical negative electrostatic force from both parts. Moreover, upon contact for a short time of 0.01s (Figure 4.18 (a)), the electrostatic interactions of

the molecules of both control PMC shell and cellulose film surface are also limited due to the electrostatic repulsion. Only when the contact time are long enough (Figure 4.19 (a)) based on the result of Figure 4.17 (a), the increased adhesive interaction was detected (about 1.3 - 1.4mN/m) which reaches the similar magnitude of those of PVF modified ones in both short and long time contacts. However, as mentioned in §4.5.2.1, the result of long time contact may be the result of other complex interactions such as van der Waals force, surface properties of both microcapsule and model cellulose film.

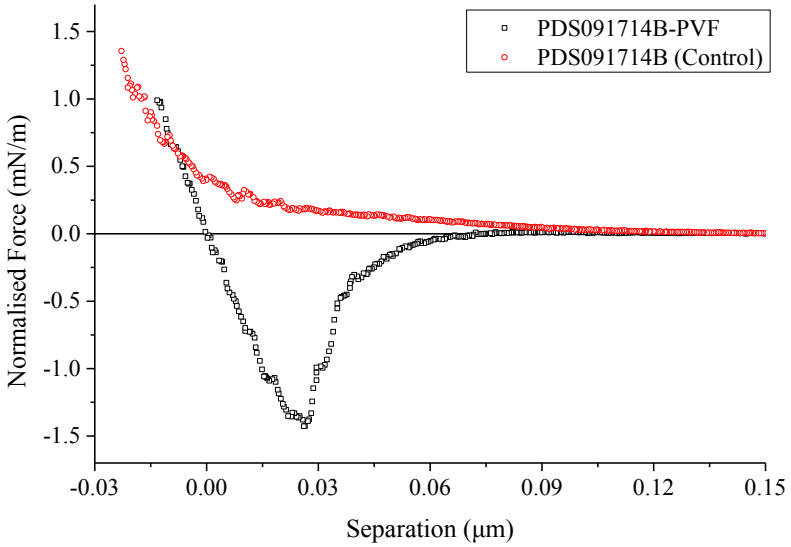

Figure 4.20 Typical force curves when PMCs approach to model cellulose film in DI water obtained using AFM.

On the contrast, PVF (Lupasol® VT) modified PMC is positively charged in water through the pH range of 3 – 11 from Zeta potential results from §4.3.5. The attractive force detected using AFM in the approach force curve of PVF modified microcapsules towards both model fabric films (Figure 4.20 and Figure 4.21) further confirmed this. In

addition, it is noted that in short contact time (Figure 4.18, Lupasol® VT samples), the detected adhesion is similar to that of long contact time (Figure 4.19) which indicates that the positive charged Lupasol® VT modification shortens the molecular interactive time to reach equilibrium from about 10s (control sample data from Figure 4.17) to less than 0.01s between PAC-PVOH PMC and the target model fabric surfaces.

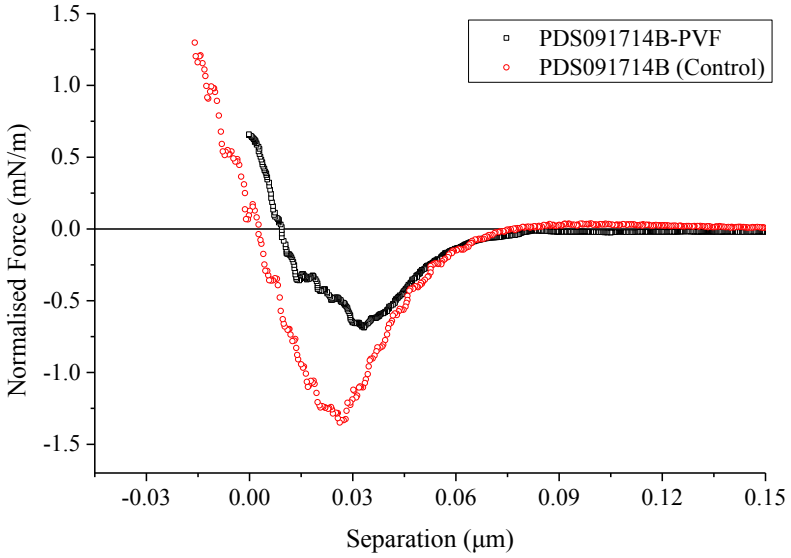

Figure 4.21 Typical force curves when PMCs approach to model PET film in DI-water obtained using AFM.

According to Table 3.2, the 1% Lupasol® VT in DI-water has a pH value of 3.5, which is significantly lower than that of other Lupamin® PVFs (typical values of 7 – 9). This confirms that Lupasol® VT polymer bears a number of weak acid functional groups which show weak negative charge when in aqueous condition. Combined with the Zeta potential results in §4.3.5, it can be concluded that Lupasol® VT has both active positive charge and negative charge centres on its molecules. In contrast, Lupamin® 9030 and 9095 are mainly composed of molecules with shorter chain length and positively charged functional groups only. Considering the surfaces of both model fabric films are

negatively charged (contributed by hydroxyl groups in cellulose film and ester groups in PET film), the positive charges of all PVF polymers make them more attractive when approaching and interacting when getting in contact with the target fabric films in aqueous condition. Moreover, the property of less positive charge centres on Lupasol® VT molecules does not prevent neither its coating on PAC-PVOH PMCs nor the ability to enhance the adhesion between the microcapsules and model fabric films. This indicates that the polymer molecular weight may be more influential than the molecular charge and charge density caused by the degree of hydrolysis for PVF modifications.

4.5.3 Surface hydrophobicity and hydrophobic interaction

Most literatures reported that hydrophilic surface of the cellulose film may attract and hold a thin layer of water by forming a considerable number of hydrogen bonds with water molecules when in an aqueous condition (Notley and Wagberg, 2005, He, 2013). This results in a physical hydrogel and may decrease the possibility of real contact with the microcapsules. On the other hand, a large amount of hydrophilic groups such as hydroxyl and amino groups from the shell material of the PAC-PVOH microcapsules, which can also attract a thin layer of water molecules and counter ions to form electrical double layer outside the microcapsule shell. All these hydrophilic interactions further reduce the overall adhesion between microcapsule and cellulose film in aqueous condition. However, as Medronho *et al.* (2012) reported that even with such a high level of hydrophilicity, a cellulose molecule is actually amphiphilic and the hydrophobicity in the molecular structure has a marked contribution to its nature of insolubility in water and most organic solvents. Thus, one can utilise the hydrophobicity to enhance the adhesion by introducing another similarly amphiphilic polymer to have hydrophobic

interactions with the cellulose molecules which swells and stretches into water phase when the cellulose film gets into aqueous solution. PVF, notably Lupasol® VT as introduced in §3.1.2.2, is one of such polymers. According to Table 3.2, with a higher mean molecular weight (about 2000k Da) and lower degree of hydrolysis (20%), Lupasol® VT is overall much larger in chain length comparing to the other Lupamin® types, bearing a relatively lower level of amino functional groups but a larger level of amide ones. It is known that in general, increase of molecular weight and decrease of the degree of hydrolysis both result in the increase of hydrophobicity of a polymer (Biggs *et al.*, 1993). This implies that Lupasol® VT may be partially hydrophilic to stretch itself in aqueous condition and form hydrogen bonds (He *et al.*, 2014), simultaneously partially hydrophobic to be able to have hydrophobic interactions when approaching and contacting cellulose fabric film to enhance the adhesion.

In contrast to cellulose film, PET film showed high level of SFE and very low polar energy in contact angle measurements (§4.2.3) which indicates it has strong hydrophobicity. When PET film is about to get contact with PAC-PVOH microcapsules in aqueous condition, polar molecules such as water molecules segregate from the space in between of both solid surfaces due to hydrophobic effect to minimise the contact surface area of polar phase to nonpolar phase thus to minimise liquid-solid SFE (Silverstein, 1998). The effect results in the long range hydrophobic force which is normally larger than the van der Waals. Figure 4.21 shows a control PMC was attracted other than repelled when it approached the model PET film in DI-water which indicates the hydrophobic force is even larger than the electrostatic repulsive force in this case. Based on above, it is highly possible that real contact was established between microcapsules and PET film in DI-water condition. Furthermore, during the process of microcapsule being pulled away from the PET film, water molecules are resisted to get

into the space created by the pulling off. All these factors consequently result in the increase of the adhesion between PMC (regardless of surface modified or not) and model PET film.

4.6 Conclusions

1. The characterisation results of both model cellulose and PET films were comparable with those of self-made fabric films (Liu, 2010, He, 2013). They also proved that the surface properties of both commercially available cellulose and PET films were similar to those of real cotton fabric and polyester fabric surfaces, respectively. Therefore, these commercial fabric films with a relatively smooth surface can be used not only to replace the self-made ones to save researcher's time and effort but also to mimic real fabric to minimise the effect of surface asperity on the adhesion.
2. Analysis on the PVF modified microcapsules showed a successful coating of the polymers on the surface of the PAC-PVOH PMCs.
3. Micromanipulation measurements of the mechanical properties of single microcapsules demonstrated that all the PAC-PVOH PMCs were strong enough and suitable for all the further AFM studies, and the applied compression force and adhesion generated can only cause very small elastic deformations to the microcapsules.
4. Initial AFM force measurement confirmed the effectiveness of PVF polymer modifications on PMCs in enhancing their adhesion to the two model fabric films in DI-water. Among the PVF polymers investigated, the one with high MOLECULAR WEIGHT and low degree of hydrolysis, i.e. Lupasol® VT with 2000 kDa and 20% hydrolysis rate, was found to be most effective in enhancing the adhesion, meaning

the surface modification of interest may need to be made by a positively charged polyelectrolyte with a reasonably large molecular weight and relatively low charge density.

5. Mechanism investigation in DI-water revealed that adhesion of PMC to model cellulose film may be influenced largely by electrostatic interactions of both film and PMC surfaces whilst adhesion of PMC to model PET film being dominated by hydrophobic interactions.

Chapter 5. Investigation of adhesion behaviour of surface modified PAC-PVOH microcapsules on both cellulose and PET films

5.1 Introduction

The work in this chapter mainly focuses on the mechanism understanding of the adhesion of PMCs to the model fabric films. Since screening different polymers is one of the purposes of this research, chitosan, as one of natural polymers which has been found in the shells of crustaceans and many other organisms including insects and fungi, was introduced to the surface modification of perfume microcapsules. Subsequently, the same analytical tools such as ESEM and Zeta Potential Measurement System in Chapter 4 were employed to characterise the effect of chitosan modification. A flow chamber and an AFM force measurement technique were also applied to measure the adhesion of the modified PMCs to model fabric films. Results were compared among non-modified control PMCs, chitosan and PVF-modified samples and further understanding of the deposition and adhesion mechanisms of surface modified PMCs on the fabric films have been developed in not only de-ionised (DI) water, but also in conditions with more environmental variables including hardness and surfactants. The surface properties of the modified PMCs in different environmental conditions are discussed and mechanism of their adhesion to target model fabric film surfaces is proposed.

5.2 Characterisation of chitosan-modified PAC-PVOH PMCs

The chitosan used for the modification in this project has a mean molecular weight of 50k Da and 75~85% (mol. %) degree of deacetylation. Since chitosan modification was achieved through the similar way to PVF modification which was made by dissolving the chemical and gentle mixing with the microcapsule slurry at 0.25% weight ratio, similar characterisations were applied to the modified PMCs.

5.2.1 Surface morphology by ESEM

Figure 5.1 presents the ESEM images of 0.25% (w/w) chitosan modified PAC-PVOH perfume microcapsules in different magnifications. Comparing to the ESEM images of microcapsules in Figure 4.7, similar surface morphology to the one of the PVF-modified microcapsules was observed. From Figure 5.1 (b) and (c), a thin layer of substances can be observed at contacting areas between particles which blurs the edge. Similar to the case of PVF modification, this phenomenon indicates that chitosan polymer was successfully deposited, which modified the target microcapsule surfaces. Moreover, the chitosan coating shown in the ESEM images is so thin that it can hardly change the size and size distribution from the original microcapsules. Therefore, measurement of such parameters may show similar results to those in Chapter 4 on PVF modifications, which will not be discussed further in this chapter.

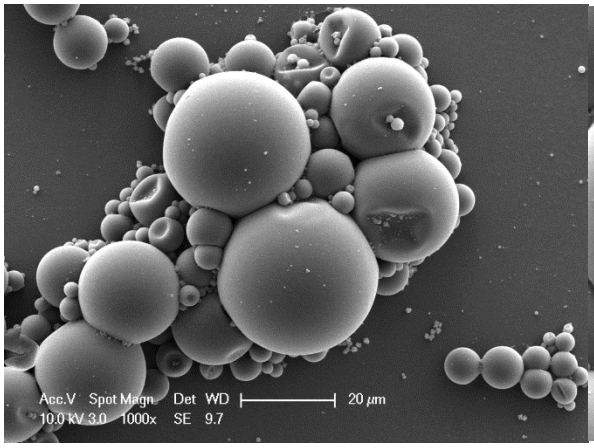

(a)

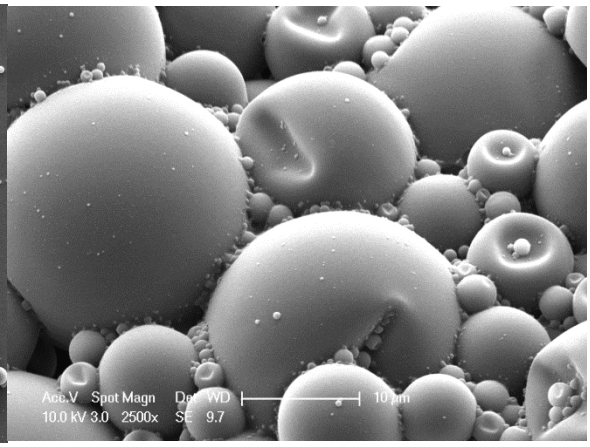

(b)

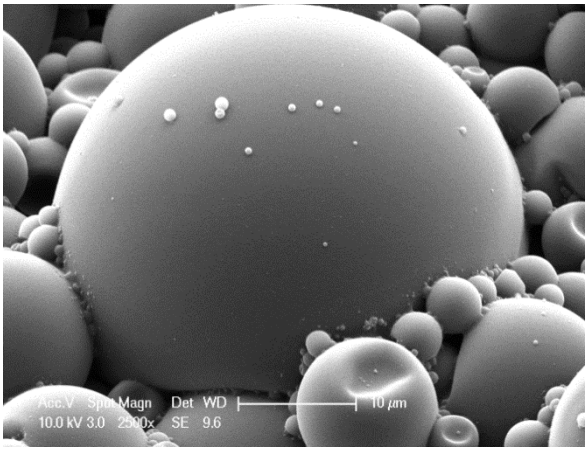

(c)

Figure 5.1 ESEM Images of 0.25% chitosan-modified PAC-PVOH microcapsules (Lot#PDS091714B-chitosan) at different magnifications.

5.2.2 Surface elemental analysis using SEM-EDX

Among the molecules related to the particle surface of chitosan-modified PAC-PVOH microcapsules, only chitosan molecule contains amide and amino functional groups in which the elemental content of nitrogen is around 8% (Yen *et al.*, 2009). Thus, N elemental analysis which was used in PVF polymer modification analysis was also applied to chitosan-modified PMCs to determine whether there is chitosan polymer

coating on the microcapsule surfaces. Therefore, SEM-EDX elemental scan was employed on the PMCs modified with 0.25% chitosan.

Representative SEM-EDX scan results of different areas are shown in Figure 5.2. (a) (b) and (e) (f) show a detective level of N element at the contact areas of microcapsules which indicates the chitosan modification to the PAC-PVOH microcapsules has been successful. However, in a larger scan area (Figure 5.2 (c) and (d)) which includes surfaces that were not in contact with any other microcapsules, no detection of N element was observed from the EDX measurement. Comparing the scan results in Figure 5.2, it can be concluded at 0.25wt.%, chitosan deposition has occurred on PAC-PVOH microcapsules but distributed unevenly on the particle surfaces.

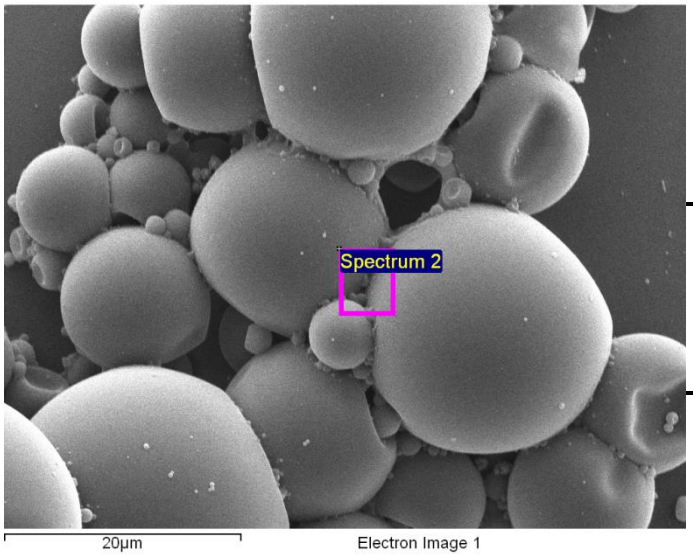

Element	Weight%	Atomic%
C	84.42	87.82
N	0.18	0.16
O	15.39	12.01
Totals	100	

(a)

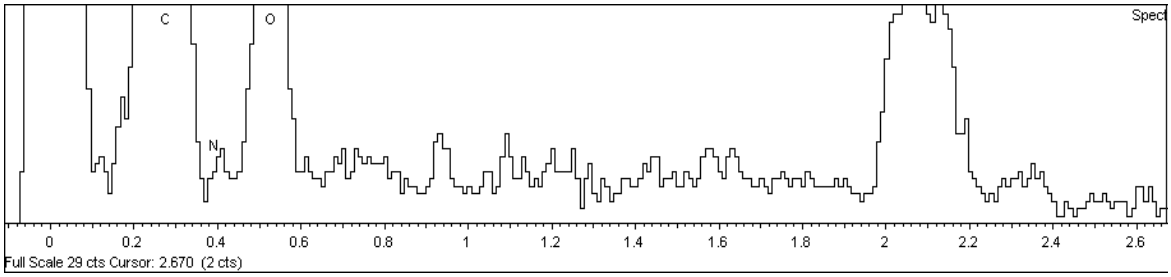

(b)

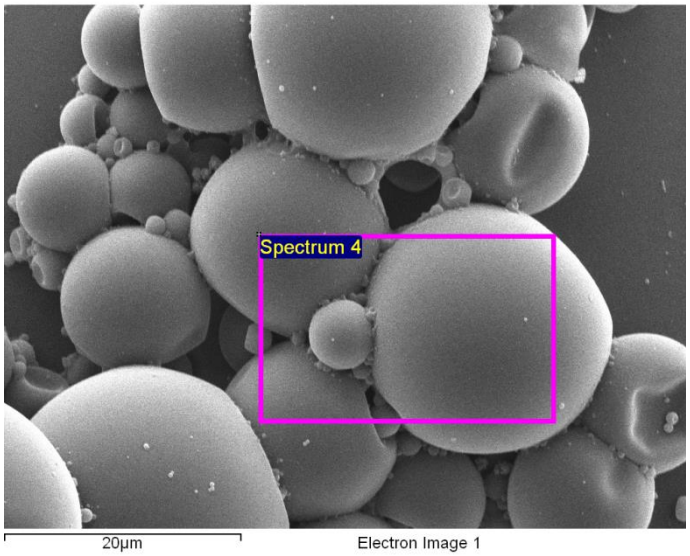

Element	Weight%	Atomic%
C	84.17	87.63
O	15.83	12.37
Totals	100	

(c)

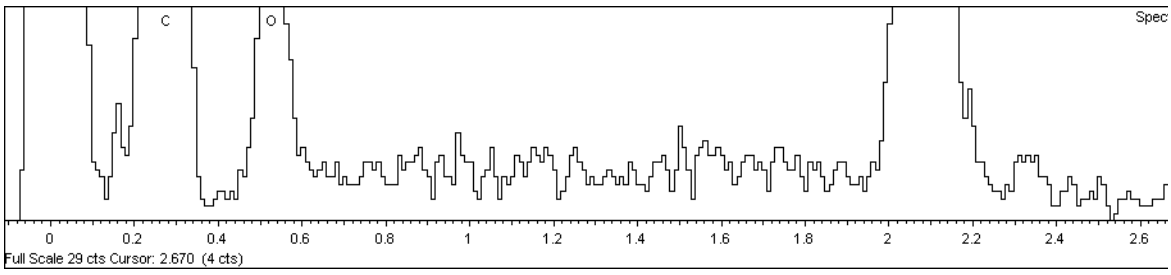

(d)

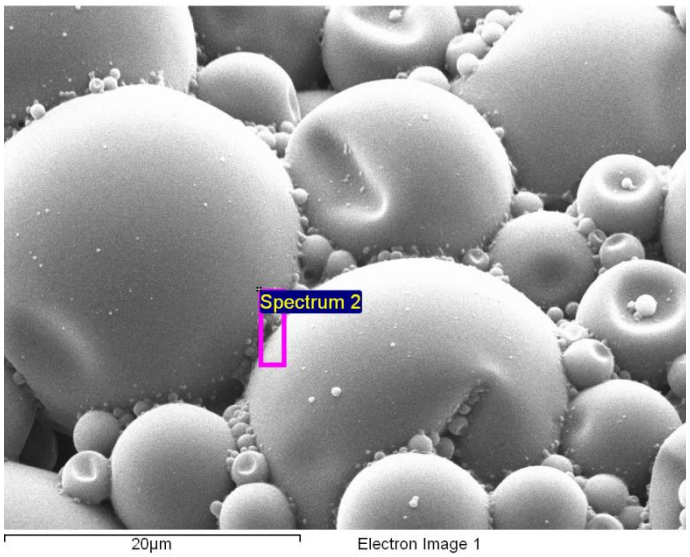

Element	Weight%	Atomic%
C	85.20	88.84
N	0.12	0.11
O	14.68	11.05
Totals	100	

(e)

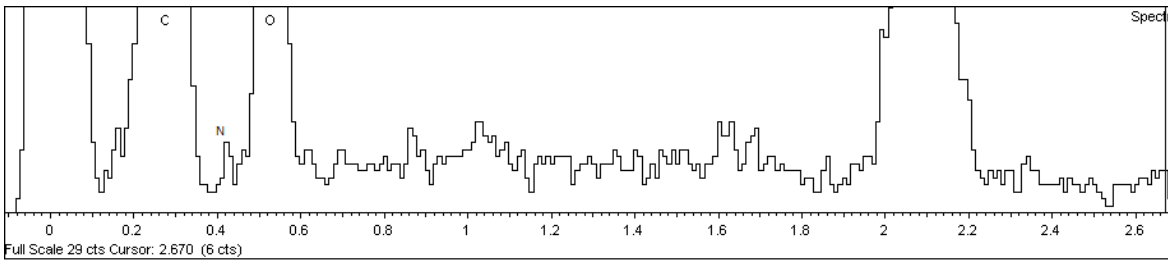

(f)

Figure 5.2 SEM-EDX elemental analysis of 0.25% chitosan-modified PAC-PVOH microcapsules (Lot#PDS091714B-chitosan) at different scanning areas.

5.2.3 Surface charge of PMCs in aqueous environment

Zeta potential analysis results (mean value of 3 measurements, each measurement lasted for 30s) of PAC-PVOH microcapsules modified with 0.25% chitosan at varying pH are plotted in Figure 5.3. It is obvious that chitosan modifications significantly increase the

surface charge of PAC-PVOH microcapsules when the pH value is below 5. However, the zeta potential of chitosan-modified microcapsules quickly decreases to negative value when pH is raised above 5 and keeps decreasing with increasing pH. Moreover, both the trend and the absolute values of the zeta potential curve of chitosan-modified PAC-PVOH microcapsules from pH 5 and 11 are found to be similar to those of control sample. Because chitosan has been proved to be positively charged due to protonation on amino functional groups in an acidic condition by multiple literature (Claesson and Ninham, 1992, Rinaudo *et al.*, 1993, Ilium, 1998, An and Dultz, 2007), these results suggest that the chitosan used in this project had significant interactions with PAC-PVOH microcapsule surface even at a low concentration (in this case 0.25wt.%) and turns the surface charge from negative to positive when pH is below 5. However, due to the pH sensitivity of chitosan itself, the deprotonation of the amino groups develops so rapidly resulting in the polymer being not able to compete with the negative charge from the original PAC-PVOH microcapsule surface at above pH 5.

As the pH for the target real laundry condition is designed to be neutral (e.g. pH 6 - 8), according to the zeta potential results here, the surface charge of chitosan-modified PMCs may not be significantly different from that of the control PMC sample. Nevertheless, zeta potential of the PMCs in aqueous solution with different hardness and surfactant was measured. PVF-modified microcapsules were tested together as a benchmark in these conditions as well. More measurement results together with data analysis and comparisons are included in later discussion section.

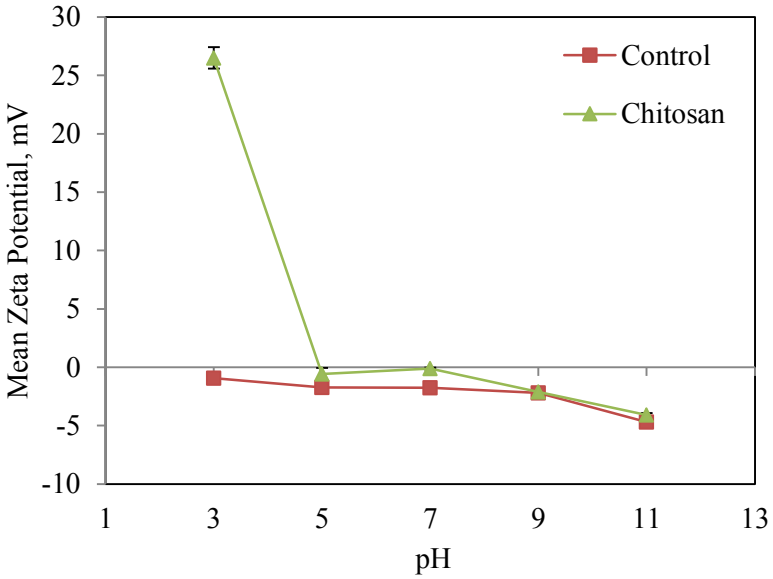

Figure 5.3 Mean Zeta Potential of 0.25% chitosan-modified microcapsules (batch# PDS091714B-chitosan) in 0.01M (580ppm) NaCl solution at varying pH. The error bar represents the standard error of the mean.

5.3 Retention of surface modified PAC-PVOH PMCs on model fabric films in a flow chamber

A flow chamber technique developed by He (2013) to understand the interactions between MF microcapsules and a model fabric film was adopted with modifications to analyse the adhesion behaviour of PAC-PVOH PMCs to model fabric films. The modifications include measurement steps and image analysis procedures, which need to be validated before systematic investigations of retention/adhesion behaviour of both PVF and chitosan-modified PAC-PVOH PMCs on model fabric films. Subsequently, different environmental conditions including hardness concentrations (ion strength), surfactant types and levels on the retention/adhesion of PMCs on the model fabric films were studied.

5.3.1 Validation of the modified flow chamber technique

The data analysis of flow chamber experimental results was based on image analysis. As a universal data processing tool, Matlab was chosen by He (2013) to be the image analysis software for the experimental results of her flow chamber technique, which was also used for calculating the area ratio of microcapsules on an image in this project.

In order to validate the modified flow chamber measurement procedures and image analysis method, six repeated flow chamber measurements and subsequent image and data analysis were conducted on both commercially available cellulose and PET films using the initial batch of control PAC-PVOH microcapsules (Lot# PDS060412) and the corresponding four PVF-modified samples (for details see §3.1.2.2, Lot# PDS060412 A to D) with the newly introduced flow chamber device (Figure 3.4). The flow chamber measurement procedures introduced in §3.2.10.3 were followed. All samples were diluted at 0.25wt.% using DI-water. As part of the validation, Image J, the open source image analysis software, was introduced to repeat the image analysis procedures (for details see §3.2.10.4) and results were compared with those obtained using Matlab. Error bar is also calculated as the standard error of the 6 repeated test results.

Figure 5.4 shows comparison of the mean area ratios occupied by microcapsules (calculated by Equation 3.2) on a cellulose film after deposition and cleaning steps. The data calculated from ImageJ and Matlab well match each other with regard to both the overall data trends from PVF-modified sample A to control sample PDS080412 as well as the absolute value of area ratio of each sample. From the deposition to the cleaning step, there was no significant change in the area ratio for each sample except the control,

which means the hydrodynamic forces generated by the cleaning were not significantly great to cause any removal of PMCs in the modified samples.

Similar data comparisons for a PET film are shown in Figure 5.5. Again, there is no significant difference in the area ratio analysed by Image J and Matlab. Overall, the area ratio of each sample on the PET film is significantly greater than that on the cellulose film. Moreover, from the deposition to cleaning step, there was no significant removal of PMCs by the hydrodynamic conditions for all samples including the control.

The above comparisons verify both Image J and Matlab as independent image analysis tools in this research. Since Matlab has much better batch data processing capability when using the code developed by Dr James W. Andrews and Dr Yanping He (2013), it was continued to be used in the later flow chamber image analysis. Furthermore, because the images were collected from six replicate measurements and all these area ratio values were calculated from the image analysis results, the flow chamber measurement procedures as well as the image analysis methods were proved capable, stable and reliable to provide consistent results. Thus, the entire flow chamber technique has been validated.

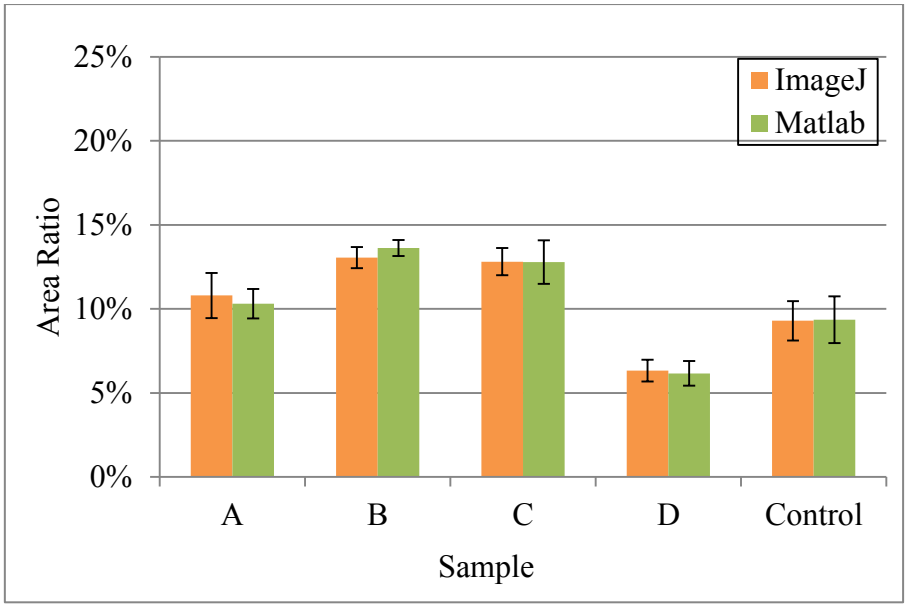

(a)

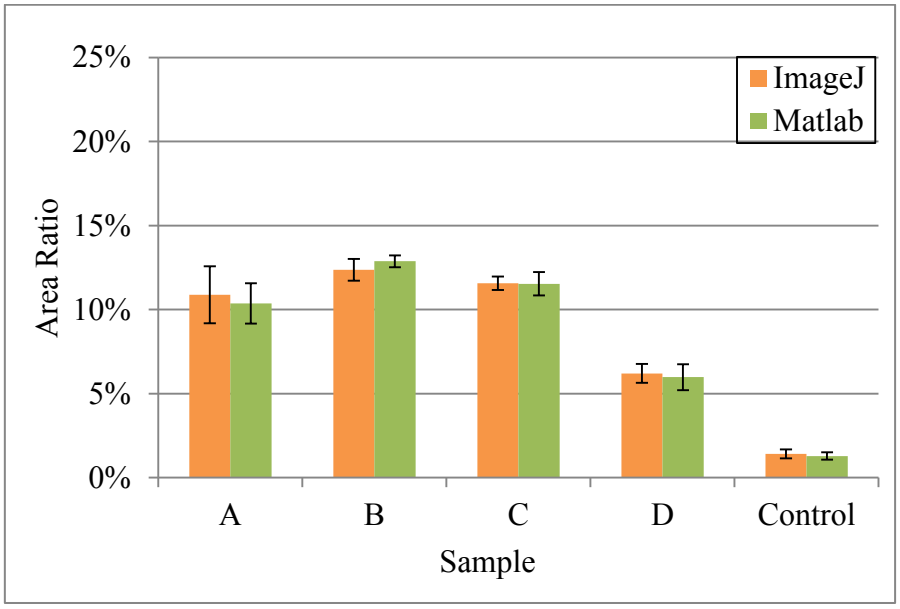

(b)

Figure 5.4 Comparison of area ratio occupied by microcapsules (mean of six measurements) from images taken on cellulose film, analysed by both ImageJ and Matlab: (a). at the end of a deposition step; (b). after cleaning step. The error bar represents the standard error of the mean. For sample details of A to D, see Table 3.1 for PVF polymer modified PAC-PVOH PMCs, Lot# PDS060412 A to D.

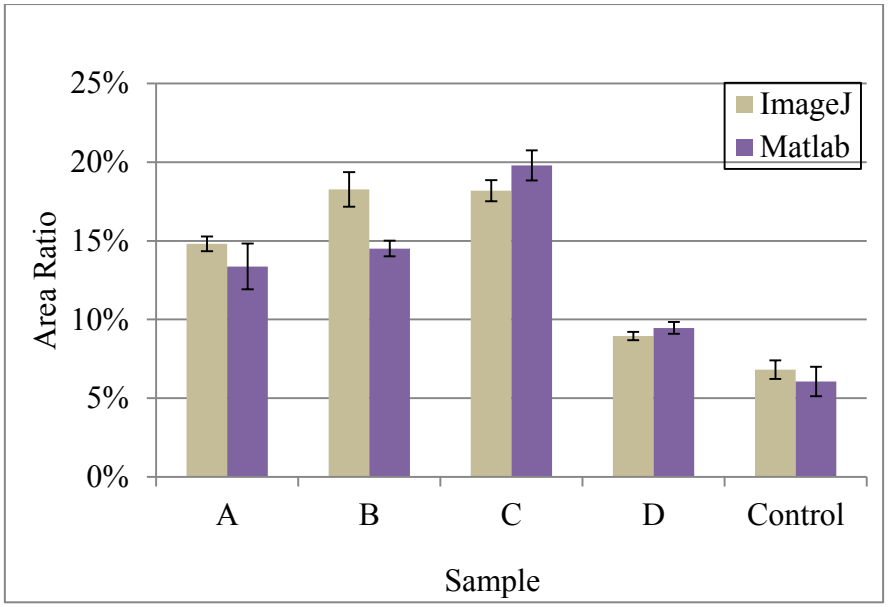

(a)

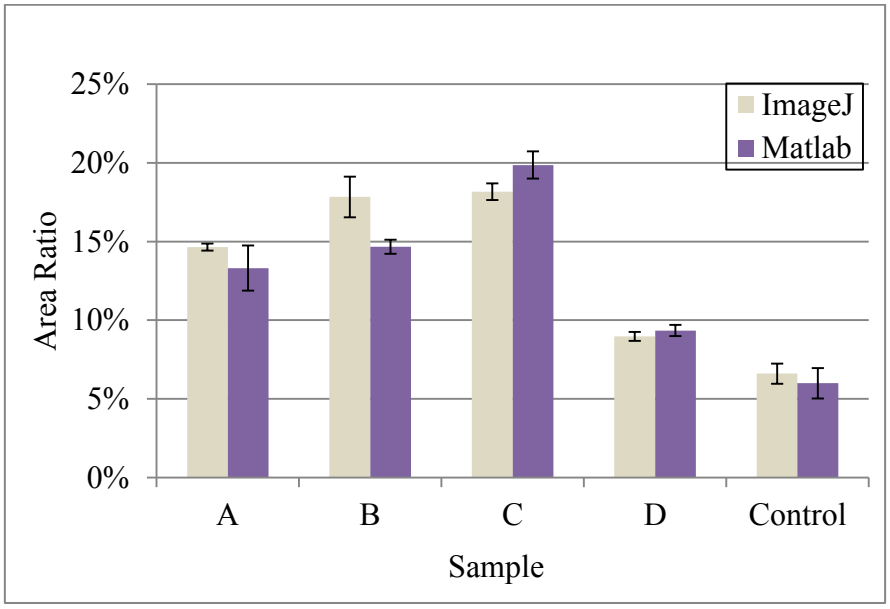

(b)

Figure 5.5 Comparison of the area ratio occupied by microcapsules (mean of six measurements) from images taken on a PET film, analysed by both Image J and Matlab: (a). at the end of deposition step; (b). after cleaning step. The error bar represents the standard error of the mean. For sample details of A to D, see Table 3.1 for PVF polymer modified PAC-PVOH PMCs, Lot# PDS060412 A to D.

5.3.2 Retention of control PAC-PVOH PMCs on model fabric films in DI-water

Figure 5.6 shows both sets of retention data on cellulose and PET films in DI-water for the three control samples of PAC-PVOH microcapsules from different batches.

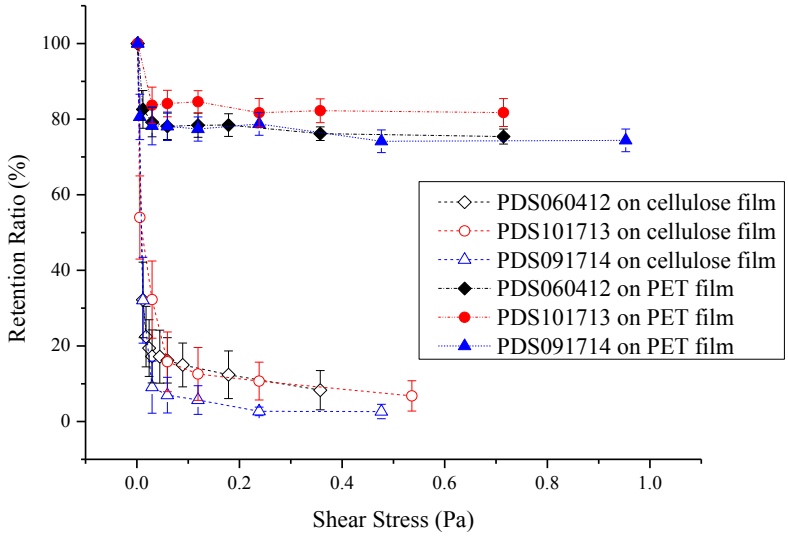

Figure 5.6 Retention ratio comparison of three control samples of PAC-PVOH PMCs from different batches on model fabric films versus shear stress in the flow chamber device with DI-water. The error bar represents the standard error of the mean.

Overall, all three control samples performed similarly on the cellulose film or PET film. As there was no additional solute, nor any surface modification of the microcapsules, the data reflect the original interactions between the control samples and the substrate film surfaces in aqueous environment. It is also clear from Figure 5.6 that on the cellulose film, the microcapsule retention ratio stays at around 3~10% once the shear stress exceeds 0.2 Pa inside the flow chamber; whilst on the PET film, the retention ratio becomes steady at about 75~85% almost right after the beginning of flushing step. These results suggest that the control PAC-PVOH microcapsules were more adhesive to

the PET film than to the cellulose film in DI-water. Considering the Zeta potential results from §4.3.5 and the discussions of surface charge of the films in §4.5.2.1, the lower retention on cellulose film could be explained by the electrostatic repulsions and overall weak interactions between the control microcapsules and cellulose film surface. However, the higher retention on PET film revealed that a strong hydrophobic force (§4.5.3) dominates the interactions between the control microcapsule and PET fabric surface.

5.3.3 Retention of surface modified PAC-PVOH PMCs on model fabric films in DI-water

In DI-water, a series of PVF-modified PAC-PVOH microcapsules and a sample of chitosan-modified microcapsules on both cellulose and PET films were tested in the flow chamber device and the results are shown in Figure 5.7 (a) and (b), respectively. The only differences between all the PVF-modified samples were the different molecular weight and hydrolysis ratio of the PVF polymers used (Table 3.1).

On cellulose film, Figure 5.7 (a) shows:

- Sample D showed the best retention performance and kept the ratio at above 96% through the entire tested shear stress in the flushing steps.
- Sample A and B showed good retention ratio above 90% when the shear stress was below 0.18 Pa but after that their performance dropped dramatically to 26±8% and 41±7%, respectively, with shear stress increasing to 0.36 Pa.
- Sample C and PDS091714B-PVF showed similarly good performances. They gave above 90% retention ratio below shear stress of 0.14 Pa and 0.24 Pa, respectively

and kept the final retention ratio of 74±5% at 0.36 Pa and 59±5% at 0.48 Pa, respectively.

- The retention ratio of sample PDS101713-PVF dropped to 72±5% after the shear stress increased above 0.03 Pa but only dropped slowly to 60±5% at 0.24 Pa and 51±6% at the shear stress of 0.54 Pa.
- The retention ratio of chitosan-modified sample quickly dropped to about 90% at the shear stress of 0.03 Pa and gradually dropped to about 60% at the shear stress of 0.54 Pa.

On PET film (Figure 5.7 (b)): all of the modified microcapsule samples performed similarly and showed approximately 100% retention ratio below a shear stress of 0.24 Pa. Above that shear stress, the modified samples were divided into two groups: retention ratios of sample A, B and PDS091714B-PVF gradually dropped to about 80-85% whilst those of sample C, D, PDS101713-PVF and PDS101713-Chitosan remained at nearly 100%.

According to the AFM experimental results from §4.4.5, the performance ranking of the PVF polymers on enhancing adhesion of PAC-PVOH microcapsules to both films is Lupasol® VT > Lupamin® 9030 ≥ Lupamin® 9095. Therefore, this conclusion was further confirmed by the flow chamber measurement results. Lupasol® VT (corresponding sample being PDS091714B-PVF) was also chosen to be the lead PVF polymer to represent the PVF surface modification in following experiments.

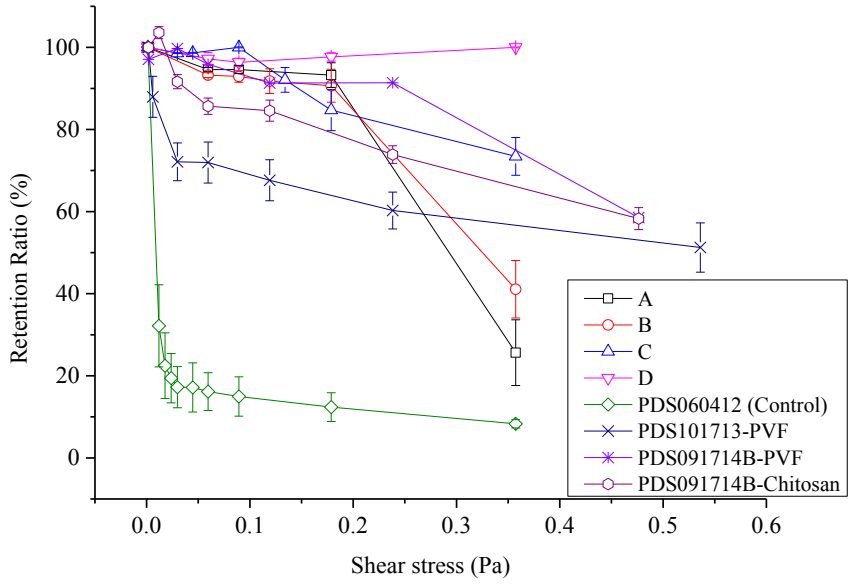

(a)

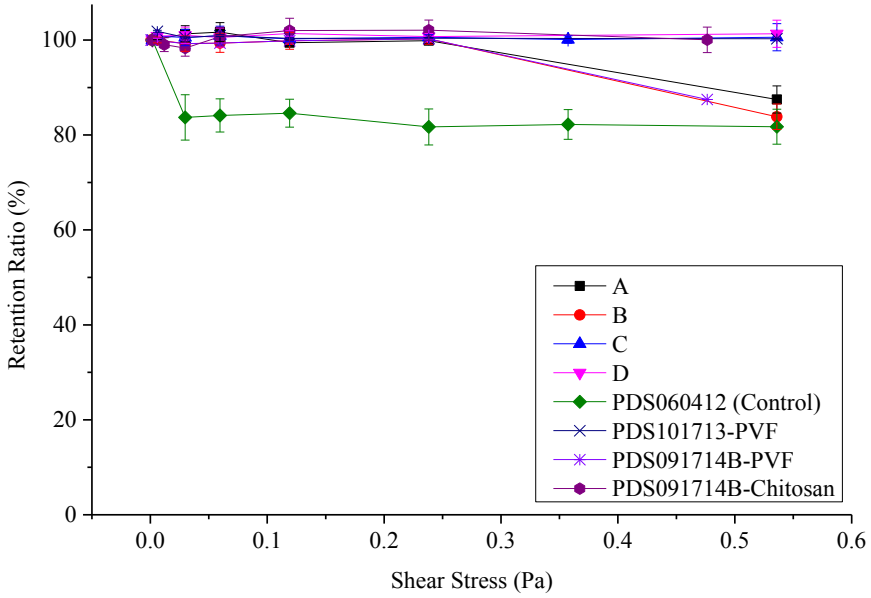

(b)

Figure 5.7 Retention ratio comparison of different surface modified PAC-PVOH PMC samples on cellulose (a) and PET (b) film versus shear stress in the flow chamber device in DI-water. The error bar represents the standard error of the mean. For sample details of A to D, see Table 3.1, Lot# PDS060412 A to D.

5.3.4 Retention of PAC-PVOH PMCs on model fabric films in hardness water

With 15gpg hardness (Ca^{2+} :Mg^{2+} = 3:1 by weight), retention of both PVF and chitosan-modified PAC-PVOH PMCs on both cellulose and PET films in the flow chamber device were measured and the results are shown in Figure 5.8 (a) and (b), respectively.

Comparing to Figure 5.6, the overall retention ratios in Figure 5.8 indicate that the addition of 15gpg hardness ions might enhance the adhesion of all the microcapsules to both films, especially at higher shear stress such as 0.4 – 0.5 Pa:

- For control sample: the hardness ions helped improve the retention from less than 10% to more than 60% on cellulose film and from about 80% to more than 90% on PET film.
- For PVF-modified sample: the retention ratio was increased from about 60% to more than 80% on cellulose film though it was not much changed on PET film.
- For chitosan-modified sample: the retention ratio was improved from about 60% to almost 100% on cellulose film whilst it kept 100% on PET film with or without hardness addition.

The mechanism of hardness improving adhesion of PAC-PVOH PMCs to model fabric films was further investigated by AFM and zeta potential analysis. More results are in later discussion sessions.

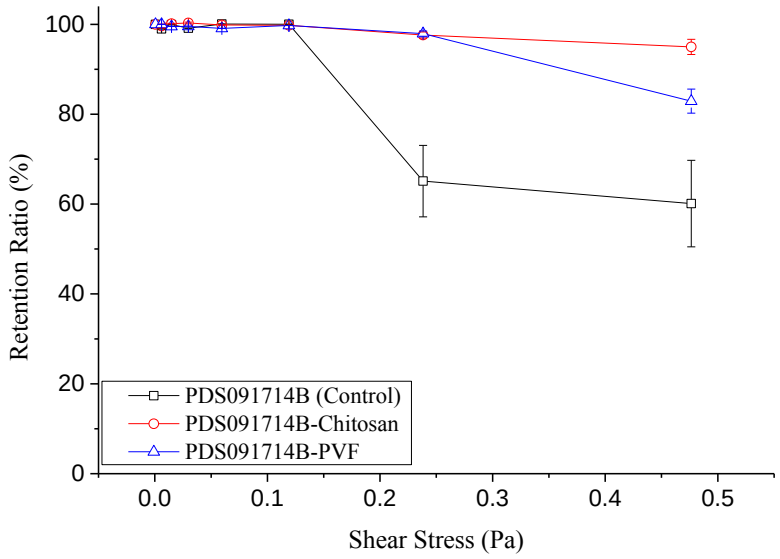

(a)

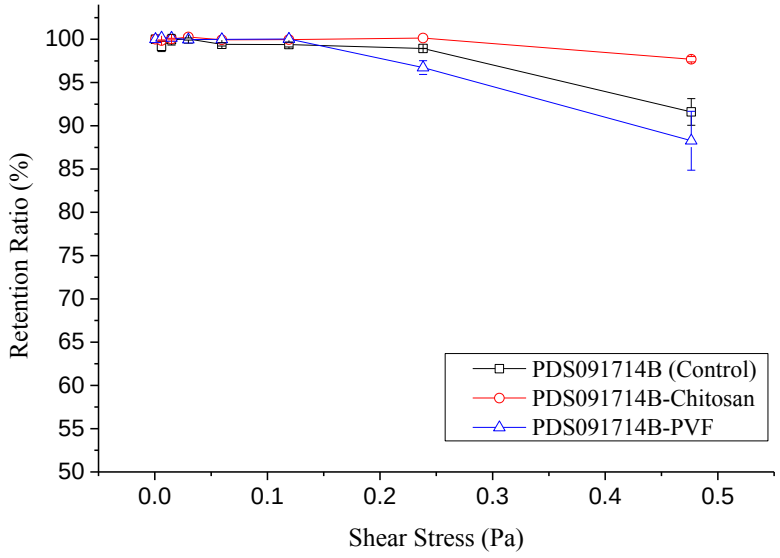

(b)

Figure 5.8 Retention ratio comparison of PAC-PVOH PMC samples on cellulose (a) and PET (b) film versus shear stress in the flow chamber device with 15gpg hardness water. The error bar represents the standard error of the mean.

5.3.5 Retention of PAC-PVOH PMCs on model fabric films in surfactant solutions

This section focuses on interpretation of the retention ratio results in surfactant solutions with different concentrations on both model fabric films using the flow chamber device. The control sample together with PVF and chitosan-modified ones were injected into the flow chamber device, deposited onto the target model fabric film and then subjected to a gradient concentration of SDS and LAS surfactant solutions, respectively. Finally, all relevant data accumulated under the same type of surfactant solution were put together in one chart.

5.3.5.1 Retention of non-modified PAC-PVOH PMCs on model fabric films in surfactant solutions

Figure 5.9 shows the retention ratio comparison of control sample in SDS surfactant solution on both cellulose and PET film using the flow chamber device, respectively. From the observation during the flow chamber experiments of all the control PMCs on cellulose film with SDS additions, it was found that most microcapsules were rolling or floating inside the chamber even at low shear stress and the phenomenon continued throughout the entire 3 minutes for a certain flow rate. This could be a sign that adhesion of the related PMCs to the film surface is relatively weak in such test conditions. Since the image taking interval was 3 minutes after which the flow rate switched to next higher level, this resulted in the microcapsule number recorded on the images taken being larger than the real number of actual retained ones, therefore, the larger calculated retention ratio and larger data variations.

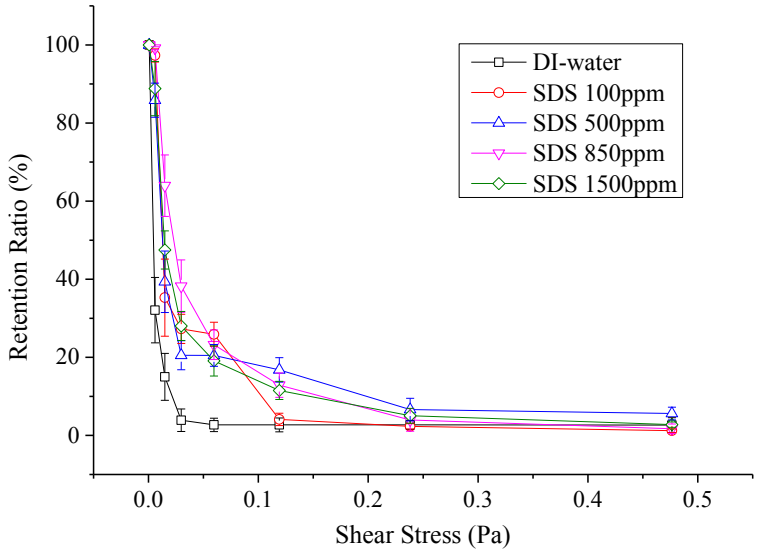

(a)

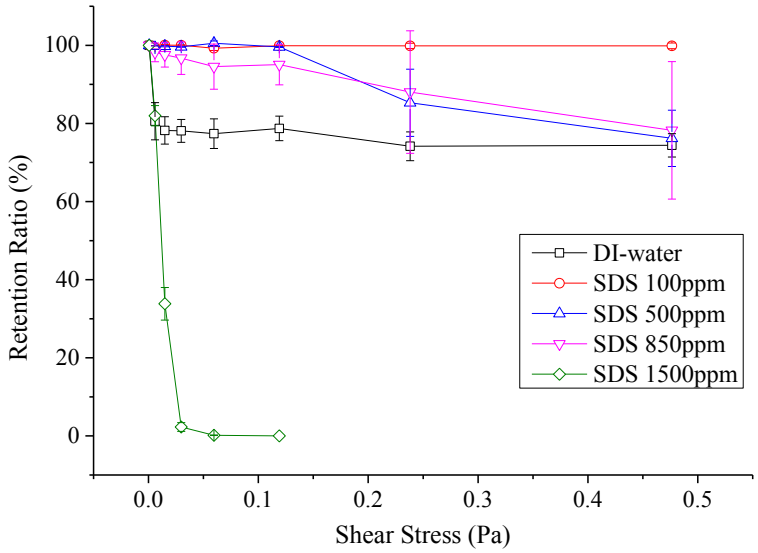

(b)

Figure 5.9 Retention ratio comparison of non-modified PAC-PVOH PMC sample (batch# PDS091714B) on cellulose (a) and PET (b) films versus shear stress in the flow chamber device with SDS surfactant solutions. The error bar represents the standard error of the mean.

From Figure5.9 (a), the overall increase of the retention ratio from nearly zero in DI-water to about 15 – 20% in various SDS solutions below the shear stress of 0.1Pa still indicates that there was some enhancement of adhesion brought by the SDS addition.

However, the decrease of the retention ratio to about zero when shear stress was increased above 0.2Pa confirms that such enhancement was overall very weak.

In contrary, it is obvious that the addition of SDS at low concentration increased the retention of the non-modified PMCs on PET film (Figure 5.9 (b)) significantly. Although the retention ratio of the PMCs on PET film was gradually reduced with the increasing SDS concentration, the overall effect of SDS addition was to enhance the retention at concentrations from 100ppm to 850ppm. However, when in 1500ppm, the effect of SDS became reversed and displacement of PMCs from PET film surface was observed which led to the retention ratio decreased to nearly zero even at a low shear stress, i.e. 0.05 Pa.

Figure 5.10 shows the retention ratio comparison of control PAC-PVOH PMCs in LAS surfactant solutions on both cellulose and PET films using the flow chamber device, respectively. Furthermore, a real wash condition using 5675ppm of P&G Senso non-fragranced HDL detergent (Lot# ETF1873-063, formula containing 15% LAS, thus corresponding to 850ppm LAS in solution) dissolved in 15gpg hardness water was used to replace the surfactant solution to make further comparison.

The retention ratio on cellulose film (Figure 5.10 (a)) shows that below shear stress of about 0.2 Pa, 100ppm LAS started to have some but limited positive influence on the retention of control PMCs on cellulose film, improving the retention from almost none to about 5 - 10% at shear stress of 0.1 – 0.5 Pa. The enhancement was further strengthened when LAS concentration was increased to 500ppm. However, the benefits disappeared and the retention ratio decreased to zero when LAS concentration was further increased to 850ppm and beyond. Furthermore, real wash condition helped

increase the retention ratio, which ranges in between that of 100ppm and 500ppm of LAS alone throughout the entire shear stress range.

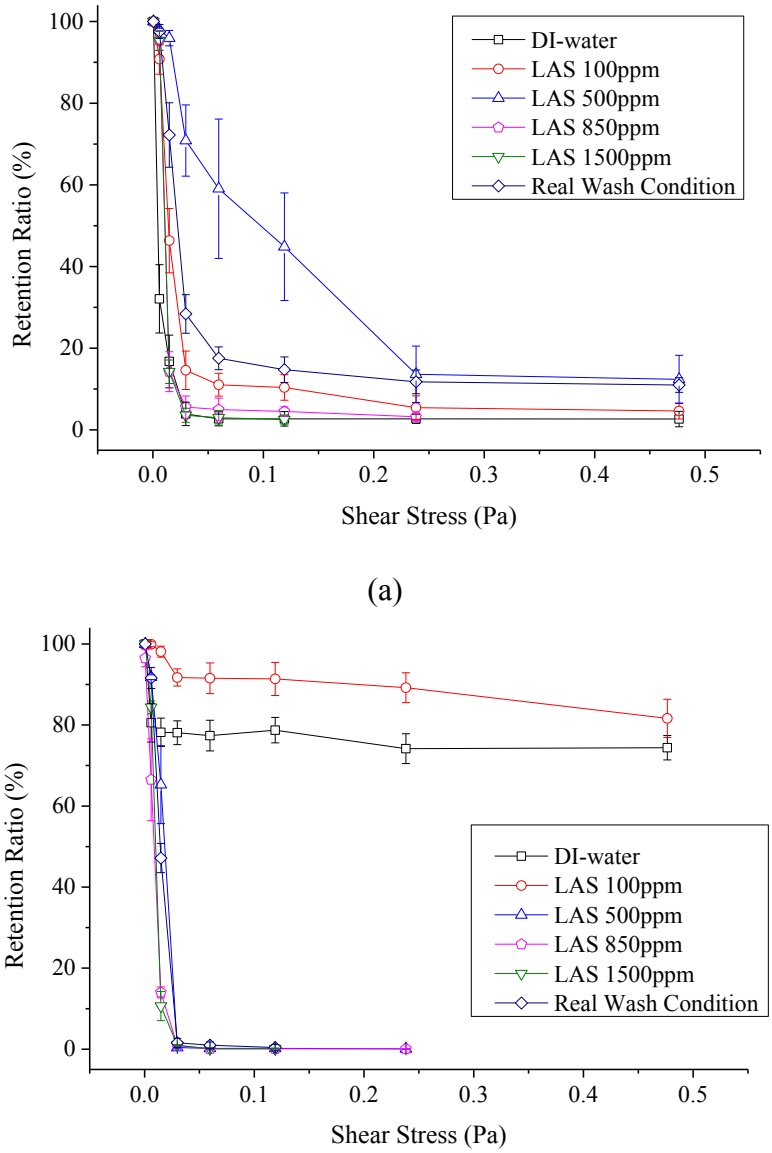

Figure 5.10 Retention ratio comparison of non-modified PAC-PVOH PMC sample (batch# PDS091714B) on cellulose (a) and PET (b) film versus shear stress in the flow chamber device with LAS surfactant solutions. The error bar represents the standard error of the mean.

On PET film (Figure 5.10 (b)), except low concentration LAS of 100ppm which increased the overall retention ratio of control PMCs from about 75% in DI-water to about 85 - 90%, all the other concentrations of LAS as well as the real wash condition showed strong negative influence on the PMC's retention which means higher concentration of LAS dramatically decreased the adhesion of control PMCs to PET film.

5.3.5.2 Retention of PVF-modified PAC-PVOH PMCs on model fabric films in surfactant-solutions

The retention ratio of PVF-modified PAC-PVOH PMCs in SDS solutions on both model fabric films are shown in Figure 5.11. Overall the retention values of PVF-modified PAC-PVOH PMCs are similar on both films in the tested SDS solutions. At SDS concentration of 100 and 500ppm, the retention ratio on cellulose film (Figure 5.11 (a)) was improved to above 95% comparing to below 70% in DI-water at shear stress above 0.45 Pa; similar improvement was found on PET film (Figure 5.11 (b)) as well. However, in 850ppm SDS solution, when the flow shear stress exceeded 0.3 Pa, the retention ratio dropped to about 50% on cellulose film and 70-80% on PET film, respectively. When the SDS concentration was increased to 1500ppm, retention ratio of PVF-modified PMCs dropped to less than 10% on both films with flow shear stress at 0.2 Pa and above.

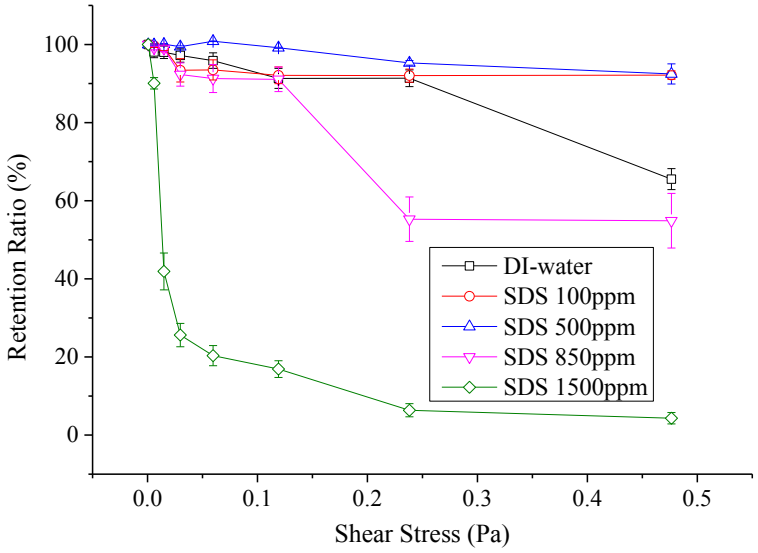

(a)

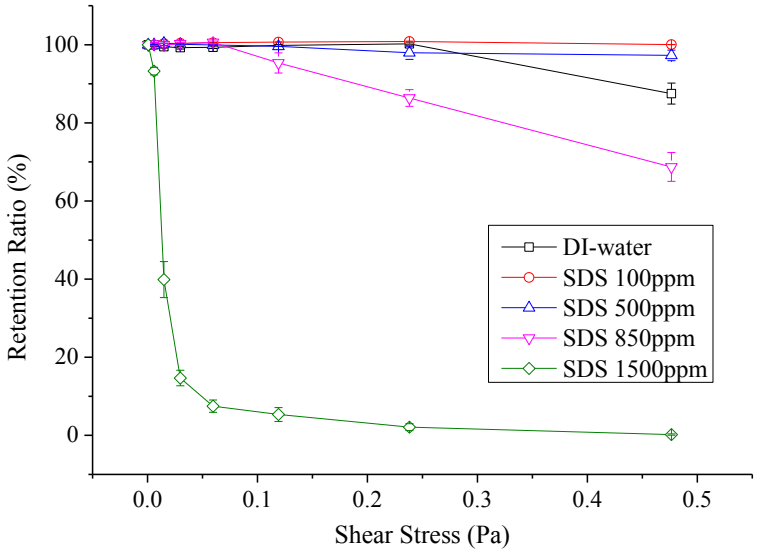

(b)

Figure 5.11 Retention ratio comparison of PVF-modified PAC-PVOH PMC sample (batch# PDS091714B-PVF) on cellulose (a) and PET (b) film versus shear stress in the flow chamber device with SDS surfactant solutions. The error bar represents the standard error of the mean.

Figure 5.12 shows the retention ratio comparison of PVF-modified PAC-PVOH PMCs in LAS solutions on both model fabric films respectively. 100ppm LAS showed slightly positive effect on improving the retention ratio of PVF-modified PAC-PVOH PMCs on cellulose film only vs that in DI-water condition on average through the tested shear stress; the same amount of LAS addition greatly reduced the retention of the PMCs on PET film from about 100% to below 60% at shear stress above 0.25 Pa. Beyond that LAS concentration, the retention ratio on both films reduced to less than 5% (for 500ppm) and almost zero (for 850ppm and 1500ppm) at shear stress above 0.05 Pa, which means almost no retention on both films in such higher concentrated LAS solutions. Furthermore, about 50 – 60% retention ratio of the PVF-modified PAC-PVOH PMCs on cellulose film was observed in real wash condition at shear stress above 0.05 Pa whilst only less than 5% of retention ratio was detected from the same condition on PET film.

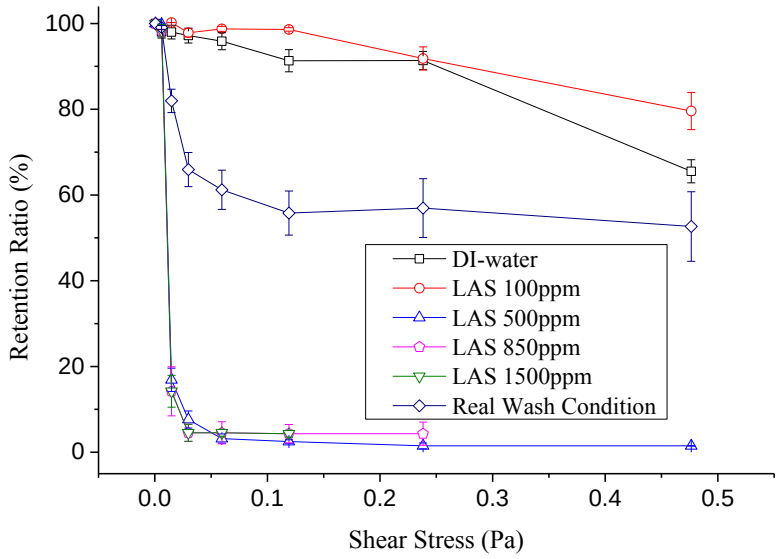

(a)

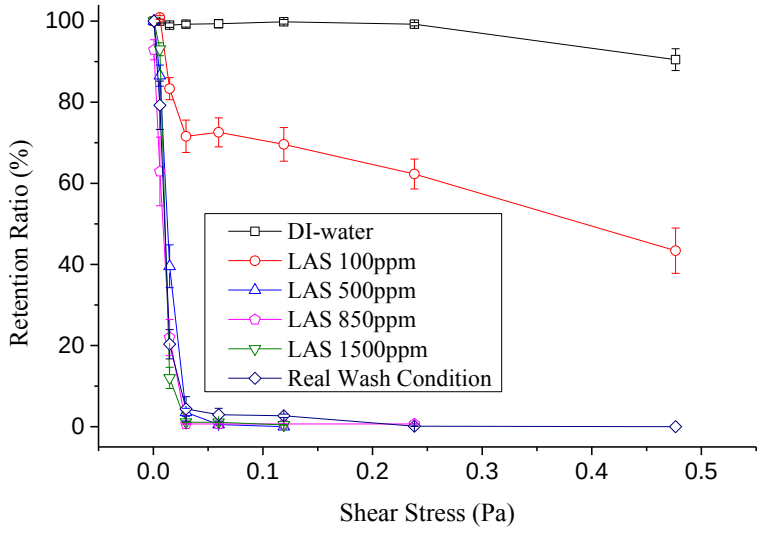

(b)

Figure 5.12 Retention ratio comparison of PVF-modified PAC-PVOH PMC sample (batch# PDS091714B-PVF) on cellulose (a) and PET (b) film versus shear stress in the flow chamber device with LAS surfactant solutions. The error bar represents the standard error of the mean.

5.3.5.3 Retention of chitosan-modified PAC-PVOH PMC on model fabric films in surfactant solutions

Figure 5.13 shows the retention ratio comparison of chitosan-modified PAC-PVOH PMCs in SDS solutions on both model fabric films respectively.

On cellulose film, the retention ratio of chitosan-modified PAC-PVOH PMCs in 100ppm SDS was similar to that in DI-water through all tested shear stresses and kept at about 60% at 0.5 Pa shear stress. By increasing the SDS concentration to 500ppm, the retention ratio reduced approximately by half in above 0.1 Pa shear stress vs that in 100ppm SDS condition; it further reduced to below 10% when the SDS concentration was increased to 850ppm and 1500ppm.

On PET film, the retention ratio decreased from almost 100% in DI-water to about 70-90% in SDS concentration below 850ppm at shear stress of 0.2 – 0.5 Pa. However, only marginal differences in the retention ratio between100, 500 and 850ppm SDS concentrations were seen, in contrast to the data for cellulose film. The retention ratio was further reduced to about 10 - 20% when SDS concentration was increased to 1500ppm.

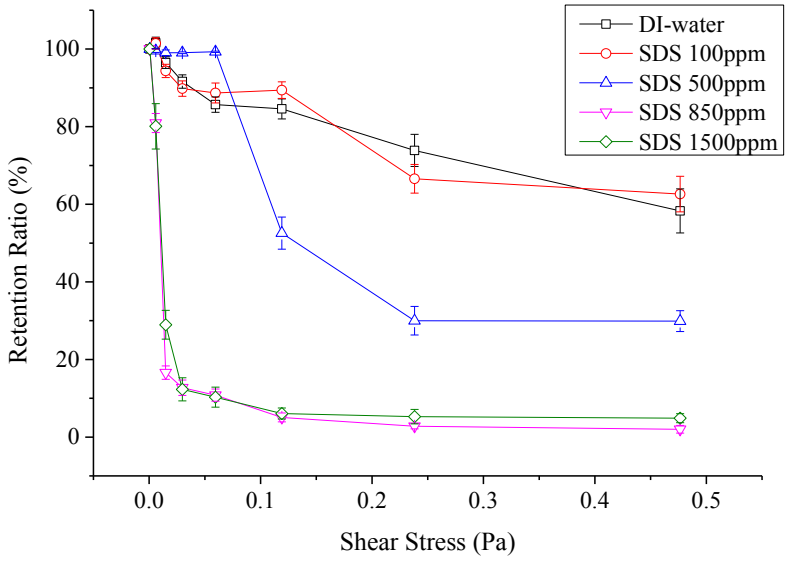

(a)

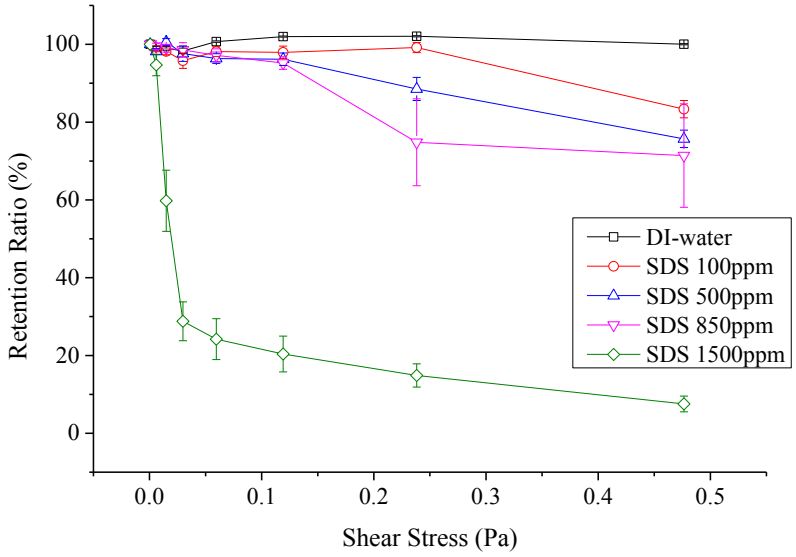

(b)

Figure 5.13 Retention ratio comparison of chitosan-modified PAC-PVOH PMC sample (batch# PDS091714B-Chitosan) on cellulose (a) and PET (b) film versus shear stress in the flow chamber device with SDS surfactant solutions. The error bar represents the standard error of the mean.

The retention ratio of chitosan-modified PAC-PVOH PMCs in LAS solutions on both model fabric films are shown in Figure 5.14. Comparing to Figure 5.13, it is obvious that it is more difficult to retain the chitosan-modified PAC-PVOH PMCs on both films in the same concentrated LAS solutions than in SDS solutions. The retention ratio at about 30 – 40% and 60 – 80% were achieved in 100ppm LAS solution at above 0.05 Pa shear stress on cellulose and PET film, respectively, which were approximately 10-20% less than the values for the corresponding films in DI-water condition. Beyond such concentration, addition of more LAS deteriorates the retention of the chitosan-modified PAC-PVOH PMCs on both films so greatly that only less than 10% retention ratio was detected in LAS 500ppm solution at above 0.1 Pa shear stress on cellulose film and almost no retention was observed from the other conditions including in LAS 500ppm solution on PET film and in LAS 850ppm and 1500ppm solutions on both films at any tested shear stress. However, in real wash condition, about 60% retention ratio of the chitosan-modified PAC-PVOH PMCs was observed on cellulose film at shear stress above 0.05 Pa whilst only less than 5% retention ratio was detected from the same condition on PET film. This finding under real wash condition is similar to that of PVF-modified PAC-PVOH PMCs, which indicates there might be some specific interactions caused by LAS of high LAS concentration (850ppm) and salt ions of high hardness level (15gpg) and possibly together with some other additional ingredients in the condition, contributing to the deposition and retention of surface-modified PAC-PVOH PMCs. More mechanism understanding and discussions are presented in later sections.

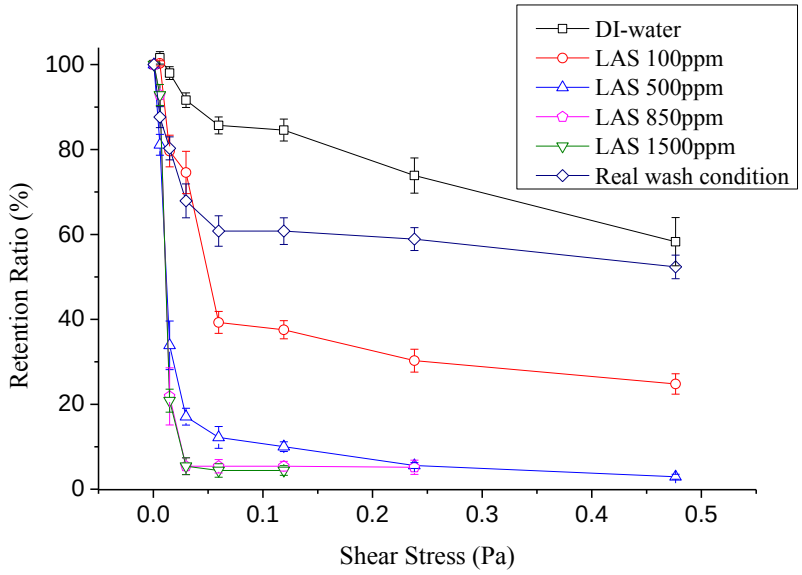

(a)

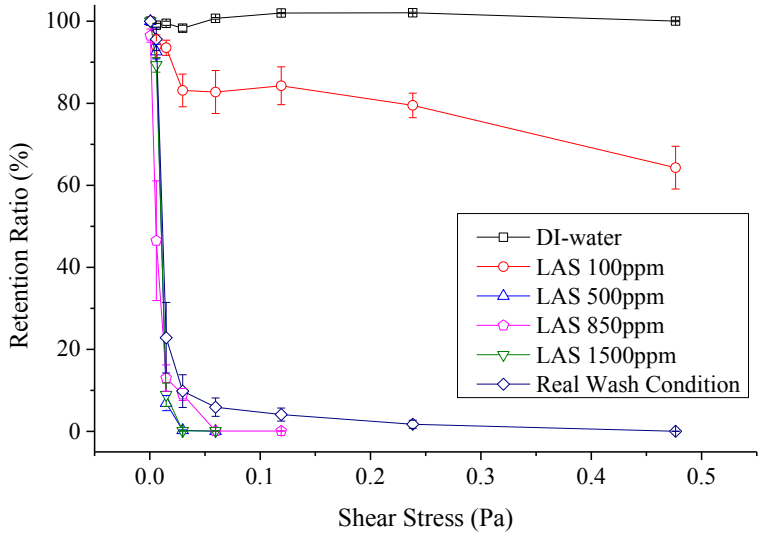

(b)

Figure 5.14 Retention ratio comparison of chitosan-modified PAC-PVOH PMC sample (batch# PDS091714B-Chitosan) on cellulose (a) and PET (b) film versus shear stress in the flow chamber device with LAS surfactant solutions. The error bar represents the standard error of the mean.

5.4 Adhesion between single surface-modified PAC-PVOH PMCs and model fabric films measured using AFM

Readily established AFM force measurement methods were applied further in this chapter. The measurements were conducted using corresponding flow chamber experimental conditions to get the adhesive properties of single surface-modified PAC-PVOH PMCs to the target model film surface. Results for the related test condition were categorised to compare with each other in order to understand the mechanism of the adhesion. Since the adhesion results of control and PVF-modified PMCs in DI-water condition have already been discussed in §4.4.5, their adhesion comparison together with that of chitosan-modified PMCs to model fabric films in other conditions are the focus in this section.

5.4.1 Adhesion measurement results of PMCs to model fabric films in hardness water

In addition to the 15gpg target water hardness (standard US laundry condition used by P&G BIC) in this study, 1gpg water hardness was also chosen in order to investigate the mechanism covering a wider hardness range in laundry conditions. Figure 5.15 and Figure 5.16 present the AFM adhesive force measurement results of single microcapsules on both model fabric films in 1gpg and 15gpg hardness conditions compared to the adhesion measured in DI-water for the same samples at both 0.01s and 10s contact time, respectively.

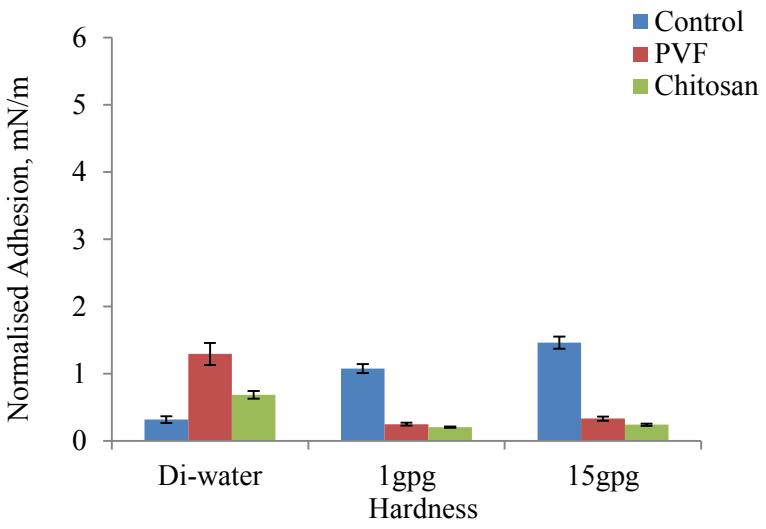

(a)

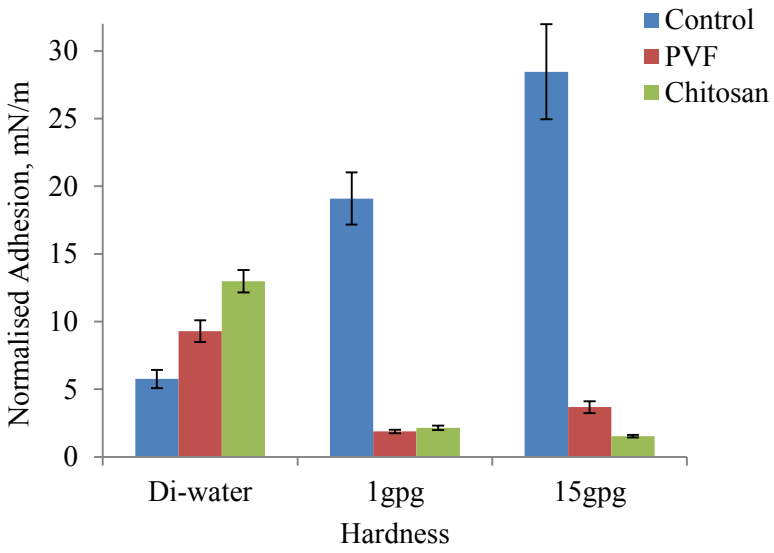

(b)

Figure 5.15 Comparison of mean normalised adhesion of single microcapsules in hardness water solution to model cellulose film (a) and PET film (b) at a contact time of 0.01s using AFM. For control sample (batch# PDS091714B), n (number of microcapsules measured) = 3; for PVF-modified sample (batch# PDS091714B-PVF), n = 3; for chitosan-modified sample (batch# PDS091714B-Chitosan), n = 2. The compression force was set to be 20nN. The error bar represents the standard error of the mean.

It is clear that the addition of hardness ions in DI-water acts differently on control PAC-PVOH PMCs and surface-modified ones. The 1gpg hardness in DI-water significantly enhanced the normalised adhesion of the control PAC-PVOH PMC to cellulose film (Figure 5.15 (a)) by approximately 4 times and to PET film (Figure 5.15 (b)) 3 times at a contact time of 0.01s and to both films about 1.5 times at a 10s contact time (Figure 5.16). Furthermore, the increase in hardness from 1gpg to 15gpg further enhanced the normalised adhesion by about 30% ~50% at 0.01s contact time and about 10% ~ 30% at 10s contact time.

On the contrary, the increase in hardness greatly decreased the normalised adhesion of both surface-modified PAC-PVOH PMCs to either film. In 1gpg hardness solution, the normalised adhesion of both surface-modified samples to either film at 0.01s contact time was reduced by about 80% from that in DI-water condition (Figure 5.15); such adhesion was decreased by approximately 60% with PVF-modified sample and about 40% with chitosan-modified one to both films at 10s contact time (Figure 5.16).

In 15gpg hardness solution:

- At 0.01s contact time (Figure 5.15), the measured normalised adhesive forces of both surface-modified samples to either film were similar to their corresponding ones in 1gpg hardness;
- At 10s contact time (Figure 5.16), the normalised adhesion of PVF-modified sample to cellulose film was found comparable to that in 1gpg condition; the normalised adhesion of the same sample to PET film was observed doubled to the one in 1gpg hardness. All these results were significantly lower than that in DI-water.
- At 10s contact time (Figure 5.16), the normalised adhesion of chitosan-modified PMC to cellulose film was further reduced by more than 60% comparing to that in

1gpg hardness condition whilst such adhesion of the same sample to PET film was comparable to the one in 1gpg hardness water.

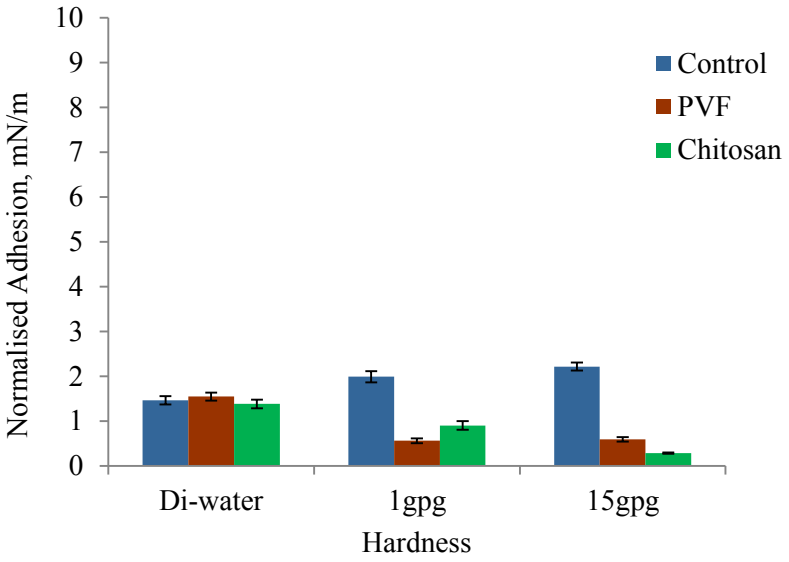

(a)

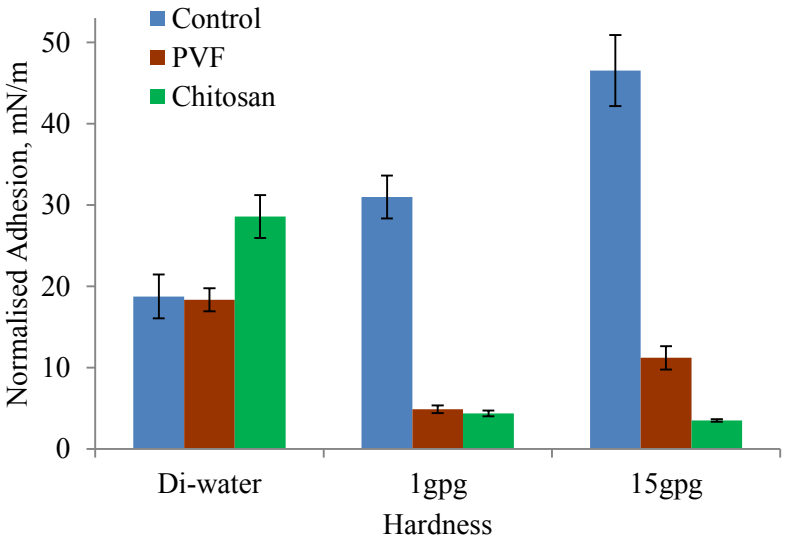

(b)

Figure 5.16 Comparison of mean normalised adhesion of single microcapsules in hardness water solution on model cellulose film (a) and PET film (b) at a contact time of 10s using AFM. For control sample (batch# PDS091714B), n = 3; for PVF-modified sample (batch# PDS091714B-PVF), n = 3; for chitosan-modified sample (batch# PDS091714B-Chitosan), n = 2. The compression force was set to be 20nN. The error bar represents the standard error of the mean.

All above results suggest strong positively charged ions such as Ca^{2+} and Mg^{2+} ions in the hardness water may promote the attraction of the negatively charged PMC to model fabric film surfaces but interrupt the adhesion of any positively charged PMC to them. Because both cellulose and PET film surfaces are originally negatively charged, it is highly possible that Ca^{2+} and Mg^{2+} ions deposit and coat the film surfaces when the films are soaked into the hardness water. Then the positively charged ions make the film surface repel the similar positively charged PMCs such as PVF and chitosan-modified ones. However, since the control PMC surface is negatively charged, the Ca^{2+} and Mg^{2+} ions coating may act like a bridge in between of the PMC and film surfaces therefore promoting the attraction of the control microcapsules to the films.

5.4.2 Adhesion of PMCs to model fabric films in surfactant solutions

The adhesion of PAC-PVOH PMCs to model fabric films in surfactant solutions was measured using AFM to find out the possible mechanism. As the main surfactant in the industry, LAS was chosen as one of the target surfactants. SDS was chosen as another target surfactant because of its simple molecular structure and the fact that it has been researched thoroughly both in academic and industry; therefore it could be easier to interpret the phenomenon observed from the experiment and to analyse the data. Due to the complex interactions among the ingredients of laundry detergent and hardness ions in water, insoluble particles of micrometre to millimetre scales form in the laundry detergent solution (Matheson *et al.*, 1985, Bajpai, 2007) which can interrupt the AFM adhesive force measurement of single microcapsules. Therefore, no real wash solution was used for the AFM measurement. Moreover, the interaction between single

microcapsules and the model fabric films may have not reached equilibrium at 0.01s contact time according to the results in §4.4.4, the combined analyses of both short (0.01s) and long (10s) contact time data may reveal the mechanism of the enhancement of adhesion by the surface modifications of PVF and chitosan in surfactant solutions.

5.4.2.1 Adhesion of PMCs to model fabric films in SDS solutions

Figure 5.17 and Figure 5.18 present the adhesive force measurement results of single PMCs in SDS solutions at a contact time of 0.01s and 10s using AFM on both model fabric films, respectively.

According to Figure 5.17, on cellulose film:

- At 0.01s contact time (Figure 5.17 (a)), the normalised adhesion of control sample was the lowest among the three samples in DI-water (SDS concentration = 0); it was further reduced to less than half of that through the addition of SDS concentration of 100ppm to 1500pm. Moreover, the normalised adhesion of chitosan-modified sample was about half of PVF-modified one in DI-water. Through the SDS concentrations from 100ppm to 1500ppm, the normalised adhesion of the both modified microcapsules were gradually reduced as well. The values of normalised adhesion of all three samples were reduced to about 0.1mN/m at 1500ppm SDS concentration.

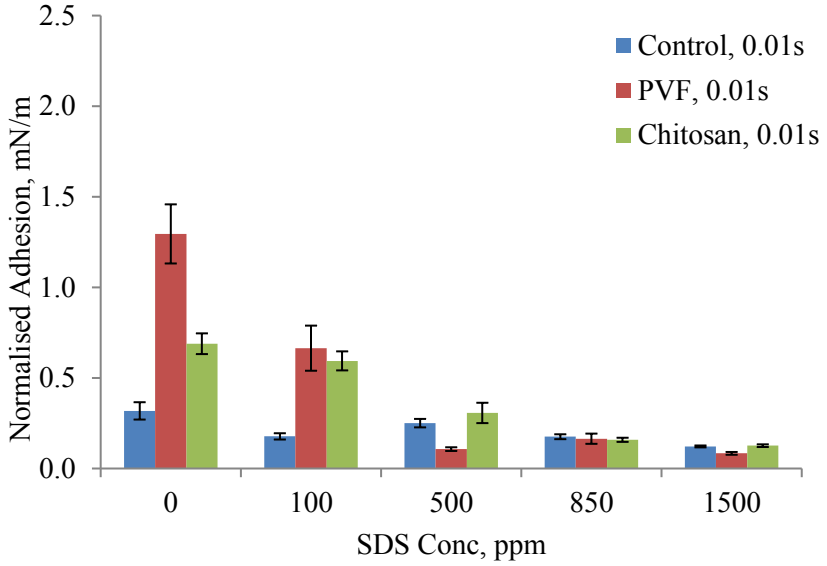

(a)

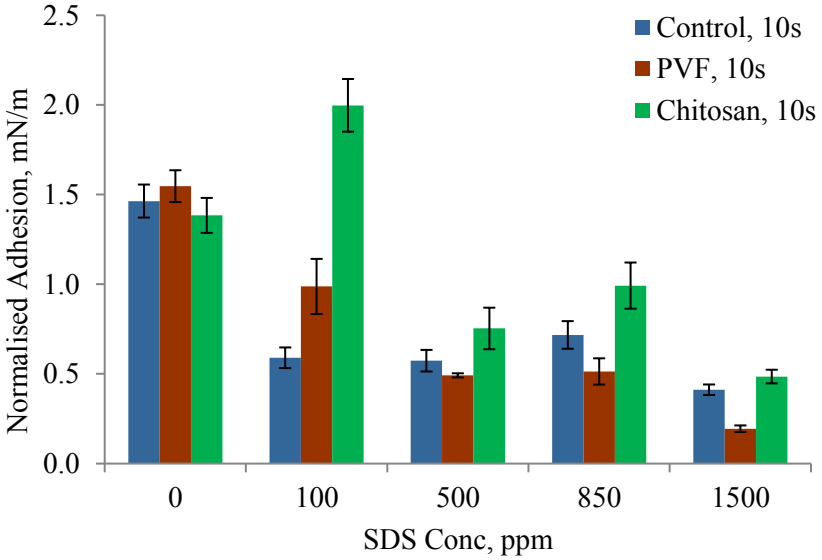

(b)

Figure 5.17 Comparison of mean normalised adhesion of single microcapsules in SDS solutions on cellulose film at a contact time of 0.01s (a) and 10s (b) using AFM. For control sample (batch# PDS091714B), n = 3; for PVF-modified sample (batch# PDS091714B-PVF), n = 3 ~ 5; for chitosan-modified sample (batch# PDS091714B-Chitosan), n = 3. The compression force was set to be 20nN. The error bar represents the standard error of the mean.

- At 10s contact time (Figure 5.17 (b)), all three samples showed similar normalised adhesion in DI-water. Through the increasing SDS concentrations, the normalised adhesion of both control and PVF-modified samples decreased. However, with 100ppm SDS concentration, the normalised adhesion of chitosan-modified sample was found to significantly increase before it decreased with increasing SDS concentration to 500ppm and beyond. Moreover, the normalised adhesion of chitosan-modified samples was greater than that of PVF-modified ones in the corresponding SDS solutions.

On PET film, at both 0.01s (Figure 5.18 (a)) and 10s (Figure 5.18 (b)) contact time: the normalised adhesion values of both control and chitosan-modified samples significantly increased from zero to 100ppm SDS solution and then decreased through the further addition of SDS. In contrast, normalised adhesion of PVF-modified samples decreased with the increasing SDS concentration. However, the decreasing rate of the normalised adhesion of PVF-modified sample was much lower than that of control or chitosan-modified one. In 850ppm SDS solution, the normalised adhesion of control sample decreased to the magnitude of 1 – 2 mN/m whilst the ones of PVF and chitosan-modified samples were at about 5 – 10 mN/m. At 1500ppm SDS concentration, the normalised adhesion of all the three samples decreased to about 1 – 2 mN/m.

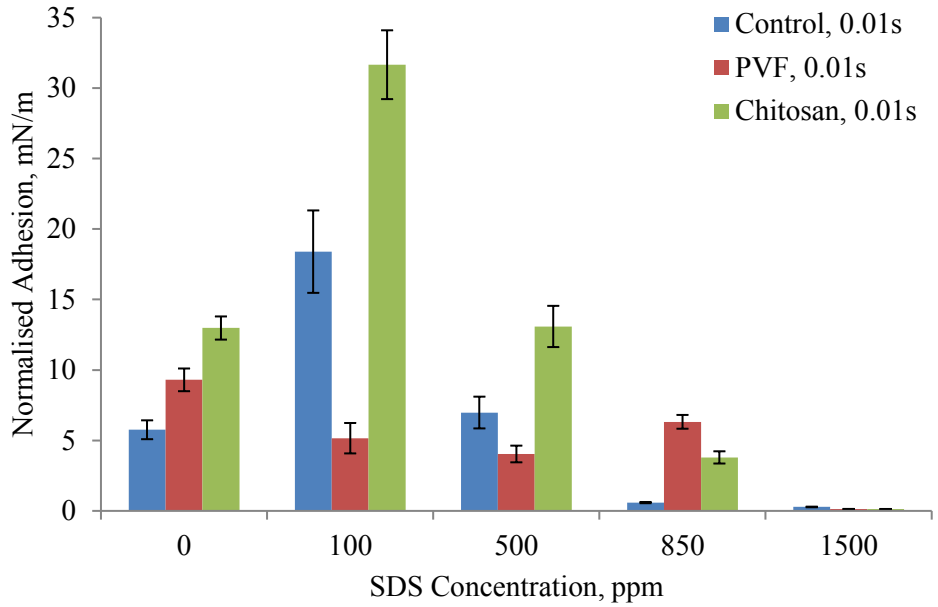

(a)

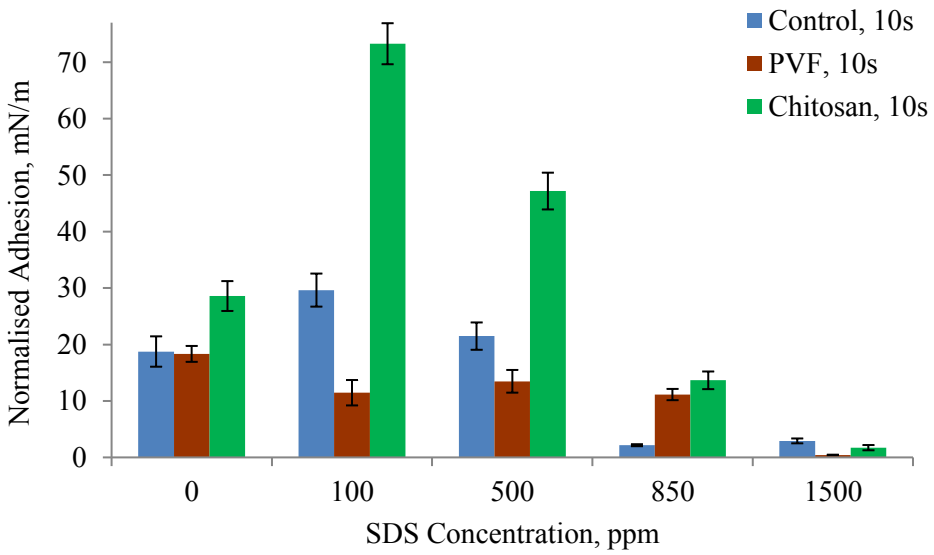

(b)

Figure 5.18 Comparison of mean normalised adhesion of single microcapsules in SDS gradient solutions on PET film at a contact time of 0.01s (a) and 10s (b) using AFM. For control sample (batch# PDS091714B), n = 3; for PVF-modified sample (batch# PDS091714B-PVF), n = 3 ~ 5; for chitosan-modified sample (batch# PDS091714B-Chitosan), n = 3. The compression force was set to be 20nN. The error bar represents the standard error of the mean.

5.4.2.2 Adhesion of PMCs to model fabric films in LAS solutions

Figure 5.19 and Figure 5.20 present the adhesive force measurement results of single PMCs in LAS solutions at a contact time of 0.01s and 10s using AFM on both model fabric films, respectively.

On cellulose film (Figure 5.19), all the normalised adhesion values are at 0.1 – 1mN/m level. Though chitosan-modified PMCs kept a similar level of normalised adhesion in 100ppm LAS concentration versus that in DI-water at both contact times, the rest of the normalised adhesion of all the three samples decreased with the increase of LAS concentration and their mean values were all smaller than the corresponding ones in DI-water.

On PET film (Figure 5.20), all the three samples showed strong adhesion in DI-water as well as in 100ppm LAS solution at both contact times; the normalised adhesion of PVF-modified sample even had a significant increase in 100ppm LAS condition than that in DI-water. However, with the increase of LAS concentration to 500ppm LAS, the magnitude of all the normalised adhesions at 0.01s contact time decreased dramatically from about 5 – 10 mN/m to less than 1 mN/m and remained at such level through the 850ppm and 1500ppm LAS conditions; at 10s contact time, such magnitude was reduced from 15 – 30 mN/m to 5 – 10 mN/m at 500ppm LAS concentration and was further reduced to about 2 – 3 mN/m at 850ppm and 1500ppm LAS concentrations.

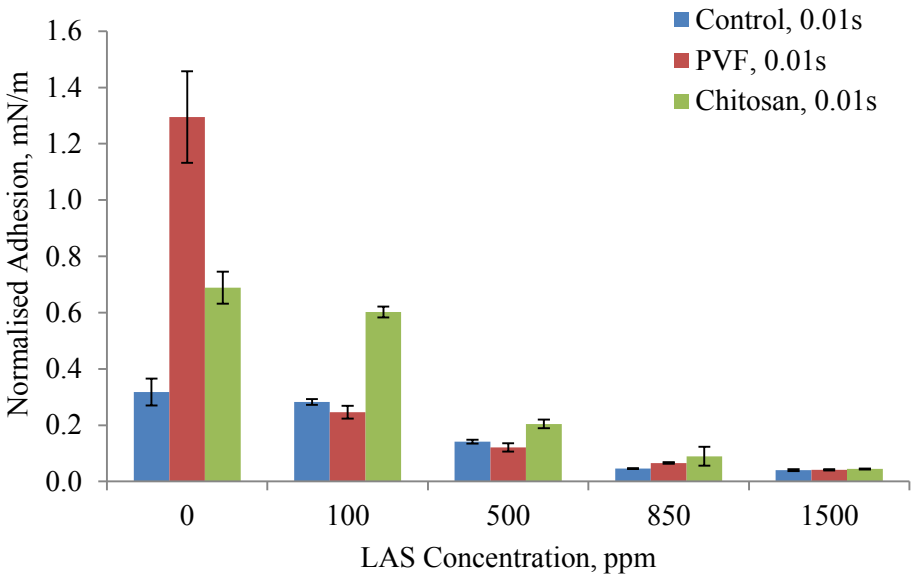

(a)

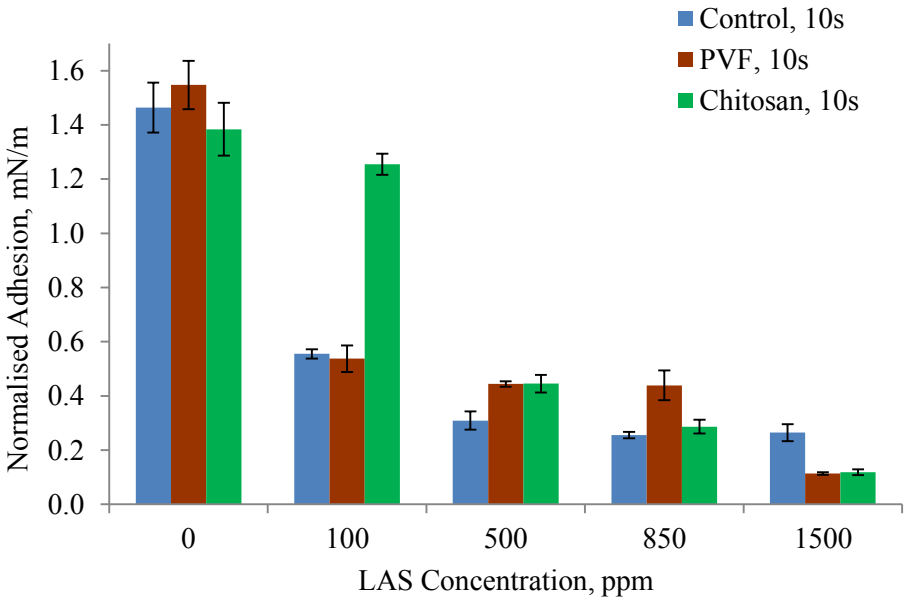

(b)

Figure 5.19 Comparison of mean normalised adhesion of single microcapsules in LAS gradient solutions on cellulose film at a contact time of 0.01s (a) and 10s (b) using AFM. For control sample (batch# PDS091714B), n = 3; for PVF-modified sample (batch# PDS091714B-PVF), n = 3; for chitosan-modified sample (batch# PDS091714B-Chitosan), n = 3. The compression force was set to be 20nN. The error bar represents the standard error of the mean.

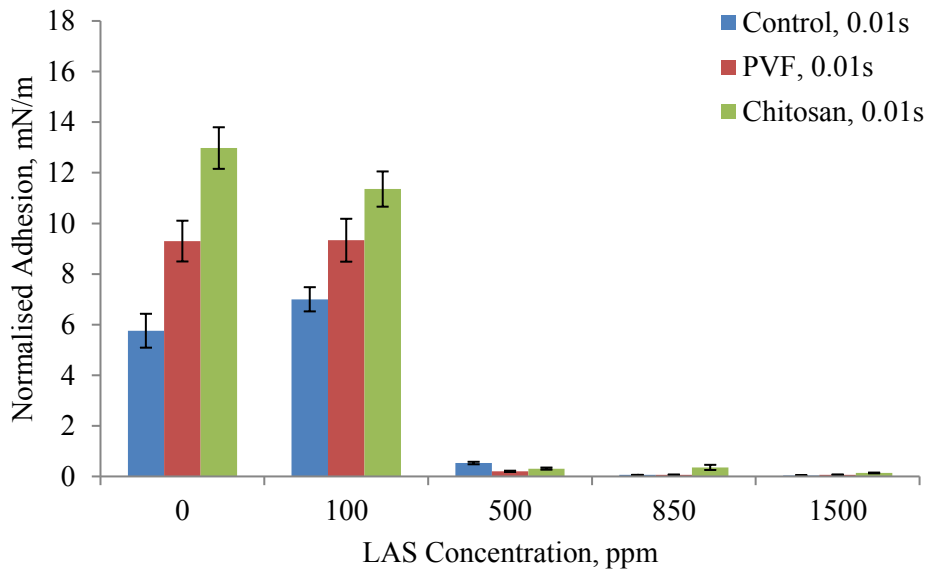

(a)

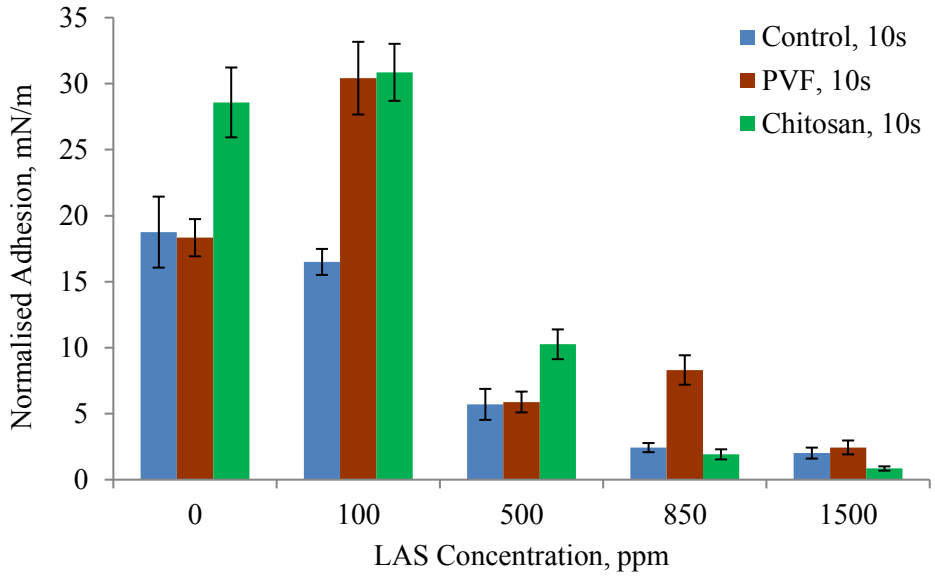

(b)

Figure 5.20 Comparison of mean normalised adhesion of single microcapsules in LAS gradient solutions on PET film at a contact time of 0.01s (a) and 10s (b) using AFM. For control sample (batch# PDS091714B), n = 3; for PVF-modified sample (batch# PDS091714B-PVF), n = 3; for chitosan-modified sample (batch# PDS091714B-Chitosan), n = 3. The compression force was set to be 20nN. The error bar represents the standard error of the mean.

5.5 Discussion

5.5.1 Properties of microcapsule surfaces that impact on adhesion

Both polymer modifications of PMC surface were evident to be uneven from §4.3.3 (for PVF modification) and §5.2.2 (for chitosan modification) because of relatively low amounts of the related polymers due to cost consideration. Although AFM measured the adhesion of single PMCs on model fabric films directly, the uneven coating could contribute to the inconsistency in AFM adhesion data because only a limited number (normally 3, maximum 4 – 5) of single microcapsules could be tested realistically for each sample in each tested condition, which could lead to overall large variations of the adhesive force data. However, since a relatively large population of microcapsules (at least 1mL 0.5% PMC suspension for each experiment) was used in each flow chamber experiment, the technique could provide statistically representative adhesion characteristics in a short period of time with relatively small variations in the deposition and retention results. Therefore, the combined analyses of AFM and flow chamber retention data together could help elaborate the mechanism of the interactions between the PMCs and model fabric films.

5.5.1.1 Surface charge and charge density

The discussion of the effect of surface charge and charge density of the modified PAC-PVOH PMCs on their adhesion to model fabric films in aqueous solutions other than DI-water follows §4.5.2. From the Zeta-potential results in §5.2.3, it can be concluded that the chitosan modification used in this project showed pH sensitivity which made the modified microcapsule surface neutral at the pH of 5.0 and negatively charged

above pH 7.0. This behaviour is similar to that of non-modified control sample since with a pK_a at about 6.5, chitosan can be only incompletely ionised and partially solubilised at pH near neutral, i.e. pH 5 – 7 (Ilium, 1998). A typical force curve from AFM measurement of a chitosan-modified PMC approaching the model cellulose film in DI-water (Figure 5.21) shows the chitosan modification made the sample particle week negatively charged; and it is different from the PVF modification which was positively charged shown in §4.5.2.2. When the distance between the tested chitosan-modified microcapsule and target cellulose film was less than 30 nm, the strong interactions such as Van der Waals force dominated and reversed the interactive force between them from repulsion to attraction. Moreover, all these data are correlated well with the Zeta-potential results.

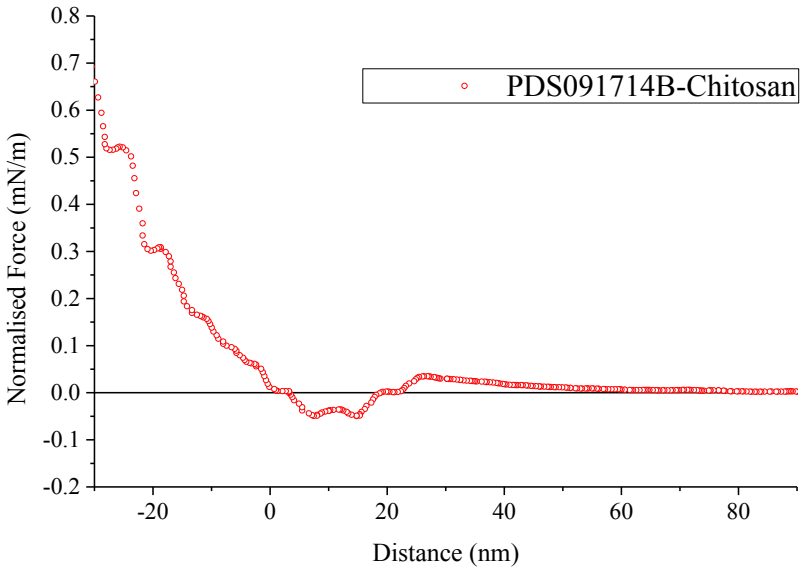

Figure 5.21 Typical force curve when single chitosan-modified PMCs approached a model cellulose film in DI-water obtained using AFM.

As the model cellulose and PET films are both negatively charged (§4.5.2.1), attraction is expected between PVF and chitosan-modified microcapsules and both films at pH ≤ 7 condition. Therefore, the strong electrostatic attraction may dominate the process of getting microcapsules closer to model fabric films (deposition process in flow chamber experiment and approach process in AFM tests). Furthermore, upon contact, charge neutralisation could take place and the bonding of the counter charged parts may trigger tangling of the polymeric molecules resulting in the partially transfer of the coated materials from microcapsules to corresponding film surfaces (Giesbers et al., 2002, He *et al.*, 2014). When separating the two parts, the bonding and tangling could extend the connected polymers in between and enlarge the force and energy required to remove the microcapsules from the film surfaces.

5.5.1.2 Adhesion as a function of ion strength

According to DLVO theories introduced in §2.4.1, strong electrolyte ions suppress the electrical double layer in the solution which means the increase of ion strength decreases the thickness of electrical double layer, resulting in the decrease of the Debye length (Israelachvili, 2011, Zoppe et al., 2011, He *et al.*, 2014). Moreover, as shown in Equation 2.2 and Equation 2.4, the Debye length is an independent parameter which is only associated to the ion strength in the solution. Calculation results of Debye length of 1gpg and 15gpg hardness solutions, using Equation 2.4 and hardness preparation information from §3.2.3, are 7.8nm and 2.1nm, respectively; whilst the Debye length in pure neutral (pH 7) DI-water was reported 960nm (Israelachvili, 2011). These results indicate the interactive range of the microcapsule and model film surface becomes short through the increase of ion strength, e.g. by the addition of hardness and surfactants.

To further elucidate the effect of the different interactions on the change of the surface charge and charge density, additional Zeta-potential measurements were conducted using the test conditions of both flow chamber and AFM experiments for all the three microcapsule samples. As hardness is composed of mixtures of salts such as Ca^{2+} and Mg^{2+} ions (15gpg equals to about 1.9mM Ca^{2+}), to make better comparisons, single $CaCl_2$ solution was prepared because Ca^{2+} has stronger electrostatic effect than Mg^{2+}. Corresponding NaCl solution was also prepared to compare the results. Subsequent Zeta-potentials of all PMC samples in both single salt solutions at pH 7.0 were measured and the results are shown in Figure 5.22.

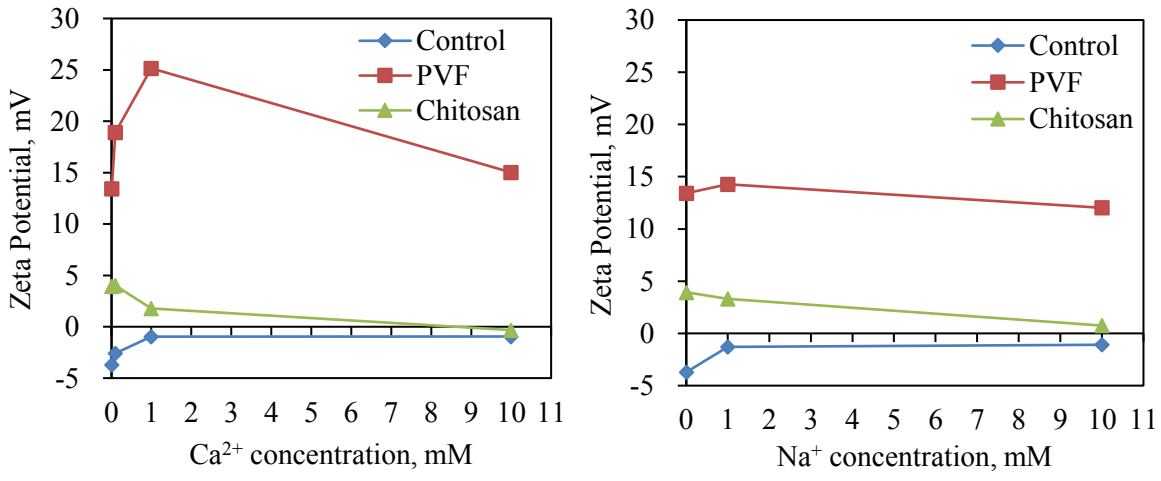

Figure 5.22 Comparison of mean Zeta-potentials (N = 3) of microcapsule samples in $CaCl_2$ (a) and NaCl (b) solutions at pH 7.0, respectively. The tested ion concentrations were 0 (DI-water), 0.1, 1 and 10mM. Sample information: control batch# PDS091714B; PVF-modified batch# PDS091714B-PVF; chitosan-modified batch# PDS091714B-Chitosan.

The Zeta-potential value of PVF-modified microcapsules experienced an increase then decrease through the increasingly addition of either Ca2+ or Na+ ion. Moreover, it kept positive above 10mV and was much greater than those of control and chitosan-modified samples (which were around 0mV). Furthermore, it is clear that the increase of ion strength decreases the net surface charge of both control and chitosan-modified microcapsules. All these results indicate the positive surface charge of the PVF-modification could be less sensitive than chitosan modification to the increase of the ion strength.

Since the main PVF polymer used in this project was Lupasol® VT with only 20% hydrolysis rate, most of the positive charge groups are in amide form. The carbonyl group (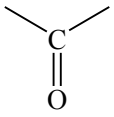) near the –N–C– bond can attract electron and may protect the positive centre from external influences. In contrast, most positively charged centres in chitosan (75~85% degree of deacetylation) are in amino form which is less protected from environment.

Figure 5.23 shows the normalised attraction measured during the approach of adhesive force measurement using AFM. It can be found that addition of hardness ions greatly increased the attraction between control microcapsules on both the films. The attraction between PVF-modified PMCs and cellulose film was almost constant through the addition of hardness concentration further confirmed the conclusion from above Zeta-potential analysis; the observed decrease of its attraction on PET film may be due to the positive hardness ion attaching to the negatively charged surface of the PET film, resulting in repelling to the PVF polymer on PMCs.

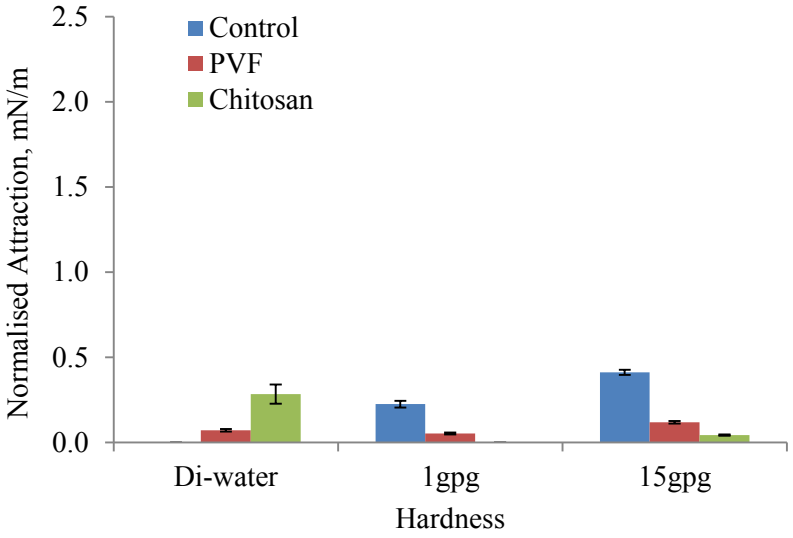

(a)

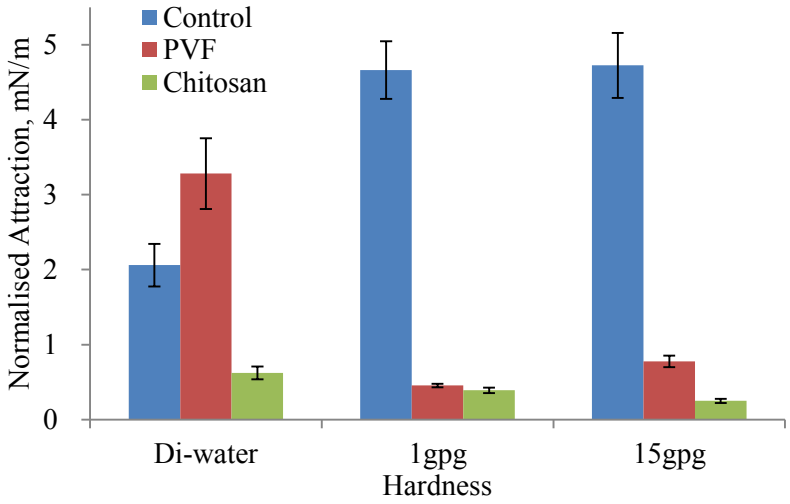

(b)

Figure 5.23 Comparison of mean normalised attraction of single microcapsules in hardness water solution on model cellulose film (a) and PET film (b) using AFM. For control sample (batch# PDS091714B), n = 3; for PVF-modified sample (batch# PDS091714B-PVF), n = 3; for chitosan-modified sample (batch# PDS091714B-Chitosan), n = 2. The error bar represents the standard error of the mean.

Figure 5.23 also shows that the attraction of chitosan-modified PMCs decreased with the increasingly addition of hardness ions. Noted that on cellulose film, the values of attractive force for control sample in DI-water and chitosan-modified sample in 1gpg

hardness solution were actually negative, therefore no data is shown in Figure 5.23 (a) for either sample. Combined with their Zeta potential data being negative in neutral condition (Figure 5.3), this means the two samples in the corresponding conditions had negatively charged surface and repulsive force was dominant when they approached the cellulose film. As the increasingly addition of hardness ions, the positively charged ions performed as a bridge to connect both negatively charged microcapsule and the film surfaces and therefore promoted the adhesion between them. Therefore, the positive hardness ions may coat on film surfaces and promote the adhesion of control samples to the film but reduce the adhesion between the modified PMC samples and the film.

5.5.1.3 Effect of surfactant on adhesion

From §5.3.5 and §5.4.2, it can be found that both SDS and LAS surfactants had overall negative influence on the adhesion of microcapsule samples to the model fabric films with the exception of 100ppm surfactants on PET film. To further explain the observations, Zeta-potential of the microcapsule samples in such surfactant solutions was measured and data are presented in Figure 5.24. The data show that after addition of surfactant, Zeta-potential of all the positively charged microcapsules became negative, indicating it is highly possible that they attracted and were coated by such surfactant molecules.

As mentioned in a number of literatures, surfactant in solution at concentration under its CMC will present at the interfaces as well as in bulk individually (Mukerjee and Mysels, 1971, Scamehorn et al., 1982, Haigh, 1996, Khan and Shah, 2008). Only after reaching its CMC, excessive surfactant molecules starts to form micelles in the solution; if interfaces of the solution increases after that (e.g. addition of oil droplets into water

phase), the surfactant will be released from the micelles and absorbed to the surface until all the new created interfaces are covered.

Since SDS has a large CMC value of about 8mM (2360ppm) in ambient condition (Mukerjee and Mysels, 1971) possibly due to its small molecular structure, it is clear that the surfactant can hardly form micelle under the tested concentrations in this research; nor could the individual SDS molecules cover all the surfaces in any of the tested conditions. Therefore, all the SDS conditions in this research may result in insufficient coatings around the microcapsule particles and on the corresponding film surfaces. The increasingly decrease of the Zeta potential results of any of the microcapsule samples through the increase of SDS concentration (Figure 5.24 (a)) is the proof. Moreover, the molecular structure of the repeating unit on PVF is smaller than that of chitosan. Thus, it is easier for the negatively charged SDS molecules to aggregate around PVF molecules resulting in a significantly more negative Zeta potential of PVF modification at the same SDS concentration versus either control or chitosan-modified samples.

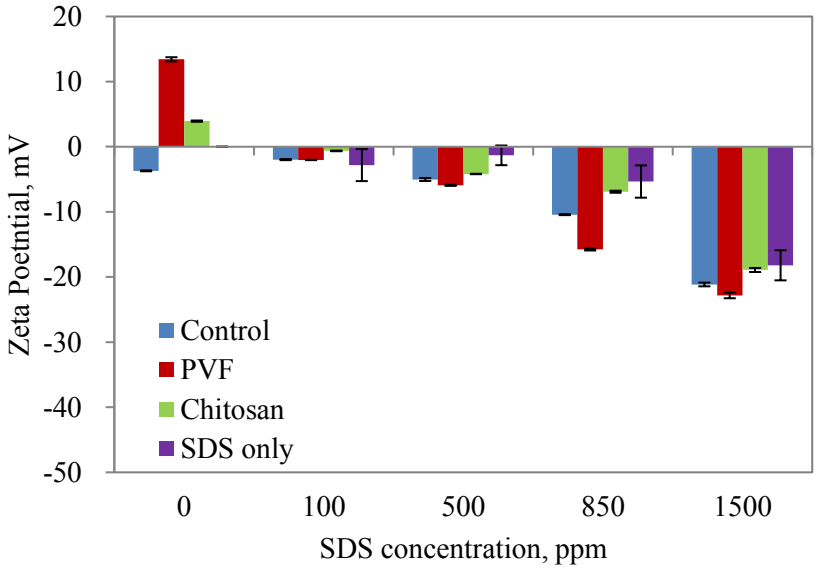

(a)

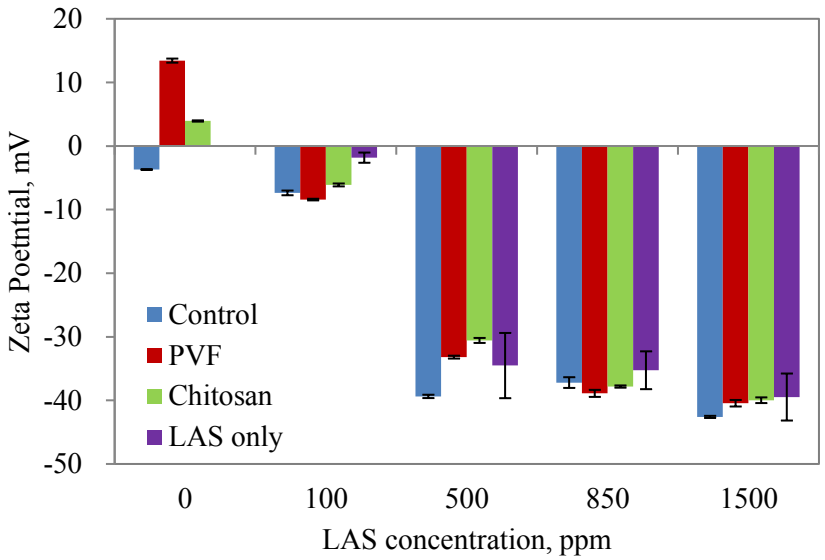

(b)

Figure 5.24 Comparison of mean Zeta-potentials (N = 3) of microcapsule samples in SDS (a) and LAS (b) solutions at pH 7.0. Sample information: control batch# PDS091714B; PVF-modified batch# PDS091714B-PVF; chitosan-modified batch# PDS091714B-Chitosan. The error bar represents the standard error of the mean. SDS only and LAS only solutions are DI-water with addition of SDS and LAS surfactants at corresponding concentrations without any microcapsule samples, respectively.

In contrast, CMC of LAS at ambient condition is around 1 – 2mM (about 350 ~ 700ppm) according to different reports (Cox *et al.*, 1985, Furton and Norelus, 1993, Khan and Shah, 2008, Samper *et al.*, 2009). Combined with the Zeta-potential data (Figure 5.24 (b)) that the LAS only solution above 500ppm had an almost stable Zeta-potential value, it is highly possible that the LAS used in this project has a CMC concentration between 100 – 500ppm. Moreover, the observation that Zeta-potential values of all microcapsule samples above 500ppm LAS were similar to the ones of LAS only solutions could further verify this inference.

The normalised attractive force data measured by AFM are shown in Figure 5.25. Upon approach, all the microcapsule samples showed repulsion on cellulose film in both SDS and LAS surfactant conditions (therefore, there is no attractive force chart for cellulose film) whilst some attractive behaviours were observed on PET film. These attractions could be due to a combined effect of the follows:

1) Partial surfactant coating of microcapsules and films at a lower surfactant concentration than the CMC.
2) Interaction between cationic polymer and anionic surfactants.

Point 1) has been elaborated in the above discussion. For point 2), when adding a small amount anionic surfactant, the ionised molecules may react with the cationic polymers and form precipitate. Only after the increase of the surfactant concentration, the precipitate can be suspended into the solution by the excessive surfactants (Goddard and Hannan, 1976, Goddard, 2017). In this case, where both polymer and surfactant concentrations were low, the precipitate would form and deposited on the surface of the microcapsule and film. Moreover, chitosan has more unprotected cationic groups than PVF does. It can be concluded that chitosan-modified PMCs will have more such precipitate on the shell surface. Since the precipitate is formed by electrostatic bonding, its outer layer would be hydrophobic (composed of surfactant tails), which is more compatible with PET film. The combined results may cause the chitosan-modified sample to generate a greater attractive force in such low concentrated surfactant solutions than the PVF-modified sample.

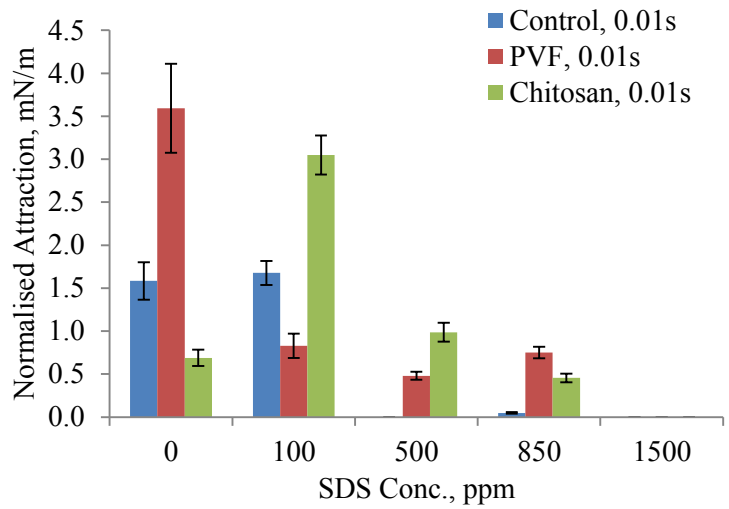

(a)

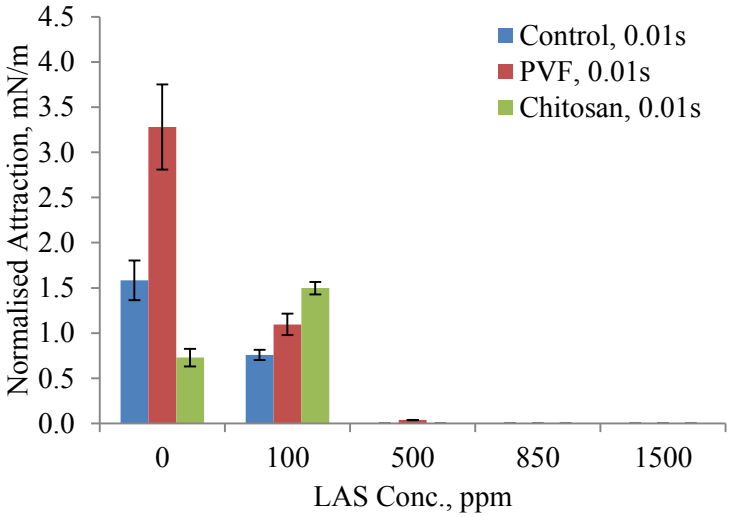

(b)

Figure 5.25 Comparison of mean normalised attraction of single microcapsules in SDS (a) and LAS (b) solutions on PET film using AFM. For control sample (batch# PDS091714B), n = 3; for PVF-modified sample (batch# PDS091714B-PVF), n = 3; for chitosan-modified sample (batch# PDS091714B-Chitosan), n = 3. The error bar represents the standard error of the mean.

In real wash condition, where a large amount of surfactants, hardness ions and other polymers, builders from the detergent formulation interact together in the solution, insoluble precipitates including different polymer-surfactant precipitates, Ca-builder

residues and $Ca(LAS)_2$ (Showell, 1997, Verge *et al.*, 2001, Yangxin *et al.*, 2008) will most likely deposit onto the surfaces of microcapsules and target fabrics. This will cause similar situations to those described above and the adhesion in such case would be a very dynamic process. However, the findings in flow chamber experiments described in §5.2.5 suggest the complicated phenomena may not necessarily bring negative impact on the retention or adhesion of the microcapsules on the fabrics. In contrast, the appearance of the other ingredients in real washing condition could result in better deposition and retention of the microcapsules on the model fabric films than in high level surfactant solutions only, as shown in Section §5.4.2.

5.5.1.4 Effect of hydrophobicity

The relationship between PVF modification and hydrophobicity in DI-water condition has been discussed in §4.5.3. Compared to the chitosan data in this chapter, the balance of hydrophobicity and hydrophilicity resulting from chitosan modification seems less important than that from PVF modification. This may be because the properties of hydrophobicity are dependent on the molecular weight and shape of the hydrophobic parts. However, the chitosan used had relatively small molecular weight (50k Da). Moreover, as a hydrogel material, chitosan contains a large number of hydroxyl and amino groups in its molecules, which makes it overall hydrophilic. Furthermore, the introduction of electrolytes like hardness ions and surfactants further deteriorated the possibility to maintain the hydrophobicity of both cellulose and PET films. As both flow chamber and AFM measurement results show, little adhesion was observed at high surfactant concentrations such as a concentration larger than the CMC of the surfactant.

Despite the above reasons, on contact, chitosan-modified PMCs still have intensive interactions with both films according to the AFM measurement results, especially with PET film. Large adhesive forces were detected between the chitosan-modified samples and PET films and such forces were 2 – 5 times larger on average than those on cellulose films. When in 100ppm SDS concentration, chitosan-modified PMCs had the largest adhesion to PET film (Figure 5.18 and 5.25). Note the Zeta potential of the sample in such condition was nearly 0 (Figure 5.24 (a)), it indicates that chitosan-modified PMCs had neutral surface in such condition resulting in minimum electrostatic repulsion to the film surface. Therefore, hydrophobic interaction including polymer-surfactant and polymer-film surface interactions and Van der Waals forces may dominate the adhesion.

On cellulose film, hydrophobic interactions are not dominant as the case with PET film, the possible mechanisms of adhesion are more complicated. Schematic diagrams showed in Figure 5.26 are proposed. The surface of unmodified control PMC is partly hydrophilic with negative charge in DI-water (Figure 5.26 (a)). Although the PMC surface has certain hydrophobicity due to its PAC-PVOH polymer nature, the same negative charged cellulose film surface repulses the capsule and makes the approaching difficult. Moreover, because of the hydrophilicity, both surfaces are covered by a thin layer of water molecules respectively, which prevent the real contact of them. Only on PET film, there is possible real contact, resulting the much higher adhesion (§4.5.3). In hardness water (Figure 5.26 (b)), the high positive charged centres Ca^{2+} and Mg^{2+} are strongly attracted by both control PMC and film surfaces, thus can act as a bridge to "bond" the two surfaces together.

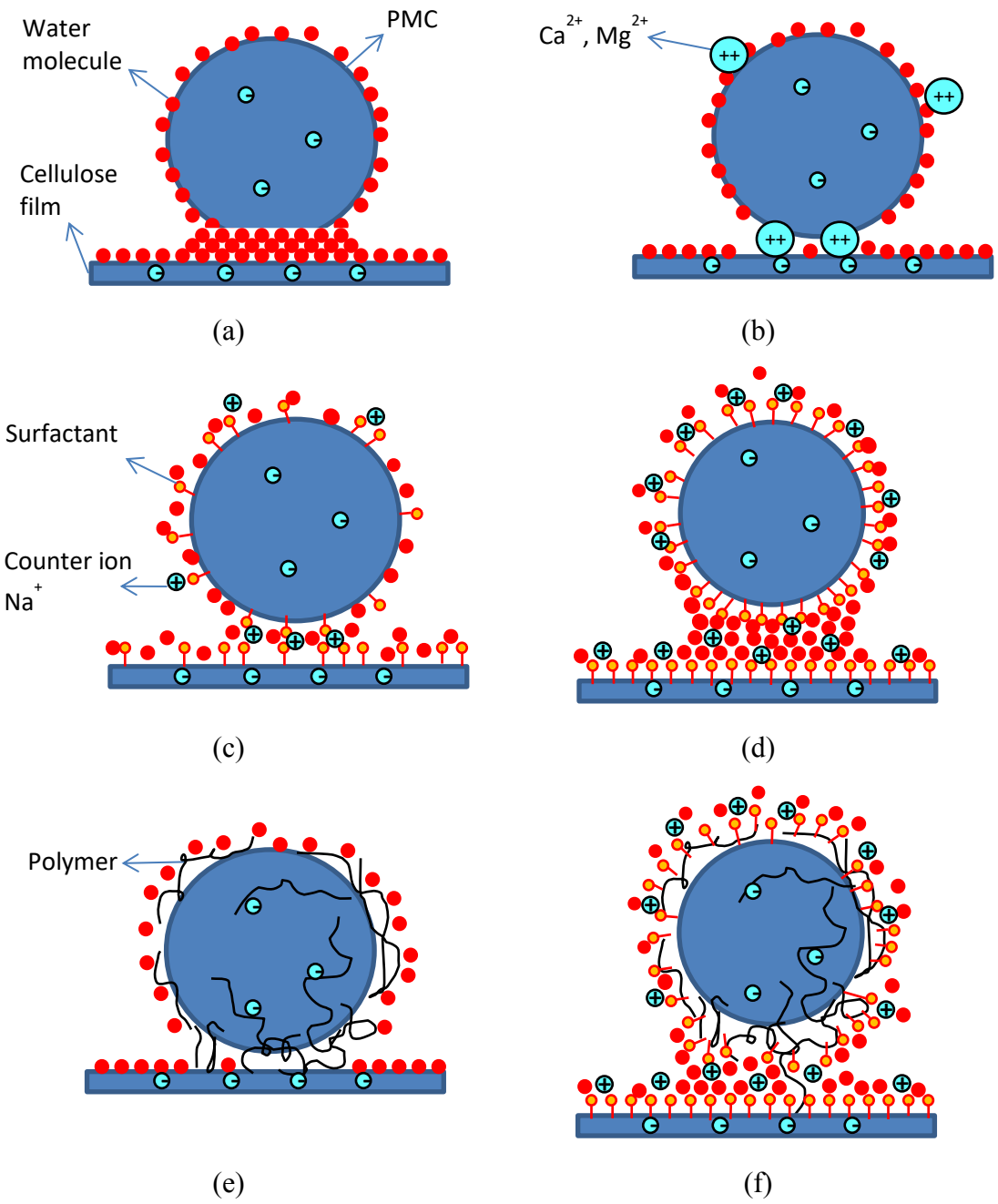

Figure 5.26 Schematic diagrams of PMC adhesion to model cellulose film and the possible impact of PMC surface modifications and different solutions: (a). unmodified control PMC in DI-water, (b) control PMC in hardness water, (c) control PMC in low concentrated (e.g. surfactant conc. < CMC) surfactant solution, (d) control PMC in high concentrated (e.g. Conc. > CMC) surfactant solution, (e) polymer (e.g. PVF or chitosan) modified PMC in DI-water, (f) polymer modified PMC in high concentrated surfactant solution.

At low surfactant concentration (Figure 5.26 (c)), the surfactant amount is not enough to cover all the interfaces in the solution (such as PMC and film surfaces) which means the surfactant molecules cannot effectively form a continuous layer around either PMC or film surface. Therefore, the weak bridging effect of the surfactant's counter ion (Na^+) may exceed the repelling force between PMC and film surfaces to enhance the adhesion. As the surfactant concentration increases (Figure 5.26 (d)), both surfaces of PMC and the model film will be covered by a complete layer of surfactant molecules and the force between them will gradually become repulsive again. With surface modification by polymer containing positive charge centres, PMC surface becomes positively charged so that it can be attractive to the film surface (Figure 5.26 (e)) and enhance the adhesion through bridging (He *et al.*, 2014) and hydrophobic effect (§4.5.3). After the addition of surfactants (Figure 5.26 (f)), though the positive charged centres on the polymer is likely to be neutralised or even reversed, resulting weak or no attraction, respectively, between the PMC and film surface, the long chain of the polymer molecules is still possible to act as a bridge to enhance the adhesion through hydrophobic interaction.

5.5.2 Correlation of flow chamber retention and AFM adhesion results

Both flow chamber retention data and AFM adhesive force results under similar test conditions were put together in order to show any correlation between them. To best reflect the possible conditions during a real laundry process, e.g. at consumer home in a washing machine, data points of flow chamber retention ratio at 0.5Pa shear stress (the highest shear stress for most flow chamber experiments) and 10s contact time from AFM adhesion test were chosen. Figure 5.27 and Figure 5.28 are the correlation charts

for both the chitosan and PVF modified PAC-PVOH PMC samples in SDS and LAS solution conditions on cellulose and PET films, respectively. The data trend and curves on all charts of Figure 5.27 and Figure 5.28, except the one for SDS conditions on cellulose film (Figure 5.27 (a)), show good correlation between flow chamber and AFM experiments. Reading from the charts, it is clear that the flow chamber retention ratio increases with the AFM adhesion for almost all of the tested conditions. However, the reason is not quite clear for the data in Figure 5.27 (a) being not quite consistent between the two experiments, and this may be worth further understanding and research in the future.

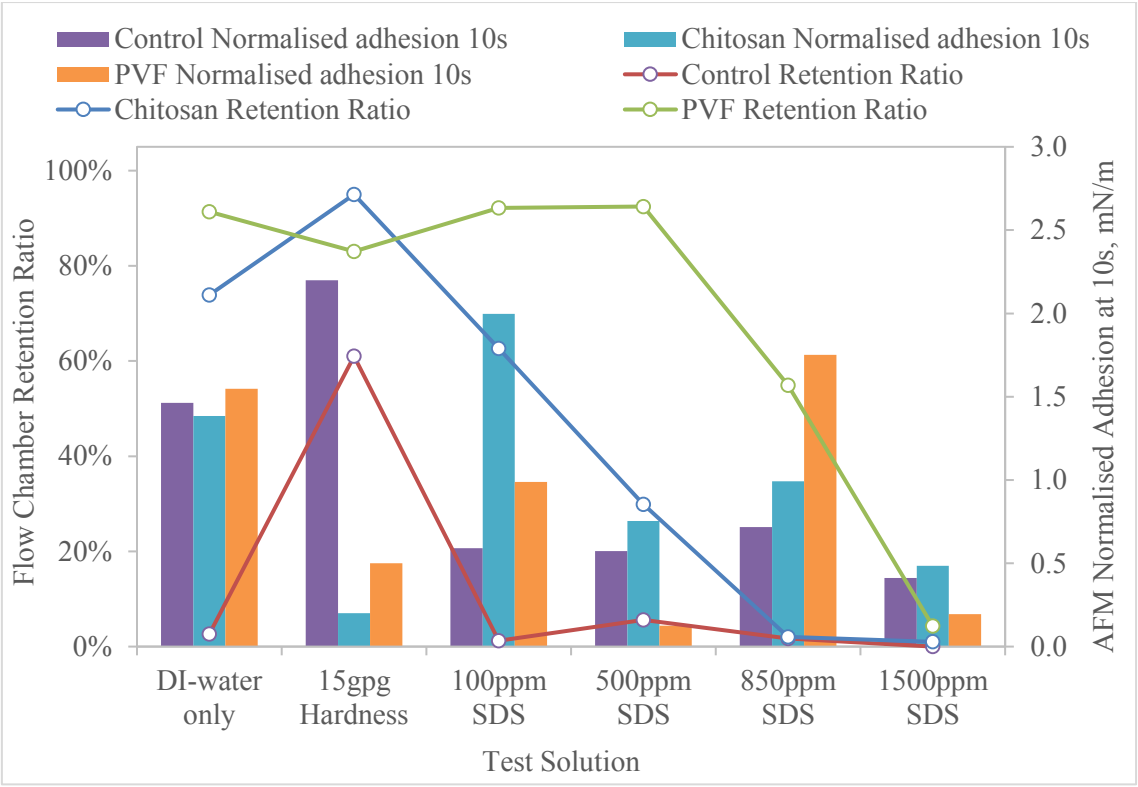

(a)

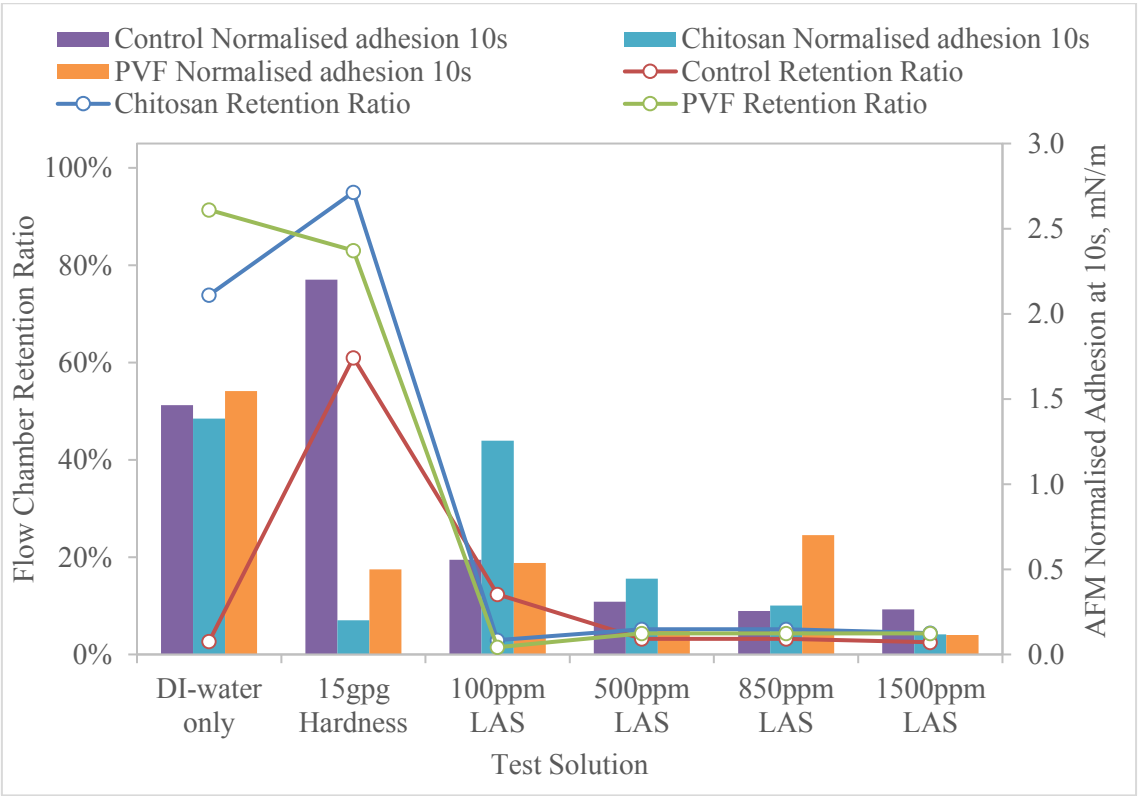

(b)

Figure 5.27 Comparison chart of PMC samples in SDS (a) and LAS (b) solutions on cellulose film. Data points are combined of the mean value of flow chamber retention ratio at 0.5Pa shear stress and AFM adhesive force after 10s contact time only.

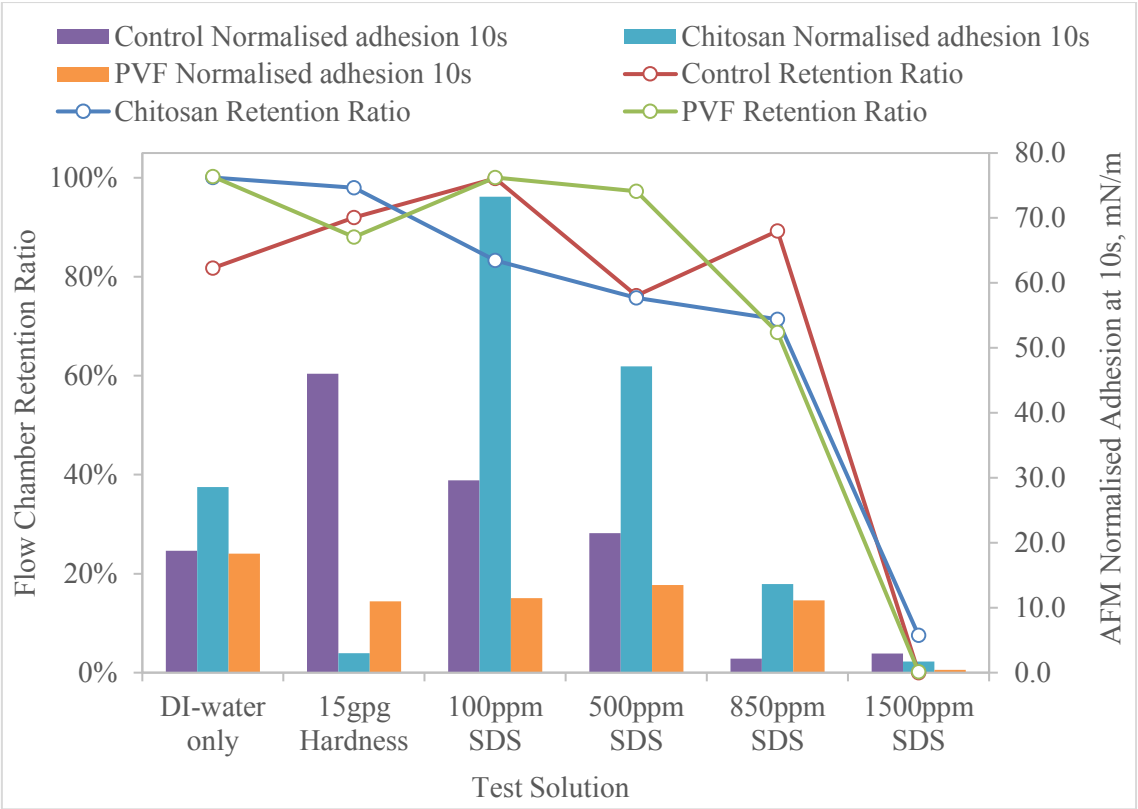

(a)

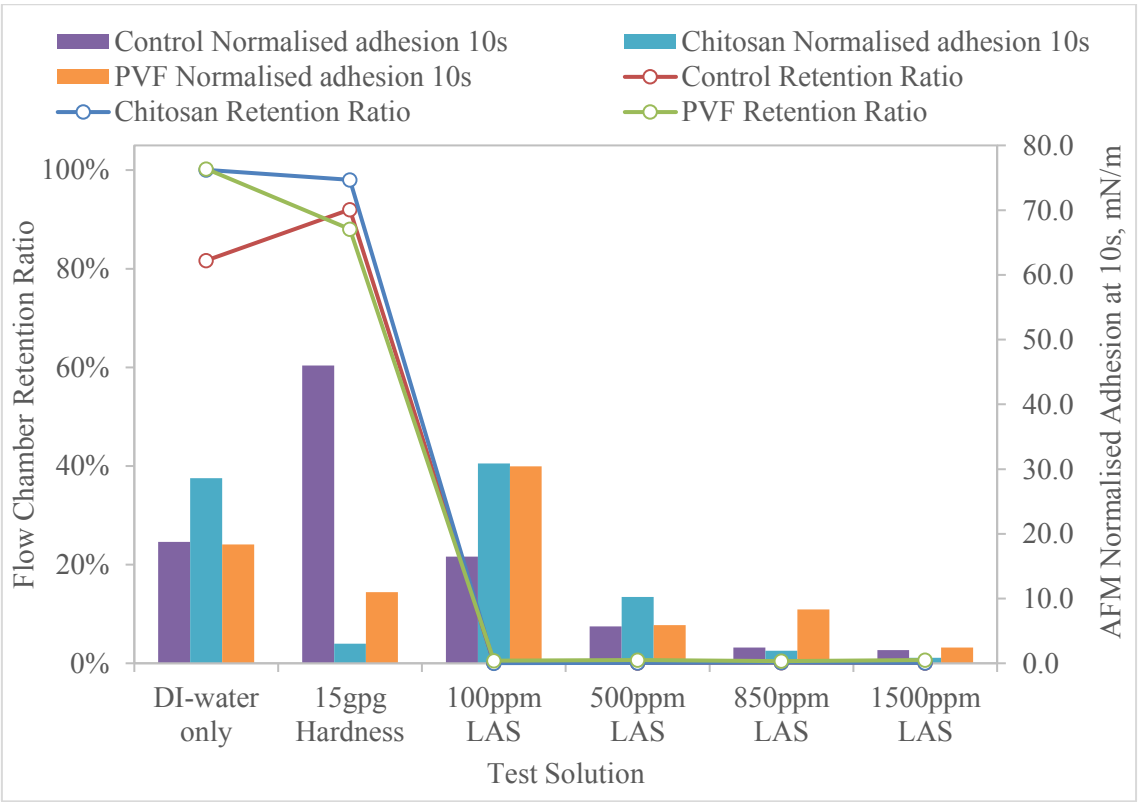

(b)

Figure 5.28 Comparison chart of PMC samples in SDS (a) and LAS (b) solutions on PET film. Data points are combined of the mean value of flow chamber retention ratio at 0.5Pa shear stress and AFM adhesive force after 10s contact time only.

5.6 Conclusions

1. Chitosan was applied to modify PAC-PVOH PMCs, and the characterisation results confirmed the coating was successful.
2. The modified flow chamber device was designed and manufactured, which proved to be robust for undertaking experiments on deposition and retention of the PAC-PVOH PMCs on model cellulose and PET films. The images of microcapsules on the two films were analysed using Matlab and Image J software, which gave consistent results.
3. The flow chamber and AFM results confirmed the effectiveness of chitosan modifications on PAC-PVOH PMCs in enhancing their adhesion to the two model fabric films in DI-water. The addition of hardness to DI-water increases the adhesion of control PMCs to both model fabric films but decreases the adhesion of surface modified ones, possibly due to electro repulsion. SDS and LAS surfactants used below CMC concentrations have less impact on the adhesion of all the tested PMC samples; beyond CMC, additional surfactants greatly decreased it.
4. On the mechanisms of the adhesion of the surface modified PAC-PVOH PMCs to model fabric films, electrostatic force has been confirmed by AFM force curve analysis to dominate the approaching process; on contact, hydrophobic interactions including interface-surfactant interactions and molecular bridging may play important roles in determining the adhesive force. Although it is difficult to investigate the dynamic process in real wash condition, the experiment results suggest the performance of deposition and retention of the surface modified PMCs on both model fabric films would not be worse than those in the high concentration surfactant solutions.

5. The flow chamber retention ratio increases with the AFM adhesion in almost all tested conditions. The data trend of flow chamber retention ratio at 0.5Pa and AFM adhesive force analysed at 10s contact time are correlated in most test conditions on both model fabric films with all three PMC samples as well, which confirms the two test methods may likely be replaceable to each other. However, the reason for the uncorrelated trend in SDS conditions on cellulose film being not quite consistent between the two experiments is not quite clear and this may be worth further understanding and research in the future.

Chapter 6. Investigation of adhesion behaviour of polydopamine-modified MF microcapsules on model fabric films

6.1 Introduction

As introduced in §2.3.6.3, a mussel-inspired polymeric product of dopamine, i.e. polydopamine (PDA) has been identified as one of the strongest adhesives known to date. Although it has become one of the most researched adhesives in multiple industrial applications (Lee et al., 2007, Anderson et al., 2010, Yang et al., 2011), the study of the PDA coatings on PMCs to enhance the perfume delivery in laundry detergent has been insufficient. Therefore, PDA was chosen to be a new coating material to further expand the exploration in this research project.

As the PAC-PVOH PMCs samples from P&G did not have sufficient amount, MF microcapsules with a core vegetable oil (§3.2.2.4) were made in the lab as a substitution. In order to enhance adhesion of MF microcapsules to fabric surface, they were coated using PDA, and its effect was investigated, and the results are presented in this chapter.

The coating of the MF microcapsules was undertaken with PDA in an aqueous solution with different pH values (§3.2.2.5). Consequently, the PDA-coated MF microcapsules were made successfully and subsequent characterisation and performance tests including adhesion of microcapsules to model fabrics measured by AFM and their retention quantified by a flow chamber technique were conducted, which is also the focus of the research presented in this chapter. Data is analysed against literature reports and comprehensive discussions reveal the details of PDA surface functional groups, their formations and related adhesion mechanisms. Finally, a comparison between PDA

surface coating and polyelectrolyte surface modifications are made, pointing out the possible future research direction for the PDA coatings.

6.2 Characterisations of MF microcapsules filled with vegetable oil

Characterisations were done to the MF microcapsules made following the process described in §3.2.2.4. Images from both optical microscope and ESEM (Figure 6.1) show the MF microcapsules were spherical with smooth surface. A few capsules showing broken in Figure 6.1 (a) were the ones with relatively large diameters, which might be caused by sample preparation for imaging. This is reasonable because larger capsules tend to have weaker strength in comparison with the smaller counterparts.

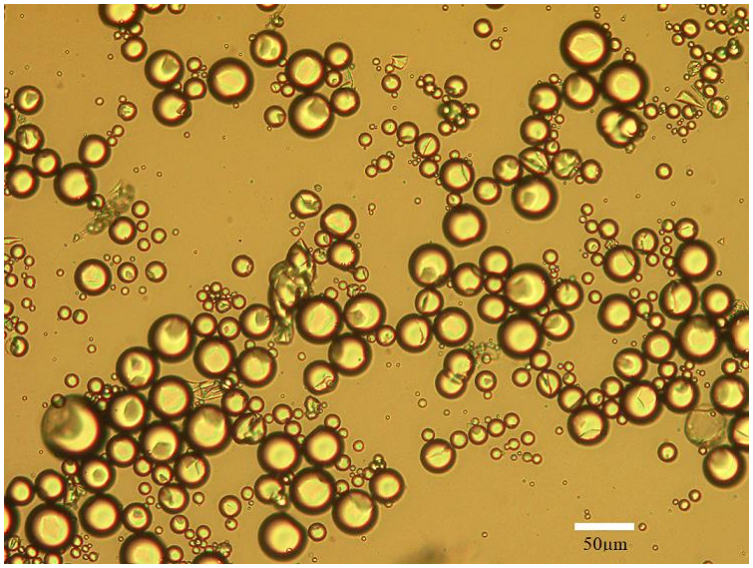

(a)

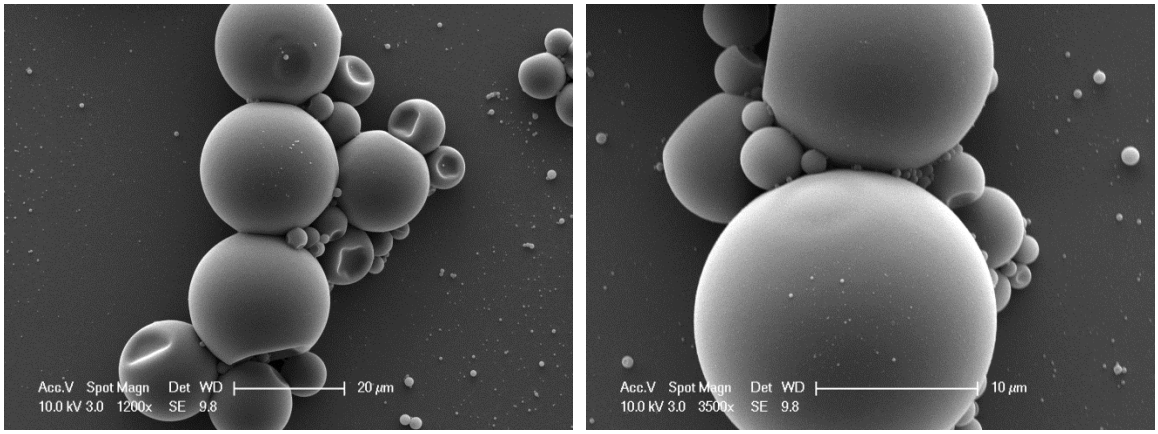

(b) (c)

Figure 6.1 Images of dried MF microcapsules obtained using optical microscope (a) and ESEM ((b) and (c), at different magnifications).

The mechanical properties of the MF microcapsules were obtained using a micromanipulation rig following the method in §3.3.8 and data analysis procedures mentioned in §4.3.4. A representative force vs displacement curve from compression of a single MF microcapsule (with a diameter of 10.8 μm) is shown in Figure 6.2. Clearly this MF microcapsule was relatively more brittle than the PAC-PVOH PMC (Figure 4.9) as it shows multiple rupture points on the compression curve. By selecting and summarising the data corresponding to the first rupture point, the overall nominal rupture stress data of 23 randomly picked MF microcapsules was plotted in Figure 6.3. It is worth noting that the overall nominal rupture stress of the MF microcapsule sample is significantly lower than that of the PAC-PVOH PMC control sample (Figure 4.10) for a given diameter, which means the lab made MF microcapsules were significantly weaker than the sample provided by P&G, which might result from different processing conditions and the core materials used. However, after analysing the elastic range on their force-displacement curves (for example, in Figure 6.2, the elastic range is the linear part at the beginning of the curve from zero point to point A), it was found that

the compressive force at elastic limit of the MF microcapsules with a diameter of 10-20 μm was at around 0.02-0.05 mN. Although the force corresponding to this elastic limit is lower than that of PAC-PVOH PMCs (which was 0.1 mN from §4.3.4.1), according to the force analysis in §4.3.4.1, it is still well above all the forces applied from the flow chamber test and AFM measurement, meaning the MF microcapsules would only experience elastic deformation in the following flow chamber and AFM adhesion tests.

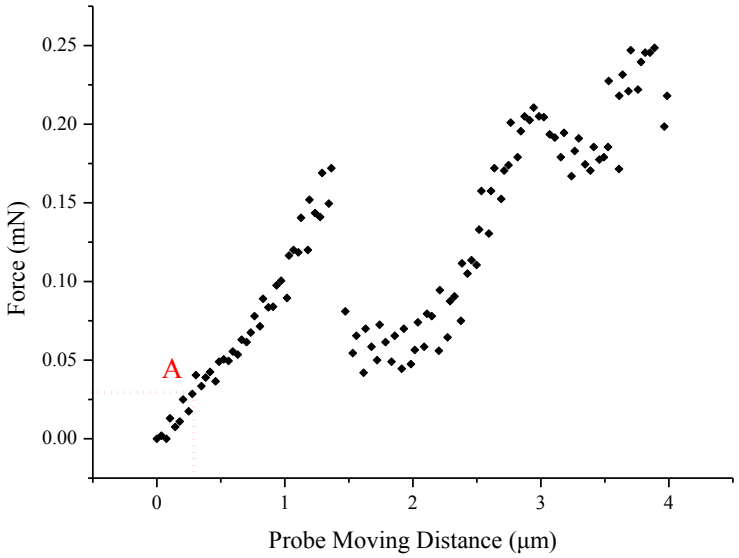

Figure 6.2 Representative force-displacement curve for compressing a single MF microcapsule (d = 10.8 μm). Linear part from the starting (zero) point to point A represents the elastic range of the curve.

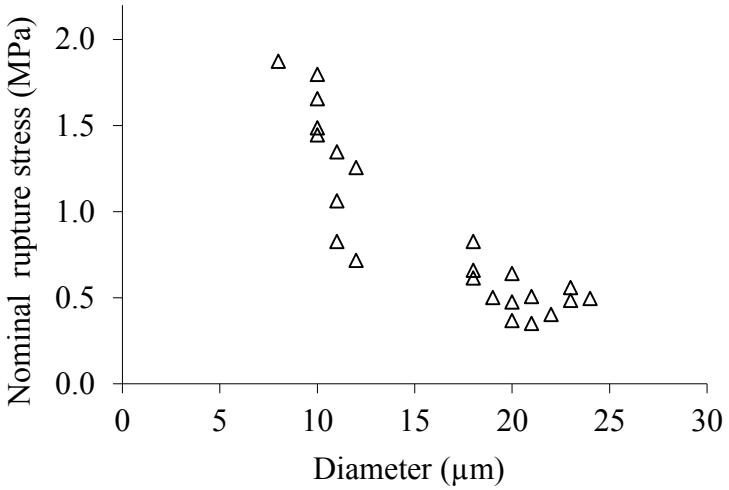

Figure 6.3 Nominal rupture stress data for the lab made MF microcapsule sample.

6.2.1 Characterisation of PDA-modified MF microcapsules

PDA was prepared by the spontaneous polymerisation of dopamine hydrochloride in a TRIS buffer solution at pH 8.4 in ambient air condition (Lee *et al.*, 2007). Figure 6.4 shows the chemical structures of dopamine and PDA, respectively.

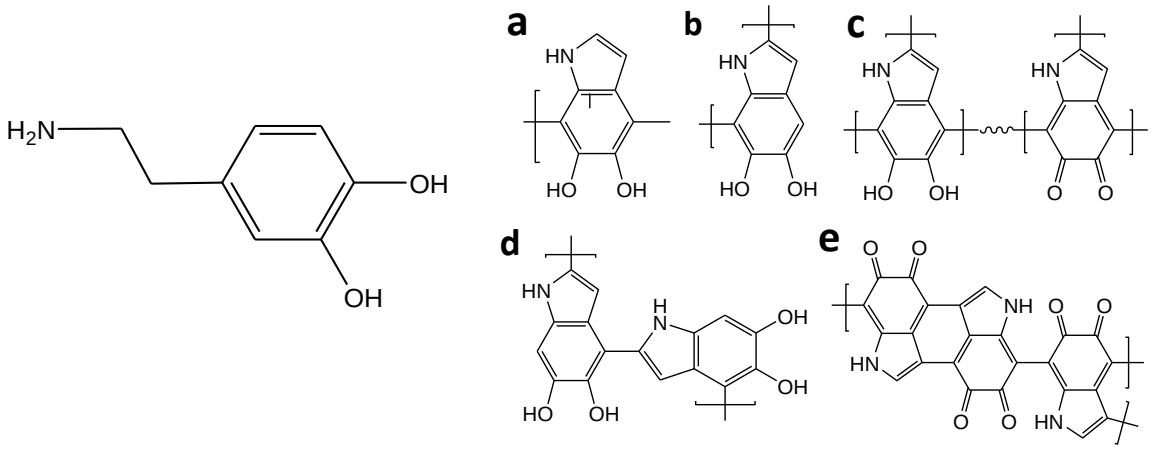

dopamine polydopamine (PDA)

Figure 6.4 Chemical structures of dopamine and PDA

As reviewed in §2.3.6.3, the catechol moieties in polydopamine are oxidised into a mixture of quinone and indole derivatives and subsequently undergo complex polymerisations to form PDA. Because most quinone and indole derivatives are coloured (Kim *et al.*, 2003a), a solution colour change from transparent to dark brown developed within 20 minutes usually accompanies the initiation of the PDA formation reaction, which can be used as an indication of the start of the reaction (Bernsmann *et al.*, 2011, Kang *et al.*, 2015b).

In this project, the lab-made MF microcapsules were divided into 3 sub-populations and each was exposed to PDA solution with different pH and additives as described in §3.2.2.5, to form the PDA-coated MF microcapsules, respectively. Since the PDA-coated MF microcapsules had dark brown colour, in order to get the clear view of their surface morphology, the dried PDA-coated MF microcapsules were observed under ESEM other than conventional optical microscope.

Moreover, the coating conditions at pH 8.4 and pH 7.0 were adapted from Lee *et al.* (2007) and Kang *et al.* (2015b), respectively. The chemical compositional analysis (e.g. Infrared (IR) and nuclear magnetic resonance (NMR) analysis) of the resulting PDA polymer has been reported by a number of researchers (Postma *et al.*, 2009, Wei *et al.*, 2010, Bernsmann *et al.*, 2011, Ye *et al.*, 2011, Jia *et al.*, 2014) confirming the PDA polymerisation in these systems is reliable and consistent. Further, the change in pH 7.0 to 5.0 was achieved with less addition of 1M NaOH solution in buffer preparation. The difference in pH is not expected to make any significant change to the oxidation of the dopamine to PDA (Ponzio et al., 2016b). Therefore, no additional chemical compositional analysis was done to the PDA-coated MF microcapsules in this project.

6.2.1.1 Surface morphology of PDA-modified MF microcapsules characterised using ESEM

Comparing to the smooth surface morphology of uncoated MF microcapsules shown in Figure 6.1 (b) (c), all the PDA-coated ones shown in Figure 6.5, Figure 6.6 and Figure 6.7 from different pH coating conditions had obviously larger surface roughness, indicating the deposition of the PDA.

The surface of the microcapsules after coating with PDA under the pH 8.4 condition (Figure 6.5) showed uneven distribution with clearly large surface roughness (with irregular particles sized about 1 - 3 μm); the PDA seemed to form agglomerates on the surface rather than evenly spread.

Similar to the pH 8.4 condition, the microcapsules coated with PDA under the pH 7.0 (Figure 6.6) showed quite a number of uneven depositions. Although some of the MF microcapsules were found to have more even surface coatings (Figure 6.6 (b)) than the others (Figure 6.6 (a)), the observation is overall different from the report from Kang *et al.* (2015b), in which the authors showed significantly smoother surface coatings in the pH 7.0 condition than in pH 8.4. Moreover, some small fibres (Figure 6.6 (a)) were observed embedded in the coatings, indicating there were some impurities in the reaction solution.

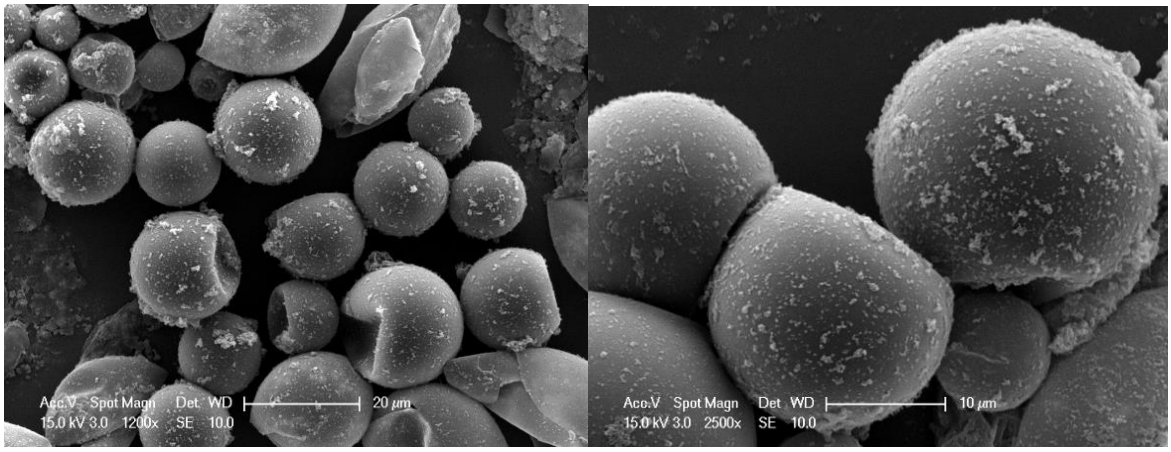

(a) (b)

Figure 6.5 ESEM images of dried PDA-modified MF microcapsules made under the pH 8.4 condition at different magnifications

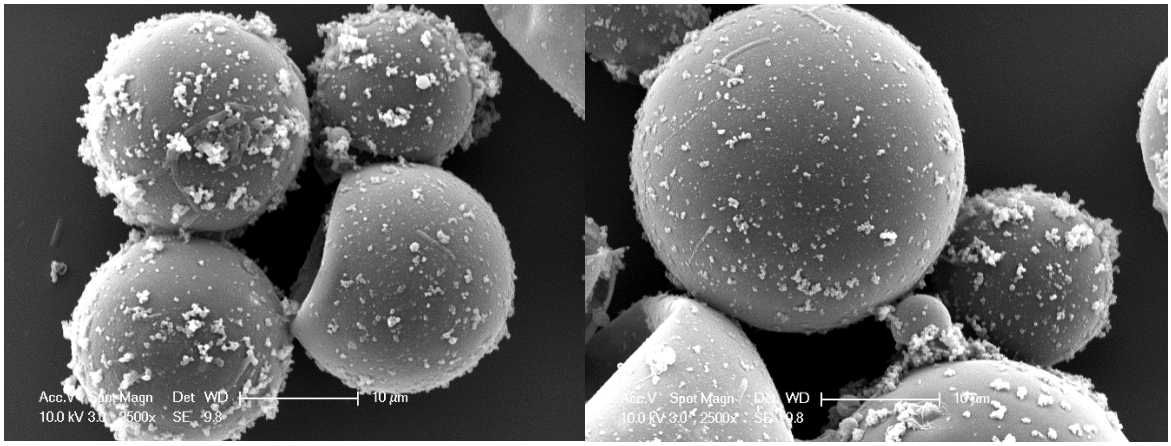

(a) (b)

Figure 6.6 ESEM images of dried PDA-modified MF microcapsules made under the pH 7.0 condition

The surface morphology of the PDA coatings from the pH 5.0 condition (Figure 6.7) was the smoothest among the three PDA coatings. With a few small spherical particles (possibly the small-sized MF microcapsules) attached, the clear texture of the coatings (Figure 6.7 (b)) on the particle surface was observed, which was smoother than either coated surface in the pH 8.4 or pH 7.0 condition.

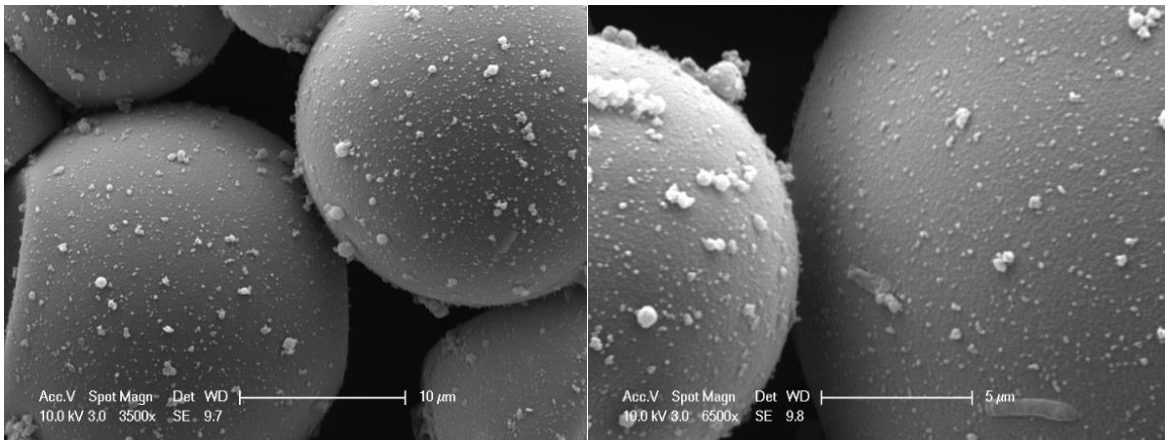

(a) (b)

Figure 6.7 ESEM images of dried PDA-modified MF microcapsules made under the pH 5.0 condition at different magnifications

6.2.1.2 Shell thickness of MF microcapsule and the PDA coatings

The shell thickness of microcapsules affects their mechanical properties and barrier functionalities. It is also related to the payload and density of the microcapsules (Sun and Zhang, 2002, Liu, 2010). Figure 6.8 presents two ESEM images showing the cross sections of broken MF microcapsule shells with PDA coatings in the acidic (pH = 5.0) and neutral (pH = 7.0) conditions, respectively. Both the shell thicknesses of MF microcapsules were estimated from the ESEM images to be about 100-200nm, which are in the similar range of the MF microcapsules reported by Liu (2010). Although it is difficult to identify and estimate the thickness of PDA coatings through these images, the measurements done by Kang *et al.* (2015b) using transmission electron microscopy (TEM) on a PDA-coated microcapsule sample made under the similar neutral condition showed such PDA coating thickness was around 50nm.

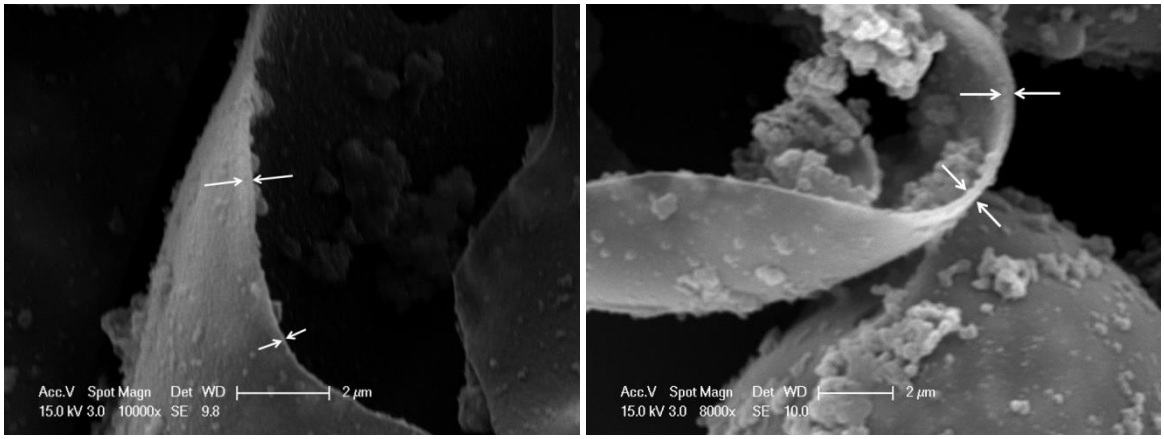

(a) (b)

Figure 6.8 ESEM images of broken MF microcapsules with PDA coatings made under the pH 5.0 condition (a) and pH 7.0 condition (b). The arrows indicate the locations of the shells.

6.3 Adhesion of PDA-modified MF microcapsules to model fabric films

6.3.1 Adhesion to model fabric films measured by AFM

Adhesion of a single PDA-coated microcapsule to model cellulose and PET films in DI-water for both 0.01s and 10s contact times were measured for all the MF microcapsule samples, and the data are summarised in Figure 6.9.

To the cellulose film, significantly larger adhesions were found with PDA-coated samples made at pH 5.0 and pH 7.0 than that at pH 8.4 for both short (0.01s) and long (10s) contact times (Figure 6.9 (a)). Though there is no significant difference in the mean normalised adhesion between pH 5.0 and pH 7.0 based on a t-test (Micceri, 1989, Raju, 2005) with confidence level of 95%, it is worth noting that the data obtained at pH 5.0shows less variation (smaller error bars) than that at pH 7.0. Furthermore, the non-coated MF microcapsules (control) showed similar level of adhesion to those coated by

PDA at pH 7.0. In other words, the PDA coating did not offer any significant increase in the adhesion.

To the PET film, at the short contact time (0.01s), the microcapsules coated with PDA at pH 7.0 showed the largest adhesion, whilst the microcapsules coated with PDA at two other pH values and the control sample exhibited similar level of adhesion. At the long contact time (10s), the adhesions of microcapsules coated with PDA at pH 5.0 and 7.0 had similar values; they both seem greater than those at pH 8.4 and the control sample, although the latter two are not significantly different.

It is also worth noting that the values of the normalised adhesion for the non-coated MF microcapsules to the model cellulose film are in the same magnitude as the reported ones to a lab-regenerated cellulose film by Liu (2010) and He *et al.* (2014) in DI-water conditions, which further confirms both measurement systems were robust and comparable.

The adhesion of these PDA-coated MF microcapsule samples to a PET film in LAS solution (850 ppm) was also measured using AFM, and the results are presented in Figure 6.10, which shows:

- At a short contact time (0.01s), the microcapsules coated with PDA at different pH all enhanced the adhesion in comparison with the control sample, and those at pH 8.4 generated the highest adhesion.

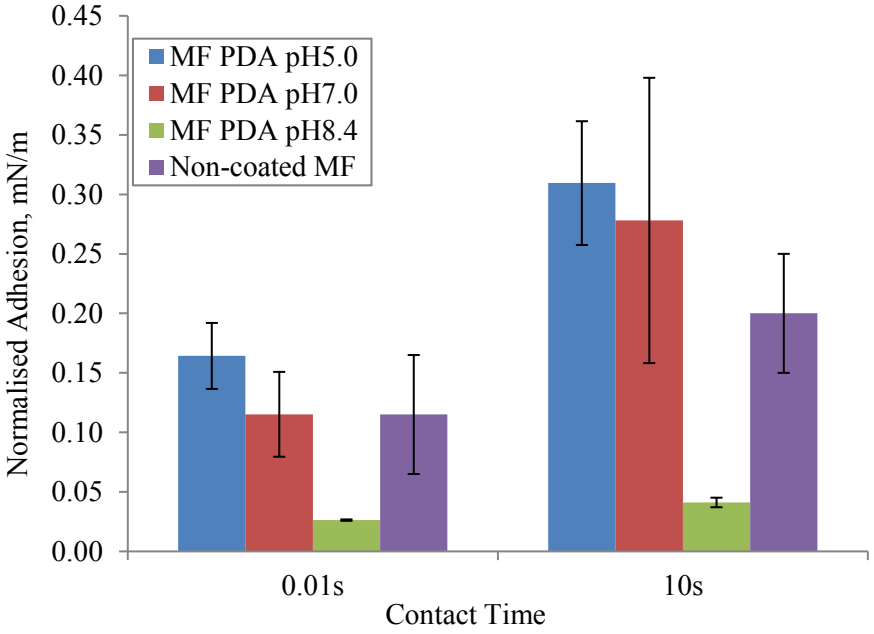

(a)

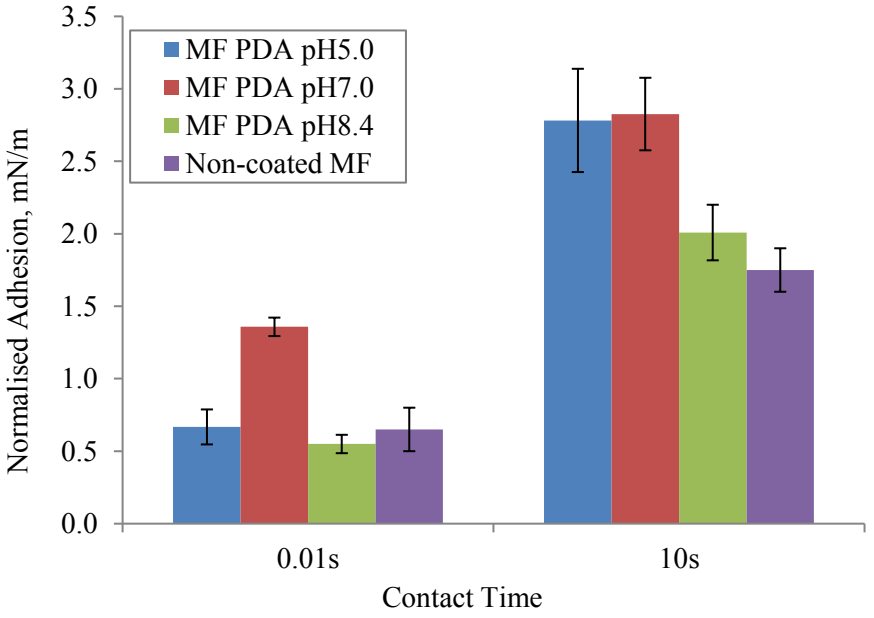

(b)

Figure 6.9 Comparison of mean normalised adhesion of single microcapsules in DI-water to cellulose film (a) and PET film (b) using AFM. For control MF microcapsule sample, N (number of microcapsules tested) = 2; for PDA-coated MF sample, N = 2. The compression force was set to be 20 nN. The error bar represents the standard error of the mean.

- At a long contact time (10s), again all the microcapsules coated with PDA at different pH showed significantly higher adhesion to the PET film than the non-coated. Actually, the differences were so explicit among the samples in this condition that they had the following ranking (from the highest adhesion achieved to the lowest): pH 8.4 > pH 5.0 > pH 7.0 > non-coated.

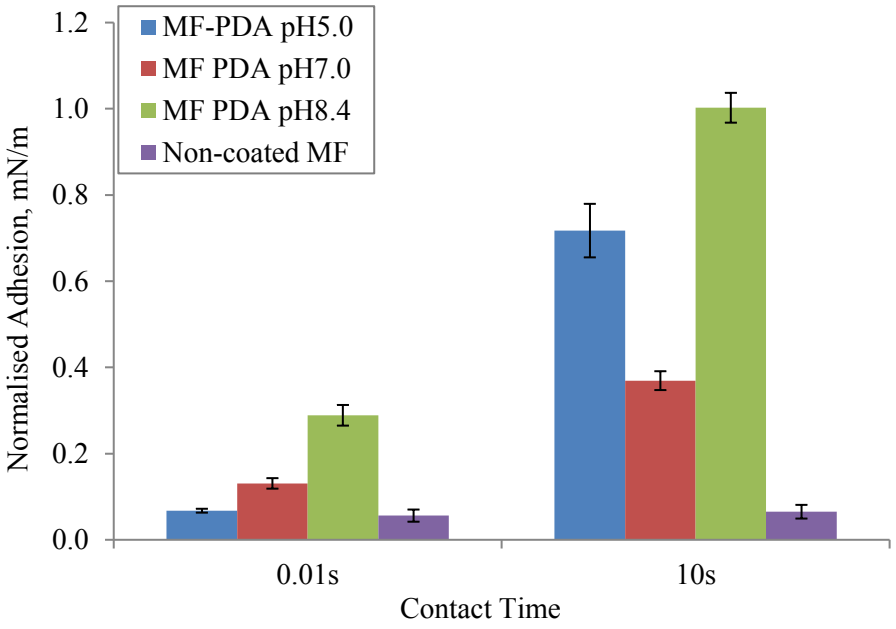

Figure 6.10 Comparison of the mean normalised adhesion of single microcapsules in LAS 850 ppm solution to the PET film using AFM. For control MF sample, N = 2; for PDA-coated MF sample, N = 2. The compression force was set to be 20nN. The error bar represents the standard error of the mean.

6.3.2 Retention of microcapsules on PET film in a flow chamber

Retention ratios of the non-coated and PDA-coated MF microcapsule samples vs shear stress in the flow chamber with DI-water and LAS 850ppm solution are shown in Figure 6.11.

In DI-water, the retention ratios of the microcapsules coated with PDA at pH 7.0 and pH 8.4 were both lower than that of the control sample for a given shear stress. Moreover, there was almost no retention of the microcapsules coated with PDA at pH 8.4. The microcapsules coated with PDA at pH 5.0 showed the greatest retention on the film in DI-water among all the tested samples. However, in the solution of 850 ppm LAS, the retention was greatly reduced (from more than 50% at about 0.5 Pa to almost none), which indicates the adhesion enhancement of PDA coating on the microcapsules was greatly reduced by the addition of such concentrated surfactant.

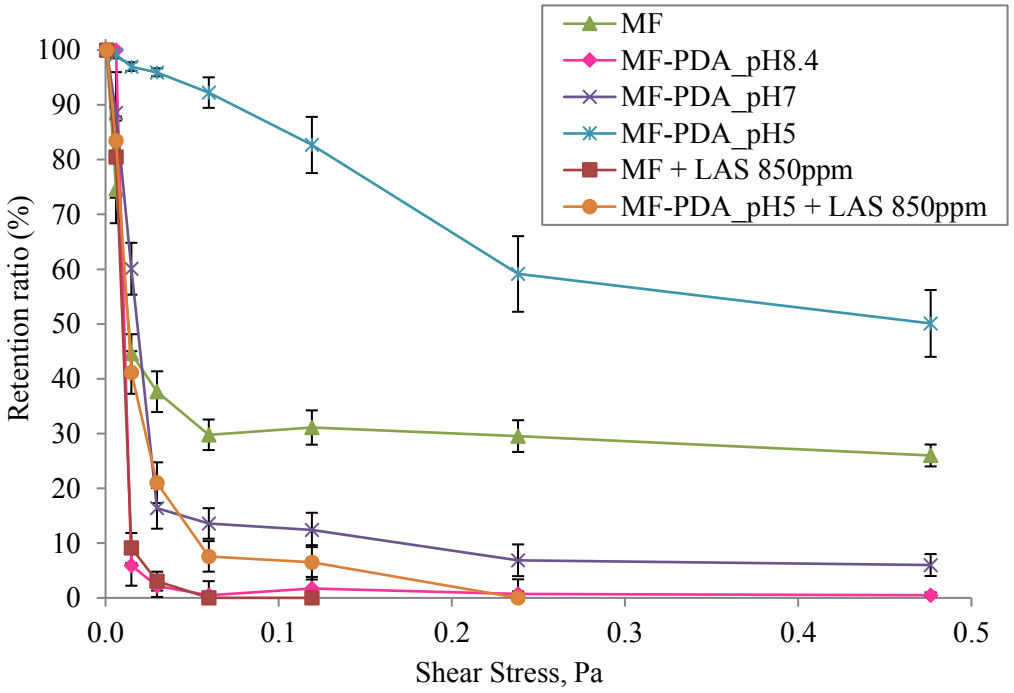

Figure 6.11 Retention ratios of the non-coated microcapsules and those coated with PDA at different pH on a PET film versus shear stress in the flow chamber device (n=3). The error bar represents the standard error of the mean.

6.4 Discussion

A number of oxidation and nucleophilic addition reactions can take place during the PDA polymerisation due to the high reactivity caused by the complex interactions of catechol moieties and amine moieties on dopamine molecules, which results in the multiple functional chemical groups on the surface of the PDA (§2.3.6.3), making it able to adhere to almost any surfaces. Details of these functional groups, their possible formation conditions and adhesion mechanisms are discussed in this section.

6.4.1 Colouring of PDA coatings

It is a typical phenomenon that the colour of aqueous-dopamine solution turns from clear transparent to dark brown (or orange-brown if the dopamine concentration is relatively low) in about 30 minutes in ambient condition because of the self-polymerisation of dopamine to form PDA (Lee et al., 2007, Postma et al., 2009). Due to the complicated oxidation and polymerisation reactions, the resulted "PDA polymer" is actually a mixture of a number of different polymers (Figure 2.10) on which no clear understanding / analysis has been made yet. Nevertheless, it is well accepted that the dopamine polymerisation process results in a dark brown coloured PDA polymer (Lee *et al.*, 2007, Liu *et al.*, 2014). Although Kohri and Kawamura (2016) recently reported a colourless PDA resulting from a co-polymerisation process which involved an atom transfer radical polymerization (ATRP) initiator prepared by the reaction of dopamine with 2-bromoisobutyryl bromide, the traditional pathway of dopamine to PDA inevitably produces the coloured components and limits the use of the PDA coatings in industrial applications such as optical materials, cosmetics and diagnostic test materials.

Since this project aims to enhance deposition of microcapsules in detergents on fabrics, the liquid laundry detergent normally contains dye (about 0.5 – 1.0 wt.% in formulation) to give the appearance of the product, and the low target usage amount (~ 0.5%) of PMC, PDA coating should not be a big concern with regards to the colour of the product. However, it could be a potential issue if PDA-coated PMC is used in powder detergent in which the formulation is without dye and the product appearance is normally white.

6.4.2 Mechanism of adhesion of PDA-modified MF microcapsules to model fabric films

6.4.2.1 Influence of pH on PDA coatings

The control of system pH has been one of the key parameters in the fabrication of PDA coating. In this study, there were two major reactions in the PDA coating solutions: polymerisation from dopamine to PDA and the deposition reaction between PDA functional groups and the MF surface chemical groups. The mechanism of the PDA coating on to the surface of MF microcapsules could be through the spontaneous reactions of the two, which means different reaction rates could impact on the resulted surface properties of the coating.

As the p*K*a values of the first -OH in catechol and amine groups in dopamine molecule were reported to be 9.0 - 9.4 and 8.8 - 9.1 (Wang *et al.*, 2009) respectively, it is possible that majority of the dopamine molecules were neutralised to the free base form at pH 8.4. Moreover, the free base form of dopamine was found to be more reactive than its protonated form by Carter *et al.* (1982). Additionally, the surface of MF microcapsule was negatively charged between pH 3-11 (Liu, 2010). The reduction of electropositivity

of the dopamine molecule caused by the transition from the protonated form to the free base form decreases the electrostatic attraction between the dopamine molecule and the MF microcapsule, resulting in the decrease of the deposition rate of the dopamine onto the MF microcapsule surface. Therefore, the polymerisation reaction rate could be higher than the deposition rate for the dopamine in this basic condition, indicating majority of PDA may be formed and agglomerated in the solution, then deposit onto the surface of the MF microcapsule, resulting in an uneven coating with large surface roughness.

In contrast, dopamine in the pH 5.0 condition may deposit on the surface of microcapsules first, and then-polymerise to form the coating, resulting in much smoother PDA-coated MF microcapsule surfaces due to the high concentration of protonated therefore less reactive dopamine molecules in the solution.

It is speculated that the reaction and deposition rates of dopamine in the pH 7.0 condition both lie between the ones in pH 5.0 and pH 8.4, which resulted in surface coating morphology with a roughness between the other two.

Thus, the ranking of surface roughness of the PDA coatings could be (from the smallest to the largest): pH 5.0 > pH 7.0 > pH 8.4. Subsequently, as mentioned in §4.5.1, greater roughness results in less adhesion. However, the fibre impurities present in the reaction solution could probably cause more unevenness / roughness of the PDA coatings in the pH 7.0 condition (Figure 6.6), which might result in a further decrease of the adhesion of the PDA-coated MF microcapsule to the target model fabric surfaces.

6.4.2.2 Surface chemistry of PDA coatings

From the TEM results of Kang *et al.* (2015b), the microcapsules coated with PDA with a neutral pH, their surface was densely packed with PDA polymers with a thickness of about 50nm. Since the same raw material and a similar coating process were adapted in the work presented in this chapter, it can be concluded that the amount of PDA was excess and the MF microcapsules could be fully covered by PDA, in which MF molecules were hindered from interacting with the model fabric film surface. Thus, the PDA-film surface might dominate the overall attraction / adhesion between the PDA-coated MF microcapsules and the target film surface.

In comparison with the two possible PDA surface functional quinone and catechol groups, it can be more difficult for amine to have effective interactions with the model fabric film due to the steric hindrance of the surface structure. Independent zeta potential analysis results published by Fu *et al.* (2015) showed that sub-micro PDA particles made in the pH 8.5 condition were negatively charged from about pH 3 - 4 onward and the negativity increased with pH. Ball (2010) also found two possible p*K*a values for PDA coating at about pH 6.0 and 9.0, based on the zeta potential titration curve, which the author attributed to the average p*K*a of quinone-imine and catechol, respectively. As an isoelectric point of about pH 4 was concerned, Ball (2010) argued it was likely that TRIS molecules were covalently bonded to PDA during the coating process and formed secondary amine on the PDA surface which was able to be protonated at a lower pH than the original steric-hindered amine groups being protonated. Based on above, it is reasonable to speculate the majority of the PDA surface was covered with catechol and quinone groups.

Recent work reported by the research team led by Israelachvili (Anderson et al., 2010, Lee et al., 2011, Yu et al., 2011, Danner et al., 2012, Yu et al., 2013, Mirshafian et al., 2016) revealed that apart from the solution pH, interfacial redox is another important factor that influences the adhesion performance of PDA coatings. Although they used a different system (with small molecular raw materials mussel foot protein-3 (mfp-3), a surface force apparatus (SFA) and mica or TiO_2 substrate), the resulted PDA surface and the adhesive force analysis results were similar to those in the current work.

As reviewed in §2.3.6.3 and Figure 2.10, the complicated oxidations process may result in the PDA surface with a combination of functional groups such as catechol, quinone, dopaminechrome and *o*-dihydroxyindole. Catechol groups are more interactive, resulting in higher adhesion than *o*-benzoquinone groups. Although *o*-benzoquinone can quickly get rearrangement / tautomerization to α, β-dehydro-catechol in the presence of Lewis base, the double bond formed on the α-carbon on the backbone during the process made the polymer less flexible, therefore more difficult to approach the target surfaces (steric effect), thus causing reduction in adhesion.

Combining the effect of pH used in the coating process and all the above analyses, the following mechanisms are proposed:

1). in basic condition (pH > 7.5), the PDA surface mainly consists of *o*-benzoquinone ending groups. Moreover, since TRIS was used as a reaction buffer in the coating of microcapsules with PDA at pH 8.4 whilst an inorganic buffer was used at two other pH conditions, it is possible that there were extra amine groups introduced by TRIS in the PDA coating corresponding to pH 8.4.

2). in acidic condition (e.g. pH < 5.5), the PDA coating is more likely composed of catechol groups due to the overall reducing environment. However, with additional

oxidant such as sodium periodate and ammonium persulfate (which was used in this study as well), the resulting coating may be partially composed of *o*-benzoquinone ending groups, but the overall resulted coating should still have more hydrophilicity, thickness and homogeneity than those in basic condition without oxidant (Ponzio et al., 2016a).

3). in neutral condition of pH around 7.0, the PDA coating could be composed of a certain ratio of both catechol and *o*-benzoquinone groups.

4). these surface functional groups are convertible under certain conditions such as solution pH, additional reagents (e.g. oxidant / reducing reagents) and even sometimes after being in contact with target surface (Anderson *et al.*, 2010).

Based on the above analysis, the PDA coatings could have surface hydrophilicity in the order of pH 5.0 (relatively more hydrophilic) > pH 7.0 > pH 8.4 (relatively more hydrophobic) due to the different pH. Figure 6.12 shows the typical PDA surface functional groups and their transition pathways.

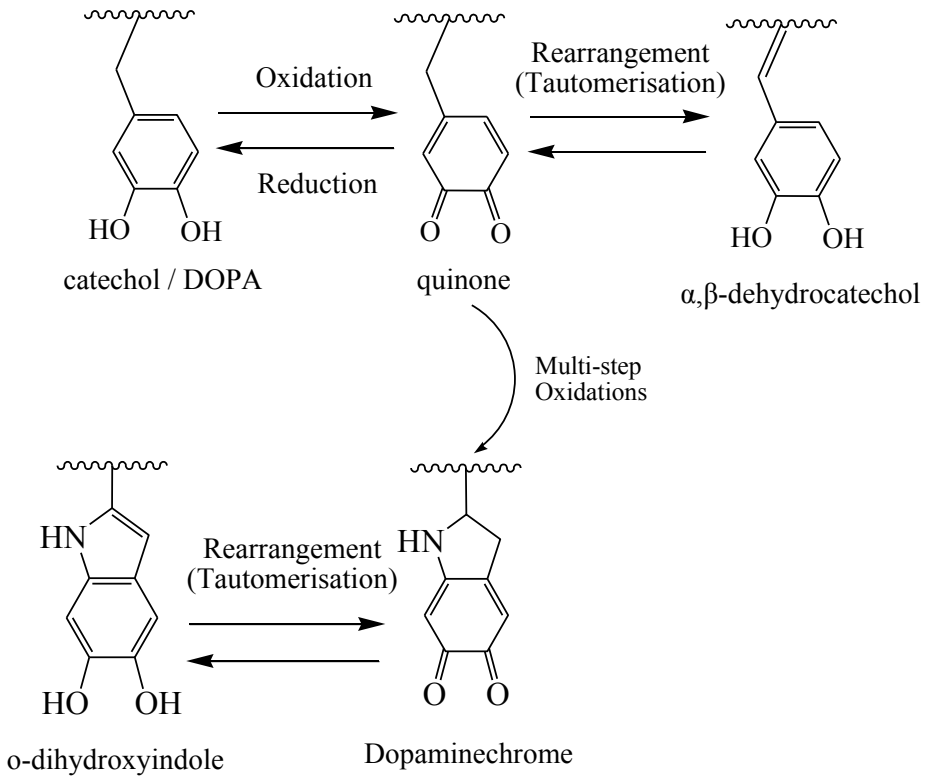

Figure 6.12 Typical transitions of surface functional groups in PDA of oxidization forms.

Representative AFM approach-retract force curves of single PDA-coated MF microcapsules interacting with cellulose and PET films are presented in Figure 6.13, which may indicate the existence of different surface functional groups of the PDA coatings and their chemical status. During approach, only the microcapsule coated with PDA at pH 5.0 interacting with PET film in DI-water showed a "jump in" event (Figure 6.13 (b) black curve) without obvious repulsion, whilst flat approach curves and slight repulsion before contact were observed from all other samples, indicating the surfaces of the PDA coatings in these samples were negatively charged. During retraction, most of the PDA-coated microcapsules showed a "jump out" event when the adhesive force reached its maximum. The microcapsule coated with PDA at pH 8.4 interacting with cellulose film in LAS 850 ppm showed almost no adhesion (Figure 6.13 (g)). The

microcapsule coated with PDA at pH 7.0 exhibited the weakest adhesion among the three samples (Figure 6.13 (d, e and f)). All these findings are in line with the proposed mechanisms in the previous sections, including the differences of the PDA surface functional groups and their hydrophilicity. Furthermore, it is worth to note that the uneven surface morphology shown in Figure 6.5 – 6.7 is also likely to contribute to such variable and inconsistent force-displacement data in Figure 6.13.

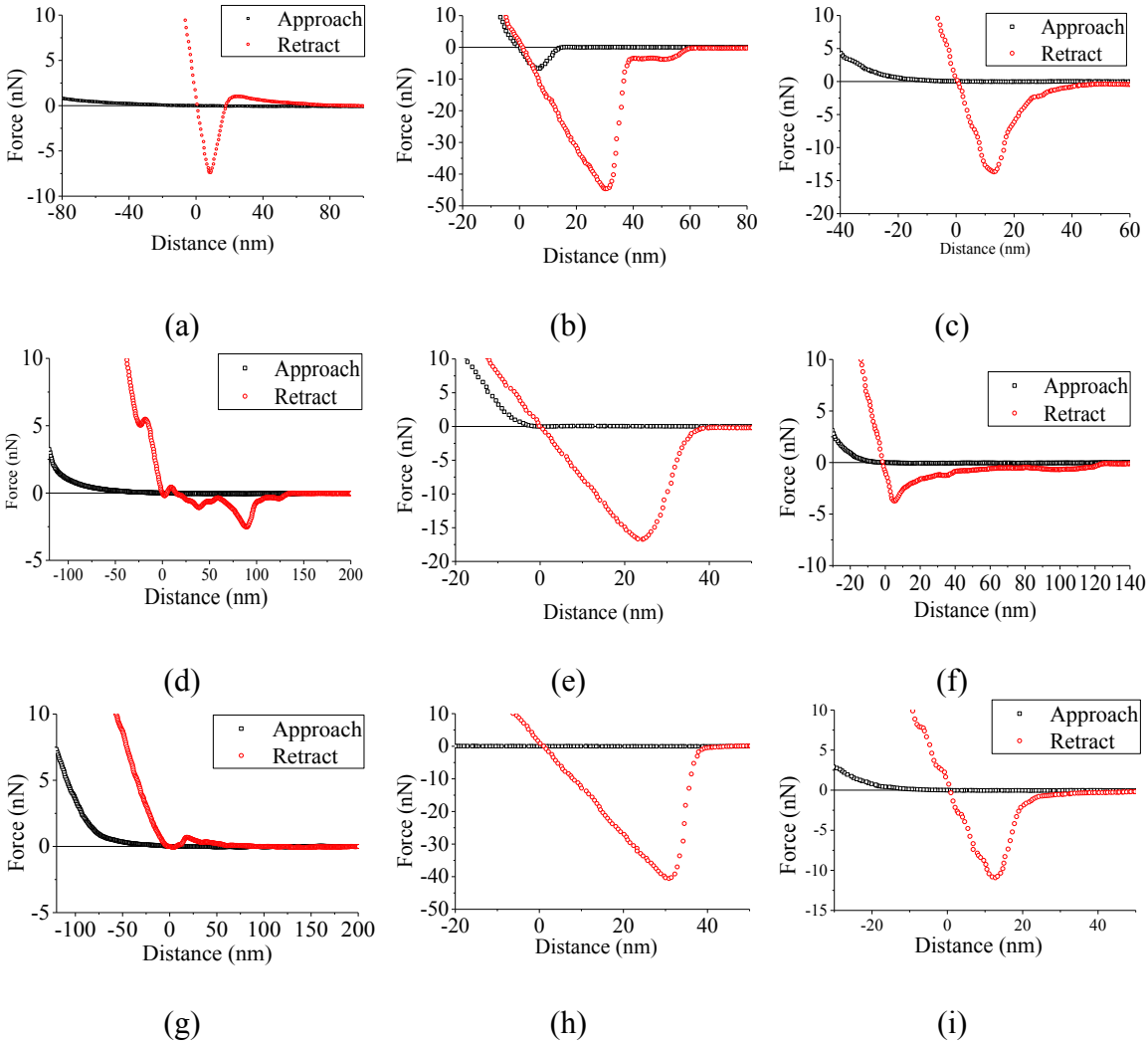

Figure 6.13 Representative AFM approach-retract force curves of single PDA-coated MF microcapsules on cellulose (a, d, g) and PET (b, c, e, f, h, i) films. Solution conditions: DI-water (a, b, d, e, g, h), LAS 850ppm (c, f, i). Samples: pH 5.0 (a, b, c), pH 7.0 (d, e, f), pH 8.4 (g, h, i). Data were collected from three different PDA-coated MF microcapsules on random parts of the substrates.

6.4.2.3 Influences of surfactant on adhesion of PDA-modified MF microcapsules

Comparing Figure 6.9 (b) and Figure 6.10, it is noticed that with the presence of 850ppm LAS in DI-water, for a contact time of 10s, the normalised adhesion was reduced by more than 75% (from 2.5 - 3.1mN/m to 0.6 - 0.8mN/m) for the PDA coating at pH 5.0 and more than 80% (from 2.6 – 3.1mN/m to about 0.4mN/m) at pH 7.0, whilst at pH 8.4, the normalised adhesion only reduced by about 50% (from 1.8 - 2.2mN/m to about 1.0mN/m). Considering the proposed mechanism in §6.4.2.2 that the PDA coating at pH 8.4 could contain a certain degree of secondary amine groups introduced by TRIS, which showed positive charges at such neutral pH condition to enhance the adhesion, it is reasonable that the PDA coating on microcapsules at the neutral and acidic conditions, due to lack of such enhancement, generated less adhesion with the presence of LAS surfactant. On the contrary, these results provide a supplementary evidence to support the conclusions in Chapters 4 and 5 on the mechanism of the adhesions that when there is neither electrostatic force nor hydrophobic interaction (PDA surface is generally hydrophilic), the overall adhesion between the microcapsule and the model fabric film could be minimised at the tested conditions.

6.4.3 Comparisons of the adhesion of MF microcapsules to fabric surface between PDA coating and polyelectrolyte modifications

The modification of PMCs using polyelectrolyte such as PVF or chitosan polymers turns their surface into positively charge, which could enhance the interactions between them and fabric surface that are negatively charged. The enhancement is normally

through the strong long-range electrostatic interaction when PMCs approach the fabric surface and their strong adhesion including the combined effects of electrostatic force and hydrophobic force. All these processes including the modification, approaching, deposition and adhesion enhancement are relatively quick and can be considered to be completed within seconds to minutes (Israelachvili, 2011).

On the contrary, PDA coating is added on to the surface of PMCs via the formation of a considerable amount of hydrogen bonds and covalent bonds and the adhesion enhancement is through the contact and molecular bridging of PDA surface functional groups and the fabric surface. However, the PDA formation and deposition on to the surface of PMCs takes quite a long time (30 min to 24 hours) to achieve the reasonably effective quality (Danner *et al.*, 2012, Yu *et al.*, 2011, Li and Li, 2015); the subsequent adhesion process requires 30 - 60 min (Lee et al., 2011, Ho and Ding, 2014) to get the force balance, which can vary with the solution pH and temperature. Moreover, the PDA interactions with a target surface are normally considered strong but relatively short ranged (for hydrogen bonds and covalent bonds). This could be one of the major reasons that the PDA coating didn't show desirable performance in adhesion enhancement. Therefore, for the tested conditions, the benefit of PDA coating cannot compete with that offered by polyelectrolyte modifications. For example, the normalised adhesions of the PDA-coated MF microcapsules in DI-water condition corresponding to a contact time were in a range of of 0.2 - 0.3 mN/m to cellulose film and 2 - 3 mN/m to PET film, which were significantly lower than those generated from the PVF modification of PAC-PVOH PMCs (1.4 - 1.6 mN/m to cellulose film and 16 - 19 mN/m to PET film, from §4.4.5) and chitosan modification (1.3 - 1.5 mN/m to cellulose film and 26 - 31 mN/m to PET film, from §5.4.1) under the same environmental conditions.

Moreover, the normalised adhesions of MF microcapsules coated by PDA to a PET film in LAS 850 ppm solution obtained at a contact time of 10s, which could be the most relevant to real laundry condition, were in a range of 0.4 - 1 mN/m, whereas the ones for the PAC-PVOH PMCs modified by PVF were of 6 - 8 mN/m, and those for the microcapsules modified by chitosan of 1 - 2 mN/m.

However, it may be unfair to directly compare the performance of PDA-modified microcapsules with those by PVF or chitosan simply because it takes much longer for PDA coating to interact with a target surface. Furthermore, the two modifications are quite different in the chemical basis; the magnitude of their resulting forces involved in the adhesion is quite different as well. Nevertheless, it's desirable to see the difference, which may be further investigated in future work.

Finally, it is worth noting that in a real industrial process to manufacture detergent, the time and potential cost of making such PDA-coated PMCs could be significantly higher than those of polyelectrolyte-modified microcapsules; it is less likely for the consumers to wait more than 30 min for the PDA-coated PMCs to fully interact with the fabrics before starting a laundry process. Therefore, the current PDA coating approach explored in this project needs to be further developed before it can meet the requirements from the industrial manufacture and consumer behaviour.

6.5 Conclusions

1. The oxidative conversion of dopamine to PDA and its coatings on MF microcapsules with a core of vegetable oil, which were made in the lab, were investigated in neutral and acidic conditions, as well as a conventional pH 8.4 TRIS

buffer with no addition of oxidant. SEM image analysis confirmed the successful coatings of the PDA in all three conditions, among which the best coating homogeneity was achieved with pH 5.0.

2. The AFM force curves together with relevant literature reports confirmed the proposed mechanisms that the surface functional groups of PDA coating MF microcapsules at pH 5.0 are more likely to be catechol groups than at the other pH values, which is preferred because they are also the most basic functional groups of mussel foot proteins. Therefore it can be concluded that the PDA coating at pH 5.0 is overall more hydrophilic than that at neutral or basic conditions.
3. Based on the AFM measurement data and the flow chamber test results, it has been demonstrated that coating of microcapsules with PDA may not be a good choice for enhancing deposition and retention of PMCs on fabric in laundry process. Future research is needed to speed up the chemical reaction for surface coating.
4. As far as the mechanisms of the adhesion of microcapsules to model fabric films are concerned, the findings from PDA-coated MF microcapsules might be applicable to other capsules including PAC-PVOH PMCs. Electrostatic force between the PDA-coated microcapsules and the model fabric film has been confirmed to dominate the approaching process from the analysis of AFM force curves; on contact, few interactions were detected possibly due to the relatively short contact time of PDA coating with PET film surface. Since it is difficult for PET surface to form hydrogen bond or any hydrophilic interactions, much longer contact time is required for PDA to obtain strong interactions than PVF or chitosan. This provided a supplementary evidence to support the conclusions in previous chapters that both electrostatic force and hydrophobic interaction are of great

importance to adhesion, whilst the other interactions contributing to the adhesion of the microcapsule to the model fabric films could be insignificant.

Chapter 7. Overall conclusions and future work

7.1 Overall conclusions

Model cellulose and PET films were characterised and the results showed similar elemental compositions and comparable surface properties to real fabrics. These commercial fabric films with a relatively smooth surface can be used not only to replace the conventional self-made fabric substrates to save researcher's time and effort but also to mimic real fabric to minimise the effect of surface asperity on the adhesion, which brought much more convenience and enabled the project going smoothly through the intensive experiment period.

Characterisations of the microcapsules modified by PVF and chitosan respectively showed successful coating of the polymers on the surface of the PAC-PVOH PMCs. Although used at a relatively low concentration (0.25% wt. in the ~50% wt. PMC raw material), both the polyelectrolyte modifications showed significant improvement towards the deposition and retention of the PAC-PVOH PMCs in the tested conditions including DI-water, hardness water, surfactant solutions under low concentrations (e.g. lower than the surfactant CMC).

Micromanipulation measurements of the mechanical properties of single microcapsules (both non-modified and surface-modified ones) demonstrated that all the microcapsules were strong enough and suitable for all the following AFM and flow chamber experiments and the applied compression force and adhesion generated can only cause very small elastic deformations to the microcapsules.

AFM force measurement and flow chamber retention tests confirmed the effectiveness of both PVF and chitosan polymer modifications on PMCs in enhancing their adhesion

to the two model fabric films in multiple tested conditions. Among the PVF polymers investigated, Lupasol® VT with 2000 kDa and 20% hydrolysis ratio was found to be the most effective in enhancing the adhesion. Hydrolysis of PVF results in positive charged amine centres, with the p*K*a of round 10.5. Chitosan with low molecular weight (5000 Da) and medium (~ 80%) DDA has been proved to be an effective adhesion enhancer in the tested conditions as well. The results indicated that a positively charged polyelectrolyte with a reasonably large molecular weight and relatively low charge density could be the most beneficial to enhance the deposition and retention of negatively charged PMCs in laundry detergent solution environment. Furthermore, the p*K*a value of the charged centre on the polyelectrolyte could be critical. Since amine group on chitosan molecule has a p*K*a of about 6.5, which makes chitosan show pH sensitivity in laundry solutions, resulting in the less reproducibility of its performance in AFM measurement and flow chamber retention tests than those of PVF polymers.

Adhesion of PMCs to model cellulose film has been demonstrated to be influenced largely by electrostatic interactions between the film and PMC surfaces, whilst the adhesion of PMCs to model PET film was dominated by hydrophobic interactions, regardless if there was surfactant in either system. Although it is difficult to investigate the dynamic process in real wash condition, the flow chamber results suggest the performance of deposition and retention of the surface-modified PMCs on both model fabric films in such condition would not be worse than those in the single surfactant solutions of high concentration (e.g. higher than the surfactant CMC). The effects of single laundry liquid parameters including surfactant type and concentration, hardness / salt concentration on the PMC adhesion to model fabric films were investigated, and the results indicated that the adhesion can also be heavily influenced by the interactions of these factors.

Table 7.1 summarises the overall effect of different categories of surface modifications of PAC-PVOH PMC to model fabric films.

Table 7.1 Summary of basic surface properties for the adhesion of PAC-PVOH PMC to model fabric films

Surface property of PAC-PVOH PMC	**Overall effect on the adhesion to model films**
Hydrophobic	Greatly enhance the adhesion on PET film; enhance the adhesion but less effective on cellulose film
Amphiphilic	Enhance the adhesion on both films
Hydrophilic	Reduce the adhesion on both films
Positive charge	Enhance both the attraction and adhesion on both films
Neutral	No effect
Negative charge	Greatly reduce the attraction and adhesion on both films

PDA coating on MF microcapsules at three different pH conditions were successful. The AFM measurements and flow chamber test results confirmed that the modifications enhanced the adhesion of MF microcapsules to model fabric films in DI-water. However, due to the need of long reaction time with the target surface, PDA coating was not able to compete with the performances produced by the surface modifications of microcapsules with polyelectrolytes such as the leading PVF and chitosan polymers in current experimental settings.

Investigation of the mechanism of the PDA coating interacting with the model fabric films revealed that an electrostatic interaction dominates the approaching process of the PMC to both model fabric surfaces based on the AFM force curves; however, few

interactions were detected between them possibly due to the relatively short contact time of PDA with the target fabric surfaces therefore lack of strong interactions.

7.2 Future work

7.2.1 Optimisation of coating materials for current PMCs

PVF continues to be the lead candidate for the PMC surface modification in the laundry application. Chitosan is also good in enhancing the adhesion of PAC-PVOH PMCs to model fabric surfaces; however, the lower p*K*a of amine group in chitosan limits its application in high-pH formulation. The search of a similar positive charged polyelectrolyte with relatively higher molecular weight (which needs to be higher than the chitosan used in this research, and could be similar to the PVF) and higher p*K*a (e.g. > 8.0) value of the functional amine groups could be desirable. Moreover, the high molecular weight could result in less hydrophilic property of the material which is also indicated as a positive factor in enhancing the adhesion of PMCs to target fabric surfaces in this project.

Mussel-inspired polydopamine continues to be the hot research topics in academia and industry. A new way to interact with the target fabric surfaces with catechol-containing functional groups of high reactivity / binding capability could be another approach to solve the current PMC deposition / retention issue.

As this research has been only focused on the application of perfume loaded microcapsules into laundry detergent and related conditions, a lot of other application areas remain unexplored, which adds not only complexity but also opportunities to future research. A possible direction or simplification approach could be to test solid

particles of known mechanical properties with and without surface medication in these different applications.

Part of the limitation of this project comes from the roughness of the substrate model fabric films as discussed in §4.5.1. The future work could be to look for smoother substrate to further reduce the possible impacts to the small sized microcapsules during the analysis. Understanding the change of the size range and size distribution of the microcapsules in the flow chamber test is also another task this project does not complete. Theoretically, under the same shear stress, larger particle tends to receive bigger shear force because of the larger cross-sectional area, therefore, easier to be removed than the smaller particles. However, it still needs to be confirmed by experiment results.

7.2.2 Other approaches to deliver perfume to target fabric surface

Since this research was based on a collaborated project funded by P&G company in 2013, all the PMCs used in this study were limited to PAC-PVOH ones which are classified as plastic-shell PMCs. As plastic continues to bring pressure to the environment (Wheeler, 2017), the urge to reduce the usage of any plastic material in laundry products has been enforced globally during the past years (Verschoor et al., 2016, Bhattacharya, 2016, Dris et al., 2015, Mason et al., 2016). In addition, some countries in Europe and North America have separately legislated to restrict and prohibit the usage of one-time-usage plastics including microbeads in certain industries and consumer products (Hohenblum et al., 2016, Winnebeck, 2014, Xanthos and Walker, 2017). It is highly possible that the plastic-based microcapsules will be

restricted in laundry applications in near future as microbeads have been banned in some of the European and North American countries.

In recent years, alternative approaches to encapsulate and deliver fragrance oils in laundry detergents have been under development using non-plastic and biodegradable shell materials. Patent application searches show that alginate, gelatine, chitosan and their derivatives based PMCs (Aussant and Harrison, 2018, Garces, 2004, Richard and Morteau, 2004, Mint et al., 2018) have been re-emphasized by major manufacturing companies of fragrance oils and consumer products including Givaudan, Ashland and P&G. Apart from the biodegradable nature, one of the additional benefits of these technologies is the microcapsule surface contains functional groups which can be turned into positive ion centres during application. Then the positive charged centre could enhance the adhesion of the PMC to the target laundry fabric surfaces. Theoretically, these PMC technologies can simplify the PMC manufacturing process by eliminating the use of additional adhesion-enhancing polyelectrolytes, reducing the overall cost, and at the same time keeping the product environmental friendly. However, due to the limitation of the technologies, all the related processing methods (either coacervation or gel formation) have difficulties in producing PMCs smaller than 20μm (Table 2.2). Moreover, comparing to *in-situ* polymerisation, the relatively complicated process and low productivity are the factors that constrain their development. Therefore, to search for more natural substitutes as well as to develop new processes to make the PMCs for future sustainable laundry products becomes imperative.

Appendix A

Detailed design drawing of the flow chamber used in this project, adapted from the report of Lane *et al.* (2012).

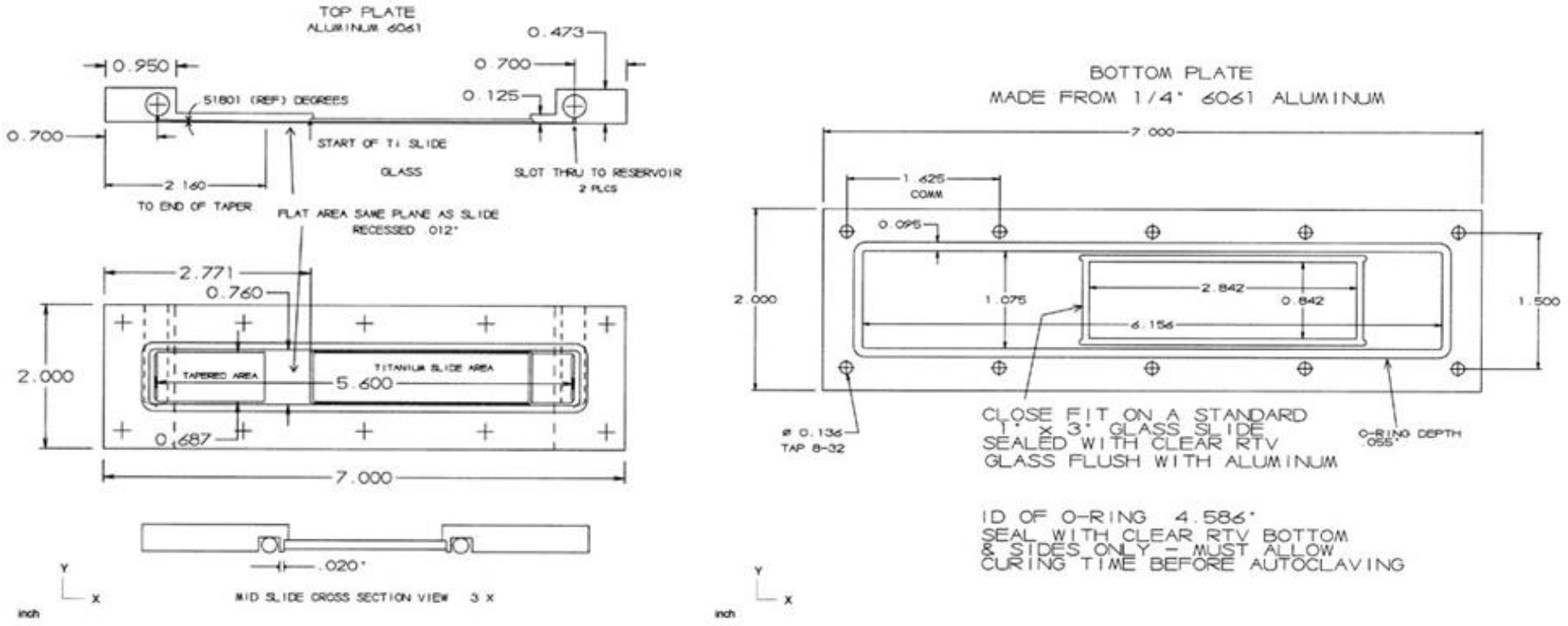

Figure A.1 Design drawing of flow chamber. Left: top plate; right: bottom plate.

Appendix B

Matlab code used for flow chamber image analysis, developed by Dr James W. Andrews and Dr Yanping He, School of Chemical Engineering, University of Birmingham (He, 2013).

```
% Script to count number of particles and produce a particle size spectrum

% Initial image processing (inverts image)
% Matlab is better at finding white on black than vice versa.
% Name files in a sequential order

folder='C:\Users\Sen\Documents\Flow Chamber\Data\2015-2-10 PET-Chitosan-WashingPremix-30min\Before'; % Root directory
pixelareas=0.62112*10^(-12); % Put the area of the pixel here units m^2

for indx=1:5
   % Get image
   % Any file matlab can be read prefferably in grey scale
   basefilename=sprintf('%d.tif',indx); % Filename
   filename=fullfile(folder,basefilename); % Full location of the file
   I1=imread(filename);
   % NB change file name above

   % Image inversion is necessary in this case
   % If your image is not true color comment out the next line
   negImage = rgb2gray(I1) ;  % Convert true colour to grayscale
   negImage=double(negImage); % Convert the image matrix to double

   negImageScale = 1.0/max(negImage(:));  % Find the max value in array
   negImage = 1 - negImage*negImageScale; % Make negative image
   figure;imshow(negImage);
   %I2=histeq(I1);        % Histogram equalization of a gray-scale image.
   I2=histeq(negImage);

   % Remove background
   negImage=imtophat(negImage,strel('disk',50));
   negImage = medfilt2(negImage,[3 3]);
   negImage=imclearborder(negImage);
   %bw=edge(negImage,'canny',level,5.5);
```

```
    I2=histeq(negImage);
    level=graythresh(I2)
    level=0.1;

    % Convert to binary image
    bw=im2bw(negImage,level);
    bw=imfill(bw,'holes');

%    figure;imshow(bw);

% Apply a morphological opening routine

    [labels,N]=bwlabel(bw,4);

% NB: N returns the number of objects found
% labels contains information about locations of objects
% The 4 indicates that particles must touch along an edge
% in order to be considered as an object

    % Extracting the size of each object

    data=regionprops(labels,'basic') %
    areas=[data.Area];
    data1=regionprops(labels,'perimeter');
    perimeter=[data1.Perimeter] % Care in using this ??
    sortareas=sort(areas) % Sorts the areas into ascending areas

    realareas=sortareas.*pixelareas;
    sizedistribution=sqrt(realareas./pi);

    % Store data
    basefilename=sprintf('ParticleShape%d.dat',indx); % Filename
    filename=fullfile(folder,basefilename); % Full location of the file
    fid = fopen(filename, 'w') ;% Open file for writing
    if fid==-1
       error('File is not open')
    end
    fprintf(fid, 'Pixel area (10^(-12) m^2): %f\n\n', pixelareas/10^(-12));
    fprintf(fid, 'Particle area (piexel^2)\tParticle perimeter (pixel)\n')
    for i=1:length(areas)
       fprintf(fid, '%e\t\t\t%e\n', areas(i), perimeter(i))
    end
    fclose(fid);
```

```
    basefilename=sprintf('ParticleSize%d.dat',indx); % Filename
    filename=fullfile(folder,basefilename); % Full location of the file
    fid = fopen(filename, 'w') ;% Open file for writing
    if fid==-1
        error('File is not open')
    end
    fprintf(fid, 'Particle diameter (10^(-6) m)\n')
    fprintf(fid, '%f\n', sizedistribution/10^(-6))
    fclose(fid)

% Plot the particle diameter in a histogram
     figure
     hist(sizedistribution);
     xlabel('Radius (m)')
     ylabel('Number of particles')
end
```

References

AKCABAY, D. T. 2007. Physics Based Washing Machine Simulations.

AKGUN, M. 2014. Assessment of the surface roughness of cotton fabrics through different yarn and fabric structural properties. *Fibers and Polymers,* 15**,** 405-413.

AKGUN, M., BECERIR, B. & ALPAY, H. R. 2012. The effect of fabric constructional parameters on percentage reflectance and surface roughness of polyester fabrics. *Textile Research Journal,* 82**,** 700-707.

AKHTAR, R., SCHWARZER, N., SHERRATT, M., WATSON, R., GRAHAM, H., TRAFFORD, A., MUMMERY, P. & DERBY, B. 2009. Nanoindentation of histological specimens: mapping the elastic properties of soft tissues. *Journal of Materials Research,* 24**,** 638-646.

ALI, Z. M. & GIBSON, L. J. 2013. The structure and mechanics of nanofibrillar cellulose foams. *Soft Matter,* 9**,** 1580-1588.

AN, J.-H. & DULTZ, S. 2007. Adsorption of tannic acid on chitosan-montmorillonite as a function of pH and surface charge properties. *Applied Clay Science,* 36**,** 256-264.

ANDERSON, T. H., YU, J., ESTRADA, A., HAMMER, M. U., WAITE, J. H. & ISRAELACHVILI, J. N. 2010. The contribution of DOPA to substrate‐peptide adhesion and internal cohesion of mussel‐inspired synthetic peptide films. *Advanced functional materials,* 20**,** 4196-4205.

ANTONCZAK, S., RUIZ-LOPEZ, M. & RIVAIL, J. 1994. Ab initio analysis of water-assisted reaction mechanisms in amide hydrolysis. *Journal of the American Chemical Society,* 116**,** 3912-3921.

ARAVINDANATH, S., PARALIKAR, K. M., BETRABET, S. M. & CHAUDHURI, N. K. 1982. Structual Study of Cellophane. *Polymer,* 23**,** 823-828.

AUSSANT, E. & HARRISON, I. M. 2018. Microcapsules. Google Patents.

AYMONIER, C., LOPPINET-SERANI, A., REVER N, H., GARRABOS, Y. & CANSELL, F. 2006. Review of supercritical fluids in inorganic materials science. *The Journal of Supercritical Fluids,* 38**,** 242-251.

BÔNE, S., VAUTRIN, C., BARBESANT, V., TRUCHON, S., HARRISON, I. & GEFFROY, C. 2011. Microencapsulated fragrances in melamine formaldehyde resins. *CHIMIA International Journal for Chemistry,* 65**,** 177-181.

BÜŞRA, A. & NEVIN, Ş. 2015. A Renewable Natural Bioactive Polysaccharide: An Overview to Chitosan. *International Journal of Nutrition and Food Sciences,* 4**,** 541-548.

BAFNA, P. 2016. Cell adhesion molecules: The important biomaterials. *International Journal of Research in Pharmaceutical Sciences,* 3**,** 526-536.

BAJPAI, D. 2007. Laundry detergents: an overview. *Journal of Oleo Science,* 56**,** 327-340.

BALASUNDARAM, G., SATO, M. & WEBSTER, T. J. 2006. Using hydroxyapatite nanoparticles and decreased crystallinity to promote osteoblast adhesion similar to functionalizing with RGD. *Biomaterials,* 27**,** 2798-2805.

BALL, V. 2010. Impedance spectroscopy and zeta potential titration of dopa-melanin films produced by oxidation of dopamine. *Colloids and Surfaces A: Physicochemical and Engineering Aspects,* 363**,** 92-97.

BANSODE, S., BANARJEE, S., GAIKWAD, D., JADHAV, S. & THORAT, R. 2010. Microencapsulation: a review. *International Journal of Pharmaceutical Sciences Review and Research,* 1**,** 38-43.

BARTH, G., LINDER, R. & BRYSON, C. 1988. Advances in charge neutralization for XPS measurements of nonconducting materials. *Surface and Interface Analysis,* 11**,** 307-311.

BARTHEL, E. 2008. Adhesive elastic contacts: JKR and more. *Journal of Physics D: Applied Physics,* 41**,** 163001.

BASHKATOV, A. N. & GENINA, E. A. Water refractive index in dependence on temperature and wavelength: a simple approximation. Saratov Fall Meeting 2002: Optical Technologies in Biophysics and Medicine IV, 2003. International Society for Optics and Photonics, 393-395.

BEAMSON, G. & BRIGGS, D. 1992. *High Resolution XPS of Organic Polymers: The Scienta ESCA300 Database*, Wiley.

BERNSMANN, F., BALL, V., ADDIEGO, F., PONCHE, A., MICHEL, M., GRACIO, J. J. D. A., TONIAZZO, V. & RUCH, D. 2011. Dopamine− melanin film deposition depends on the used oxidant and buffer solution. *Langmuir,* 27**,** 2819-2825.

BHATTACHARYA, P. 2016. A review on the impacts of microplastic beads used in cosmetics. *Acta Biomed. Sci.,* 3**,** 4.

BHATTARAI, N., GUNN, J. & ZHANG, M. 2010. Chitosan-based hydrogels for controlled, localized drug delivery. *Advanced drug delivery reviews,* 62**,** 83-99.

BIGGS, S., SELB, J. & CANDAU, F. 1993. Copolymers of acrylamideN-alkylacrylamide in aqueous solution: the effects of hydrolysis on hydrophobic interactions. *Polymer,* 34**,** 580-591.

BINNIG, G., QUATE, C. F. & GERBER, C. 1986. Atomic force microscope. *Physical review letters,* 56**,** 930.

BITTELLI, M., CAMPBELL, G. S. & FLURY, M. 1999. Characterization of particle-size distribution in soils with a fragmentation model. *Soil Science Society of America Journal,* 63**,** 782-788.

BLAKEWAY, J., FREY, M., LACROIX, S. & SALERNO, M. 1987. Chemical reactions in perfume ageing. *International journal of cosmetic science,* 9**,** 203-214.

BOWEN, J., CHENELER, D., WALLIMAN, D., ARKLESS, S. G., ZHANG, Z., CLWARD, M. & ADAMS, M. J. 2010. On the calibration of rectangular atomic force microscope cantilevers modified by particle attachment and lamination. *Meas. Sci. Technol.,* 21**,** 106-115.

BOWEN, W. R. & DONEVA, T. A. 2000. Atomic force microscopy studies of membranes: Effect of surface roughness on double-layer interactions and particle adhesion. *Journal of Colloid and Interface Science,* 229**,** 544-549.

BRADLEY, R. S. 1932. LXXIX. The cohesive force between solid surfaces and the surface energy of solids. *The London, Edinburgh, and Dublin Philosophical Magazine and Journal of Science,* 13**,** 853-862.

BRIGGS, D. & BEAMSON, G. 1992. Primary and secondary oxygen-induced C1s binding energy shifts in X-ray photoelectron spectroscopy of polymers. *Analytical chemistry,* 64**,** 1729-1736.

BROWN, R. W. & BOWMAN, R. P. 1985. Capsule manufacture. Google Patents.

BRYDSON, J. A. 1999. *Plastics materials*, Butterworth-Heinemann.

BURNHAM, N., COLTON, R. & POLLOCK, H. 1992. Work-function anisotropies as an origin of long-range surface forces. *Physical review letters,* 69**,** 144.

BUTT, H.-J., CAPPELLA, B. & KAPPL, M. 2005. Force measurements with the atomic force microscope: Technique, interpretation and applications. *Surface science reports,* 59**,** 1-152.

BUTT, H.-J. & KAPPL, M. 2009. Normal capillary forces. *Advances in colloid and interface science,* 146**,** 48-60.

CAO, J., USAMI, S. & DONG, C. 1997. Development of a side-view chamber for studying cell-surface adhesion under flow conditions. *Annals of Biomedical Engineering,* 25**,** 573-580.

CARPICK, R. W., OGLETREE, D. F. & SALMERON, M. 1999. A general equation for fitting contact area and friction vs load measurements. *Journal of Colloid and Interface Science,* 211**,** 395-400.

CARTER, J. E., JOHNSON, J. H. & BAASKE, D. M. 1982. Dopamine Hydrochloride. *Analytical Profiles of Drug Substances.* Elsevier.

CHASTAIN, J., KING, R. C. & MOULDER, J. 1992. *Handbook of X-ray photoelectron spectroscopy: a reference book of standard spectra for identification and interpretation of XPS data*, Physical Electronics Division, Perkin-Elmer Corporation Eden Prairie, Minnesota.

CHENG, S., YUEN, C., KAN, C., CHEUK, K., DAOUD, W., LAM, P. & TSOI, W. 2010. Influence of atmospheric pressure plasma treatment on various fibrous materials: Performance properties and surface adhesion analysis. *Vacuum,* 84**,** 1466-1470.

CHO, J. M. & SIGMUND, W. M. 2002. Direct surface force measurement in water using a nanosize colloidal probe technique. *Journal of Colloid and Interface Science,* 245**,** 405-407.

CHUA, P.-H., NEOH, K.-G., KANG, E.-T. & WANG, W. 2008. Surface functionalization of titanium with hyaluronic acid/chitosan polyelectrolyte multilayers and RGD for promoting osteoblast functions and inhibiting bacterial adhesion. *Biomaterials,* 29**,** 1412-1421.

CLAESSON, P. M. & NINHAM, B. W. 1992. pH-dependent interactions between adsorbed chitosan layers. *Langmuir,* 8**,** 1406-1412.

COOPER, K., OHLER, N., GUPTA, A. & BEAUDOIN, S. 2000. Analysis of contact interactions between a rough deformable colloid and a smooth substrate. *Journal of Colloid and Interface Science,* 222**,** 63-74.

COWAN, R. S. 1976. The" industrial revolution" in the home: Household technology and social change in the 20th century. *Technology and Culture***,** 1-23.

COX, M. F., BORYS, N. F. & MATSON, T. P. 1985. Interactions between LAS and nonionic surfactants. *Journal of the American Oil Chemists' Society,* 62**,** 1139-1143.

CRAWFORD, M., GARDNER, M. & MORRIS, J. 1968. Mortality and hardness of local water-supplies. *The Lancet,* 291**,** 827-831.

CRAWFORD, R. L. 1981. *Lignin biodegradation and transformation*, John Wiley and Sons.

CUISSINAT, C. & NAVARD, P. Swelling and Dissolution of Cellulose Part 1: Free Floating Cotton and Wood Fibres in N‐Methylmorpholine‐N‐oxide–Water Mixtures. Macromolecular Symposia, 2006a. Wiley Online Library, 1-18.

CUISSINAT, C. & NAVARD, P. Swelling and dissolution of cellulose part II: Free floating cotton and wood fibres in NaOH–water–additives systems. Macromolecular symposia, 2006b. Wiley Online Library, 19-30.

CUISSINAT, C. & NAVARD, P. 2008. Swelling and dissolution of cellulose, Part III: plant fibres in aqueous systems. *Cellulose,* 15**,** 67-74.

CUISSINAT, C., NAVARD, P. & HEINZE, T. 2008. Swelling and dissolution of cellulose. Part IV: Free floating cotton and wood fibres in ionic liquids. *Carbohydrate Polymers,* 72**,** 590-596.

DANKOVICH, T. A. & GRAY, D. G. 2011. Contact angle measurements on smooth nanocrystalline cellulose (I) thin films. *Journal of Adhesion Science and Technology,* 25**,** 699-708.

DANNER, E. W., KAN, Y., HAMMER, M. U., ISRAELACHVILI, J. N. & WAITE, J. H. 2012. Adhesion of mussel foot protein Mefp-5 to mica: an underwater superglue. *Biochemistry,* 51**,** 6511-6518.

DASH, M., CHIELLINI, F., OTTENBRITE, R. M. & CHIELLINI, E. 2011. Chitosan—A versatile semi-synthetic polymer in biomedical applications. *Progress in Polymer Science,* 36**,** 981-1014.

DE GROOT, P. & DECK, L. 1995. Surface Profiling by Analysis of White-light Interferograms in the Spatial Frequency Domain. *Journal of Modern Optics,* 42**,** 389-401.

DE JONG, W. H. & BORM, P. J. 2008. Drug delivery and nanoparticles: applications and hazards. *International Journal of Nanomedicine,* 3**,** 133.

DECUZZI, P., GENTILE, F., GRANALDI, A., CURCIO, A., CAUSA, F., INDOLFI, C., NETTI, P. & FERRARI, M. 2007. Flow chamber analysis of size effects in the adhesion of spherical particles. *International Journal of Nanomedicine,* 2**,** 689-696.

DERJAGUIN, B. V., MULLER, V. M. & TOPOROV, Y. P. 1975. Effect of contact deformations on the adhesion of particles. *Journal of Colloid and Interface Science,* 53**,** 314-326.

DESAI, K. G. H. & JIN PARK, H. 2005. Recent developments in microencapsulation of food ingredients. *Drying technology,* 23**,** 1361-1394.

DIHORA, J. O. & BROWN, M. A. 2012. Shampoo compositions with increased deposition of polyacrylate microcapsules. Google Patents.

DIHORA, J. O., CETTI, J. R., WITT, S. E. & LI, J. J. 2014. Spray drying microcapsules. Google Patents.

DRIS, R., IMHOF, H., SANCHEZ, W., GASPERI, J., GALGANI, F., TASSIN, B. & LAFORSCH, C. 2015. Beyond the ocean: contamination of freshwater ecosystems with (micro-) plastic particles. *Environmental Chemistry,* 12**,** 539-550.

DUCKER, W. A., SENDEN, T. J. & PASHLEY, R. M. 1992. Measurement of Forces in Liquids Using A Force Microscope. *Langmuir,* 8**,** 1831-1836.

DUGDALE, D. S. 1960. Yielding of steel sheets containing slits. *Journal of the Mechanics and Physics of Solids,* 8**,** 100-104.

ELLISON, A. & ZISMAN, W. 1954. Wettability studies on nylon, polyethylene terephthalate and polystyrene. *The Journal of Physical Chemistry,* 58**,** 503-506.

ENESCU, D. 2008. Use of chitosan in surface modification of textile materials. *Roumanian Biotechnological Letters,* 13**,** 4037.

F RCH, R., SCH NHERR, H. & JENKINS, A. T. A. 2009. *Surface design: applications in bioscience and nanotechnology*, John Wiley & Sons.

FALT, S., WAGBERG, L. & VESTERLIND, E. L. 2003. Swelling of model films of cellulose having different charge densities and comparison to the swelling behavior of corresponding fibers. *Langmuir,* 19**,** 7895-7903.

FALT, S., WAGBERG, L., VESTERLIND, E. L. & LARSSON, P. T. 2004. Model films of cellulose II - improved preparation method and characterization of the cellulose film. *Cellulose,* 11**,** 151-162.

FARROW, G. & PRESTON, D. 1960. Measurement of crystallinity in drawn polyethylene terephthalate fibres by X-ray diffraction. *British journal of applied physics,* 11**,** 353.

FELTON, L. A. & MCGINITY, J. W. 1999. Adhesion of polymeric films to pharmaceutical solids. *European journal of pharmaceutics and biopharmaceutics,* 47**,** 3-14.

FENG, X., POUW, K., LEUNG, V. & PELTON, R. 2007. Adhesion of colloidal polyelectrolyte complexes to wet cellulose. *Biomacromolecules,* 8**,** 2161-2166.

FINCH, C. A. 1973. *Polyvinyl alcohol; properties and applications*, John Wiley & Sons.

FINK, H. P., WEIGEL, P., PURZ, H. J. & GANSTER, J. 2001. Structure formation of regenerated cellulose materials from NMMO-solutions. *Progress in Polymer Science,* 26**,** 1473-1524.

FISHER, A. A. & DOOMS‐GOOSSENS, A. 1976. The effect of perfume "ageing" on the allergenicity of individual perfume ingredients. *Contact Dermatitis,* 2**,** 155-159.

FLETCHER, M. 1996. *Bacterial adhesion: molecular and ecological diversity*, John Wiley & Sons.

FOWKES, F. M. 1964. Attractive forces at interfaces. *Industrial & Engineering Chemistry,* 56**,** 40-52.

FU, J., CHEN, Z., WANG, M., LIU, S., ZHANG, J., ZHANG, J., HAN, R. & XU, Q. 2015. Adsorption of methylene blue by a high-efficiency adsorbent (polydopamine microspheres): kinetics, isotherm, thermodynamics and mechanism analysis. *Chemical Engineering Journal,* 259**,** 53-61.

FULLER, K. 1975. The effect of surface roughness on the adhesion of elastic solids. *Proc. R. Soc. Lond. A,* 345**,** 327-342.

FURTON, K. G. & NORELUS, A. 1993. Determining the critical micelle concentration of aqueous surfactant solutions: using a novel colorimetric method. *Journal of chemical education,* 70**,** 254.

G TZINGER, M., WEIGL, B., PEUKERT, W. & SOMMER, K. 2007. Effect of roughness on particle adhesion in aqueous solutions: a study of Saccharomyces cerevisiae and a silica particle. *Colloids and Surfaces B: Biointerfaces,* 55**,** 44-50.

GALLIFUOCO, A., D'ERCOLE, L., ALFANI, F., CANTARELLA, M., SPAGNA, G. & PIFFERI, P. 1998. On the use of chitosan-immobilized β-glucosidase in wine-making: kinetics and enzyme inhibition. *Process Biochemistry,* 33**,** 163-168.

GANGULI, K. & VAN EENDENBURG, J. 1980. Mass transfer in a laboratory washing machine. *Textile Research Journal,* 50**,** 428-432.

GANZA-GONZALEZ, A., ANGUIANO-IGEA, S., OTERO-ESPINAR, F. J., MENDEZ, J. B. & BURI, P. 2002. Polyacrylate-based microparticles for sustained release of metoclopramide. *Stp Pharma Sciences,* 12**,** 103-107.

GARCES, J. G. 2004. Microcapsules and processes for making the same using various polymers and chitosans. Google Patents.

GARDNER, D. J., OPORTO, G. S., MILLS, R. & SAMIR, M. A. S. A. 2008. Adhesion and surface issues in cellulose and nanocellulose. *Journal of Adhesion Science and Technology,* 22**,** 545-567.

GASSAN, J., GUTOWSKI, V. S. & BLEDZKI, A. K. 2000. About the surface characteristics of natural fibres. *Macromolecular materials and engineering,* 283**,** 132-139.

GERIN, P., DENGIS, P. & ROUXHET, P. 1995. Performance of XPS analysis of model biochemical compounds. *Journal de chimie physique,* 92**,** 1043-1065.

GIBSON, L. J. 2012. The hierarchical structure and mechanics of plant materials. *Journal of the Royal Society Interface***,** rsif20120341.

GIBSON, L. J., ASHBY, M. F. & HARLEY, B. A. 2010. *Cellular materials in nature and medicine*, Cambridge University Press.

GIESBERS, M., KLEIJN, J. M. & STUART, M. A. C. 2002. Interactions between acid-and base-functionalized surfaces. *Journal of Colloid and Interface Science,* 252**,** 138-148.

GIESSIBL, F. J. 2003. Advances in atomic force microscopy. *Reviews of modern physics,* 75**,** 949.

GIRO-PALOMA, J., MART NEZ, M., CABEZA, L. F. & FERN NDEZ, A. I. 2016. Types, methods, techniques, and applications for microencapsulated phase change materials (MPCM): a review. *Renewable and Sustainable Energy Reviews,* 53**,** 1059-1075.

GODDARD, E. 2017. Polymer-Surfactant Interaction: Part II. Polymer and Surfactant of Opposite Charge. *Interactions of surfactants with polymers and proteins.* CRC Press.

GODDARD, E. & HANNAN, R. 1976. Cationic polymer/anionic surfactant interactions. *Journal of Colloid and Interface Science,* 55**,** 73-79.

GOLDSTEIN, J., NEWBURY, D. E., ECHLIN, P., JOY, D. C., ROMIG JR, A. D., LYMAN, C. E., FIORI, C. & LIFSHIN, E. 2012. *Scanning electron microscopy and X-ray microanalysis: a text for biologists, materials scientists, and geologists*, Springer Science & Business Media.

GONZALEZ, F. 2012. Stabilization of Functional Ingredients by Microencapsulation-Interfacial Polymerisation. *PhD Thesis, University of Birmingham, UK*.

GOOD, R. J. 1992. Contact angle, wetting, and adhesion: a critical review. *Journal of Adhesion Science and Technology,* 6**,** 1269-1302.

GOOD, R. J. 2012. Contact angles and the surface free energy of solids. *Surface and colloid science,* 11**,** 1-29.

GOTOH, K., YASUKAWA, A. & TANIGUCHI, K. 2011. Water contact angles on poly (ethylene terephthalate) film exposed to atmospheric pressure plasma. *Journal of Adhesion Science and Technology,* 25**,** 307-322.

GRIBOVA, V., AUZELY-VELTY, R. & PICART, C. 2011. Polyelectrolyte multilayer assemblies on materials surfaces: from cell adhesion to tissue engineering. *Chemistry of Materials,* 24**,** 854-869.

GRIERSON, D., FLATER, E. & CARPICK, R. 2005. Accounting for the JKR–DMT transition in adhesion and friction measurements with atomic force microscopy. *Journal of Adhesion Science and Technology,* 19**,** 291-311.

GUILLEMOT, G., LORTHOIS, S., SCHMITZ, P. & MERCIER-BONIN, M. 2007. Evaluating the adhesion force between Saccharomyces cerevisiae yeast cells and polystyrene from shear-flow induced detachment experiments. *Chemical Engineering Research and Design,* 85**,** 800-807.

GUMBINER, B. M. 1996. Cell adhesion: the molecular basis of tissue architecture and morphogenesis. *Cell,* 84**,** 345-357.

GUNNARS, S., WAGBERG, L. & STUART, M. A. C. 2002. Model films of cellulose: I. Method development and initial results. *Cellulose,* 9**,** 239-249.

GUPTA, V., BASHIR, Z. & FAKIROV, S. 2002. Handbook of thermoplastic polyesters. *Handbook of thermoplastic polyesters*.

HAIGH, S. D. 1996. A review of the interaction of surfactants with organic contaminants in soil. *Science of the Total Environment,* 185**,** 161-170.

HASHIM, M., KULANDAI, J. & HASSAN, R. 1992. Biodegradability of branched alkylbenzene sulphonates. *Journal of Chemical Technology & Biotechnology,* 54**,** 207-214.

HAYS, D. A. 1995. Toner adhesion. *The Journal of Adhesion,* 51**,** 41-48.

HE, Y. 2013. Understanding the Interactions between Microcapsules and Fabric Surfaces. . *PhD Thesis, University of Birmingham, UK*.

HE, Y., BOWEN, J., ANDREWS, J. W., LIU, M., SMETS, J. & ZHANG, Z. 2014. Adhesion of perfume-filled microcapsules to model fabric surfaces. *Journal of Microencapsulation,* 31**,** 430-439.

HEGEMANN, D., BRUNNER, H. & OEHR, C. 2003. Plasma treatment of polymers for surface and adhesion improvement. *Nuclear instruments and methods in physics research section B: Beam interactions with materials and atoms,* 208**,** 281-286.

HO, C.-C. & DING, S.-J. 2014. Structure, properties and applications of mussel-inspired polydopamine. *Journal of biomedical nanotechnology,* 10**,** 3063-3084.

HODGES, C. S., CLEAVER, J. A., GHADIRI, M., JONES, R. & POLLOCK, H. M. 2002. Forces between polystyrene particles in water using the AFM: Pull-off force vs particle size. *Langmuir,* 18**,** 5741-5748.

HODGES, C. S., LOOI, L., CLEAVER, J. A. & GHADIRI, M. 2004. Use of the JKR model for calculating adhesion between rough surfaces. *Langmuir,* 20**,** 9571-9576.

HOFMANN, S. 1986. Practical surface analysis: state of the art and recent developments in AES, XPS, ISS and SIMS. *Surface and Interface Analysis,* 9**,** 3-20.

HOHENBLUM, P., VERSCHOOR, A., B NSCH-BALTRUSCHAT, B., BREUNINGER, E., REIFFERSCHEID, G. & KOSCHORRECK, J. 2016. European overview on management options and measures in place for plastics in freshwater environments. European Conference on Plastics in Freshwater Environments 21–22 June 2016 in Berlin, 2016. 55.

HOLMBERG, M., BERG, J., STEMME, S., ODBERG, L., RASMUSSON, J. & CLAESSON, P. 1997. Surface force studies of Langmuir-Blodgett cellulose films. *Journal of Colloid and Interface Science,* 186**,** 369-381.

HOLME, I. 2007. Innovative technologies for high performance textiles. *Coloration Technology,* 123**,** 59-73.

HONG, K. & PARK, S. 1999. Melamine resin microcapsules containing fragrant oil: synthesis and characterization. *Materials Chemistry and Physics,* 58**,** 128-131.

HOU, R., ZHANG, G., DU, G., ZHAN, D., CONG, Y., CHENG, Y. & FU, J. 2013. Magnetic nanohydroxyapatite/PVA composite hydrogels for promoted osteoblast adhesion and proliferation. *Colloids and Surfaces B: Biointerfaces,* 103**,** 318-325.

HU, Q., TAN, Z., LIU, Y., TAO, J., CAI, Y., ZHANG, M., PAN, H., XU, X. & TANG, R. 2007. Effect of crystallinity of calcium phosphate nanoparticles on adhesion, proliferation, and differentiation of bone marrow mesenchymal stem cells. *Journal of Materials Chemistry,* 17**,** 4690-4698.

HULT, E. L., IVERSEN, T. & SUGIYAMA, J. 2003. Characterization of the supermolecular structure of cellulose in wood pulp fibres. *Cellulose,* 10**,** 103-110.

HUTTER, J. L. & BECHHOEFER, J. 1993. Calibration of atomic‐force microscope tips. *Review of Scientific Instruments,* 64**,** 1868-1873.

ILIUM, L. 1998. Chitosan and its use as a pharmaceutical excipient. *Pharmaceutical research,* 15**,** 1326-1331.

INAGAKI, N., TASAKA, S., NARUSHIMA, K. & KOBAYASHI, H. 2002. Surface modification of PET films by pulsed argon plasma. *Journal of Applied Polymer Science,* 85**,** 2845-2852.

INDEST, T., LAINE, J., KLEINSCHEK, K. S. & ZEMLJIČ, L. F. 2010. Adsorption of human serum albumin (HSA) on modified PET films monitored by QCM-D, XPS and AFM. *Colloids and Surfaces A: Physicochemical and Engineering Aspects,* 360**,** 210-219.

INDEST, T., LAINE, J., RIBITSCH, V., JOHANSSON, L.-S., STANA-KLEINSCHEK, K. & STRNAD, S. 2008. Adsorption of chitosan on PET films monitored by quartz crystal microbalance. *Biomacromolecules,* 9**,** 2207-2214.

IOELOVICH, M. & LEYKIN, A. 2008. Structural Investigations of Various Cotton Fibers and Cotton Celluloses. *Bioresources,* 3**,** 170-177.

ISRAELACHVILI, J., MIN, Y., AKBULUT, M., ALIG, A., CARVER, G., GREENE, W., KRISTIANSEN, K., MEYER, E., PESIKA, N. & ROSENBERG, K. 2010. Recent advances in the surface forces apparatus (SFA) technique. *Reports on Progress in Physics,* 73**,** 036601.

ISRAELACHVILI, J. N. 2011. Intermolecular and surface forces - 3rd Ed. .

ISRAELACHVILI, J. N. & MCGUIGGAN, P. M. 1990. Adhesion and short-range forces between surfaces. Part I: New apparatus for surface force measurements. *Journal of Materials Research,* 5**,** 2223-2231.

JAIN, S. 1999. Mechanical properties of powders for compaction and tableting: an overview. *Pharmaceutical Science & Technology Today,* 2**,** 20-31.

JIA, X., SHENG, W.-B., LI, W., TONG, Y.-B., LIU, Z.-Y. & ZHOU, F. 2014. Adhesive polydopamine coated avermectin microcapsules for prolonging foliar pesticide retention. *Acs Applied Materials & Interfaces,* 6**,** 19552-19558.

JOB, A. E., HERRMANN, P. S., VAZ, D. O. & MATTOSO, L. H. 2001. Comparison between different conditions of the chemical polymerization of polyaniline on top of PET films. *Journal of Applied Polymer Science,* 79**,** 1220-1229.

JOHNSON, K. & GREENWOOD, J. 1997. An adhesion map for the contact of elastic spheres. *Journal of Colloid and Interface Science,* 192**,** 326-333.

JOHNSON, K. L. 1987. *Contact mechanics*, Cambridge university press.

JOHNSON, K. L., KENDALL, K. & ROBERTS, A. 1971. Surface energy and the contact of elastic solids. *Proc. R. Soc. Lond. A,* 324**,** 301-313.

JONES, R., POLLOCK, H. M., CLEAVER, J. A. & HODGES, C. S. 2002. Adhesion forces between glass and silicon surfaces in air studied by AFM: Effects of relative humidity, particle size, roughness, and surface treatment. *Langmuir,* 18**,** 8045-8055.

JOY, D. C. 2006. *Scanning electron microscopy*, Wiley Online Library.

JPK INSTRUMENTS 2009a. AFM Handbook General Guidance.

JPK INSTRUMENTS 2009b. NanoWizard® AFM Handbook.

KANG, S., BAGINSKA, M., WHITE, S. R. & SOTTOS, N. R. 2015a. Core-shell polymeric microcapsules with superior thermal and solvent stability. *ACS applied materials & interfaces,* 7**,** 10952-6.

KANG, S., BAGINSKA, M., WHITE, S. R. & SOTTOS, N. R. 2015b. Core–shell polymeric microcapsules with superior thermal and solvent stability. *Acs Applied Materials & Interfaces,* 7**,** 10952-10956.

KANG, S. M., RHO, J., CHOI, I. S., MESSERSMITH, P. B. & LEE, H. 2009. Norepinephrine: Material-Independent, Multifunctional Surface Modification Reagent. *Journal of the American Chemical Society,* 131**,** 13224-13225.

KHABBAZ, F. 2007. Adhesive system. Google Patents.

KHAN, A. M. & SHAH, S. S. 2008. Determination of critical micelle concentration (Cmc) of sodium dodecyl sulfate (SDS) and the effect of low concentration of pyrene on its Cmc using ORIGIN software. *Journal-Chemical Society Of Pakistan,* 30**,** 186.

KHAN, S. & NEWAZ, G. 2010. A comprehensive review of surface modification for neural cell adhesion and patterning. *Journal of Biomedical Materials Research Part A: An Official Journal of The Society for Biomaterials, The Japanese Society for Biomaterials, and The Australian Society for Biomaterials and the Korean Society for Biomaterials,* 93**,** 1209-1224.

KIM, J., LEE, K., KIM, Y. & KIM, C. K. 2003a. Production of dyestuffs from indole derivatives by naphthalene dioxygenase and toluene dioxygenase. *Letters in applied microbiology,* 36**,** 343-348.

KIM, J., PARK, Y., YUN, C. & PARK, C. H. 2015. Comparison of environmental and economic impacts caused by the washing machine operation of various regions. *Energy Efficiency,* 8**,** 905-918.

KIM, Y. S., LEE, H. H. & HAMMOND, P. T. 2003b. High density nanostructure transfer in soft molding using polyurethane acrylate molds and polyelectrolyte multilayers. *Nanotechnology,* 14**,** 1140.

KIRBY, B. J. 2010. *Micro-and nanoscale fluid mechanics: transport in microfluidic devices*, Cambridge University Press.

KLEMM, D., HEUBLEIN, B., FINK, H.-P. & BOHN, A. 2005. Cellulose: Fascinating Biopolymer and Sustainable Raw Material. *Angewandte Chemie International Edition,* 44**,** 3358-3393.

KOHRI, M. & KAWAMURA, A. 2016. Colorless polydopamine coatings for creating functional interfaces. *Polymer Science: Research Advances, Practical Applications and Educational Aspects***,** 159-168.

KRAJEWSKA, B. 2004. Application of chitin-and chitosan-based materials for enzyme immobilizations: a review. *Enzyme and microbial technology,* 35**,** 126-139.

KUMIRSKA, J., WEINHOLD, M. X., TH MING, J. & STEPNOWSKI, P. 2011. Biomedical activity of chitin/chitosan based materials—influence of physicochemical properties apart from molecular weight and degree of N-acetylation. *Polymers,* 3**,** 1875-1901.

KUSUMA, A. M., LIU, Q. X. & ZENG, H. B. 2014. Understanding interaction mechanisms between pentlandite and gangue minerals by zeta potential and surface force measurements. *Minerals Engineering,* 69**,** 15-23.

KWOK, D. Y. & NEUMANN, A. W. 1999. Contact angle measurement and contact angle interpretation. *Advances in colloid and interface science,* 81**,** 167-249.

L PEZ, G. P., CASTNER, D. G. & RATNER, B. D. 1991. XPS O 1s binding energies for polymers containing hydroxyl, ether, ketone and ester groups. *Surface and Interface Analysis,* 17**,** 267-272.

LAITY, P. R., GLOVER, P. M., GODWARD, J., MCDONALD, P. J. & HAY, J. N. 2000. Structural studies and diffusion measurements of water-swollen cellophane by NMR imaging. *Cellulose,* 7**,** 227-246.

LANE, W. O., JANTZEN, A. E., CARLON, T. A., JAMIOLKOWSKI, R. M., GRENET, J. E., LEY, M. M., HASELTINE, J. M., GALINAT, L. J., LIN, F.-H., ALLEN, J. D., TRUSKEY, G. A. & ACHNECK, H. E. 2012. Parallel-plate Flow Chamber and Continuous Flow Circuit to Evaluate Endothelial Progenitor Cells under Laminar Flow Shear Stress. e3349.

LAZZARONI, M., PEZZOTTA, E., MENDUNI, G., BOCCHIOLA, D. & WARD, D. Remote measurement and monitoring of critical washing process data directly inside the washing machine drum. Instrumentation and Measurement Technology Conference, 2000. IMTC 2000. Proceedings of the 17th IEEE, 2000. IEEE, 478-482.

LEE, B. P., MESSERSMITH, P. B., ISRAELACHVILI, J. N. & WAITE, J. H. 2011. Mussel-inspired adhesives and coatings. *Annual Review of Materials Research,* 41**,** 99-132.

LEE, D. W., LIM, C., ISRAELACHVILI, J. N. & HWANG, D. S. 2013. Strong adhesion and cohesion of chitosan in aqueous solutions. *Langmuir,* 29**,** 14222-14229.

LEE, H., DELLATORE, S. M., MILLER, W. M. & MESSERSMITH, P. B. 2007. Mussel-inspired surface chemistry for multifunctional coatings. *science,* 318**,** 426-430.

LEE, L.-H. 2013. *Fundamentals of adhesion*, Springer Science & Business Media.

LEI, X., LAWRENCE, M. & DONG, C. 1999. Influence of cell deformation on leukocyte rolling adhesion in shear flow. *Journal of biomechanical engineering,* 121**,** 636-643.

LEPPANEN, K., ANDERSSON, S., TORKKELI, M., KNAAPILA, M., KOTELNIKOVA, N. & SERIMAA, R. 2009. Structure of cellulose and microcrystalline cellulose from various wood species, cotton and flax studied by X-ray scattering. *Cellulose,* 16**,** 999-1015.

LI, H., JIA, Y., FENG, X. & LI, J. 2017. Facile fabrication of robust polydopamine microcapsules for insulin delivery. *Journal of Colloid and Interface Science,* 487**,** 12-19.

LI, L. & LI, H. 2015. Dopamine deposited rapidly on the surface of PET fabric by UV radiation and electroless nickel plating. *Materials Research Innovations,* 19**,** S8-174-S8-179.

LIANG, W., XU, L., SUN, S., LAN, L., QIU, X., CHEN, R. & LI, Y. 2016. Polystyrenesulfonate Dispersed Dopamine with Unexpected Stable Semiquinone Radical and Electrochemical Behavior: A Potential Alternative to PEDOT:PSS. *ACS Sustainable Chemistry & Engineering,* 5**,** 460-468.

LIANG, Y., HILAL, N., LANGSTON, P. & STAROV, V. 2007. Interaction forces between colloidal particles in liquid: Theory and experiment. *Advances in colloid and interface science,* 134**,** 151-166.

LIEBERMANN, H., LACHMAN, L. & KANIG, J. 1990. The theory and practice of industrial pharmacy. *Ed,* 3**,** 253-296.

LIEBSCHER, J. R., MRÓWCZYŃSKI, R., SCHEIDT, H. A., FILIP, C., HĂDADE, N. D., TURCU, R., BENDE, A. & BECK, S. 2013. Structure of polydopamine: a never-ending story? *Langmuir,* 29**,** 10539-10548.

LIM, H.-T., JEONG, W.-B. & KIM, K.-J. 2010. Dynamic modeling and analysis of drum-type washing machine. *International Journal of Precision Engineering and Manufacturing,* 11**,** 407-417.

LIU, K. M., PREECE, J. A., YORK, D., BOWEN, J. & ZHANG, Z. 2013. Measurement of the adhesion between single melamine-formaldehyde resin microparticles and a flat fabric surface using AFM. *Journal of Adhesion Science and Technology,* 27**,** 973-987.

LIU, M. 2010. Understanding the Mechanical Strength of Microcapsules and Their Adhesion on Fabric Surfaces. . *PhD Thesis, University of Birmingham, UK*.

LIU, X. D., TOKURA, S., HARUKI, M., NISHI, N. & SAKAIRI, N. 2002. Surface modification of nonporous glass beads with chitosan and their adsorption property for transition metal ions. *Carbohydrate Polymers,* 49**,** 103-108.

LIU, Y., AI, K. & LU, L. 2014. Polydopamine and its derivative materials: synthesis and promising applications in energy, environmental, and biomedical fields. *Chemical reviews,* 114**,** 5057-5115.

LIU, Y., HE, T. & GAO, C. 2005. Surface modification of poly (ethylene terephthalate) via hydrolysis and layer-by-layer assembly of chitosan and chondroitin sulfate to construct cytocompatible layer for human endothelial cells. *Colloids and Surfaces B: Biointerfaces,* 46**,** 117-126.

LONDON, F. 1937. The general theory of molecular forces. *Transactions of the Faraday Society,* 33**,** 8b-26.

LUCASSEN-REYNDERS, E. H. 1981. *Anionic surfactants: physical chemistry of surfactant action*, Marcel Dekker.

LUCOVSKY, G., LIN, S., RICHARD, P., CHAO, S., TAKAGI, Y., PAI, P., KEEM, J. & TYLER, J. 1985. Local atomic structure of silicon suboxides (SiOx, x< 2). *Journal of Non-Crystalline Solids,* 75**,** 429-434.

LYNGE, M. E., SCHATTLING, P. & ST DLER, B. 2015. Recent developments in poly (dopamine)-based coatings for biomedical applications. *Nanomedicine,* 10**,** 2725-2742.

MAC NAMARA, C., GABRIELE, A., AMADOR, C. & BAKALIS, S. 2012. Dynamics of textile motion in a front-loading domestic washing machine. *Chemical Engineering Science,* 75**,** 14-27.

MADENE, A., JACQUOT, M., SCHER, J. & DESOBRY, S. 2006. Flavour encapsulation and controlled release–a review. *International journal of food science & technology,* 41**,** 1-21.

MALVERN INSTRUMENTS LTD, U. 2007. *Mastersizer 2000 User Manual*.

MALVERN INSTRUMENTS LTD, U. 2013. *Zetasizer Nano Series User Manual*, Malvern Instruments Ltd, UK.

MARTINS, I. M., BARREIRO, M. F., COELHO, M. & RODRIGUES, A. E. 2014. Microencapsulation of essential oils with biodegradable polymeric carriers for cosmetic applications. *Chemical Engineering Journal,* 245**,** 191-200.

MASON, S. A., GARNEAU, D., SUTTON, R., CHU, Y., EHMANN, K., BARNES, J., FINK, P., PAPAZISSIMOS, D. & ROGERS, D. L. 2016. Microplastic pollution is widely detected in US municipal wastewater treatment plant effluent. *Environmental Pollution,* 218**,** 1045-1054.

MATHESON, K. L., COX, M. F. & SMITH, D. L. 1985. Interactions between linear alkylbenzene sulfonates and water hardness ions. I. Effect of calcium ion on surfactant solubility and implications for detergency performance. *Journal of the American Oil Chemists' Society,* 62**,** 1391-1396.

MATIJEVIC, E. & GOOD, R. J. 2012. *Surface and colloid science*, Springer Science & Business Media.

MAUGIS, D. 1992. Adhesion of spheres: the JKR-DMT transition using a Dugdale model. *Journal of Colloid and Interface Science,* 150**,** 243-269.

MCNAUGHT, A. D. 1997. *Compendium of chemical terminology*, Blackwell Science Oxford.

MCNEIL, I. 2002. *An Encyclopedia of the History of Technology*, Taylor & Francis.

MEDRONHO, B., ROMANO, A., MIGUEL, M. G., STIGSSON, L. & LINDMAN, B. 2012. Rationalizing cellulose (in) solubility: reviewing basic physicochemical aspects and role of hydrophobic interactions. *Cellulose,* 19**,** 581-587.

MERCAD -PRIETO, R., NGUYEN, B., ALLEN, R., YORK, D., PREECE, J. A., GOODWIN, T. E. & ZHANG, Z. 2011. Determination of the elastic properties of single microcapsules using micromanipulation and finite element modeling. *Chemical Engineering Science,* 66**,** 2042-2049.

MERCAD ‐ PRIETO, R., ALLEN, R., ZHANG, Z., YORK, D., PREECE, J. A. & GOODWIN, T. E. 2012. Failure of elastic ‐ plastic core ‐ shell microcapsules under compression. *AIChE Journal,* 58**,** 2674-2681.

MERCADE-PRIETO, R., NGUYEN, B., ALLEN, R., YORK, D., PREECE, J. A., GOODWIN, T. E. & ZHANG, Z. B. 2011. Determination of the elastic properties of single microcapsules

using micromanipulation and finite element modeling. *Chemical Engineering Science,* 66**,** 2042-2049.
MERCADE-PRIETO, R. & ZHANG, Z. B. 2012. Mechanical characterization of microspheres - capsules, cells and beads: a review. *Journal of Microencapsulation,* 29**,** 277-285.
MERKUS, H. G. 2009. *Particle size measurements: fundamentals, practice, quality*, Springer Science & Business Media.
MEYER, E. E., LIN, Q., HASSENKAM, T., OROUDJEV, E. & ISRAELACHVILI, J. N. 2005. Origin of the long-range attraction between surfactant-coated surfaces. *Proceedings of the National Academy of Sciences of the United States of America,* 102**,** 6839-6842.
MICCERI, T. 1989. The unicorn, the normal curve, and other improbable creatures. *Psychological bulletin,* 105**,** 156.
MINT, A., VIRGOE, J. R., PALMER, D. V. & KERR, A. R. 2018. Capsules. Google Patents.
MIR SPECOS, M. M., ESCOBAR, G., MARINO, P., PUGGIA, C., DEFAIN TESORIERO, M. V. & HERMIDA, L. 2010. Aroma finishing of cotton fabrics by means of microencapsulation techniques. *Journal of industrial textiles,* 40**,** 13-32.
MIRSHAFIAN, R., WEI, W., ISRAELACHVILI, J. N. & WAITE, J. H. 2016. α, β-Dehydro-Dopa: a hidden participant in mussel adhesion. *Biochemistry,* 55**,** 743-750.
MITCHELL, R., CARR, C., PARFITT, M., VICKERMAN, J. & JONES, C. 2005. Surface chemical analysis of raw cotton fibres and associated materials. *Cellulose,* 12**,** 629-639.
MITTAL, K. L. & JAISWAL, R. 2015. *Particle adhesion and removal*, John Wiley & Sons.
MORENT, R., DE GEYTER, N., VERSCHUREN, J., DE CLERCK, K., KIEKENS, P. & LEYS, C. 2008. Non-thermal plasma treatment of textiles. *Surface and Coatings Technology,* 202**,** 3427-3449.
MUKERJEE, P. & MYSELS, K. J. 1971. Critical micelle concentrations of aqueous surfactant systems. National Standard reference data system.
MURNAGHAN, F. 1944. The compressibility of media under extreme pressures. *Proceedings of the National Academy of Sciences,* 30**,** 244-247.
NAGARAJAN, R. 2002. Molecular packing parameter and surfactant self-assembly: the neglected role of the surfactant tail. *Langmuir,* 18**,** 31-38.
NEDOVIC, V., KALUSEVIC, A., MANOJLOVIC, V., LEVIC, S. & BUGARSKI, B. 2011. An overview of encapsulation technologies for food applications. *Procedia Food Science,* 1**,** 1806-1815.
NELSON, G. 2001. Microencapsulation in textile finishing. *Coloration Technology,* 31**,** 57-64.
NODA, A., YAMAGUCHI, M., AIZAWA, M. & KUMANO, Y. 1992. Cosmetic containing fine soft microcapsules. Google Patents.
NOTLEY, S. M. & W GBERG, L. 2005. Morphology of modified regenerated model cellulose II surfaces studied by atomic force microscopy: Effect of carboxymethylation and heat treatment. *Biomacromolecules,* 6**,** 1586-1591.
NOTLEY, S. M. & WAGBERG, L. 2005. Morphology of modified regenerated model cellulose II surfaces studied by atomic force microscopy: Effect of carboxymethylation and heat treatment. *Biomacromolecules,* 6**,** 1586-1591.
ONO, A., FUSE, T., MIYAMOTO, O., MAKINO, S., YAMATO, Y., KAMETANI, H., TOKURA, S., TANAKA, H., ITO, T. & NAKAO, H. 1990. Fibrous structures having a durable fragrance and a process for preparing the same. Google Patents.
OSTERBERG, M. & CLAESSON, P. M. 2000. Interactions between cellulose surfaces: effect of solution pH. *Journal of Adhesion Science and Technology,* 14**,** 603-618.
OWENS, D. K. & WENDT, R. 1969. Estimation of the surface free energy of polymers. *Journal of Applied Polymer Science,* 13**,** 1741-1747.
PAKULA, C. & STAMMINGER, R. 2010. Electricity and water consumption for laundry washing by washing machine worldwide. *Energy Efficiency,* 3**,** 365-382.

PALANISAMY, S. 2015. SD Denesh kumaar." Stress Analysis of Washing Machine Drum. *International Journal of Innovative Research in Science, Engineering and Technology*, 610-614.

PAPAKONSTANTINOU, D., AMANATIDES, E., MATARAS, D., IOANNIDIS, V. & NIKOLOPOULOS, P. 2007. Improved surface energy analysis for plasma treated PET films. *Plasma Processes and Polymers,* 4, S1057-S1062.

PARIA, S., MANOHAR, C. & KHILAR, K. C. 2005. Adsorption of anionic and non-ionic surfactants on a cellulosic surface. *Colloids and Surfaces A: Physicochemical and Engineering Aspects,* 252, 221-229.

PERESSADKO, A., HOSODA, N. & PERSSON, B. 2005. Influence of surface roughness on adhesion between elastic bodies. *Physical review letters,* 95, 124301.

PERRIN, D. D., DEMPSEY, B. & SERJEANT, E. P. 1981. *pKa prediction for organic acids and bases*, Springer.

PICKERING, S. J. 2006. Recycling technologies for thermoset composite materials—current status. *Composites Part A: Applied Science and Manufacturing,* 37, 1206-1215.

PIERRES, A., BENOLIEL, A. M. & BONGRAND, P. 2008. Studying Molecular Interactions at the Single Bond Level with a Laminar Flow Chamber. *Cellular and Molecular Bioengineering,* 1, 247-262.

PODCZECK, F. 1998. *Particle-particle adhesion in pharmaceutical powder handling*, Imperial College Pr.

PONCELET, D., LEUNG, R., CENTOMO, L. & NEUFELD, R. J. 1993a. Microencapsulation of silicone oils within polyamide—polyethylenimine membranes as oxygen carriers for bioreactor oxygenation. *Journal of Chemical Technology and Biotechnology,* 57, 253-263.

PONCELET, D., LEUNG, R., CENTOMO, L. & NEUFELD, R. J. 1993b. MICROENCAPSULATION OF SILICONE OILS WITHIN POLYAMIDE POLYETHYLENIMINE MEMBRANES AS OXYGEN CARRIERS FOR BIOREACTOR OXYGENATION. *Journal Of Chemical Technology And Biotechnology,* 57, 253-263.

PONZIO, F., BARTH S, J., BOUR, J., MICHEL, M., BERTANI, P., HEMMERL , J., D'ISCHIA, M. & BALL, V. 2016a. Oxidant Control of Polydopamine Surface Chemistry in Acids: A Mechanism-Based Entry to Superhydrophilic-Superoleophobic Coatings. *Chemistry of Materials,* 28, 4697-4705.

PONZIO, F., BARTHÈS, J., BOUR, J. R. M., MICHEL, M., BERTANI, P., HEMMERLÉ, J., D'ISCHIA, M. & BALL, V. 2016b. Oxidant control of polydopamine surface chemistry in acids: A mechanism-based entry to superhydrophilic-superoleophobic coatings. *Chemistry of Materials,* 28, 4697-4705.

POPOV, V. L. 2010. *Contact mechanics and friction*, Springer.

POSTMA, A., YAN, Y., WANG, Y., ZELIKIN, A. N., TJIPTO, E. & CARUSO, F. 2009. Self-polymerization of dopamine as a versatile and robust technique to prepare polymer capsules. *Chemistry of Materials,* 21, 3042-3044.

PREVORSEK, D., KWON, Y. & SHARMA, R. D. 1977. Structure and properties of Nylon 6 and PET fibres: the effects of crystallite dimensions. *Journal of materials science,* 12, 2310-2328.

R WILLIAMS, D. 2015. Particle engineering in pharmaceutical solids processing: surface energy considerations. *Current pharmaceutical design,* 21, 2677-2694.

RABANEL, J. M., BANQUY, X., ZOUAOUI, H., MOKHTAR, M. & HILDGEN, P. 2009. Progress Technology in Microencapsulation Methods for Cell Therapy. *Biotechnology Progress,* 25, 946-963.

RABINOVICH, Y. I., ADLER, J. J., ATA, A., SINGH, R. K. & MOUDGIL, B. M. 2000. Adhesion between nanoscale rough surfaces: I. Role of asperity geometry. *Journal of Colloid and Interface Science,* 232, 10-16.

RABINOVICH, Y. I., ADLER, J. J., ESAYANUR, M. S., ATA, A., SINGH, R. K. & MOUDGIL, B. M. 2002. Capillary forces between surfaces with nanoscale roughness. *Advances in colloid and interface science,* 96**,** 213-230.

RAJU, T. N. 2005. William Sealy Gosset and William A. Silverman: two "students" of science. *Pediatrics,* 116**,** 732-735.

RATNER, B. D., CHILKOTI, A. & LOPEZ, G. P. 1990. Plasma deposition and treatment for biomaterial applications. *Plasma deposition, treatment and etching of polymers***,** 463-516.

REIMER, L. 2000. Scanning electron microscopy: physics of image formation and microanalysis. IOP Publishing.

REN, Y., DONALD, A. & ZHANG, Z. 2007a. Investigation of radiation damage to microcapsules in environmental SEM. *Materials science and technology,* 23**,** 857-864.

REN, Y. L., DONALD, A. M. & ZHANG, Z. B. 2007b. Investigation of radiation damage to microcapsules in environmental SEM. *Materials Science and Technology,* 23**,** 857-864.

RICHARD, J. & MORTEAU, S. 2004. Plant protein-based microcapsules. Google Patents.

RINAUDO, M., MILAS, M. & LE DUNG, P. 1993. Characterization of chitosan. Influence of ionic strength and degree of acetylation on chain expansion. *International Journal of Biological Macromolecules,* 15**,** 281-285.

RODRIGUES, S., MARTINS, I., FERNANDES, I., GOMES, P., MATA, V., BARREIRO, M. & RODRIGUES, A. 2009. Scentfashion®: Microencapsulated perfumes for textile application. *Chemical Engineering Journal,* 149**,** 463-472.

RODRIGUESA, S. N. 2010. Microencapsulation of Perfumes for Application in Textile Industry. *PhD Thesis, University of Porto, Portugal*.

RUMPF, H. 2012. *Particle technology*, Springer Science & Business Media.

SACHDEV, A. & KRISHNAN, S. 1996. Heavy-duty liquid detergents. *Surfactant science series***,** 261-324.

SAFRAN, S., ROBBINS, M. O. & GAROFF, S. 1986. Tilt and splay of surfactants on surfaces. *Physical Review A,* 33**,** 2186.

SAJIC, B., RYKLIN, I. & MALIK, A. 1999. Heavy duty liquid detergent compositions comprising salts of α-sulfonated fatty acid methyl esters and use of α-sulphonated fatty acid salts to inhibit redeposition of soil on fabric. Google Patents.

SALLOUM, D. S., OLENYCH, S. G., KELLER, T. C. & SCHLENOFF, J. B. 2005. Vascular smooth muscle cells on polyelectrolyte multilayers: hydrophobicity-directed adhesion and growth. *Biomacromolecules,* 6**,** 161-167.

SAMPER, E., RODR GUEZ, M., DE LA RUBIA, M. & PRATS, D. 2009. Removal of metal ions at low concentration by micellar-enhanced ultrafiltration (MEUF) using sodium dodecyl sulfate (SDS) and linear alkylbenzene sulfonate (LAS). *Separation and Purification Technology,* 65**,** 337-342.

SAVARINO, P., MONTONERI, E., MUSSO, G. & BOFFA, V. 2010. Biosurfactants from urban wastes for detergent formulation: surface activity and washing performance. *Journal of surfactants and detergents,* 13**,** 59.

SCAMEHORN, J., SCHECHTER, R. & WADE, W. 1982. Micelle formation in mixtures of anionic and nonionic surfactants. *Journal Of Dispersion Science And Technology,* 3**,** 261-278.

SCHAEFER, D. M., CARPENTER, M., GADY, B., REIFENBERGER, R., DEMEJO, L. P. & RIMAI, D. S. 1995. Surface-Roughness And Its Influence on Particle Adhesion Using Atomic-Force Techniques. *Journal of Adhesion Science and Technology,* 9**,** 1049-1062.

SCHANZE, K. S., LEE, H. & MESSERSMITH, P. B. 2018. Ten Years of Polydopamine: Current Status and Future Directions. ACS Publications.

SCHEIBEL, J. J. 2004. The evolution of anionic surfactant technology to meet the requirements of the laundry detergent industry. *Journal of surfactants and detergents,* 7**,** 319-328.

SCHEIRS, J. & LONG, T. E. 2005. *Modern polyesters: chemistry and technology of polyesters and copolyesters*, John Wiley & Sons.
SCHWANTES, T. A. 2011. Cationic microcapsule particles. Google Patents.
SCHWANTES, T. A. & SANDS, P. D. 2010. Oil-in-water capsule manufacture process and microcapsules produced by such process. Google Patents.
SCHWARZ, U. D. 2003. A generalized analytical model for the elastic deformation of an adhesive contact between a sphere and a flat surface. *Journal of Colloid and Interface Science,* 261**,** 99-106.
SEITZ, M. E. 1988. Microcapsules, printing inks and their production. Google Patents.
SHARMA, M. M., CHAMOUN, H., SARMA, D. S. R. & SCHECHTER, R. S. 1992. Factors controlling the hydrodynamic detachment of particles from surfaces. *Journal of Colloid and Interface Science,* 149**,** 121-134.
SHIMIZU, R. N. & DEMARQUETTE, N. R. 2000. Evaluation of surface energy of solid polymers using different models. *Journal of Applied Polymer Science,* 76**,** 1831-1845.
SHOWELL, M. 1997. *Powdered detergents*, CRC Press.
SIA, S. K. & WHITESIDES, G. M. 2003. Microfluidic devices fabricated in poly(dimethylsiloxane) for biological studies. *Electrophoresis,* 24**,** 3563-3576.
SILVERSTEIN, T. P. 1998. The real reason why oil and water don't mix. *Journal of chemical education,* 75**,** 116.
SMETS, J., SANDS, P. D., GUINEBRETIERE, S. J., PINTENS, A. & DIHORA, J. O. 2011. Benefit agent containing delivery particle. Google Patents.
SOBOTTKA, R. 1994. Anti-blocking agent containing modified amorphous silica. Google Patents.
SOHAIL, T., TANG, T. & NADLER, B. 2013. Adhesive contact of a fluid-filled membrane driven by electrostatic forces. *International Journal of Solids and Structures,* 50**,** 2678-2690.
SPEIGHT, J. G. 2005. *Lange's handbook of chemistry*, McGraw-Hill New York.
SRIDHAR, I., JOHNSON, K. & FLECK, N. 1997. Adhesion mechanics of the surface force apparatus. *Journal of Physics D: Applied Physics,* 30**,** 1710.
STAMM, M. 2008. Polymer surfaces and interfaces. *Polymer Surfaces and Interfaces: Characterization, Modification and Applications, ISBN 978-3-540-73864-0. Springer Berlin Heidelberg,* 1.
STELLNER, K. L. & SCAMEHORN, J. F. 1989a. Hardness tolerance of anionic surfactant solutions. 1. Anionic surfactant with added monovalent electrolyte. *Langmuir,* 5**,** 70-77.
STELLNER, K. L. & SCAMEHORN, J. F. 1989b. Hardness tolerance of anionic surfactant solutions. 2. Effect of added nonionic surfactant. *Langmuir,* 5**,** 77-84.
STEVENSON, W. T. & SEFTON, M. 1992. Development of polyacrylate microcapsules. *Fundamentals of Animal Cell Encapsulation and Immobilization***,** 143-181.
SU, J. F., WANG, X. Y. & DONG, H. 2012. Micromechanical properties of melamine-formaldehyde microcapsules by nanoindentation: Effect of size and shell thickness. *Materials Letters,* 89**,** 1-4.
SULTANOVA, N., KASAROVA, S. & NIKOLOV, I. Investigation of optical properties of thin polymer films. Journal of Physics: Conference Series, 2012. IOP Publishing, 012049.
SUN, G. & ZHANG, Z. 2001. Mechanical properties of melamine-formaldehyde microcapsules. *Journal of Microencapsulation,* 18**,** 593-602.
SUN, G. & ZHANG, Z. 2002. Mechanical strength of microcapsules made of different wall materials. *International Journal of Pharmaceutics,* 242**,** 307-311.
TABOR, D. 1977. Surface forces and surface interactions. *Plenary and Invited Lectures.* Elsevier.
TALENS, F., PATON, P. & GAYA, S. 1998. Micelar flocculation of anionic surfactants. *Langmuir,* 14**,** 5046-5050.
TAN TAI, L. H. 2000. Formulating detergents and personal care products. A complete guide to product development. AOCS Press.
TEIXEIRA, C. S. N. R. 2010. Microencapsulation of perfumes for application in textile industry.

THIES, C. 2005 Microencapsulation. *Kirk-Othmer Encyclopedia of Chemical Technology.*
THYGESEN, A., ODDERSHEDE, J., LILHOLT, H., THOMSEN, A. B. & ST HL, K. 2005. On the determination of crystallinity and cellulose content in plant fibres. *Cellulose,* 12**,** 563.
TONEY, M. D. & KIRSCH, J. F. 1989. Direct Bronsted analysis of the restoration of activity to a mutant enzyme by exogenous amines. *science,* 243**,** 1485-1488.
TSUJI, K. 1999. Microcapsules in agriculture. *MML SERIES,* 1**,** 349.
TSUJI, K. 2001. Microencapsulation of pesticides and their improved handling safety. *Journal of Microencapsulation,* 18**,** 137-147.
ULGUT, B. & SUZER, S. 2003. XPS studies of SiO2/Si system under external bias. *The Journal of Physical Chemistry B,* 107**,** 2939-2943.
UPDEGRAFF, D. M. 1969. Semimicro determination of cellulose inbiological materials. *Analytical Biochemistry,* 32**,** 420-424.
VAN DEN BREKEL, L. D. M. 1987. Hydrodynamics and mass transfer in domestic drum-type fabric washing machines.
VAN HONSCHOTEN, J. W., TAS, N. R. & ELWENSPOEK, M. 2010. The profile of a capillary liquid bridge between solid surfaces. *American Journal of Physics,* 78**,** 277-286.
VEMMER, M. & PATEL, A. V. 2013. Review of encapsulation methods suitable for microbial biological control agents. *Biological Control,* 67**,** 380-389.
VERBOOM, G. 2011. Method for strengthening keratinous fibers. Google Patents.
VERBOOM, G. M. 2013. Method for strengthening keratinous fibers. EU Patents.
VERGE, C., MORENO, A., BRAVO, J. & BERNA, J. L. 2001. Influence of water hardness on the bioavailability and toxicity of linear alkylbenzene sulphonate (LAS). *Chemosphere,* 44**,** 1749-1757.
VERSCHOOR, A., DE POORTER, L., DR GE, R., KUENEN, J. & DE VALK, E. 2016. Emission of microplastics and potential mitigation measures: Abrasive cleaning agents, paints and tyre wear.
VERWEY, E. J. W., OVERBEEK, J. T. G. & OVERBEEK, J. T. G. 1999. *Theory of the stability of lyophobic colloids*, Courier Corporation.
W GBERG, L. 2000. *Spreading of droplets of different liquids on specially structured papers*, Mitthögskolan, FSCN.
WAGBERG, L. 2000. Polyelectrolyte adsorption onto cellulose fibres - A review. *Nordic Pulp & Paper Research Journal,* 15**,** 586-597.
WAITE, J. H. 2008. Surface chemistry: Mussel power. *Nature materials,* 7**,** 8.
WAKELYN, P. J., BERTONIERE, N. R., FRENCH, A. D., THIBODEAUX, D. P., TRIPLETT, B. A., ROUSSELLE, M.-A., GOYNES JR, W. R., EDWARDS, J. V., HUNTER, L. & MCALISTER, D. D. 2006. *Cotton fiber chemistry and technology*, CRC Press.
WANG, P., YANG, L. & HSIEH, A. H. 2011. Nucleus Pulposus Cell Response to Confined and Unconfined Compression Implicates Mechanoregulation by Fluid Shear Stress. *Annals of Biomedical Engineering,* 39**,** 1101-1111.
WANG, Y., LI, P. & KONG, L. 2013. Chitosan-modified PLGA nanoparticles with versatile surface for improved drug delivery. *Aaps Pharmscitech,* 14**,** 585-592.
WANG, Y., LI, Y., TANG, L., LU, J. & LI, J. 2009. Application of graphene-modified electrode for selective detection of dopamine. *Electrochemistry Communications,* 11**,** 889-892.
WARD, D. 2000. Modelling of a horizontal-axis domestic washing machine. *Journal of the Textile Institute,* 91**,** 207-234.
WARD, D. 2003. A novel remote measurement and monitoring system for the measurement of critical washing parameters inside a domestic washing machine. *Measurement,* 34**,** 193-205.
WARHEIT, D. B., SAYES, C. M., REED, K. L. & SWAIN, K. A. 2008. Health effects related to nanoparticle exposures: environmental, health and safety considerations for assessing hazards and risks. *Pharmacology & therapeutics,* 120**,** 35-42.

WARMOESKERKEN, M., VAN DER VLIST, P., MOHOLKAR, V. & NIERSTRASZ, V. 2002. Laundry process intensification by ultrasound. *Colloids and Surfaces A: Physicochemical and Engineering Aspects,* 210**,** 277-285.
WEEKS, B. L., VAUGHN, M. W. & DEYOREO, J. J. 2005. Direct imaging of meniscus formation in atomic force microscopy using environmental scanning electron microscopy. *Langmuir,* 21**,** 8096-8098.
WEI, Q., ZHANG, F., LI, J., LI, B. & ZHAO, C. 2010. Oxidant-induced dopamine polymerization for multifunctional coatings. *Polymer Chemistry,* 1**,** 1430-1433.
WEINBERGER, H. 1983. Heavy duty liquid detergent. Google Patents.
WEING RTNER, H., FRANCK, E., WEIGAND, G., DAHMEN, N., SCHWEDT, G., FRIMMEL, F., GORDALLA, B., JOHANNSEN, K., SUMMERS, R. & H LL, W. 2000. Ullmann's Encyclopedia of Industrial Chemistry. *Wiley-VCH Verlag GmbH & Co. doi,* 10**,** a28_001.
WEISENHORN, A., MAIVALD, P., BUTT, H.-J. & HANSMA, P. 1992. Measuring adhesion, attraction, and repulsion between surfaces in liquids with an atomic-force microscope. *Physical Review B,* 45**,** 11226.
WHEELER, A. F. 2017. Intentionally added microplastics in products. *Final report. Report*.
WINNEBECK, K. 2014. *Clean, Green & Healthy.* US Environmental Protection Agency.
WOO, Y.-K. 1985. Fragrance impregnated fabric. Google Patents.
WOO, Y.-K. 1988. Capsule impregnated fabric. Google Patents.
WOOD, D. 2004. Heavy-duty liquid detergent composition comprising anionic surfactants. Google Patents.
WU, D. Y., LI, S. & STANISLAW, G. W. 1999. Surface treatment of polymers. Google Patents.
WU, S. Calculation of interfacial tension in polymer systems. Journal of Polymer Science: Polymer Symposia, 1971. Wiley Online Library, 19-30.
WU, S. 1973. Polar and nonpolar interactions in adhesion. *The Journal of Adhesion,* 5**,** 39-55.
XANTHOS, D. & WALKER, T. R. 2017. International policies to reduce plastic marine pollution from single-use plastics (plastic bags and microbeads): a review. *Marine pollution bulletin,* 118**,** 17-26.
XANTHOS, M. 2010. *Functional fillers for plastics*, John Wiley & Sons.
XU, D., LIECHTI, K. M. & RAVI-CHANDAR, K. 2007. On the modified Tabor parameter for the JKR–DMT transition in the presence of a liquid meniscus. *Journal of Colloid and Interface Science,* 315**,** 772-785.
YANG, S. H., KANG, S. M., LEE, K.-B., CHUNG, T. D., LEE, H. & CHOI, I. S. 2011. Mussel-inspired encapsulation and functionalization of individual yeast cells. *Journal of the American Chemical Society,* 133**,** 2795-2797.
YANGXIN, Y., JIN, Z. & BAYLY, A. E. 2008. Development of surfactants and builders in detergent formulations. *Chinese Journal of Chemical Engineering,* 16**,** 517-527.
YE, Q., ZHOU, F. & LIU, W. 2011. Bioinspired catecholic chemistry for surface modification. *Chemical Society Reviews,* 40**,** 4244-4258.
YEN, M.-T., YANG, J.-H. & MAU, J.-L. 2009. Physicochemical characterization of chitin and chitosan from crab shells. *Carbohydrate Polymers,* 75**,** 15-21.
YOSHIDA, S., HAGIWARA, K., HASEBE, T. & HOTTA, A. 2013. Surface modification of polymers by plasma treatments for the enhancement of biocompatibility and controlled drug release. *Surface and Coatings Technology,* 233**,** 99-107.
YOUNG, R. A. & ROWELL, R. M. 1986. *Cellulose: Structure, Modification, and Hydrolysis*, Wiley.
YOUNG, T. 1805. III. An essay on the cohesion of fluids. *Philosophical transactions of the royal society of London,* 95**,** 65-87.
YU, J., WEI, W., DANNER, E., ISRAELACHVILI, J. N. & WAITE, J. H. 2011. Effects of interfacial redox in mussel adhesive protein films on mica. *Advanced materials,* 23**,** 2362-2366.

YU, J., WEI, W., MENYO, M. S., MASIC, A., WAITE, J. H. & ISRAELACHVILI, J. N. 2013. Adhesion of mussel foot protein-3 to TiO2 surfaces: the effect of pH. *Biomacromolecules,* 14**,** 1072-1077.

YUN, C. & PARK, C. H. 2015. The effect of fabric movement on washing performance in a front-loading washer II: under various physical washing conditions. *Textile Research Journal,* 85**,** 251-261.

ZAUSCHER, S. & KLINGENBERG, D. J. 2001. Friction between cellulose surfaces measured with colloidal probe microscopy. *Colloids and Surfaces A: Physicochemical and Engineering Aspects,* 178**,** 213-229.

ZAUSCHER, S. & KLINGENBERG, D. J. 2003. *Surface forces and friction between cellulose surfaces in aqueous media,* Norwell, Kluwer Academic Publishers.

ŻENKIEWICZ, M. 2007. Methods for the calculation of surface free energy of solids. *Journal of Achievements in Materials and Manufacturing Engineering,* 24**,** 137-145.

ZHANG, Z. 1999. Mechanical strength of single microcapsules determined by a novel micromanipulation technique. *Journal of Microencapsulation,* 16**,** 117-124.

ZOETEWEIJ, M., VAN DER DONCK, J. & VERSLUIS, R. 2009. Particle removal in linear shear flow: model prediction and experimental validation. *Journal of Adhesion Science and Technology,* 23**,** 899-911.

ZOPPE, J. O., OSTERBERG, M., VENDITTI, R. A., LAINE, J. & ROJAS, O. J. 2011. Surface interaction forces of cellulose nanocrystals grafted with thermoresponsive polymer brushes. *Biomacromolecules,* 12**,** 2788-2796.